Coordination polymers based on divergent terpyridine ligands

Inauguraldissertation

zur
Erlangung der Würde eines Doktors der Philosophie
vorgelegt der
Philosophisch-Naturwissenschaftlichen Fakultät
der Universität Basel

von
Srboljub Vujovic

aus Österreich

Basel, 2017

Genehmigt von der Philosophisch-Naturwissenschaftlichen Fakultät auf Antrag von:

Prof. Dr. Catherine E. Housecroft

Prof. Dr. Dennis Gillingham

Basel, den 21.04.15

Prof. Dr. Jörg Schibler

Dekan

"Ever tried. Ever failed. No matter. Try Again. Fail again. Fail better."

Samuel Beckett

"I've failed over and over and over again in my life and that is why I succeed."

Michael Jordan

"Don't get too excited when I am winning, and don't get too depressed when I am losing. Just keep it cool."

Marat Safin

"So many of our dreams at first seem impossible, then they seem improbable, and then, when we summon the will, they soon become inevitable."
"Don't give up. Don't lose hope. Don't sell out."

Christopher Reeve

Contents

Most of the figures in this thesis are reproduced using the original artwork used in the following publications:

Molecular recognition between 4'-(4-biphenylyl)-4,2':6',4"-terpyridine domains in the assembly of d9 and d10 metal ion-containing one-dimensional coordination polymers
E. C. Constable, C. E. Housecroft, M. Neuburger, J. Schönle, S. Vujovic and J. A. Zampese
Polyhedron, 2013, 60, 120-129

Coordination polymers with 4'-(4-(anthracen-9-yl)phenyl)- and 4'-(4-(naphthalen-1-yl)phenyl)-4,2':6',4"-terpyridines: Mono-, di and heptazinc(II) nodes
E. C. Constable, C. E. Housecroft, M. Neuburger, J. Schönle, S. Vujovic and J. A. Zampese
Polyhedron, 2013, 62, 260-267

Do perfluoroarene..arene and C–H...F interactions make a difference to 4,2':6',4"-terpyridine-based coordination polymers?
E. C. Constable, C. E. Housecroft, S. Vujovic, J. A. Zampese, A. Crochet and S. R. Batten
CrystEngComm, 2013, 15, 10068-10078

Metallohexacycles containing 4'-aryl-4,2':6',4"-terpyridines: conformational preferences and fullerene capture
E. C. Constable, C. E. Housecroft, S. Vujovic and J. A. Zampese
CrystEngComm, 2014, 16, 328–338.

2D -> 2D Parallel interpenetration of (4,4) sheets constructed from a ditopic bis(4,2':6',4''-terpyridine)
E. C. Constable, C. E. Housecroft, S. Vujovic and J. A. Zampese
CrystEngComm, 2014, 16, 3494-3497

Environmental control in the assembly of metallomacrocycles and one-dimensional polymers with 4,2':6':4''-terpyridine linkers and zinc(II) nodes
E. C. Constable, C. E. Housecroft, A. Prescimone, S.Vujovic and J. A. Zampese
CrystEngComm, 2014, 16, 8691-8699

Engineering 2D→2D parallel interpenetration using long alkoxy-chain substituents
S. Vujovic, E. C. Constable, C. E. Housecroft, C. D. Morris, M. Neuburger and A. Prescimone
Polyhedron, 2015, in press.

Acknowledgements

First and foremost I would like to express my gratitude towards Prof. Dr. Catherine E. Housecroft and Prof. Dr. Edwin C. Constable for being my research supervisors and doctoral "parents". I am very grateful that you took me in and gave me the opportunity to do research and complete my studies. It goes without saying that I learned and improved a lot of skills related to science but what I particularly cherish is that you believed in me and gave me the opportunity to grow as a person. It was an experience that made me stronger and taught me how to deal with a lot of stuff, all at once and I am sure it will serve me very well in the future. I will proudly look back and say I, we came a long way. Catherine, it was a pleasure to work on one of the projects that everyone referred to as "your baby" and hopefully "our baby". I really liked it from the first time you introduced it to me and the fact that there were already nice results in the past just made me hopeful that we could achieve more of the same together. Ed, thank you for caring about the project, for being interested and always having some helpful advice even though this project was being referred to as "not your baby" I certainly never felt that way.

Then, I'd like to thank Prof. Dr. Dennis Gillingham for accepting to be my co-examiner. We know each other since you came to Basel and I am very impressed how you built your lab from scratch. I still remember some very nice discussions during organic chemistry problem sessions. But what I will never forget is one private discussion that we had during a critical moment in my time here in Basel when I felt that you clearly related to me. "Chemical work in the lab is about expressing your intelligence through your hands, if you are smart you can get away without studying too much for an exam, but in the lab where failure is part of the process there is no way around hard work". I don't remember if those were your exact words but I clearly got the message (not that I am smart but that I need to work hard) and understood what I had to do in order to succeed. Maybe, I never thanked you enough for this moment but I'd like to do it here and now, thank you.

Essential to the success of my project was the crystallography team consisting of: Dr. Jennifer Zampese, Dr. Markus Neuburger and Dr. Alessandro Prescimone. I am especially grateful to Jennifer for giving me a lot of tips about crystal growing when I started and for not only doing a lot of structures for me but also teaching me about the whole process. It is something I truly enjoyed and it made me realize that I do work in a team. Thanks to Markus for running the crystallography lab, your patience, kindness and knowledge are just impressive. Also, thanks to Alex for solving the structures that allowed me to start writing this thesis. After Jennifer left, Dr. Collin Morris was working with me in the crystallography lab and I'd like to thank you for that. We didn't have the best of luck, but what we found out was very important for the subsequent work.

Takodje, hteo bih da se zahvalim Dr. Biljani Bozic-Weber na svemu. Biljo od kad sam došao si uvek imala vreme za mene, slušala si me kako kukam i kako se žalim i svaki put si znala da me smiriš i da mi ulijes dodatno samopouzdanje. Puno sam naučio od tebe, ne samo na naučnom planu nego i kako da se nosim sa odredjenim situacijama i ljudima. Sve do samog kraja sam mogao da računam na tebe i ne znam kako bih isplivao bez tvojih saveta. Sad znam da ne mogu u svakoj situaciji da odreagujem prosto "balkanski" i da ponekad treba spustiti loptu. Nedostajaće mi kafica sa tobom ali se nadam da će ih jos biti.

VIII

naučio me mnogo toga pa sam tako napredovao mnogo i fizicčki i psihički. Radovao sam se svakoj fukici i svakom treningu kao i rostiljanju. Hvala ti pre svega sto si se mojim uspesima radovao kao da su tvoji. Drago mi je da si uspeo da ostaneš i da ti dobro ide i baš se nadam i veselim skorašnjem gledanju. Hvala takodje Mariu Lovriću aka Ljubi aka stari moj sto je zamenio Marka mada nam je prerano otišao. Naravno i kafice sa Biljom su takodje doprinele balkanskom uživanju.

Danke auch an buba švaba Sascha Keller aka Sale. Ich erinnere mich immer noch an das Departmentsfest als wir uns kennengelernt haben und seither sind wir echt Freunde geworden. Mit dir kann man echt über alles reden, vom Training bis zu den Frauen. "Jaa", "und", "läuft" und "muss" gehören da natürlich dazu. Thanks also to the members of the Seebeck group especially Kikina, Roxana Lemnaru, Laetitia Misson and Pascal Engi for "tolerating" my company and for hanging out with me in and outside of the Uni.

Hvala takodje mojim "našim" prijateljima van fakulteta u Mordoru, najduže znam Mirana brkana Mišica. Brko stvarno ti hvala za druženje, za tenis koji nismo igrali sto godina, za bezbroj pivi kod brke kao i za izlaske tu i tamo. Posebno sam ti zahvalan što si organizovao provod u Splitu i na Hvaru, to stvarno pamtim kao jedno od najlepsih putovanja i obećavam da ću uzvratiti istom merom u Beogradu. Hvala Džoniju "Alenu" Jekeru mom bivsem studentu koji je u medjuvremenu krenuo u bolje vode. Lepo smo se uklopili stvarno za trening, bleju, sport i zezanje. Drago mi je da napokon ja imam ulogu "velikog brata" i da te gledam kako napreduješ. Potencijal je veliki ali mladom majmunu nije lako. Hvala takodje Džonijevim roditeljima Dari i Goranu na podršci i druženju. Od mladog lava Leona očekujemo velika dela. Miši Jovanoviću hoću takodje da se zahvalim na druženju i novom prijateljstvu u teretani ali i izvan nje. Jedva čekam da probam tu rakijicu što je matora kao i ti. Komšiji Borislavu Iliću se zahvaljujem na druženju i blejanju uz pivicu i utakmice kao i za odelo koje mi je donelo sreću za poslovni razgovor pa se nadam da ce isto tako biti i za odbranu.

Merci aussi a Yves-Andre Graf avec qui mon chemin c'est croisé dans trois villes consécutives, c'est vraiment une amitié de longue date et c'est dommage que tu n est plus a Bâle. Un grand grand merci á mon brate Guillaume Glauser et a ses parents Fabienne et André Glauser qui m'ont accueilli ici comme si j'étais un des leurs. Je suis content GG que tu te plais dans ta nouvelle vie á Bordeaux mais tu manques ici. A mes parents alsaciens je suis vraiment reconaissant de tout ce que vous faites pour moi, les nombreux repas de Fabienne, les bricolages de Dédé. Je me suis vraiment moins seul ici grâce a vous. Merci aussi de vouloir bien venir a ma soutenance, ce serait pas la meme chose sans vous.

Gracias también a mi amigo, el Dr. David Muñoz Torres, me hace falta practicar el español contigo. Me acuerdo todavía de nuestro viaje a Tenerife mientras que estabas acabando tu tesis y espero verte pronto.

Sports has always been a big part of my life and I am thankful for everything it thought me, which is to fight, never to give up and try to find a way when it seems impossible. A cet endroit je veux et dois remercier le Dr. Damien Mauron pour m'avoir remis sur les pieds vraiment et m'avoir aidé a reprendre le sport. Je suis très content de toujours pouvoir compter sur votre soutien car on a fait beaucoup de chemin ensemble et on continuera d'en faire. Egalement l'équipe de Neuroradiologie du nouveau CHU de Strasbourg mérite mon gratitude. Particulièrement, le Dr. Fabrice Bing qui a réalisé l'intervention, la PLDD. Si je suis capable de toujours écrire ma thèse au bout de nombreux mois et si je suis aussi capable de faire du sport comme je n'ai pas pu en faire pendant des années, c'est bien grâce a vous. Merci infiniment!

X

Hteo bih takodje da se zahvalim Jovanu Zlatanoviću Joci koji me je trenirao u TK Partizan. Joco, mnogo ste me naučili ne samo o tenisu, nego o zivotu. Naucio sam da nema popustanja i da svaki poen mora da se zaradi. Isto kao sto me niste mazili na terenu tako me i u zivotu niko nece maziti. Nikad mi iste popustili nimalo i hvala vam na tome. Obećao sam vam da ću da pokažem ovde ko smo is šta smo i nadam se da vas nisam razočarao. Zahvaljujem se svom trenutnom treneru Urošu Bičaninu koji me je trenirao jos kad sam bio mnogo mladji. Hvala ti Uroše na strpljenju i što nisi poludeo pored mene. Nadam se da imamo još puno da napredujemo zajedno mada si već mnogo napredovao kao trener a ja nadam se kao teniser.

I am very happy that I started going to Karate again and I really regret that I ever stopped. It really is not just a sport for the body but also for the mind. Je voulais remercier Emmanuel Labouebe, qui est mon professeur de Karaté, pour son influence, ses conseils, son approche et pour la passion qu'il me transmet à chaque entrainement. Pour avoir ma thèse, je vais essayer le coup de brique comme vous m'avez conseillé. Après ma soutenance un de mes grands projets et souhaits est d'avoir le premier dan. Je me réjouis de tout le travail qui m'attend sous votre oeil observateur pour y arriver. Merci également aux amis du Karaté pour la belle ambiance qu'on a dans notre club, je pense à Manu, Jérem, les Nico's, Greg, Florian, Sophie et bien d'autres.

Ich denke auch an meine vielen Freunde in Wien, vor allem an Geza Frank, meinen ersten Kumpel und an Patrick Maurer meinen Lieblingssvabo und Nachbarn. Rado se sećam ''našeg'' drustvanceta u Beču: Ivana, Vlakija, Ratka, Ivana, Acka, Marka, Arsenija sto je sad u Londonu, porodice Jakić.

Takodje mislim i na moje drugove, bisere rasute svuda po malo. Većina je ipak u Bgu kao i moje drugarice Tara i Isidora Karajica sa kojima se uvek slatko ispričam i nasmejem. Takodje, njihovi roditelji Branka i Fedja su mi mnogo dragi i uvek se obradujem da ih vidim i mnogo puta su mi pružili podršku i uputili ohrabrujuće reči.

Zahvalan sam takodje Milošu Djokiću, mom drugu iz ranog detinjstva kao i mom komšiji Milošu Ilinčiću što će da mi dodju na odbranu i što ćemo da proslavimo zajedno. Ne vidjamo se baš često ali kad se vidimo, uvek je kao da se nikad nismo razišli. Nažalost moj kumić iz Brazila neće moći da dodje ali siguram sam da će u mislima biti uz mene kao i kumići Bojan i Bogdan. Hvala Beki što si me izabrao za venčanog kuma i jedva čekam da opet dodjem kod tebe.

Sta-ri moj lud sam sta-ri moj!! Que dire brate, heureusement je suis allé au Karate sinon qui sait comment on aurait fait pour se connaitre ici à Saint-Louis mêtropole. Comme le prophète a annoncé, LudviK était censé partir en Serbie pour ses conquètes. Il te reste encore du territoire a parcourir mais on fera ça ensemble kad mu ga DA, DA DA DA! Je ne sais pas pourquoi te remercier d'abord, merci de: m'avoir initié a la méthode, m'aider pour mon entrainement, gérer ma diète, m'avoir aidé pour le passage de grade pour la ceinture marron, m'aider a me préparer pour la ceinture noire, m'ammener un red bull quand il m'en faut (hvala Gosp. Matešiću za priozvod btw) ou tout simplement m'écouter pour tout et n'importe quoi. Tu n'est pas juste un drug, tu est un prijatelj et brate. Qui sait comment ce serait passé ma période de rédaction sans les soirées shisha et zik. Merci aussi de bien vouloir t'occuper de la musique lors de ma soutenance. Je suis vraiment content de t'avoir comme brate et qu'on va fêter ça ensemble. Tu as vraiment su me motiver et soutenir quand j'avais pas envie! Suffit que tu viennes allumer une shisha en me donnant un red bull et en mettant une de nos chansons préférés et ca allait déjà mieux. Vu que tu as pas voulu lire ces mots avant ma soutenance j'ai juste a rajoutter: ZAPALI GRAAD!

Zahvaljujem se takodje mojoj braći, mojim burazerima Andji, Dekiju i Bokiju kao i mojoj sestrici Dei. Hvala vam na podršci i što ste verovali da mogu da uspem šta god ja mutio tamo. Svi mi mnogo značite i zaista uživam u dobroj klopi i serijama sa Deom, izlascima sa Bokijem, razgovorima i roštilju sa Dekijem, tenisu i akciji sa Andjom. Mnogo mi je lepo bilo dok smo živeli u istom gradu brate, i nadam se da će se ponoviti. Mislim i na tvoju porodicu, pogotovu na Pericu i Aleksandricu. Hvala i Desi i Danki što sa vama mogu da pričam o svemu i što me uvek slušate i savetujete kao da sam vaše dete. Takodje veliko hvala Mimi i Ceciju sto me čuvaju od malena i što su me pogotovu u skorije vreme podržali u teskim trenucima. Zahvaljujem se takodje ujacima Lakiju i Dekiju na podršci. Sanji Djordjević se zahvaljujem što mi dolazi na odbranu i što si mi kao i Milan ostala porodični prijatelj. Stvarno se družimo od kad znam za sebe i radujem se što cemo da proslavimo zajedno. Šteta sto Stefan i Aleksandar ne mogu da dodju ali mi je drago što se opet više družimo pa cemo da nadoknadimo sve to.

Jejo, ti si moj najveći poklon ikada, ne samo za četvrti rodjendan nego za ceo život, moj najveći izvor energije, moja motivacija i moja inspiracija. Hvala ti što postojiš i što si baš moja sestra. Sreća me je pogledala. Da nije tebe ko zna gde bih bio i mnogo me raduje što ćes biti prisutna kad će sve da bude gotovo i da taj trenutak proživimo zajedno. Zahvalan sam ti na podršci koju si mi pružila za vreme teze kao i u svakom periodu u životu. Volim te najviše na svetu i ceo ovaj rad i trud posvećujem tebi. Nadam se da ćemo uvek da se pazimo i čuvamo iako nismo bas u blizini. Nije zato što si moja ali si najbolja sestra na svetu svih vremena. Mogu bez mnogih stvari u životu, ali bez tebe nikako.

Voleo bih takodje ovaj rad i sve što sam postigao do sad da posvetim najpre svojoj dragoj mami Mileni, kojoj dugujem sve u životu, vaspitanje, obrazovanje i nadam se ljubav prema drugima. Najzahvalniji sam ti što si mi rodila Jeju da nikad ne budem sam. Siguram sam da bi bila presrećna što sam napokon završio ovaj poduhvat i znam da bi bila ponosna na mene. Puno mi nedostaješ svakog dana života ali pogotovu na ovakvim bitnim dogadjajima. Volim te i zauvek te čuvam u srcu i u mislima. Istom merom posvećujem ovaj rad mojoj dragoj nani Stojanki što me je očuvala od malena, sve mi dala i volela više od same sebe kao i mom dedi, imenjaku Srboljubu sa kojim sam mnogo voleo da pričam o nauci. Za kraj, posvećujem ovaj rad mom stricu Miodragu, koji je takodje bio doktor i mom dedi Mitru koga stalno čujem da sam jako voleo.

Abbreviations

Å	Ångström
a, b, c	lattice parameters (X-ray)
AcO	Acetate
α, β, γ	interaxial angles (X-ray)
aq.	Aqueous
a.u.	Arbitrary unit
calc.	calculated
conc.	concentration/concentrated
^{o}C	degree Celsius
CH_2Cl_2	dichloromethane
COSY	correlation spectroscopy
DC	calculated density (X-ray)
δ	chemical shift [ppm]
DMF	*N*,*N*-dimethylformamide
DMSO	dimethyl sulfoxide
EA	elemental analysis
eq.	equivalent
ESI	electron spray ionisation
Et_2O	diethyl ether
ε	extinction coefficient
g	gram
h	hour
HMBC	heteronuclear multiple bond correlation
HMQC	heteronuclear multiple quantum coherence
IR	infrared
J	coupling constant in Hz
L	litre
$λ_{abs}$	absorption wavelength
$λ_{em}$	emission wavelength
$λ_{ex}$	excitation wavelength
MALDI	matrix-assisted laser desorption ionization
Me	methyl
MeCN	acetonitrile
MeOH	methanol
mmol	millimole
mL	millilitre
MS	mass spectrometry
m/z	mass-to-charge ratio (MS)
μ(M-Kα)	absorption coeffcient of the radiation source M (X-ray)
nm	nanometer
NMR	nuclear magnetic resonance
NOESY	nuclear overhauser enhancement spectroscopy
Ph	phenyl
phen	1,10---phenanthroline

PMMA	1-(4-methoxyphenyl)-*N*-methyl-propan-2-amine/ polymethylmethacrylate
ppm	parts per million
R1	agreement factor (X-ray)
rt	room temperature
TMS	tetramethylsilane
tpy	4,2':6',4''-terpyridine
UV-Vis	ultra violet and visible light
U	volume of the unit cell (X-ray)
wR2	weighted agreement factor (X-ray)
z	formula units (X-ray)

Abstract

This work describes the design and synthesis of 4,2':6',4''-terpyridine ligands and their use in coordination polymers with various metal salts. In that goal, a series of novel mono-4,2':6',4''-terpyridines bearing aryl substituents on the 4' position was prepared. Then, a series of back-to-back 4,2':6',4''-terpyridines, which is a new class of compounds, connected through the same 4' positions with various rigid spacers were synthesized. First, their synthesis, NMR, UV-VIS, fluorescence and most importantly single crystal X-ray structures are presented and compared. The next section describes the reactions of the mono-4,2':6',4''-terpyridines with metal acetates (mainly Zn(II)), which yielded various one-dimensional coordination polymers. Afterwards the reactions of the same ligands with various Zn(II) halides to produce mostly metalloxexacycles are discussed. Also, a number of host-guest attempts are presented. In the last section, the reactions of the back-to-back 4,2':6',4''-terpyridines with various Zn(II) halides, which resulted in the formation of 2D nets, are displayed and the effect of the spacers was considered.

Summary

Chapter I: Introduction
The first chapter begins with an introduction of supramolecular chemistry and its concepts. Examples from nature where supramolecular interactions occur are presented followed by examples from research. Then, crystal engineering and coordination polymers are introduced followed by the 4,2':6',4''-terpyridine. Lastly, previous results from our research group with this ligand class are presented.

Chapter II: Synthesis and characterization of 4'-substituted mono-4,2':6',4''-terpyridines and back-to-back 4,2':6',4''-terpyridines
In this section the various strategies that led to the formation of new mono-4,2':6',4''-terpyridines bearing aromatic substituents on the 4' position is presented as well as the synthesis of the novel class of back-to-back 4,2':6',4''-terpyridines. The full characterization of the compounds is included. Obtained crystal structures, including the packing-effects of the different substituents, are discussed.

Chapter III: Reactions of 4'-substituted 4,2':6',4''-terpyridines with metal acetate salts
Chapter III shows reactions with Zn(II), Cd(II) and Cu(II) acetate. Different reaction conditions and metal-to-ligand ratios are examined. The obtained one-dimensional coordination polymers and their configurations are analyzed as well as the interactions between adjacent chains. Furthermore, the effect of the size and the electronic properties of the aromatic substituent are explored.

Chapter IV: Reactions of 4'-substituted 4,2':6',4''-terpyridines with Zn(II) halides
The fourth chapter presents the reactions with $ZnCl_2$, $ZnBr_2$ and ZnI_2. The influence of the halide and of the 4' substituent of the ligand are discussed as well as the formation of different conformers. A host-guest complex is illustrated and other inclusion attempts are reviewed.

Chapter V: Reactions of back-to-back 4,2':6',4''-terpyridines with Zn(II) halides

Here, the first reactions of the new back-to-back 4,2':6',4''-terpyridines with $ZnCl_2$, $ZnBr_2$ and ZnI_2 are displayed. The formation of the different 2-dimensional nets and their topology is explained. Consequences of reducing the length of the alkoxy substituent on the spacers on the structures is investigated and discussed.

Instruments section

Data were collected on a Bruker-Nonius KappaAPEX diffractometer with data reduction, solution and refinement using the programs APEX2, SIR92, CRYSTALS, and SHELXL97 or 13 or on a Stoe IPDS diffractometer using Stoe IPDS software and SHELXL97. ORTEP diagrams were drawn using ORTEP-3 for WINDOWS, TOPOS or with Mercury, and the latter was used to analyse the packing. If rapid solvent loss influenced data quality and therefore the structure was subsequently refined using SQUEEZE. Powder diffractograms were measured on a STOE STADI P diffractometer equipped with Cu Kα1 radiation (λ = 1.540598 Å) and a Mythen1K detector.

^{1}H and ^{13}C NMR spectra were recorded using a Bruker Avance III-250, 400 or 500 NMR spectrometer with chemical shifts referenced to residual solvent peaks with respect to δ(TMS) = 0 ppm.

Absorption spectra were recorded on a Cary-5000 spectrophotometer or on an Agilent 8453 spectrophotometer

Solution emission spectra were recorded on a Shimadzu RF-5301 PC spectrofluorometer. Solution and solid state quantum yield measurements were recorded on a Hamamatsu 11347-11 (Standard type) Absolute PL Quantum Yield Measurement System.

FT-IR spectra were recorded on a PerkinElmer UATR Two spectrometer or on a Shimadzu 8400S instrument with Golden Gate accessory for solid samples.

Electrospray ionisation (ESI) and MALDI TOF mass spectra were measured using Bruker Esquire 3000plus and Bruker microflex instruments, respectively.

Solution electronic absorption spectra were recorded using an Agilent 8453 spectrophotometer.

Melting points were measured on a Bibby Melting Point Apparatus SMP3.

Elemental analyses were measured on a Leco CHN-900 microanalyser.

Chapter I: Introduction

1.1 Supramolecular chemistry

1.1.1 What is supramolecular chemistry?

As Prof. Jean-Marie Lehn explained during his banquet speech upon receiving the Nobel Prize in 1987 (together with Donald J. Cram and Charles J. Pedersen) "Beyond the chemistry of strong bonds, that forge the atoms into molecules, the chemistry of weak interactions was rewarded this year, one in which unity is strength, where players join hands to better embrace the object of their desire, where the matching of shapes allows the recognition of one another. This chemistry that can be called supramolecular forms a sort of molecular sociology. Interactions between molecules define the interspecific link, the action and reaction, the stability of an organization and the "elective affinities" that prevail, in short, the behavior of individuals and molecular populations."[1]

Sub-atomic particles associate to form atoms, which in turn connect to form molecules. Traditionally, chemistry mainly focuses on the properties of atoms and chemical reactions that form bonds between them. Such a covalent bond, which involves sharing of electron pairs, is a strong interaction and therefore carries the notion of irreversibility to a large extent. Instead, supramolecular chemistry focuses on the weaker (noncovalent) interactions that have a reversible character and that occur between molecules. Those interactions, that make up the tool box of supramolecular chemistry[2,3] are pictured in Fig. 1.
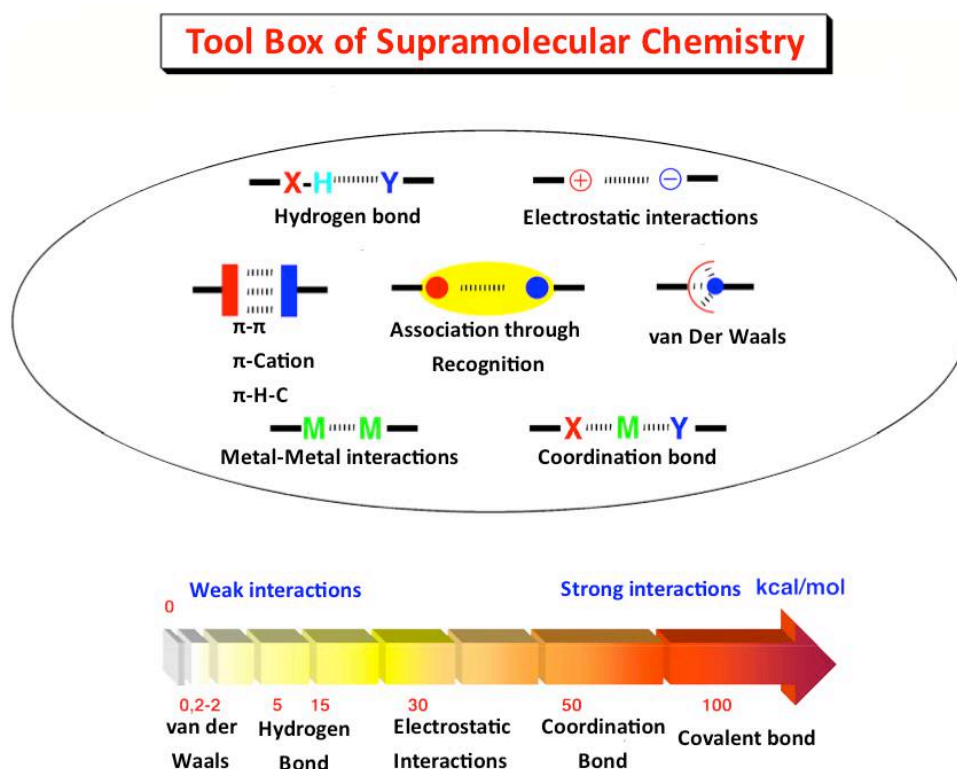
Fig. 1.Tool box of supramolecular chemistry showing the different types of weak interactions that can occur between molecules and comparison of some of their relative energies (figure from references 2 and 3).

1.1.2 Supramolecular chemistry in nature

Even though supramolecular chemistry is a research topic that has gathered pace quite recently it has been omnipresent ever since molecules started to exist. Nature is full of beautiful examples of supramolecular interactions and without them life as we know it would not be possible. As far as chemical reactions in our body are concerned, supramolecular interactions are involved every step of the way. The molecule that is the symbol of life, DNA, is held together by hydrogen bonds when in its double-stranded form as shown in Fig. 2.
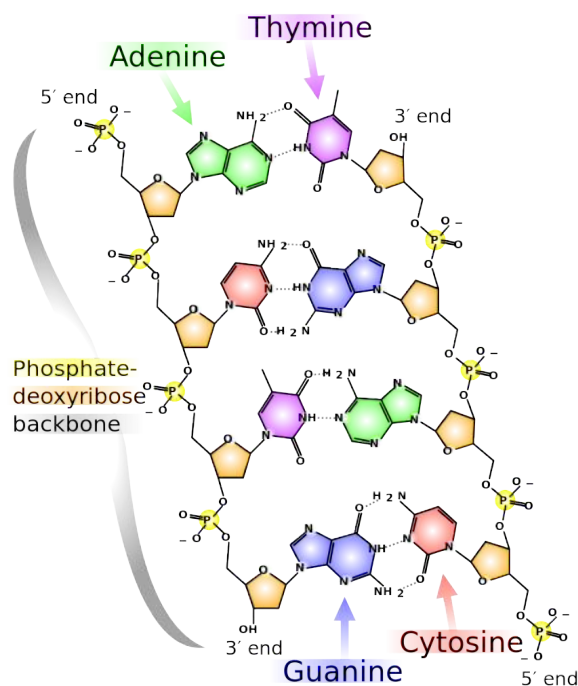
Fig. 2. Hydrogen bonds between matching base pars between two strands of DNA.

Due to those hydrogen bonds being reversible, the DNA molecule can either stay closed or open when needed, for example during replication. After a transcription/translation cycle a protein is obtained and via a multitude of those weak interactions like H-bonds, electrostatic interactions, coordination bonds if a metal is present, it folds together into its three dimensional structure. Those enzymes catalyze chemical reactions by first recognizing their substrate. An enzyme-substrate interaction via the famous "lock and key" concept suggested by Nobel laureate Hermann Emil Fischer[4] is a very important principle for molecular recognition and host-guest chemistry. Next to the fact that there has to be a complementarity as far as the shapes are concerned, the two species that associate also engage in van der Waals interactions. As can be seen in Fig. 3, which shows a step in the mechanism of the alcohol oxidation by alcohol dehydrogenase[5], H-bonds, association through recognition and coordination bonds are among the interactions that take place in this enzyme-catalyzed reaction. As such, supramolecular interactions do not just hold proteins together but also more complex systems.
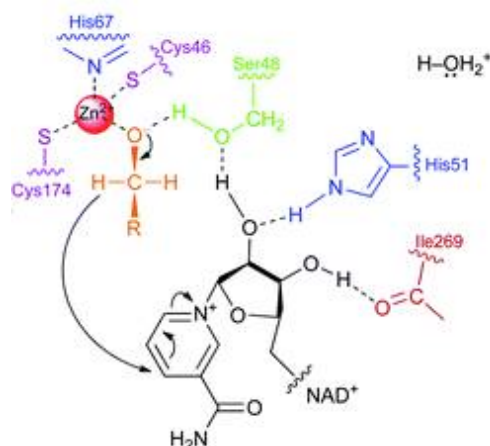
Fig. 3. Proposed catalytic mechanism for alcohol dehydrogenase: Proton relay system in horse liver alcohol dehydrogenase (HLADH). Different supramolecular interactions occur simultaneously.

1.1.3 Supramolecular chemistry in research

As is often the case, nature served as a source of inspiration for chemists to try to mimic concepts found in organisms all around us but also to use some of those principles for new goals. Even though the chemists use the same tool box of supramolecular interactions as nature, they have the advantage that using synthetic techniques almost any building block can be prepared. In 1967 Charles Pedersen reported the binding properties of crown ethers[6], in the case shown in Fig. 4 the compound 18-crown-6 recognises and binds to a potassium ion. The group of Jean-Marie Lehn managed in 1969 to create an even better "cage" for the same cation by preparing the macrobicyclic cryptand [2,2,2][7] (also shown in Fig. 4).

(a) Crown ether   **(b) Cryptand**
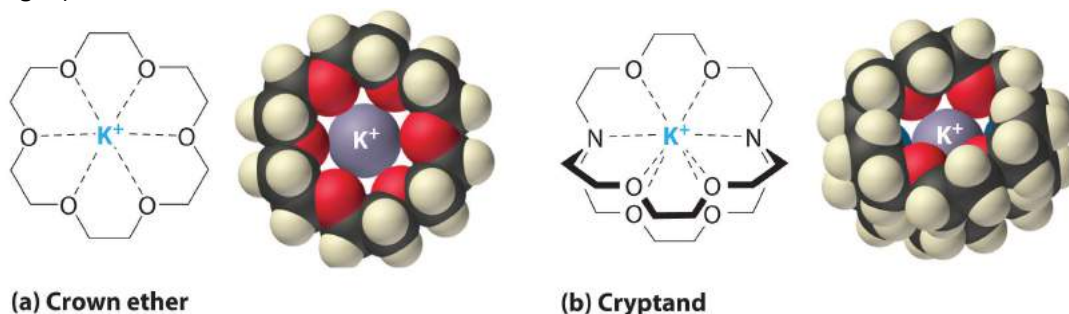
Fig. 4. a) Crown ether 18-C-6 prepared by Pedersen and b) cryptand [2,2,2] prepared by Lehn; both recognize and "imprison" the potassium cation.

Soon, chemists began to realize that metal ions are not only a motif that can be recognized but that can also prearrange, or template different organic fragments. One of the firsts, if not the first example, is a metallocatenane[8, 9] synthesized by Sauvage in 1983. The synthetic strategy was based on the copper(I) having a preference for a tetrahedral geometry and thus coordinating two phenanthroline units, which preorganizes the system. Furthermore the phenylene unit engages in a stacking interaction with the phenanthroline, which further stabilizes the system. After the coordination, the polyether substituents can be installed and the system stays interlocked.
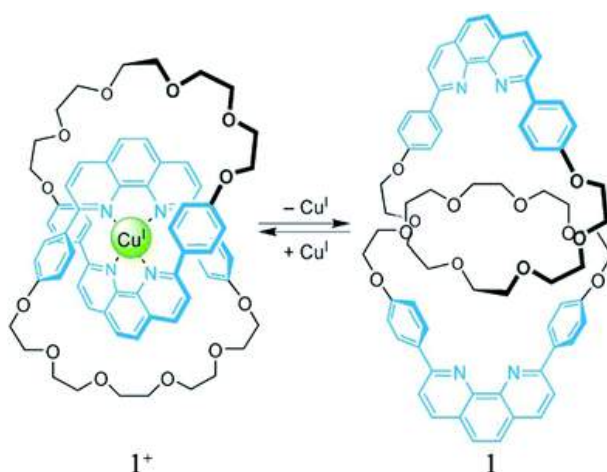
Fig. 5. The first copper-complexed [2]catenane (1^+) and its metal-free form (1) (figure from reference 8).

Obviously, the coordination bond is a very popular choice among the tools of supramolecular chemistry because of its versatility, predetermined geometry, strength and reversibility to some extent. A very beautiful example of the π–stacking being the driving force behind the formation of a supramolecular structure was made by Lehn and is called a foldamer[10] (Fig. 6). A chain containing a succession of hydrazine-pyrimidine units was prepared and allowed to crystallize. Due to the fact that the compound contains bonds around which it can rotate and aromatic moieties that interact between each other via π–stacking the structure folds into a helix. The term folding implicitly means that the molecule does not only assemble but self assemble in an intramolecular manner, since the motifs recognize one another without external influence. This folding is reminiscent to protein folding and DNA folding, even though both use H-bond interactions to do so.
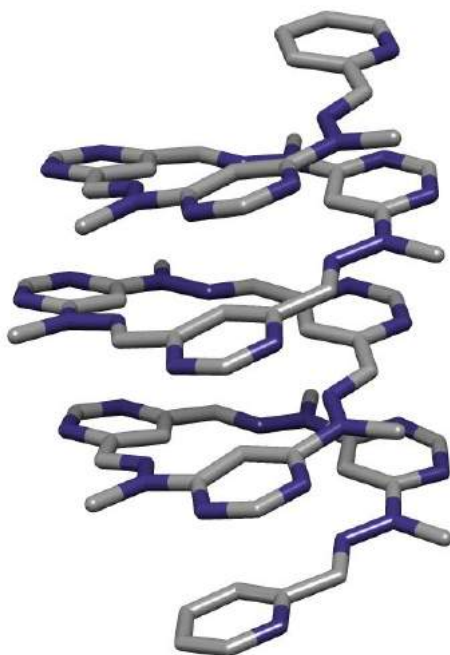
Fig. 6. Intramolecular self-assembly via π–stacking of a foldamer.

1.2 Coordination polymers in crystal engineering

1.2.1 Crystals

A crystal is a solid-state material that is made up from atoms, ions or entire molecules, which are arranged in a highly organized manner. The crystal lattice contains a basic motif that is repeated periodically an "infinite" number of times. Due to the fact that the interactions that hold the constituents together are weak (non-convalent), "a crystal is, in a sense, the supramolecule par excellence" as described by Dunitz[11]. A very popular example for a structure where the components are ions and therefore held together by ionic bonds is the structure of NaCl or table salt. The structure consists of repeating units of Na^+ and Cl^- ions that arrange in a regular cubic pattern as shown in Fig. 7[12]. Repeating of this pattern makes up a NaCl crystal. There is more than one way to visualize and describe the structure but for example the central sodium ion (red) is surrounded by 6 chloride ions (that form an octahedron). Of course, if the diagram would be centered on a chloride ion, it would be surrounded by 6 sodium ions. It can also be said that the chloride ions are located in a cubic array while the smaller sodium ions fill the gaps between them. This basic structure is typical for many other ionic compounds as is commonly called halite or rock-salt crystal structure.
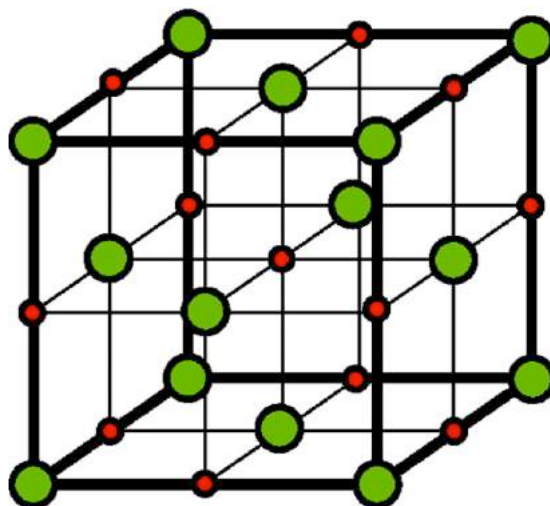
Fig. 7. Schematic representation of the conventional unit cell of the NaCl structure, where the green spheres represent Cl^- and the red spheres represent Na^+ (figure from reference 12).

However, molecules that are not charged cannot associate via ionic bonds and therefore associate via different supramolecular interactions. As previously discussed, many biological molecules and systems bind through H-bonds, which is a very versatile binding mode. Aromatic molecules that do not have hydrogen donors and acceptors associate via different types of π-π stacking. Naphthalene, the simplest fused aromatic molecule is one example and its crystal packing follows a herringbone motif, which is dominated by C-H…π interactions as shown in Fig. 8. Six naphthalene molecules arrange around a central one[13].

6
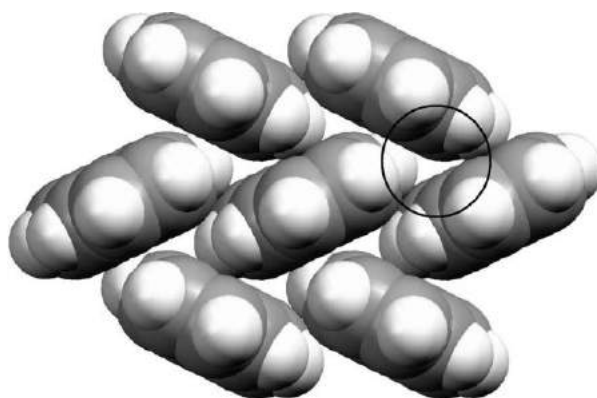
Fig. 8. Space-filling plots for the crystal structure of naphthalene at ambient pressure.

1.2.2 Crystal engineering

Gautam R. Desiraju defined crystal engineering in 1988 as: "the understanding of intermolecular interactions in the context of crystal packing and the utilization of such understanding in the design of new solids with desired physical and chemical properties."[14] Two popular interactions for the formation of crystals are H- and coordination bonds. E. J. Corey, recipient of the Nobel Prize in Chemistry in 1990 introduced retrosynthetic analysis to the art of organic total synthesis[15]. His methodology involves the transformation of the often-complicated target molecule into simpler precursors via idealizes fragments called synthons. Desiraju drew an analogy to Corey's retrosynthetic approach to organic synthesis and introduced the term "supramolecular synthon"[16] in order to describe certain building blocks that have a known geometry and association pattern so that they can be used to engineer novel solid state structures. The difference is that in the organic retrosynthetic analysis the target molecule is well defined (in terms of covalent bond connectivity), whereas in the supramolecular retrosynthetic analysis a topological characteristic and geometrical connectedness (noncovalently bonded) is the target and the exact nature of the molecules is not as important. An example of his methodology can be seen in Fig. 9. The target is the linear ribbon shown at the top of Fig. 9 and the suggested synthon exploits the iodo...nitro interaction formed from two convergent, polarization induced I...O interactions. The suggested solution is either to use 4-iodonitrobenzene or complex 3.
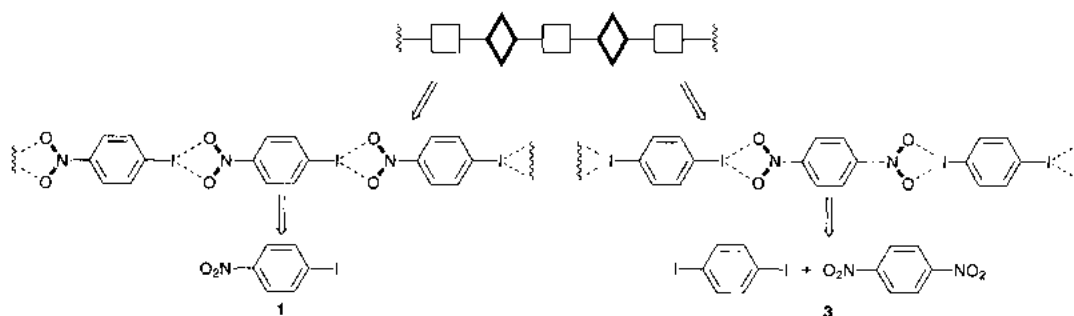
Fig. 9. Retrosynthetic analysis for the linear ribbon pattern leading to 4-iodonitrobenzene (1) or alternatively to complex 3. Supramolecular synthons are shown as heavy lines. Notice the equivalence of these two structures (figure from references 16).

1.2.3 Self-assembly

A central concept in crystal engineering (and in supramolecular chemistry generally speaking) is self-assembly. Contrary to the formation of strong, covalent bonds that necessitate the addition of reactants and often energy in the form of heating, in self-assembly the compounds (disordered in the beginning) adopt a certain organized arrangement without intervention from an outside source. All that this type of assembly requires is the information that the components need to recognize each other to be "encoded" within them. Furthermore, once a covalent bond is formed it is practically irreversible whereas due to the fact that supramolecular interactions are weaker, the bonds can be reversible. This means that if mistakes or imperfections were to happen, the system has the possibility to repair them. Two popular interactions for the formation of crystals are H- and coordination bonds. An example from nature, the association of two DNA strands via H-bonds to form the double helix was previously described and shown in Fig. 2. A synthetic self-assembly example was published by Meijer in 1998[17] and is shown in Fig. 10. The auto-complementary molecule contains an array of H-bond donor (D) and acceptor (A) sites (which has to be an even number).
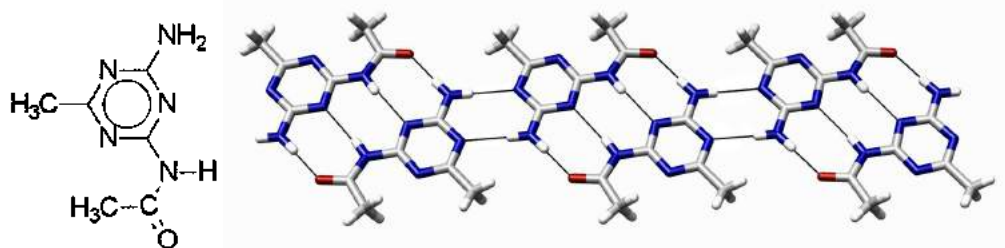
Fig. 10. Chemical structure of the auto-complementary molecule and its PLUTON representation (figure from reference 10).

In this example the molecule features a total of four adjacent H-bonding sites (DADA), which the authors claim were absent from the supramolecular literature until that time. The compound is derived from diaminotriazine and also contains an amido group forming a dimer in the solid state, which is held together by four hydrogen bonds between self-complementary DADA arrays. Furthermore, the dimer forms an infinite chain by a double hydrogen bond of an amino group to one of the triazine-ring nitrogen atoms.

1.2.4 Coordination polymers

By definition, a coordination polymer uses coordination bonds as the connecting interaction and is a hybrid inorganic/organic structure that contains metal cation centers linked by organic ligands. In other words, it is a polymer whose repeating units are coordination complexes. An important way to classify coordination polymers is by dimensionality, which can be 1D, 2D or 3D depending on the number of directions in space the polymer extends in. A 1D-chain structure extends in a straight line (along the x axis for example), a 2D-sheet in a plane (two directions, x and y for example) and a 3D-network into all three directions (x, y and z)[18]. The dimensionality of a given structure depends on the coordination number and preferred coordination geometry of the metal center (node) and on the donor abilities of the ligands (linkers). A nice example published by Shimizu in 2003 shows how the

dimensionality of a coordination polymer can be changed easily by varying the metal only[19]. Ligand L (shown in Fig. 11) was used in all the reactions with different metal cations from group 2 and the dimensionality increased with the metal size from Ca to Sr to Ba.
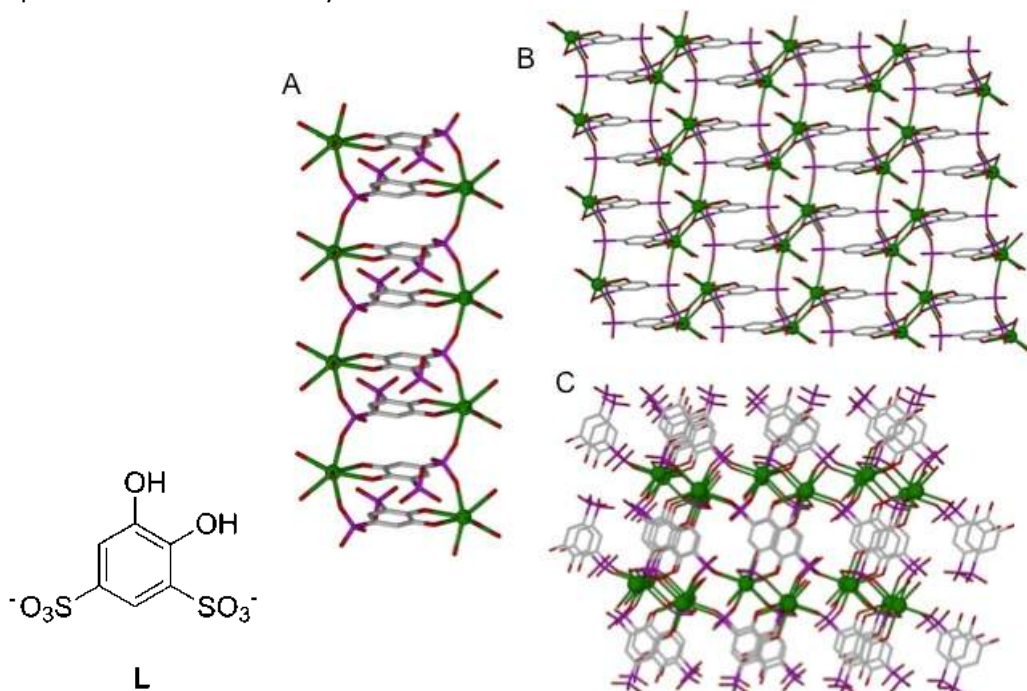
Fig. 11. Coordination polymers A, B and C of different dimensionality made from ligand L and a Group 2 metal. A: [Ca(L)(H$_2$O)$_4$].H$_2$O B: [Sr(L)(H$_2$O)$_4$].H$_2$O C: [Ba(L)(H$_2$O)].H$_2$O. In each case, the metal is represented in green (figure from reference 19).

Of course, coordination polymers in the solid state are prepared by self-assembling co-crystallization of a ligand with a metal salt. The exact methods used to obtain such a crystal are the same ones used to grow any crystal if the solubilities of the two components allow it. If not, the layering system is a very powerful method as each component can be dissolved in a favorable solvent and the constituents meet and crystallize out in the zone in the middle where the solvents diffuse. Alternatively, the hydrothermal method can be used, which consists in the mixture being heated up in an autoclave and cooled down slowly. It is important to obtain a good quality crystal, since X-ray crystallography is the method of choice for analyzing coordination polymers.

1.3 Previous results with 4,2':6',4''-Terpyridine

The 2,2':6',2''-terpyridine ligand is a well established supramolecular motif[20]. It offers a chelating *N,N',N''*-domain which drives it to bind to single metal centers. On the other hand, the 4,2':6',4''-terpyridine offers a diverging *N,N'*-donor set with the nitrogen of the central pyridine ring remaining uncoordinated, which makes it an ideal linker for combination with metal nodes in polymers. The N-donors of the coordinating outer pyridine rings span an angle of 120 °C. Another advantage of this tpy isomer is the functionalization in the 4'-position. The first coordination polymer containing the 4,2':6',4''-terpyridine was reported back in 1998 and by now (as of 2014) over 60 structures of coordination polymers with the same moiety have been published.

1.3.1 Helical structure

In those examples, 4,2':6',4''-terpyridine was reacted typically with Zn(II) halides. Various 4'-substituted tpy ligands formed helical coordination polymers just as in an example published by our own research group where 4'-tBu-4,2':6',4''-tpy was reacted with ZnI_2[21] as can be seen in Fig. 12.
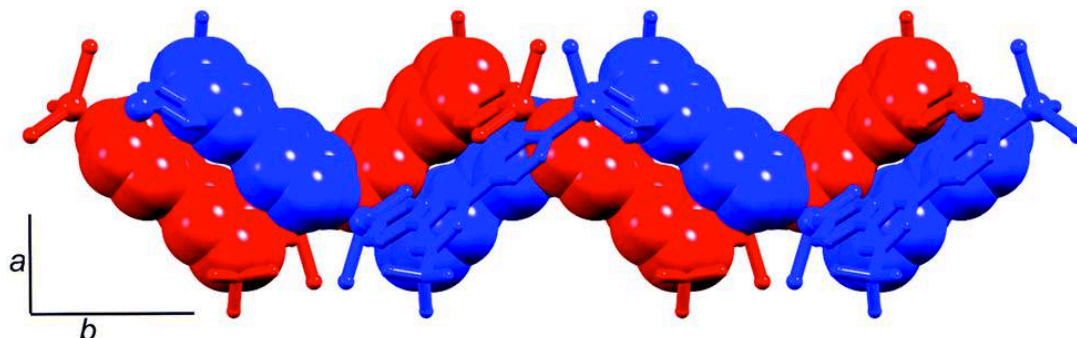
Fig. 12. Interlocking of P- and M-helices in rac-[ZnI_2(4'-tBu-4,2':6',4''-tpy)]n; face-to-face interactions of tpy domains are shown in space-filling representations.

Pyridine rings of tpy domains in adjacent P- and M-helices engage in π–stacking, which leads to interconnection of the chains throughout the lattice.

1.3.2 Metallohexacycle

When 4'-HC≡CC_6H_4-4,2':6',4''-tpy was reacted with $ZnCl_2$, a metallohexacycle was obtained[22] with a chair-like conformation (up/up/up/down/down/down arrangement of ligands. This represented a unique example in the literature at the beginning of this doctoral research project.
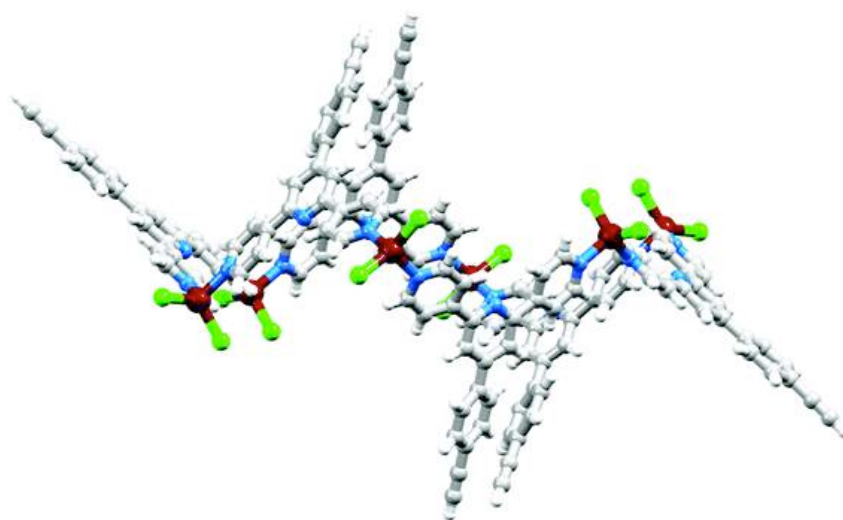
Fig. 13. Chair-like conformation of [{$ZnCl_2$(4'-HC≡CC_6H_4-4,2':6',4''-tpy)}$_6$]

1.3.3 Zig-zag chain

Switching to $Zn(OAc)_2 \cdot 2H_2O$, which was reacted with 4'-(4-BrC_6H_4)-4,2':6',4''-tpy a one-dimensional coordination polymer was obtained[23]. In this case, as shown in Fig. 14, tpy domains of adjacent chains engage in face-to-face π–interactions. The individual chains propagate in a zig-zag manner and nest with one-another to form planar sheets (Fig.14 b) where every 4-bromophenyl group in one chain is accommodated in the V-shaped cavity formed by a tpy unit from the neighboring chain (Fig. 14 a). As can be seen in Fig. 14 a), the cavity is large enough to accommodate larger substituents.

(a)

(b)
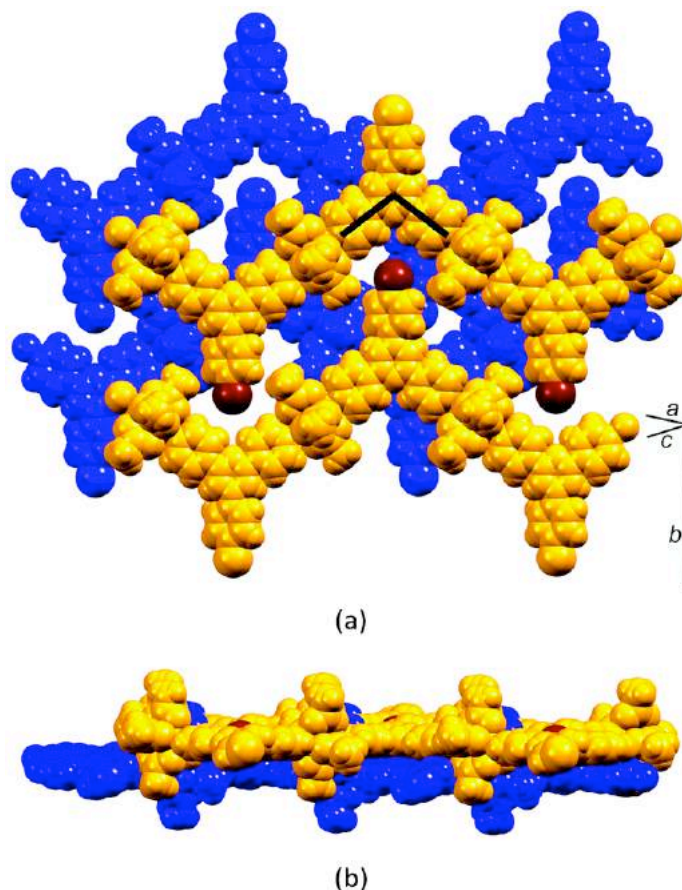
Fig. 14. Packing of zigzag chains in $[Zn_2(\mu\text{-}OAc)_4(4'\text{-}(4\text{-}BrC_6H_4)\text{-}4,2':6',4''\text{-}tpy)]_n$. (a) Zigzag chains nest with one another to give sheets (blue and orange), and tpy domains (one is represented by a ^) in one sheet stack over tpy domains in the next sheet. (b) The sheets are flat.

1.4 This thesis

The goal of this thesis was to design and synthesize new ligands and react them with a number of metals in order to form coordination polymers in the solid state. Initially, we were interested in photoactive polymers. First, a series of mono-4,2':6',4''-terpyridines bearing aryl substituents on the 4' position was prepared. Then, a novel class of back-to-back bis(4,2':6',4''-terpyridine) ligands connected through the 4'-positions via different spacers has been synthesized. Their behavior in the solid state as well as formation of coordination complexes with various metals has been investigated.

1.5 References

1. "Jean-Marie Lehn - Banquet Speech". *Nobelprize.org.* Nobel Media AB 2014. Web. 21 Mar 2015. http://www.nobelprize.org/nobel_prizes/chemistry/laureates/1987/lehn-speech.html

2. http://lcco.u-strasbg.fr/wp-content/uploads/2011/09/Cours-Supramol-copie.pdf

3. http://lcco.u-strasbg.fr/wp-content/uploads/2011/09/Cours-AutoassemblageOctobre2011.pdf

4. E. Fischer, Chem. Ber. 1894, 27, 2985.

5. C. Lee, D. L. Bedgar, L. B. Davin and N. G. Lewis. *Org. Biomol. Chem.*, 2013, 11, 1127.

6. C. J. Pedersen, J. Am. Chem. Soc., 89 (1967), 7017.

7. B. Dietrich, J. M. Lehn and J.-P. Sauvage, Tetrahedron Lett 1969. 2885, 2889.

8. S. Durot, R. Reviriego and J.-P. Sauvage, Dalton Trans., 2010, 39, 10557-10570.

9. C. Dietrich-Buchecker, J.-P. Sauvage and J.-P. Kintzinger, Tetrahedron Lett., 1983, 24, 5095.

10. J.-L. Schmitt, A.-M. Stadler, N. Kyritsakas and J.-M. Lehn, Helv. Chim. Acta, 2003, 86, 5, 1598.

11. J. D. Dunitz, Pure App. Chem., 1991, 63, 177.

12. E. C. M. Vermolen, A. Kuijk, L. C. Filion, M. Hermes, J. H. J. Thijssen, M. Dijkstra and A. van Blaaderen, PNAS, 2009, 106, 16063.

13. F. P. A. Fabbiani, D. R. Allan, S. Parsons and C. R. Pulham, Acta Cryst. 2006, B62, 826.

14. G. R. Desiraju, Crystal Engineering: The design of Organic Solids, Elsevier, 1989, Amsterdam.

15. E.J. Corey, Angew. Chem. Int. Ed. 1991, 30, 455.

16. V. R. Thalladi, B. S. Goud, V. J. Hoy, F. H. Allen, J. A. K. Howard and G. R. Desiraju, Chem. Commun., 1996, 401.

17. F.H. Beijer, H. Kooijman, A. L. Spek, R.P. Sijbesma, and E.W. Meijer, Angew. Chem. Int. Ed., 1998, 37, 75.

18. B.-H. Ye, M.-L. Tong and X.-M. Chen, Coord. Chem. Rev., 2005, 249, 545.

19. A. P.Côté, and G. K. H. Shimizu, Chem. Eur. J., 2003, 9, 5361.

20. E. C. Constable, Chem. Soc. Rev., 2007, 36, 246.

21. E. C. Constable, C. E. Housecroft, P. Kopecky, M. Neuburger, J. A. Zampese and G. Zhang, CrystEngComm, 2012, 14, 446.

22. E. C. Constable, G. Zhang, C. E. Housecroft and J. A. Zampese, CrystEngComm, 2011, 13, 6864.

23. E. C. Constable, G. Zhang, E. Coronado, C. E. Housecroft and M. Neuburger, CrystEngComm, 2010, 12, 2139.

Chapter II: Synthesis and characterization of 4'-substituted mono-4,2':6',4''-terpyridines and back-to-back 4,2':6',4''-terpyridines

2.1. Target first generation ligands

1　　**2**　　**3**

4　　**5**　　**6**
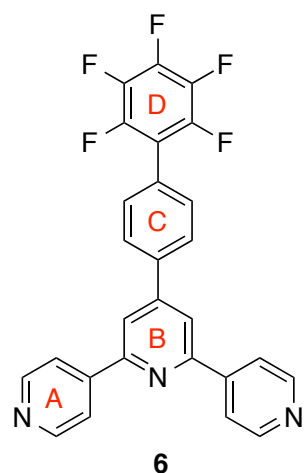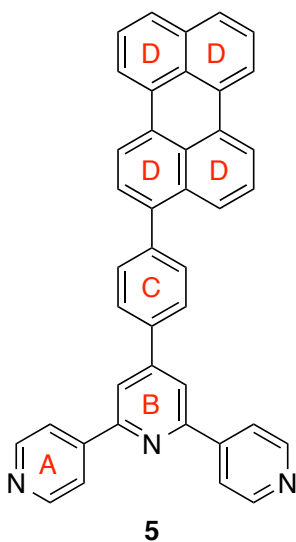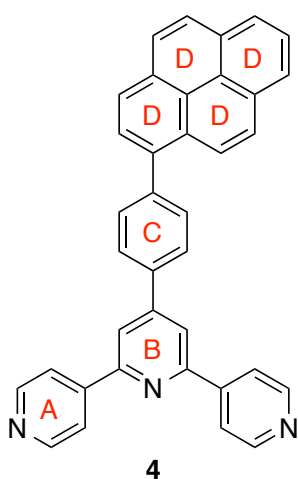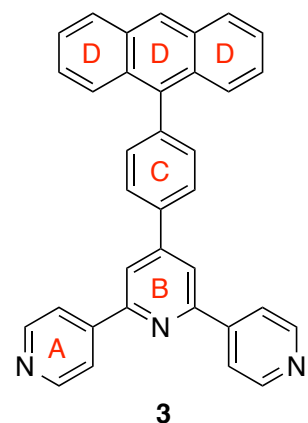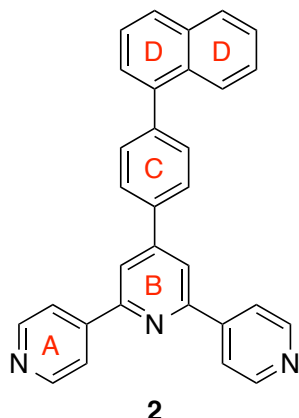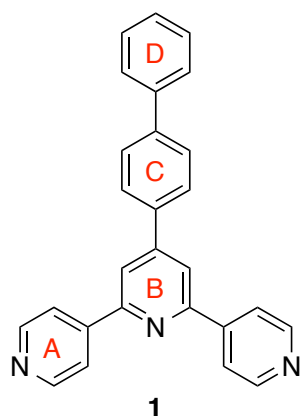
2.1.1 Retrosynthetic plan

X = Br or B(OH)$_2$
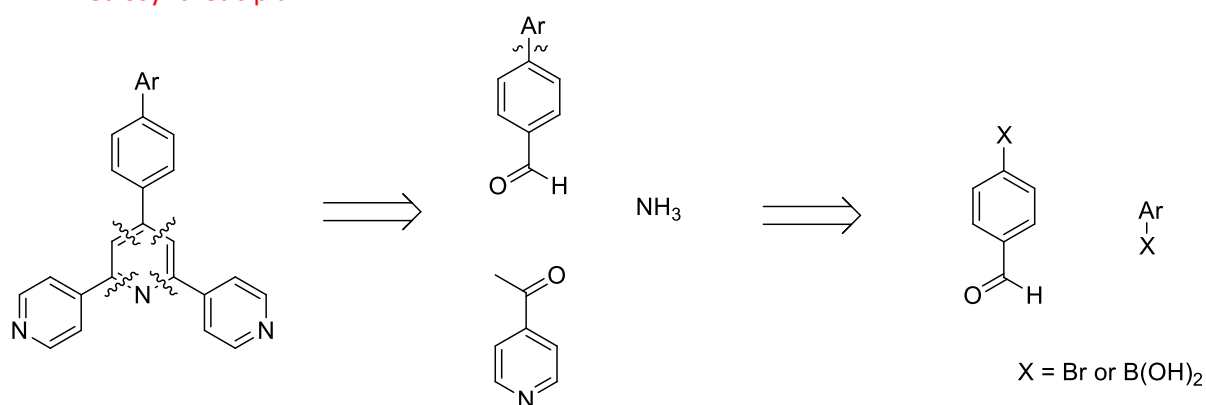
First a four-bond disconnection can be envisioned in order to assemble the middle pyridine ring. This particular ring of the terpyridine fragment can be formed via a one pot reaction between two equivalents of 4-acetylpyridine, the aromatic aldehyde and ammonia that includes four condensation steps[1]. The second disconnection consists of breaking the bond between the aromatic backbone (Ar)

and the phenylene substituent. Such a bond can be formed easily by using the versatile Suzuki-Miyaura cross coupling[2]. Depending on whether the bromide or boronic acid substituted Ar is commercially available, the other coupling partner will bear the complementary substituent.

2.1.2 Synthesis of the Ar backbones

a) Synthesis of the biphenyl and naphthylphenyl substituents

Before the ligands were made using the retrosynthetic procedure outlined before, the idea was to have 4'-(4-bromophenyl)-4,2':6',4''-terpyridine as the common precursor and synthesize the desired ligands via a cross coupling using the corresponding boronic acids (Scheme 1).
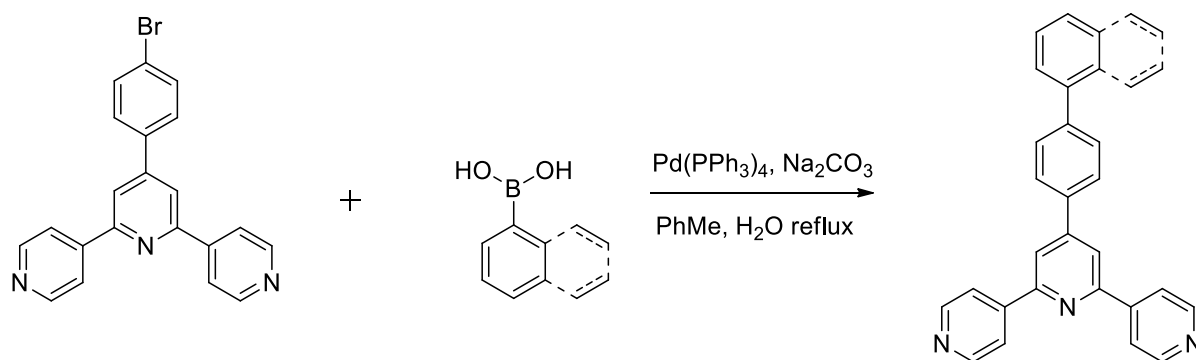
Scheme 1. Synthesis attempt of ligands **1** and **2** from a common tpy precursor.

According to the TLC the desired product seemed to form, as a fluorescent spot was present in both reaction mixtures. The formation of ligand **1** was further confirmed by MALDI mass spectrometry as an ion with an m/z 385.59 corresponding to [M+H]$^+$ was obtained. In both cases the starting material was not completely consumed and the reduction product in respect of the starting halide was obtained. This presented a problem because the side-product could not be separated from the product by TLC and in turn by flash chromatography. This prompted us to rethink the synthetic strategy and have the terpyridine-forming reaction as the final step.
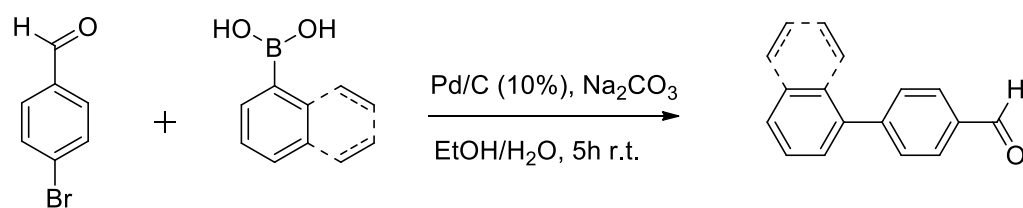
Scheme 2. Suzuki coupling yielding the phenyl- and naphthalene-functionalised aldehydes.

The biphenyl backbone ([1,1'-biphenyl]-4-carbaldehyde) was prepared in 94% yield according to a previously published procedure[3] (Scheme 2) describing the synthesis of the same compound. The naphthyl backbone (4-(naphthalen-1-yl)benzaldehyde) was made via the same procedure and a yield of 84% was obtained. In this particular procedure the metal catalyst is Pd/C which is arguably not the "classical" catalyst for that coupling. Furthermore the reactions have been carried out at room temperature and the product was isolated by simply filtering the reaction mixture over celite. Both products were obtained with a satisfactory level of purity, which allowed them to be used for the next step.

b) Synthesis of the anthracene-functionalized aldehyde

At first, the synthesis of the anthracene backbone was attempted in the same way as for the biphenyl and naphthyl backbones. The reaction shown in Scheme 3 was run at room temperature and then at 100°C over three days but according to the ^{1}H NMR spectrum, the starting halide as well as the anthracene-functionalized aldehyde were recovered.
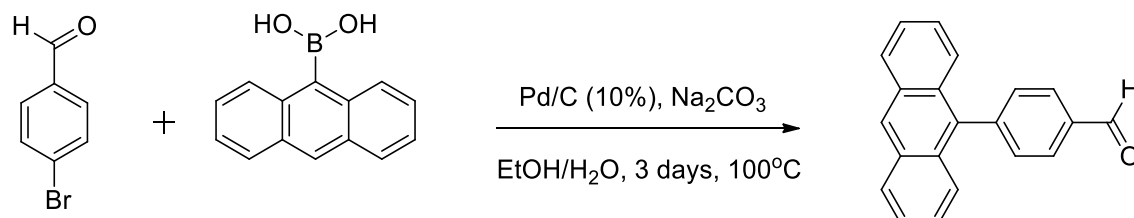
Scheme 3. Synthesis of the anthracene-functionalised aldehyde via a Suzuki coupling with Pd/C.

Next, we tried a reaction with the starting materials roles being inverted, namely 9-bromoanthracene and (4-formylphenyl)boronic acid were used instead of the compounds shown in Scheme 3. This was attempted in a more "classical" fashion as shown in Scheme 4.
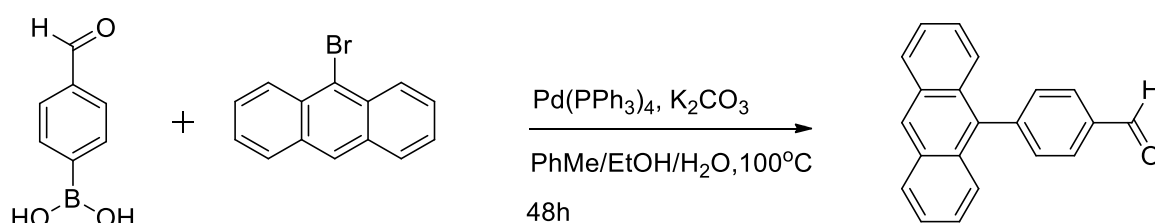
Scheme 4. Synthesis of the anthracene-functionalised aldehyde via a "classical" Suzuki coupling.

The anthracyl backbone 4-(anthracen-9-yl)benzaldehyde was finally obtained in 46% yield which is lower than expected[4]. In an attempt to improve the yield the reaction was performed in the microwave reactor which gave an even lower yield. This method was therefore abandoned.

c) Synthesis of the pyrene-functionalized aldehyde precursor substituent

The coupling of bromo and boronic acid precursors was tried using Pd/C in an EtOH/H$_2$O mixture (Scheme 5) but once more, the starting materials were recovered.
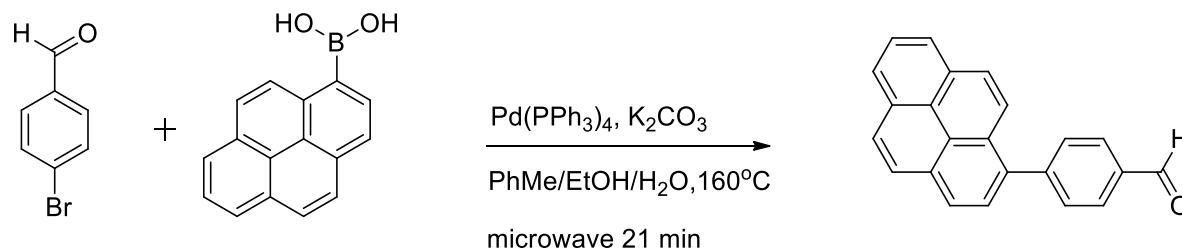
Scheme 5. Synthesis of the pyrene-functionalized aldehyde via a Suzuki coupling.

Using the same conditions as for the anthracene-substituted derivative, substituent 4-bromobenzaldehyde and pyren-1-ylboronic acid were reacted in a microwave reactor for 21 min as shown in Scheme 5. After a flash column, 4-(pyren-1-yl)benzaldehyde was isolated in a yield of 88%. This time, the microwave conditions not only accelerated the reaction but also allowed the use of a lesser amount of solvent needed to solubilize the starting materials.

16

d) Synthesis of the perylene-functionalized aldehyde

Since neither the perylene moiety containing a boronic acid nor the one containing a Br or I was readily available, the precursor for the coupling had to be synthesized as shown in Scheme 6.
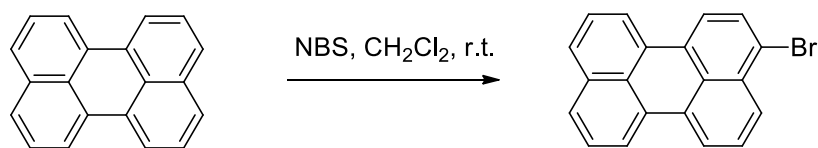
Scheme 6. Bromination of perylene to yield 3-bromoperylene.

Therefore perylene was monobrominated using NBS as the halide source according to a published procedure. It is important that the reaction mixture was quite dilute, that the addition of NBS was performed in a slow manner using an addition funnel and that the reaction was run in absence of light in order to prevent undesired side reactions. In order to ensure complete consumption of the NBS and starting material (monitored by ^{1}H NMR spectroscopy) the reaction was left over the weekend and the 3-bromoperylene was specifically obtained in a 72% yield. The crude material was used for the next step because the starting material and the product have the same Rf so a separation would be only possible after the next step.
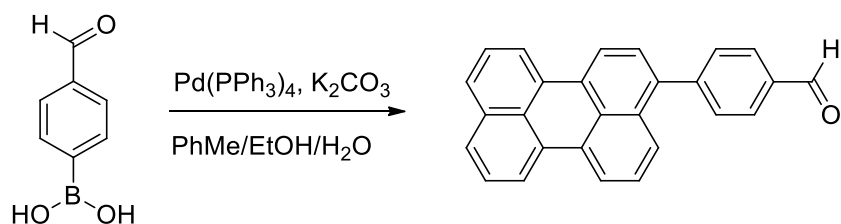
Scheme 7. Synthesis of the perylene-functionalised aldehyde via a Suzuki coupling.

Then, (4-formylphenyl)boronic acid was reacted with 3-bromoperylene under Suzuki conditions (Scheme 7). After an unsuccessful attempt under microwave conditions the reaction was done using a classical reflux setup. Due to the very insoluble starting material, PhMe was added until everything was solubilized. After a flash column, the product 4-(perylen-3-yl)benzaldehyde was obtained in 52% yield.

e) Synthesis of the pentafluorophenyl-functionalized aldehyde

Starting from commercial 1,2,3,4,5-pentafluoro-6-iodobenzene and (4-formylphenyl)boronic acid using Na_2CO_3 instead of K_2CO_3 as described in the previous procedure, 2',3',4',5',6'-pentafluoro-[1,1'-biphenyl]-4-carbaldehyde was obtained (Scheme 8).
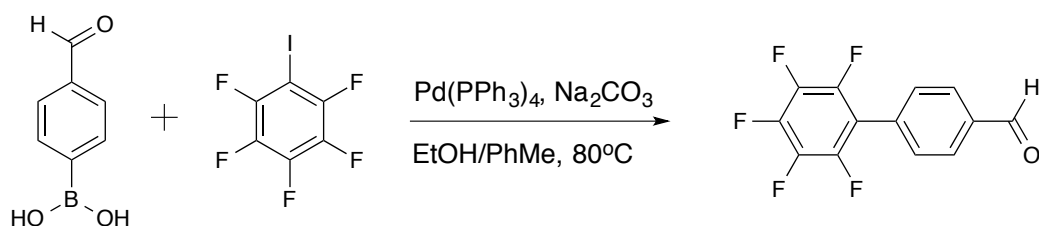
Scheme 8. Suzuki coupling yielding the pentafluorophenyl-functionalised aldehyde.

The starting materials were completely consumed but an impurity (probably triphenylphosphine oxide) was present as well. Due to the fact that no other aldehydes are present, the product was kept for the next step without further purification.

2.1.3 Formation of the 4,2':6',4''- terpyridine (tpy) fragment

The formation of the tpy fragment is the last and common step of the synthesis of each ligand for multiple reasons. As discussed earlier, the simpler the starting material for the Suzuki reaction the better as demonstrated by the fact that the couplings with tpy starting materials's proved to be difficult. The beauty of this reaction is that everything is happening in one pot and that the product precipitates out after completion of the reaction, the advantage being that aldehydes which are not entirely pure can still be used as starting materials for this reaction.
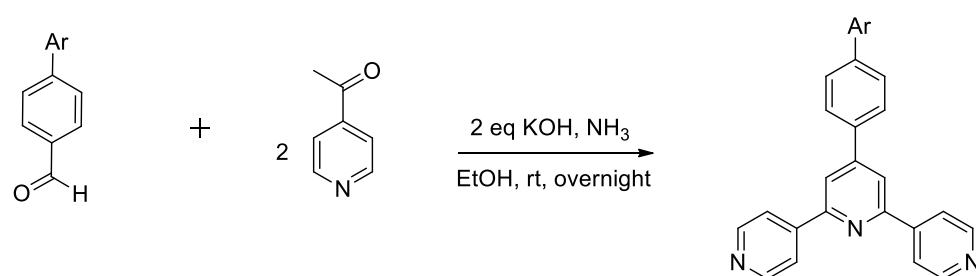
Scheme 9. Common tpy-forming reaction.

The starting aldehyde is mixed with 2 equivalents of 4-acetylpyridine, 2 of KOH and an excess of NH_3 aq in EtOH. For the less soluble starting material, EtOH was added and heated up until the aldehyde was completely dissolved. KOH deprotonates the acetyl substituent in order to form the enolate, which in turn condenses with the aldehyde. Then, a second enolate performs a Michael addition on the condensation product to yield the dibromoketone. Finally NH_3 condenses with the latter two times in order to yield the desired tpy.

Ligand	Yield (%)	Scale
1	54	100 mg
2	49	100 mg
3	30	1 g
4	35	1 g
5	28	400 mg
6	25 (over 2 steps)	1 g

Table 1. Reaction scales and yields for the first-generation ligands.

As far as the yield is concerned, it ranges between 25 and 54%. The scale of the reaction seems to be a factor, as reactions run on a 100 mg scale had a yield around 50% whereas reactions run on a gram scale only had one around 30% (Table 1).

18

2.1.4. Experimental part

Ligand 1

4-Acetylpyridine (116 mg, 0.957 mmol) was added to a solution of biphenyl-4-carbaldehyde (85 mg, 0.47 mmol) in EtOH (2.4 cm^3). Powdered KOH pellets (53 mg, 0.95 mmol) were added in one portion, followed by aqueous NH$_3$ (25%, 2.4 cm^3). The reaction mixture was stirred at room temperature for 20 h, after which a white precipitate had formed. The solid was collected by filtration, washed well with H$_2$O and EtOH, dried in vacuo over P$_2$O$_5$, and recrystallized from EtOH to give **1** as a white solid (92 mg, 0.24 mmol, 51%). M.pt. 230.4 °C. ^{1}H NMR (500 MHz, CDCl$_3$) δ/ppm: 8.80 (d$_{AB}$, J = 6.1 Hz, 4H, H^{A2}), 8.09 (d$_{AB}$, J = 6.2 Hz, 4H, H^{A3}), 8.07 (s, 2H, H^{B3}), 7.83 (m, 2H, H^{C2}), 7.79 (m, 2H, H^{C3}), 7.67 (d$_{AB}$, J = 7.1 Hz, 2H, H^{D2}), 7.50 (m, 2H, H^{D3}), 7.41 (m, 1H, H^{C4}). ^{13}C NMR (500 MHz, CDCl$_3$) δ/ppm: 155.4 (C^{B2}), 150.75 (C^{C4}), 150.7 (C^{A2}), 146.1 (C^{A4}), 142.7 (C^{B4}), 140.1 (C^{D1}) 136.7 (C^{C1}), 129.1 (C^{D3}), 128.15 (C^{C3}), 128.1 (C^{D4}), 127.7 (C^{C2}), 127.2 (C^{D2}), 121.3 (C^{A3}), 118.9 (C^{B3}). IR (solid) v/cm^{-1}: 3030w, 1682w, 1593s, 1556m, 1537m, 1393m, 1315w, 1215w, 1061w, 993m, 820s, 762s, 696s, 600w, 546m. UV–Vis (EtOH, 1.0×10^{-5} mol dm^{-3}) λ/nm 231 (ε/dm^3 mol^{-1} cm^{-1} 33100), 278 (38200), 307 (28100). ESI-MS (MeCN) m/z 386.2 [M+H]$^+$ (calc. 386.2). *Anal*. calc. for C$_{27}$H$_{19}$N$_3$·0.5H$_2$O: C, 82.21; H, 5.11; N, 10.65. Found: C, 82.46; H, 4.96; N, 10.37%.

Ligand 2

4-Acetylpyridine (104 mg, 0.84 mmol) was added to a solution of 4-(naphthalen-1-yl)benzaldehyde (97.3 mg, 0.42 mmol) in EtOH (2.4 cm^3). KOH pellets (47 mg, 0.84 mmol) were added in one portion, followed by aqueous NH$_3$ (25%, 2.4 cm^3). The reaction mixture was stirred at room temperature for 20 h, during which time a white precipitate formed. The solid was collected by filtration, washed well with H$_2$O and EtOH, and dried in vacuo over P$_2$O$_5$. Compound **3** was recrystallized from EtOH and isolated as a white solid (89 mg, 49%). m.pt. = 236.2 °C. ^{1}H NMR (500 MHz, CDCl$_3$) δ/ppm: ^{1}H NMR (500 MHz, CDCl$_3$) δ (ppm) 8.81 (d, J = 6.1 Hz, 4H, H^{A2}), 8.14 (s, 2H, H^{B3}), 8.12 (d, J = 6.1 Hz, 4H, H^{A3}), 7.95 (overlapping d, $J \approx$ 8.4 Hz, 2H, H^{D5+D8}), 7.92 (d, J = 8.2 Hz, 1H, H^{D4}), 7.89 (d, J = 8.2 Hz, 2H, H^{C2}), 7.71 (d, J = 8.2 Hz, 2H, H^{C3}), 7.58 (t, J = 7.4 Hz, 1H, H^{D3}), 7.54 (t, J = 7.4 Hz, 1H, H^{D6}), 7.49 (m, 2H, H^{D2+D7}). ^{13}C NMR (500 MHz, CDCl$_3$) δ/ppm: 155.4 (C^{B2}), 150.9 (C^{B4}), 150.7 (C^{A2}), 146.2 (C^{A4}), 142.4 (C^{B4}), 139.2 (C^{D1}), 136.9 (C^{C1}), 134.0 C$^{D4a/D8a}$), 131.5 (C$^{D4a/D8a}$), 131.2 (C^{C3}), 128.6 (C$^{D4/D8}$), 128.3 (C$^{D4/D8}$), 127.2 (C^{C2}), 127.1 (C$^{D2/D7}$), 126.5 (C$^{D2/D7}$), 126.1 (C^{D6}), 125.7 (C^{D5}), 125.5 (C^{D3}), 121.3 (C^{A3}), 119.0 (C^{B3}). (solid, v, cm^{-1}) 3634 (w), 2361 (w), 2341 (w), 2332 (w), 1684 (w), 1653 (m), 1593 (m), 1558 (s), 1506 (w), 1394 (w), 1315 (w), 1221 (w), 1047 (w), 993 (s), 945 (w), 916 (m), 847 (m), 829 (m), 812 (m), 773 (s), 748 (w), 658 (m), 617 (w), 552 (w). ESI-MS (MeOH/CHCl$_3$) m/z 436.2 [M+H]$^+$. Found: C 81.22, H 4.67, N 9.09; C$_{31}$H$_{21}$N$_3$·H$_2$O requires C 82.10, H 5.11, N 9.27%.

Ligand 3

4-Acetylpyridine (700 mg, 5.66 mmol) was added to a solution of 4-(anthracen-9-yl)benzaldehyde (800 mg, 2.83 mmol) in EtOH (25 cm^3). Powdered KOH pellets (318 mg, 5.66 mmol) were added in one portion, followed by aqueous NH$_3$ (25%, 15 cm^3). The reaction mixture was stirred at room temperature for 20 h, during which time a precipitate formed. The solid was collected by filtration, washed well with H$_2$O and EtOH, and dried in vacuo over P$_2$O$_5$. Compound **2** was recrystallized from EtOH and isolated as a yellow solid (410 mg, 30%). m.pt. = 291.2 °C. ^{1}H NMR (500 MHz, CDCl$_3$) δ/ppm: 8.83 (d, J = 6.1 Hz, 4H, H^{A2}), 8.55 (s, 1H, H^{D10}), 8.21 (s, 2H, H^{B3}), 8.15 (d, J = 6.2 Hz, 4H, H^{A3}), 8.08 (d, J = 8.5 Hz, 2H, H^{D4}), 7.98 (d, J = 8.2 Hz, 2H, H^{C2}), 7.72 (d, J = 9.4 Hz, 2H, H^{D1}), 7.65 (d, J = 8.2 Hz,

2H, H^{C3}), 7.49 (m, 2H, H^{D3}), 7.40 (m, 2H, H^{D2}). ^{13}C NMR (125 MHz, CDCl$_3$) δ (ppm) 155.4 (C^{B2}), 151.0 (C^{B4}), 150.7 (C^{A2}), 146.2 (C^{A4}), 140.7 (C^{C4}), 137.1 (C^{C1}), 135.8 (C^{D9}), 132.4 (C^{C3}), 131.4 ($C^{D4a/D9a}$), 130.2 ($C^{D4a/D9a}$), 128.6 (C^{D4}), 127.4 (C^{C2}), 127.2 (C^{D10}), 126.5 (C^{D1}), 125.8 (C^{D1}), 125.3 (C^{D3}), 121.3 (C^{A3}), 119.1 (C^{B3}). IR (solid, v, cm^{-1}) 3917 (w), 3900 (w), 3032 (w), 2359 (w), 2341 (w), 2330 (w), 1701 (w), 1684 (w), 1653 (w), 1593 (m), 1533 (w), 1516 (w), 1387 (w), 1113 (w), 1061 (w), 993 (m), 949 (w), 910 (w), 878 (w), 829 (m), 818 (s), 785 (w), 727 (m), 669 (w), 652 (w), 631 (m), 609 (m), 550 (w), 519 (m), 511 (w). ESI-MS (MeOH/CHCl$_3$) m/z 486.2 [M+H]$^+$. Found: C 80.99, H 4.61, N 8.17; $C_{35}H_{23}N_3\cdot 2H_2O$ requires C 80.59, H 5.22; N 8.06%.

Ligand 4

Synthesis of 4-(pyren-1-yl)benzenealdehyde with improved yield: 4-bromobenzaldehyde (648 mg, 3.5 mmol), pyren-1-ylboronic acid (1034 mg, 4.2 mmol) and K$_2$CO$_3$ (1510 mg, 10.9 mmol) were inserted into a microwave vial containing a PhME/EtOH/H$_2$O (6/1.3/2.7 mL) solvent mixture. The mixture was degassed with N$_2$ for about 1h and then tetrakis(triphenylphosphine)palladium (30 mg, 0.026 mmol) was added under a positive stream of gas. The mixture was heated for 21 min in the microwave. After the solution cooled down it was worked up with PhMe and brine then purified by column chromatography (cyclohexane/ethyl acetate 5%). The product was isolated as a brown solid (940 mg, 88%).

Synthesis of 4'-(4-(pyren-1-yl)phenyl)-4,2':6',4''-terpyridine: 4-Acetylpyridine (759 mg, 6.14 mmol) was added to a solution of 4-(pyren-1-yl)benzenealdehyde (940 mg, 3.07 mmol) in EtOH (250 cm^3). KOH pellets (345 mg, 3.07 mmol) were added in one portion, followed by aqueous NH$_3$ (25%, 15 cm^3). The reaction mixture was stirred at room temperature for 20 h, during which time a orange precipitate formed. The solid was collected by filtration, washed well with H$_2$O and EtOH, and dried in vacuo over P$_2$O$_5$ (540 mg, 35%). ^{1}H NMR (500 MHz, CDCl$_3$) d (ppm) 8.80 (d, J = 6.1 Hz, 4H, H^{A2}), 8.09 (d, J = 6.2 Hz, 4H, H^{A3}), 8.07(s, 2H, H^{B3}), 7.83 (d, J = 8.5 Hz, 2H, H^{C2}), 7.79 (d, J = 8.6 Hz, 2H, H^{C3}), 7.67 (d, J = 7.1 Hz, 2H, H^{D2}), 7.50 (t, J = 7.6 Hz, 2H, H^{D3}), 7.41 (t, J = 7.4 Hz, 1H, H^{C4}). ^{13}C NMR (500 MHz, CDCl$_3$) d (ppm) 155.4 C^{B2}, 150.7 C^{B4}, 150.7 C^{A2}, 146.1 C^{A4}, 142.7 C^{C4}, 140.1 C^{D1}, 136.7 C^{C1}, 129.1 C^{D3}, 128.13 C^{C3}, 128.08 C^{D4}, 127.7 C^{C2}, 127.2 C^{D2}, 121.3 C^{A3}, 118.9 C^{B3}. IR (neat): v = 3973 (w), 3948 (w), 3904 (w), 3854 (w), 3628 (w), 3032 (w), 2920 (w), 2359 (w), 2341 (w), 2330 (w), 1684 (w), 1653 (m), 1591 (m), 1555 (m), 1522 (m), 1456 (w), 1394 (w), 1213 (w), 1196 (w), 1113 (w), 1059 (w), 991 (m), 966 (m), 951 (m), 908 (m), 833 (s), 818 (s), 760 (w), 746 (w), 719 (m), 719 (m), 669 (w), 648 (m), 629 (m), 606 (w), 567 (w), 552 (w), 519 (m) cm-1. ESI-MS (MeCN) m/z 510.4 [M + H]$^+$ m.p. 310.2^{o}C.

Ligand 5

Synthesis of 4'-(4-(perylen-3-yl)phenyl)-4,2':6',4''-terpyridine : 4-Acetylpyridine (277 mg, 2.24 mmol) was added to a solution of 3-(4-Formylphenyl)perylene (400 mg, 1.12 mmol) in EtOH (250 cm^3). Ground KOH pellets (126 mg, 2.24 mmol) were added in one portion, followed by aqueous NH$_3$ (25%, 5.61 cm^3). The reaction mixture was stirred at room temperature for 20 h, during which time an brown precipitate formed. The solid was collected by filtration, washed well with H$_2$O and EtOH, and dried in vacuo over P$_2$O$_5$ (177 mg, 28.2%). ^{1}H NMR (500 MHz, CDCl$_3$) d (ppm) 8.83 (d, J = 6.1 Hz, 4H, H^{A2}), 8.26 (m, 4H, $H^{D1/6/7/12}$), 8.16 (s, 2H, H^{B3}), 8.15 (d, J = 6.2 Hz, 4H, H^{A3}), 7.91 (d, J = 8.5 Hz, 2H, H^{C2}), 7.81 (d, J=, 1H, H^{D4}), 7.75 (d, J = 8.6 Hz, 2H, H^{C3}), 7.72 (?, 2H, $H^{D9/10}$), 7.50 (m, 4H, $H^{D2/5/8/11}$). ^{13}C NMR (500 MHz, CDCl$_3$) d (ppm) 155.2 C^{B2}, 150.7 C^{B4}, 150.5 C^{A2}, 146.2 C^{A4}, 142.3 C^{C4}, 138.52 C^{D3}, 136.8 C^{C1}, 129.1 C^{D3}, 131.0 C^{C3}, 128 $C^{D9/10}$, 127.7 C^{C2}, 126.7 C^{D2}, 125.7 C^{D4} 121.3 C^{A3}, 120.5 Cd 120.1 C^{D1}, 119.0 C^{B3}. IR (neat): v = 3973 (w), 3942 (w), 3917 (w), 3734 (w), 3599 (w), 3036 (w), 2922 (w), 2359 (w), 20

2341 (w), 1684 (w), 1653 (m), 1591 (w), 1556 (m), 1506 (w), 1456 (w), 1387 (w), 1211 (w), 1196 (w), 1113 (w), 1059 (w), 991 (m), 949 (w), 908 (w), 833 (m), 818 (s), 760 (w), 746 (w), 719 (w), 719 (w), 669 (w), 648 (w), 629 (m), 606 (w), 575 (w), 567 (w) cm-1.ESI-MS (MeCN) m/z 560.4 [M + H]$^+$ m.p. decomposes over 320°C. Found C 54.88, H 4.24, N 5.53 %; $C_{35}H_{31}N_3O_8Zn_2$ + 1/5 MeOH requires C 55.49, H 4.33, N 5.47%.

Ligand 6

4-Acetylpyridine (1.7 g, 13.7 mmol) was added to a solution of 2',3',4',5',6'-pentafluorobiphenyl-4-carbaldehyde (1.87 g, 6.87 mmol) in EtOH (25 cm^3). KOH pellets (0.77 g, 13.7 mmol) were added in one portion, followed by aqueous NH$_3$ (25%, 25 cm^3). The reaction mixture was stirred at room temperature for 20 h, during which time a white precipitate formed. This solid was collected by filtration, washed well with H$_2$O and EtOH, and dried *in vacuo* over P$_2$O$_5$. Compound 2 was recrystallized from EtOH and was isolated as a white solid (0.733 g, 22.5%). Decomp. > 290 °C. ^{1}H NMR (500 MHz, CDCl$_3$) δ/ppm: 8.82 (d, J = 6.1 Hz, 4H, H^{A2}), 8.10 (d, J = 6.2 Hz, 4H, H^{A3}), 8.09 (s, 2H, H^{B3}), 7.89 (d, J = 8.5 Hz, 2H, H^{C2}), 7.5 (d, J = 8.6 Hz, 2H, H^{C3}). ^{13}C NMR (126 MHz, CDCl$_3$) δ/ppm: 155.6 (C^{B2}), 150.7 (C^{A2}), 150.4 (C^{B4}), 146.0 (C^{A4}), 139.1 (C^{C1}), 131.3 (C^{C3}), 127.7 (C^{C2+C4}), 121.3 (C^{A3}), 119.1 (C^{B3}), 114.9 (C^{D1}), signals for C^{D2,D3,D4} not resolved. ^{19}F NMR (376 MHz, CDCl$_3$) δ/ppm: −143.0 (m, 2F, F$^{D2/D3}$), −154.3 (m, 1F, F^{D4}), −161.5 (m, 2F, F$^{D2/D3}$). IR (solid, v/cm$^{−1}$): 3035 (w), 1705 (w), 1595 (s), 1513 (m), 1480 (s), 1393 (m), 1318 (w), 1276 (w), 1217 (w), 1194 (w), 1132 (w), 1090 (w), 1061 (m), 1042 (w), 985 (s), 897 (w), 859 (m), 852 (m), 827 (s), 814 (m), 780 (m), 749 (w), 737 (m), 718 (w), 680 (s), 621 (s). UV-vis (EtOH, 2.5 × 10$^{−4}$ mol dm$^{−3}$) λ/nm: 225 (ε/dm^3 mol$^{−1}$ cm$^{−1}$: 26 500), 268 (43 100). ESI MS (MeCN) m/z 476.1 [M + H]$^+$ (calc. 476.1). Found: C 67.52, H 3.26, N 8.55; $C_{27}H_{14}F_5N_3$ requires C 68.21, H 2.97, N 8.84%.

2.1.5. Absorption and emission properties

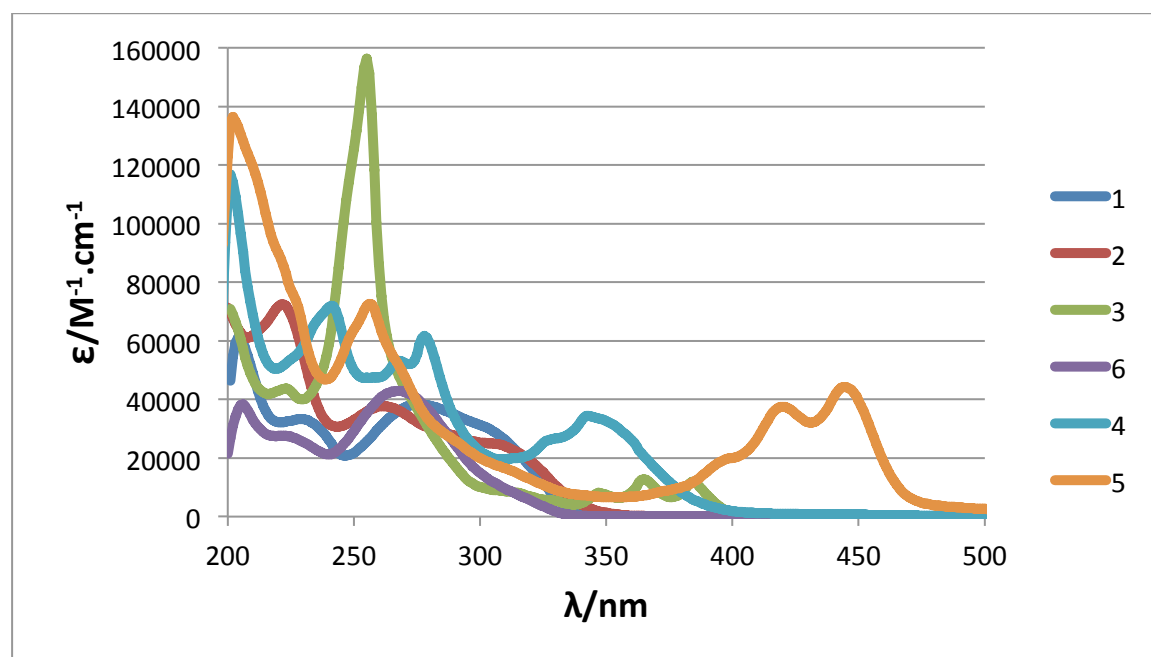
Fig. 1. Absorption spectra of EtOH solutions of all first generation ligands 1-6.

All the electronic absorption spectra were recorded in EtOH and the ligand absorbances were converted into the respective extinction coefficients. Ligand 1 displays broad bands at 231, 278 and

307 nm originating from π'⟵π transitions. A blue shift from 278 to 268 nm is observed when the terminal phenyl ring is replaced by a pentafluorophenyl one (ligand **6**). By switching to a fused substituent namely a naphthyl group (ligand **2**) the two bands at 260 and 300 nm are clearly visible. Adding a further phenyl group to the fused moiety gives the anthracene substituent (ligand **3**) whose characteristic absorptions between 350 and 400 nm are lower in energy, which is consistent with the extension of the π system. Compared to the naphthalene substituent the pyrene (ligand **4**), which is a peri-fused aromatic compound, follows the same trend and shows absorptions at 321 and 338 nm. Finally, ligand **5** has the largest and most delocalized aromatic part and is therefore the most shifted as it absorbs at 391, 414 and 441 nm. The UV-VIS spectrum shows two regions, the UV one mainly contains the absorptions of the tpy domain whereas the VIS part contains the lower energy transitions of some of the substituents. Before 300 nm the absorption of the terpyridine part overlaps with the one of the substituent, which is not the case for ligands **3**, **4** and **5** that have a larger, and more delocalized aromatic part. The red-shifting trend is consistent with the structure. A more extended π conjugation generates more π-molecular orbitals which results in more possible transitions and a vibrational structure becomes visible.

Excitation of the ligands **1**-**6** (in EtOH solution) at λ_{ex} = 304, 305, 384, 342, 444 and 281 nm respectively resulted in the emission maxima shown in Table 2.

Ligand	λ_{em} (nm)
1	385
2	440
3	480
4	474
5	467/488
6	353

Table 2. Emission maxima in EtOH for first-generation ligands **1**-**6**.

Generally due to very fast deactivation processes, which concerns the excited states, all the emission spectra are characterized by a unique band due to the S1 to S0 transition, which is centered on the substituent. For polycyclic aromatic compounds it also possible to have an intersystem crossing to the T1 state which results in phosphorescence[5]. This phenomenon is likely at 77 K, but at room temperature it is negligible and in fact such emission was not detected. The presence of a phenyl ring between the two units allows electronic communication. In fact it is normal to see the emission of the polycyclic unit upon its excitation and we were able to see it by exciting the tpy domain, for intramolecular energy transfer reasons. As for the UV-VIS spectrum the expected red-shift trend is seen here as well. Even though polycyclic aromatic compounds show an emission, which is the mirror image of the lower energy absorption, unfortunately due to the low emitting character the slits were opened to such an extent that the vibrational structure is lost.

2.1.6. Crystal structures

Ligand **1**: polymorph 1

Single crystals of ligand **1** were obtained using the slow evaporation technique on a two solvent system. First, the ligand was dissolved in $CHCl_3$, which is the good solvent for the compound and then about 25% of MeOH was added and the solution was mixed. The idea is that $CHCl_3$ is more volatile than MeOH and as it evaporates the percentage of MeOH increases and the solubility drops. Using

just CHCl$_3$ was tried as well, but the solubility being too high, no single crystals were obtained. Ligand **1** crystallizes in the space group P2$_1$/c, which is monoclinic. It is very interesting that the unit cell contains five independent molecules as can be seen in Fig. 2. Steed has pointed out that structures with Z'>4 are extremely rare[6] and in 2008, Bond reported that there were only seven examples of structures with Z' = 5 in monoclinic space groups, representing 0.007% of all structures in this crystal system[7].
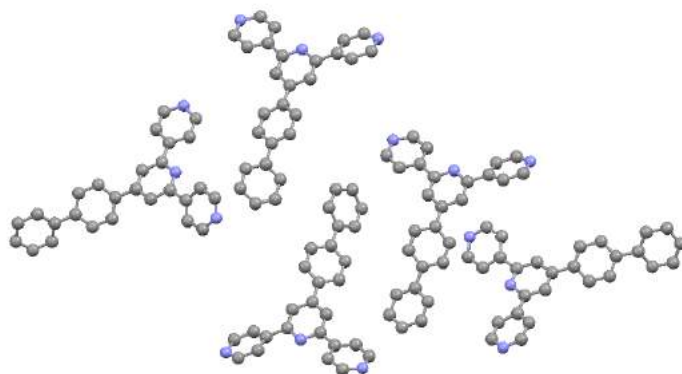
Fig. 2. Contents of the asymmetric unit in crystal structure of **1**.

One of those molecules is shown in Fig. 3. As expected for such a polyaromatic system the bond lengths and angles are unremarkable but due to the fact that there are five independent molecules there is a divergence in the relative orientation of the aromatic rings and therefore a difference in conformation for each molecule. The crystal packing includes face-to-face π-stacking and CH…N interactions. There is an interaction between neighboring tpy domains but because of the different twisting of the biphenyl moiety complete stacking of two molecules is impossible.
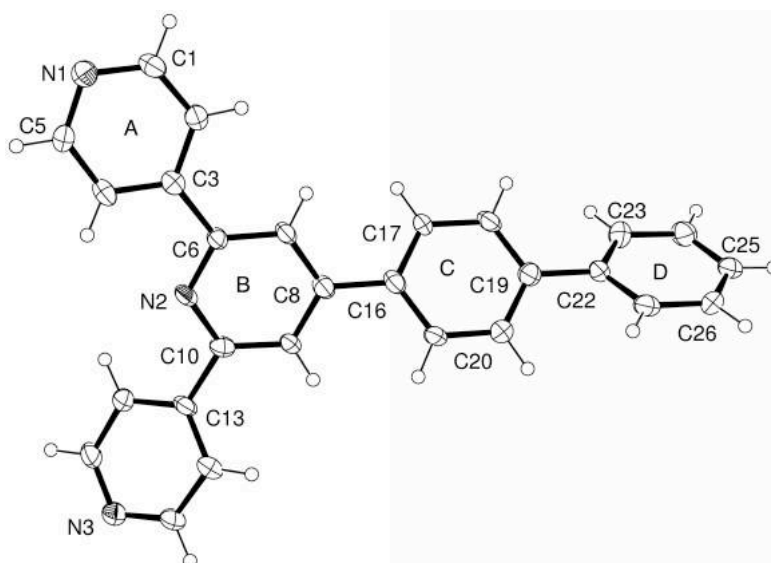
Fig. 3. Structure of one of the five independent molecules of **1**. Ellipsoids plotted at 40% probability level.

Alternatively, stacking between a pyridine ring with a central phenyl ring, without stacking with the terminal phenyl ring, of the bordering molecule is also observed. Lastly, the whole central part of the molecule can interact with a tpy domain.

Ligand 1: polymorph 2

While a reaction between ligand 1 and a Zn(II) halide was performed (to be discussed in more detail in one of the next chapters) more than one type of crystal was obtained. One of them turned out to be the desired coordination polymer whereas the other crystal was a second polymorph of ligand 1. In this case the compound crystallizes in the space group P-1 and there are three molecules in the asymmetric unit (Fig. 4).
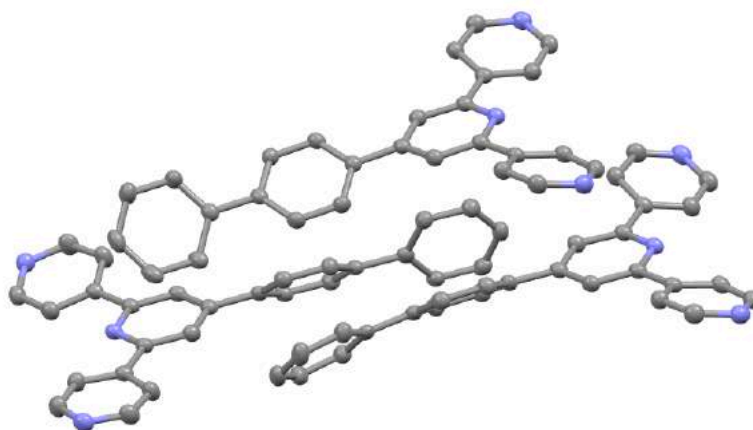
Fig. 4. Contents of the asymmetric unit in polymorph 2 of the crystal structure of 1.

There is significant twisting between the rings in all of the three molecules. All the values are compared in table 3 below (ring labels as in Fig. 3). Generally the angle is bigger in the biphenylene part (D-C, C-B) then in the tpy part (B-A1, B-A2), which is the flattest part of the molecules.

| Angle (^{o}) | D-C | C-B | B-A1 | B-A2 |
Molecule				
Molecule 1	35	25	20	18
Molecule 2	35	40	12	3
Molecule 3	10	34	21	18

Table 3. Interplane angles in the three independent molecules of 1. For ring labels, see 2.1.

Looking down the a-axis (Fig. 5.), it is evident that the biphenyl parts are facing each other and interdigitate. Rings C and D engage in edge-to-face π–stacking with a CH…centroid distance of 3.33 Å. On the other end of the molecule the tpy fragments engage in CH…N interactions without interpenetrating each other.
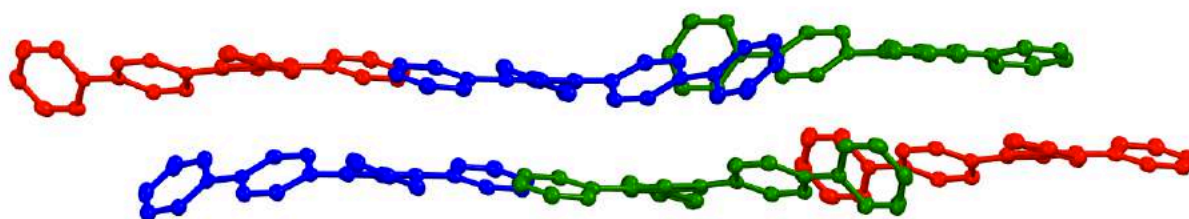
Fig. 5. View down the a-axis.

Those interactions lead to the formation of sheets that come on top of one another (Fig. 6). They are held together between face-to-face π–stacking of A rings of the tpy's (seen in the figure when looking at the molecules in blue, interplane distance 3.18 Å). Finally, there are also some edge-to-face π–interactions, mainly between the D ring of the phenylene part and the B ring of the tpy part (molecules in green for example CH..centroid distance 3.09 Å).
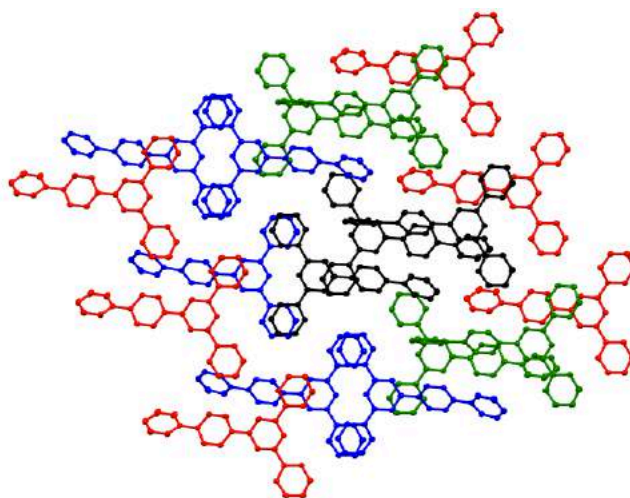
Fig. 6. Face-to-face π–stacking of tpy units between adjacent sheets.

Ligand 6

Ligand **6** is nicely soluble in $CHCl_3$ and an almost saturated solution was prepared, put in a thin vial and hexane was carefully layered over it in order to grow single crystals. The compound crystallizes in a monoclinic space group as well, namely Cc. The structure, shown in Fig. 7 is much like the one of the phenyl ligand does not have bond lengths and angles worth discussing in detail. Almost the whole molecule, except for the ring containing atom C16 (Fig. 7), lies in one plane. This particular ring being bent (34.9° with respect to the tpy part and 32.5° with respect to the pentafluorophenyl ring) allows the minimization of steric hindrance between the H and F atoms located on the *ortho* posi-
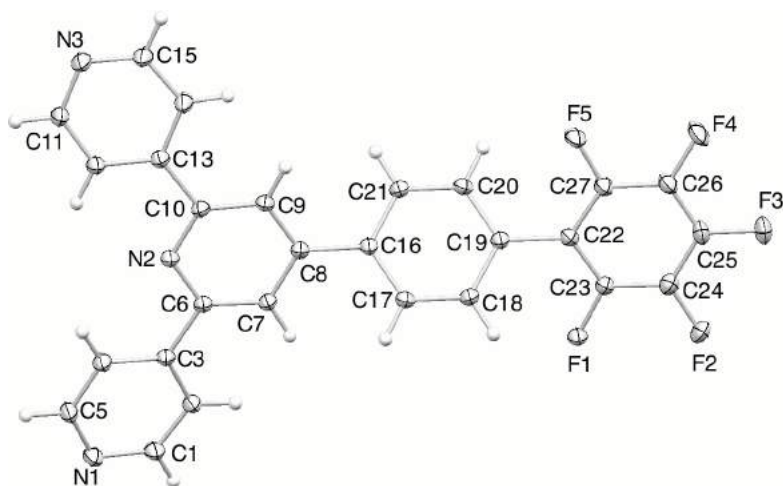
Fig. 7. ORTEP diagram of the structure of **6** with ellipsoids plotted at the 40% probability level.

tions of adjacent rings. Contrary to the biphen ligand where due to the differences in conformation between the different molecules a simple packing description is impossible, in this case slipped π_H(py)...π_F (centroid-centroid distances 4.24 and 3.88 Å) contacts between the molecules produce chains, which are parallel to the c-axis (Fig. 8).
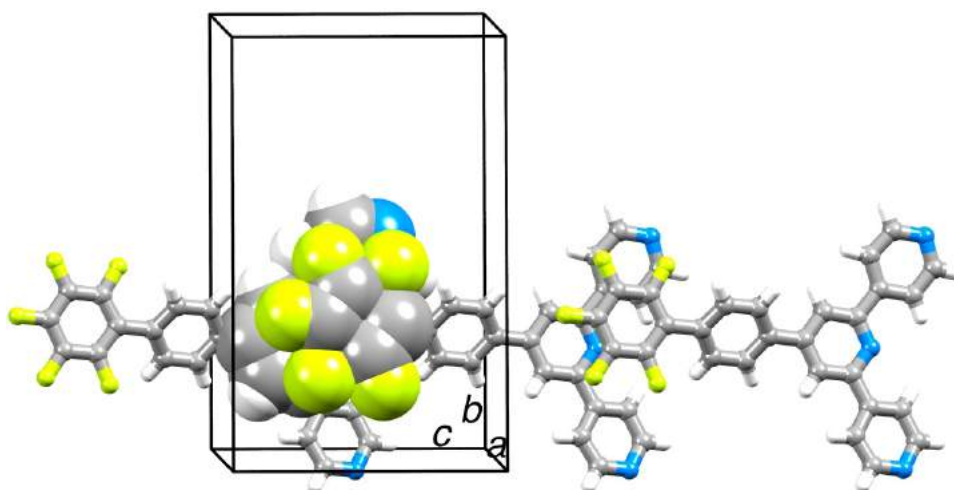
Fig. 8. Packing interactions in **6**: chains following the c-axis with slipped intermolecular π_H(py)...π_F contacts.

The pentafluorophenyl part stacks either with the tpy domain or with the phenylene one of a neighboring molecule and the two latter ones also interact between themselves. Fig. 9 illustrates those packing modes between adjacent chains where the π_H(py)...π_H(arene), π_H(py)...π_F and π_H(arene)...π_F contacs (which considering centroid distances of 4.21 and 4.63 Å are quite inefficient) take place. Finally CH...N and CH...F contacts further contribute to the packing by connecting the molecules within a sheet together.

Initially, the idea behind the design of ligand **6** (which has an electron poor π–system in the terminal ring) was for it to be complementary in the solid state to the biphen one, that has a rather electron rich one. Therefore, the co-crystallisation of those two was explored by dissolving a 1:1 mixture in CH$_2$Cl$_2$/MeOH and then carefully layering with hexane. Single crystals were grown successfully but unfortunately the unit cell dimensions either corresponded to the structure of pure ligand **1** of **6**

26

previously obtained. Maybe, replacing the middle phenylene ring by a tetrafluorophenylene would have increased the interaction as thus the complementarity of the two fragments. Nevertheless, the cocrystallisation between the two in the presence of a metal was also tested and will be discussed in one of the next chapters.
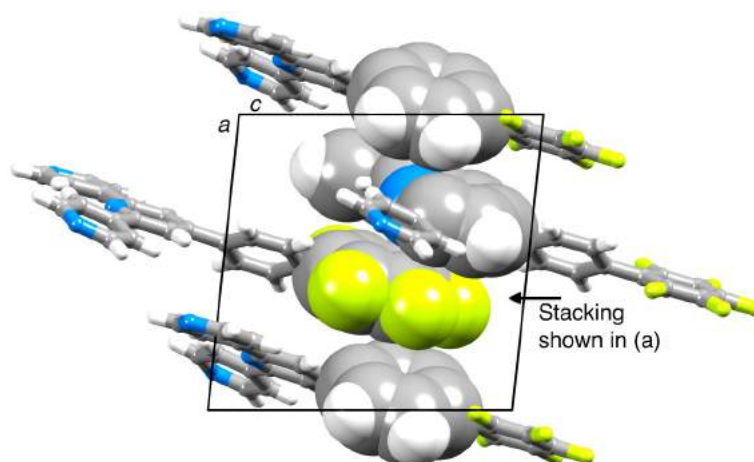
Fig. 9. Packing interactions in **6**: relatively inefficient π–stacking (space filling representation) along the a-axis.

Ligand **3**

A CH_2Cl_2/MeOH solution of the anthracene ligand was subjected to slow evaporation, which yielded single crystals. The space group P-1, that this compound crystallizes in, is centrosymmetric and three independent molecules are found in the asymmetric unit (Z'=3). One of those three molecules is represented in Fig. 10. Again the bond lengths and angles are ordinary and what differentiates the three molecules from one another are the angles between the three rings of the tpy part. The difference in angles between the middle pyr ring and the phenylene spacer is less significant and the difference between the latter one and the anthracene substituent is smallest.
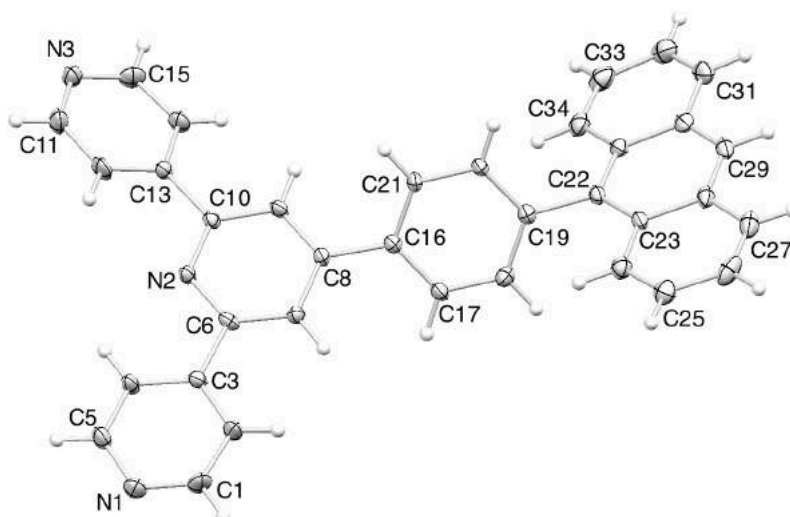
Fig. 10. Structure of one of the three independent molecules of 3 in the asymmetric unit (ellipsoids plotted at 40% probability level).

This is confirmed by the fact that the 4-(anthracen-9-yl)phenyl moieties of adjacent molecules stack together via edge-to-face CH…π interactions as can be seen in Fig. 11 (CH..centroid distance is 2.82 Å). One such block on molecules interacts with the next one through face-to-face π-stacking of anthracene fragments with an interplane distance of 3.53 Å. In the crystal packing CH…N contacts, which connect neighboring tpy groups are also present.
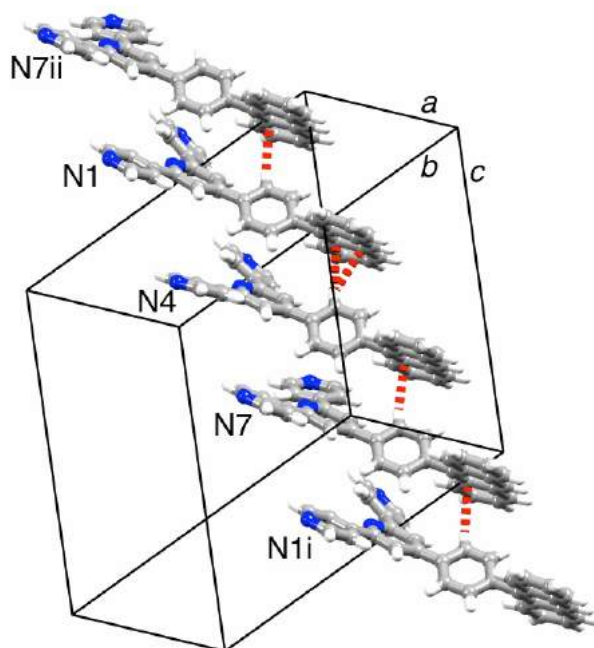
Fig. 11. Edge-to-face CH…π interactions between independent molecules and symmetry generated analogs (symmetry codes: i = -1 + x, y, 1 + z; ii = 1 + x, y, -1 + z).

Crystal structure of the pyrene-functionalized aldehyde precursor substituent

Single crystals suitable for X-ray crystallography were grown by leaving a big vial containing a pure fraction of the product (obtained from flash column chromatography) to slowly evaporate overnight. The compound crystallizes in the space group P-1, with one molecule in the asymmetric unit whose structure is shown in Fig. 12. The pyrene moiety is almost planar and the benzaldehyde fragment is twisted 61.92^{o} with respect to that plane.
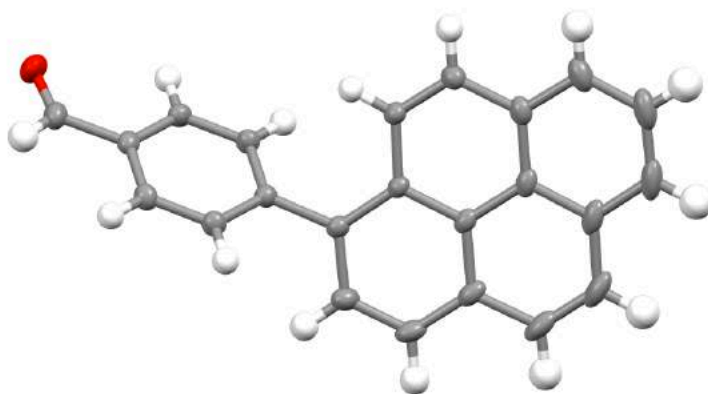
Fig. 12. Contents of the asymmetric unit of the crystal structure of the pyrene-functionalized aldehyde substituent.

28

The pyrene part of a particular molecule (in blue see Fig. 13.) engages in edge-to-face stacking with the phenylene part of a molecule (CH…centroid distance 2.87 Å) located above and in face-to-face stacking with the perylene part (plane-plane distance 3,43 Å) from a molecule from below. Its phenylene part interacts in edge-to-face stacking with the pyrene part from another molecule from below. Finally CH…O interactions with another two molecules round up the packing mode.
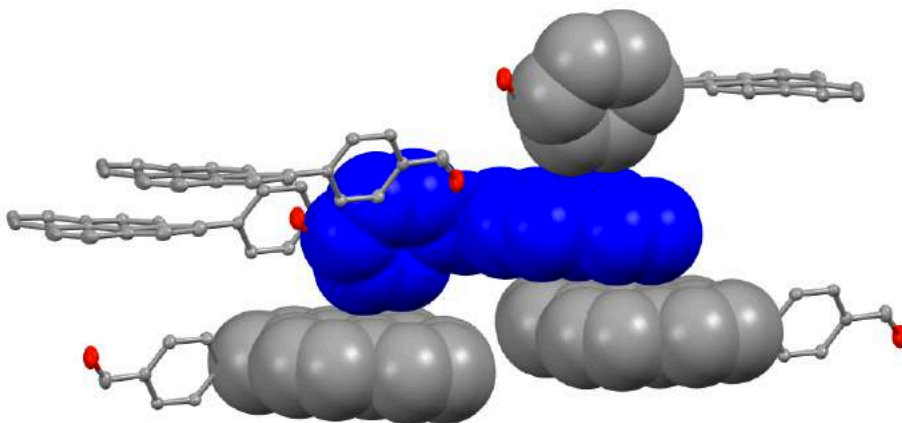
Fig. 13. Different π–stacking modes in the crystal structure of the pyrene-functionalized aldehyde substituent.

Ligand **4**

The compound, like its previously described precursor, crystallizes in the space group P-1 and its asymmetric unit contains one molecule shown it Fig. 14. The pyrene part is planar and the phenylene part is twisted some 47.80° relative to that plane. Two of the pyridine rings (one of the A rings and the B ring) of the tpy moiety are in the same plane but the second A ring is 17.68° twisted with respect to that plane. Finally the twist angle between the middle pyridine ring and the phenylene ring is 35.12°.
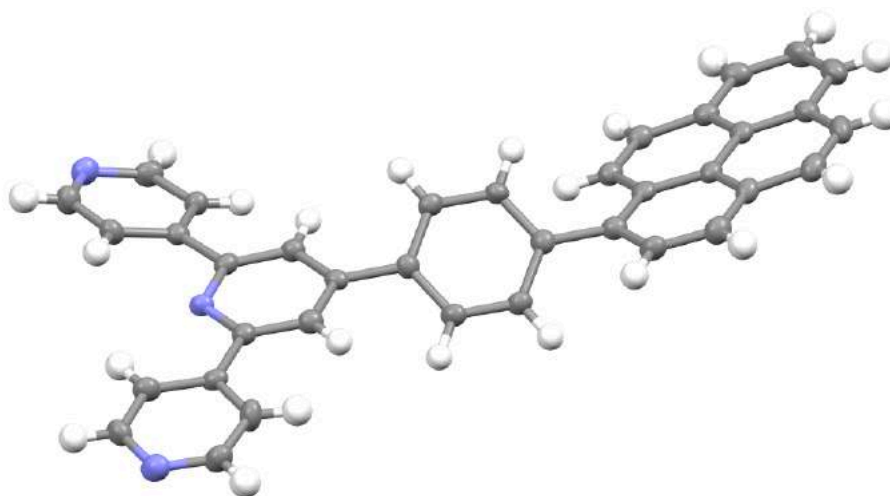
Fig. 14. Structure of **4** in the asymmetric unit.

Each molecule of ligand **4** is engaged in interactions with two of its neighbors as shown in Fig. 15. Namely, the pyrene part of one such molecule engages in face-to-face π-stacking with the pyrene part of an adjacent one from above (3.54 Å distance between the planes). Much in the same way the tpy part interacts by face-to-face π-stacking with the tpy part from below (3.53 Å distance between the planes). With those interactions the structure propagates in a stair-like fashion. Lastly, CH…N interactions between adjacent molecules supplement the packing interactions.
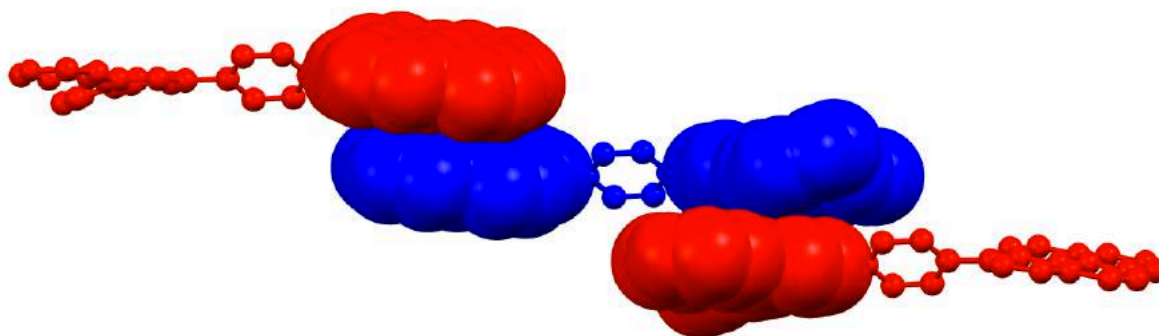
Fig. 15. Face-to-face π-stacking between pairs of pyrene fragments and between pairs of tpy moieties.

Ligand **5**

Single crystals suitable for X-ray crystallography were grown from a CHCl$_3$ solution and the compound crystallizes in the space group P-1 together with a molecule of the solvent (Fig. 16). The perylene and the tpy part of the molecule are approximately coplanar. On the other hand the phenylene part is twisted by 47.6° with respect to the plane of the perylene part and by 44.61° with respect to the tpy moiety.
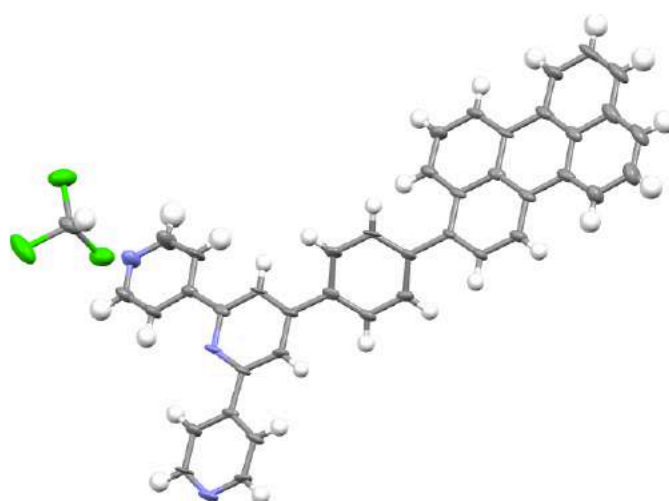
Fig. 16. Contents of the asymmetric unit in the crystal structure of **5**.

A large part of the molecule is engaged is face-to-face π–stacking. The phenylene part stacks with a symmetry-related phenylene obtained by inversion (-x, -y, -z) while the perylene moiety stacks with two out of three rings of the tpy fragment (distance between the planes 3.45 Å). It can be said that the molecules are stacked on each other in an anti-parallel manner, a consequence of it being a centrosymmetric pair, and build up columns like that (Fig. 17). Further CH…N contacts connect molecules that are located within the same plane to form a sheet. It is interesting that they all point in the same direction and then an antiparallel sheet comes on top followed by a parallel one. The voids between the columns of sheets are filled by solvent molecules.
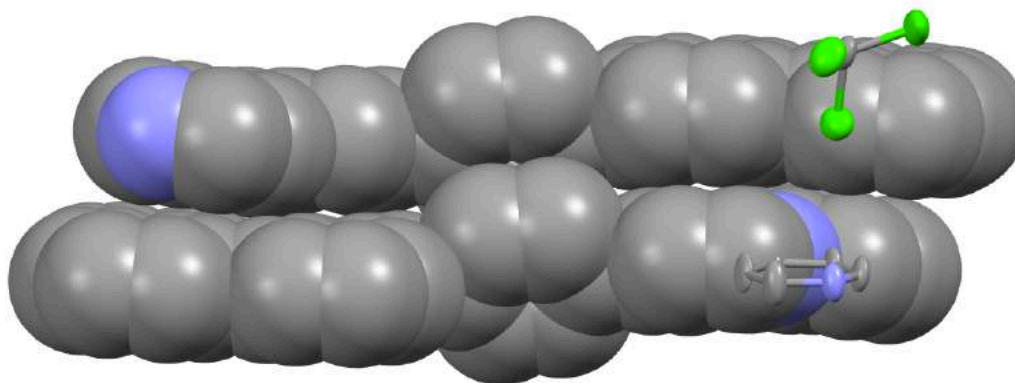
Fig. 17. Face-to-face π–stacking between a molecule **5** and its partner generated by inversion (-x, -y, -z).

Crystal data

Compound, Formula	**1**, $C_{27}H_{19}N_3$	**6**, $C_{27}H_{14}F_5N_3$	**3**, $C_{35}H_{23}N_3$
Formula weight	385.47	475.41	485.59
Z, calculated density	20, 1.328 Mg $\cdot$ m^{-3}	4, 1.552 Mg $\cdot$ m^{-3}	6, 1.341 Mg $\cdot$ m^{-3}
F(000)	4040	968	1524
Description and size of crystal	colourless needle, 0.020 $\cdot$ 0.070 $\cdot$ 0.260 mm^3	colourless Block, 0.040 $\cdot$ 0.100 $\cdot$ 0.250 mm^3	colourless plate, 0.050 $\cdot$ 0.170 $\cdot$ 0.280 mm^3
Absorption coefficient	0.079 mm^{-1}	1.071 mm^{-1}	0.079 mm^{-1}
min/max transmission	0.99 / 1.00	0.879 / 0.958	0.99 / 1.00
Temperature	123K	123(2)K	123K
Radiation(wavelength)	Mo K_α (λ = 0.71073 Å)	CuK_α (λ = 1.54178 Å)	Mo K_α (λ = 0.71073 Å)
Crystal system, space group	Monoclinic, P 2$_1$/c	Monoclinic Cc	Triclinic, P -1
a	26.942(2) Å	10.6918(11) Å	10.6630(7) Å
b	10.7793(8) Å	17.4451(17) Å	18.2526(13) Å
b	34.802(3) Å	10.9674(11) Å	19.9113(14) Å
α	90°	90°	77.069(5)°
β	107.519(4)°	96.054(4)°	82.996(5)°
γ	90°	90°	73.179(5)°
V	9638.4(13) Å^3	2034.2(4) Å^3	3608.6(4) Å^3
min/max Θ	1.585° / 25.027°	4.871° / 68.249°	1.737° / 30.032°
Number of collected reflections	62220	15280	76538
Number of independent refections	17015 (merging r = 0.129)	3453 (merging r = 0.0281)	21012 (merging r = 0.084)
Number of observed reflections	16935 (I>2.0σ(I))	3453 (I > 2σ(I))	10594 (I>2.0σ(I))
Number of refined parameters	1351	316	1027
r	0.0918	0.0293	0.0925
rW	0.3128	0.0782	0.2419
Goodness of fit	1.2204	1.061	1.0878

2.2 Target second generation ligands

7

8

9

10

11
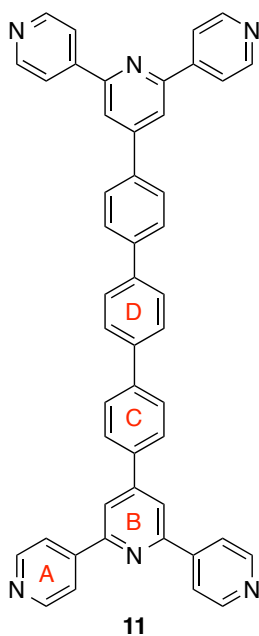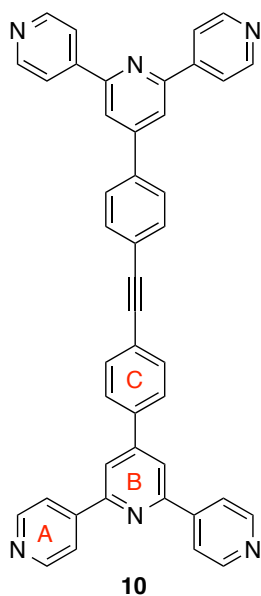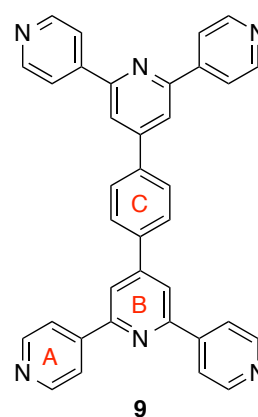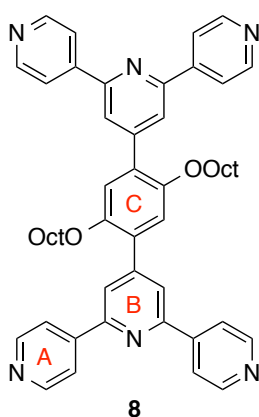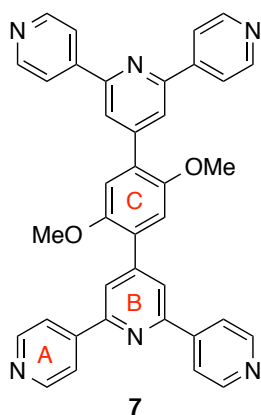
2.2.1 Retrosynthetic plan

= rigid spacer
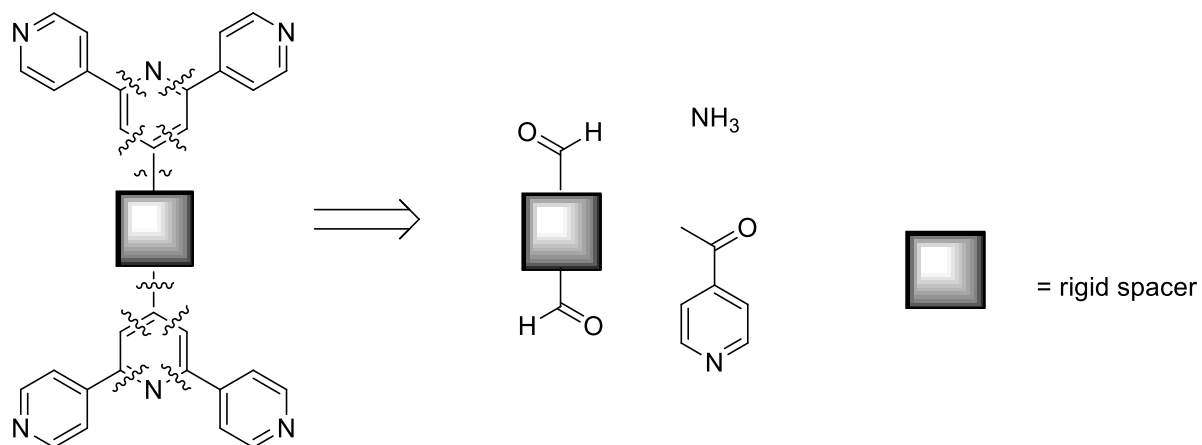
As for the first generation, the first disconnection for the preparation of the second generation (or back to back) ligands is the formation of the middle pyridine ring. The resulting dialdehyde can either

be purchased or in some cases the spacer may be synthesized using cross coupling reactions as described below.

2.2.2 Synthesis of the ligands 7, 8 and 9

In the case of the C_6H_4, 2,5-$(MeO)_2C_6H_4$, and 2,5-$(n-octylO)_2C_6H_4$ spaced ditopic ligands, the starting materials were namely terephthalaldehyde, 2,5-dimethoxyterephthalaldehyde and 2,5-bis(octyloxy)-terephthalaldehyde and were commercialy available.

R = H, OMe, OOct
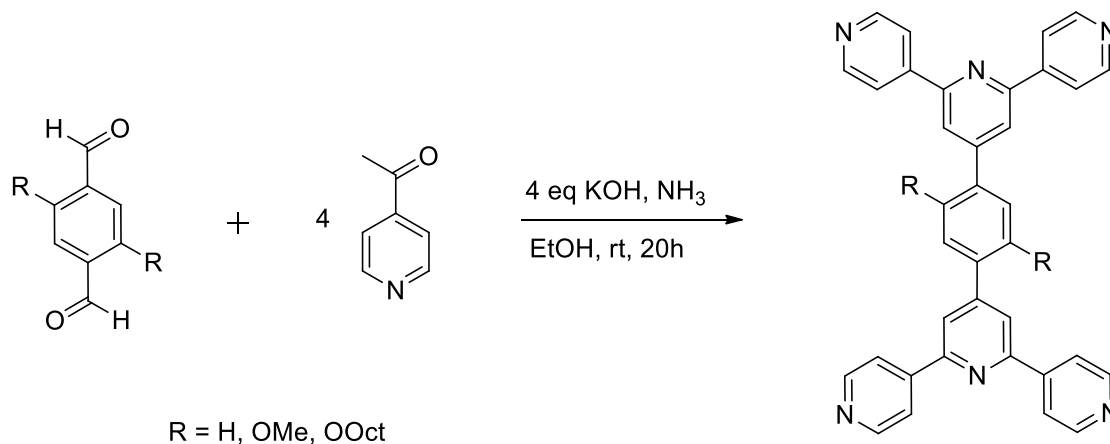
Scheme 10. Synthesis of ligands 7, 8 and 9 via a double tpy-forming reaction.

The starting dialdehydes are mixed with 4 equivalents of 4-acetylpyridine, 4 of KOH and an excess of NH_3 aq in EtOH. All three reactions were performed on a gram scale (Scheme 10).

Ligand	Yield (%)
7	30
8	30
9	40

Table 4. Yields for ligands 7, 8 and 9.

Compared to the syntheses of ligands 1-6 where one tpy domain is assembled in a one-pot reaction (Scheme 9), the synthesis of 7-9 involves the assembly of two tpys, again in a one-pot reaction. It is quite surprising therefore, that the yields of both 1st and 2nd generation ligands are comparable.
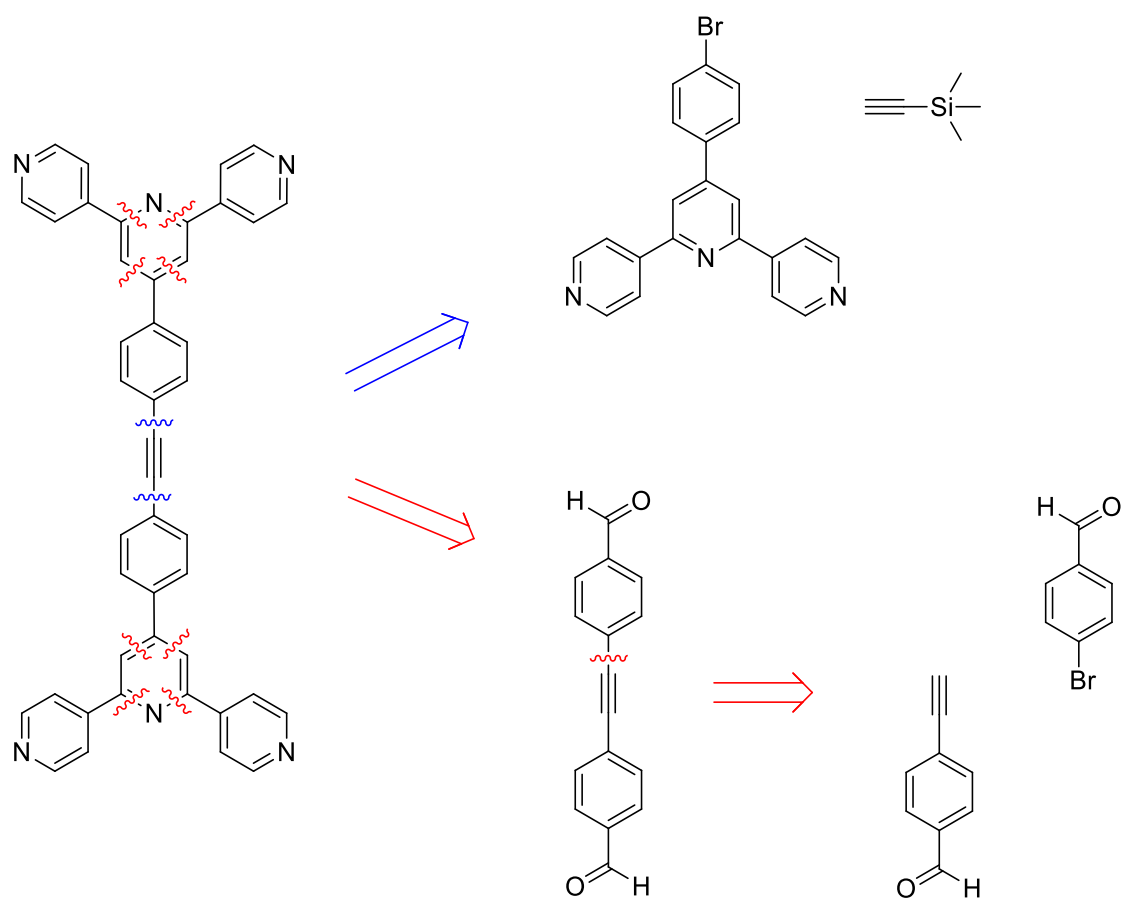
For the preparation of ligand **10** the same four-bond disconnection forming the middle terpyridine can be used at first. Then, the necessary dialdehyde can be prepared by an unsymmetrical Sonogashira reaction. Alternatively, the same ligand can be synthesized by disconnecting the bonds between the phenyl rings and the acetylene part via a double Sonogashira reaction.

a) Via a double Sonogashira reaction
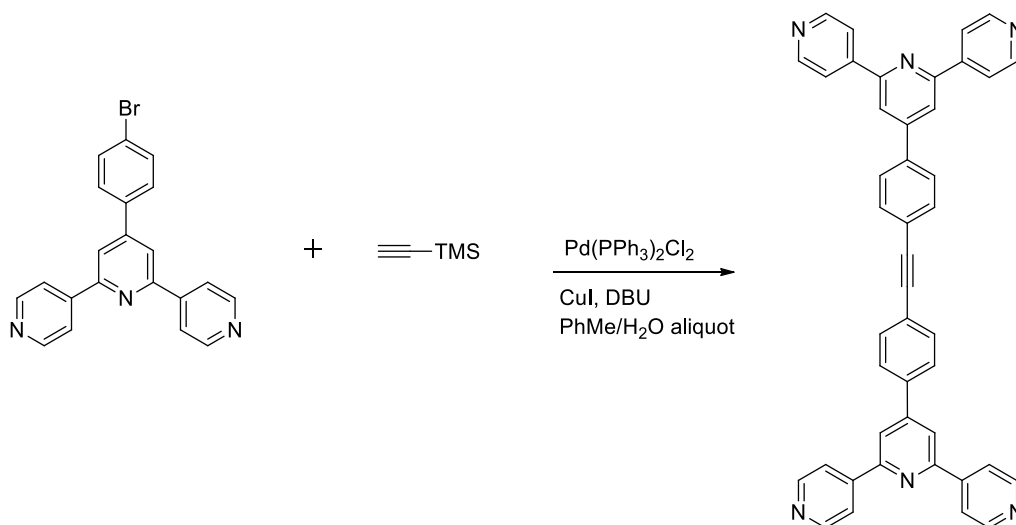
Scheme 11. Synthesis of ligand **10** via a double Sonogashira reaction.

Using two equivalents of 4'-(4-bromophenyl)-4,2':6',4''-terpyridine and trimethylsilylethyne, a double Sonogashira coupling was performed in the presence of $Pd(PPh_3)_2Cl_2$ and CuI (Scheme 11). DBU was used as the base and PhMe with an aliquot of water as the solvent. The desired 1,2-bis(4-([4,2':6',4''-terpyridin]-4'-yl)phenyl)ethyne was obtained in 83% yield which is in line with the yields described for the synthesis of symmetrical bisarylethylenes albeit some of the substrates described were arguably less challenging. The authors argue that the utilization of an amidine base and the presence of a substoichiometric amount of water are central to the synthetic protocol. After the first cross coupling, the silane-protected aryl-ethylene converges with Cu^+ and a water/DBU salt (acting as a proton shuttle) resulting in protodesililation to yield the terminal ethynylene. Then, the aryl-substituted terminal ethynylene is resubmitted to the cross-coupling cycle generating the bisarylethynyl product after a second round[8].

b) Via a simple Sonogashira reaction
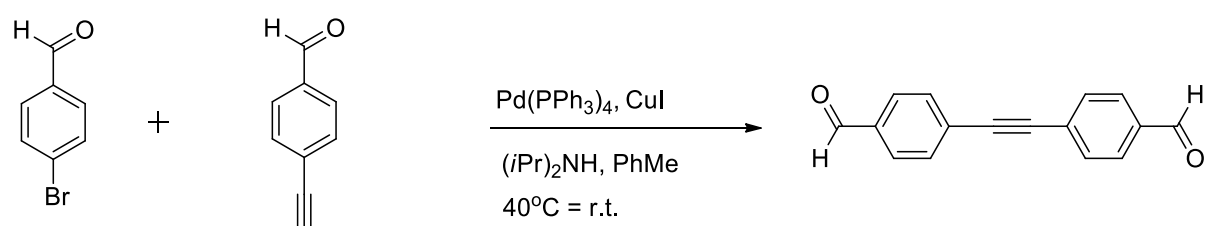
Scheme 12. Synthesis of the spacer for ligand **10** via a simple Sonogashira reaction.

Under more typical Sonogashira conditions, namely using a pure organic solvent and anhydrous conditions, 4-bromobenzaldehyde and 4-ethynylbenzaldehyde were coupled together to yield 4,4'-(ethyne-1,2-diyl)dibenzaldehyde in quantitative yield (Scheme 12). The product was used without further purification for the next step.
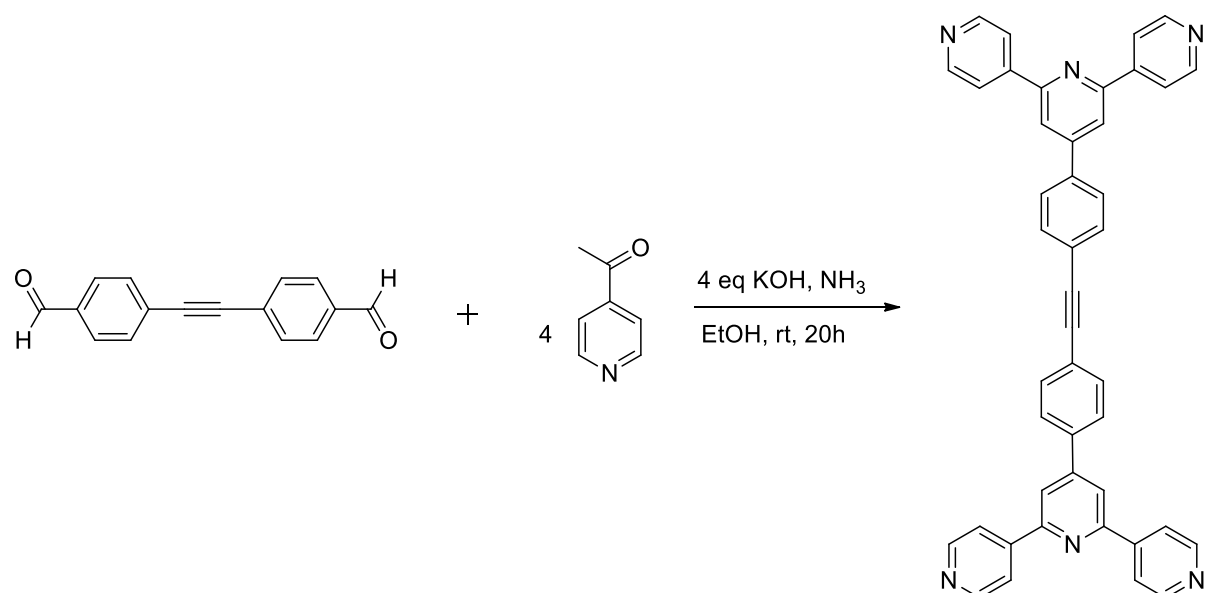
Scheme 13. Formation of ligand **10** via a double tpy-forming reaction.

As shown in Scheme 13 the starting 4,4'-(ethyne-1,2-diyl)dibenzaldehyde was mixed with 4 equivalents of 4-acetylpyridine, 4 of KOH and an excess of NH_3 aq in EtOH to yield ligand **10** (30%).
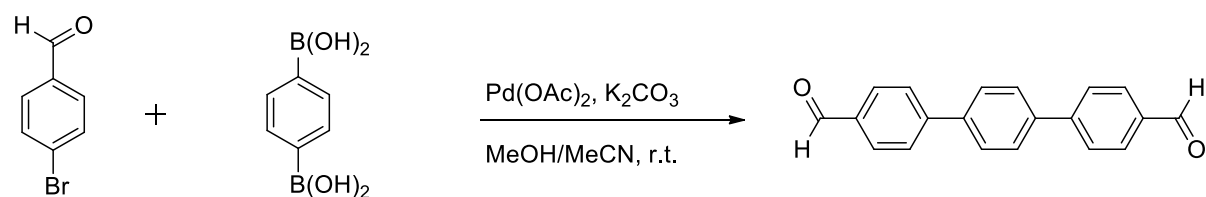
Scheme 14. Synthesis oft he spacer for ligand **11** via a double Suzuki reaction.

A double Suzuki between two equivalents of 4-bromobenzaldehyde and one equivalent of 1,4-phenylenediboronic acid was performed according to a published procedure[9]. The reaction has some interesting and maybe slightly unusual characteristics. First, a Pd(II) catalyst is used instead of directly using a Pd(0) source. Therefore palladium acetate is reduced in situ by simply dissolving it and stirring in the solvents under air for 3h. Then, the starting materials were added and the reaction was stirred at room temperature (Scheme 14). The product can also be isolated in a simple way by filtering the reaction mixture over celite and washing out the product with CH_2Cl_2. The [1,1':4',1''-terphenyl]-4,4''-dicarbaldehyde was obtained with a yield of 63% and was pure enough to be used as such for the next step.
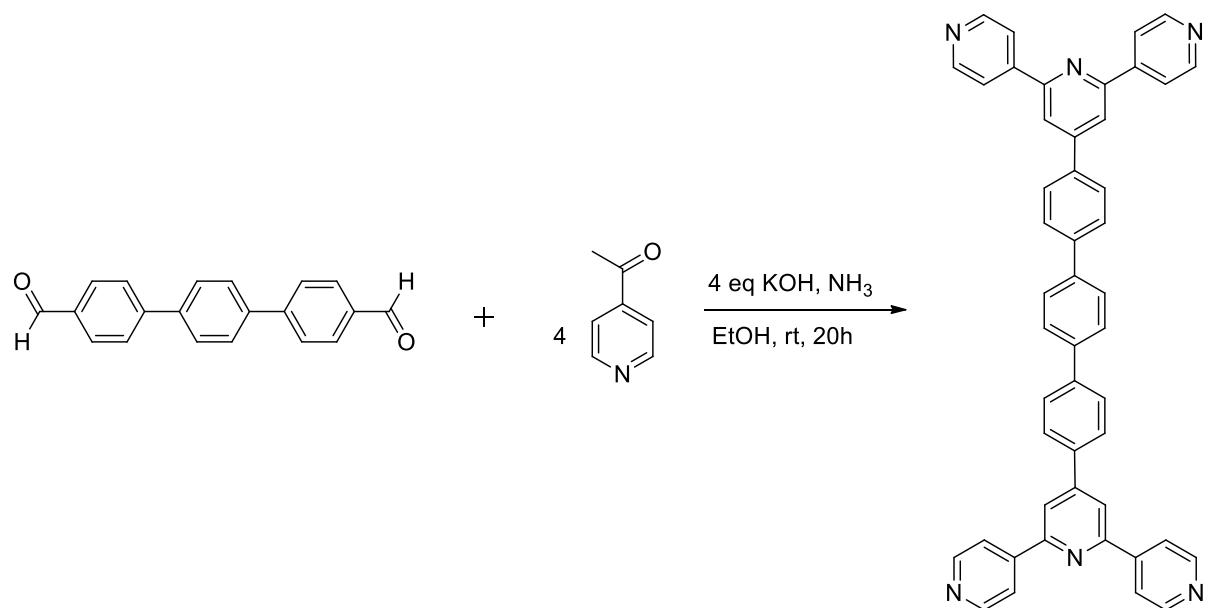
Scheme 15 Formation of ligand **11** via a double tpy-forming reaction.

As shown in Scheme 15 the starting [1,1':4',1''-terphenyl]-4,4''-dicarbaldehyde was mixed with 4 equivalents of 4-acetylpyridine, 4 of KOH and an excess of NH_3 aq in EtOH to yield ligand **11** in 30%.

2.2.5 Experimental part

Ligand 7

4-Acetylpyridine (2.04 g, 16.8 mmol) was added to a solution of 2,5-bis(methoxy)benzene-1,4-dicarbaldehyde (0.80 g, 4.12 mmol) in EtOH (250 mL). KOH pellets (0.93 g, 16.6 mmol) were added in one portion, followed by aqueous NH3 (25%, 15 mL). The reaction mixture was stirred at room temperature for 20 h. The precipitate that formed was collected by filtration, washed with H_2O and EtOH, and dried in vacuo over P_2O_5. Compound 2 was recrystallized from EtOH/CHCl$_3$ and was isolated as a pale yellow solid (0.81 g, 1.35 mmol, 32.8%). Decomp > 320 ^{o}C. ^{1}H NMR (500 MHz, CDCl$_3$) δ / ppm 8.81 (m, 8H, H^{A2}), 8.09 (m, 8H, H^{A3}), 8.07 (s, 4H, H^{B3}), 7.15 (m, 2H, H^{C3}), 3.92 (s, 6H, H^{OMe}). ^{13}C NMR (126 MHz, CDCl$_3$) ð / ppm 154.8 (C^{B2}), 150.6 (C^{A2}), 148.1 (C^{C2}), 146.1 (C^{B4}), 129.0 (C^{C1}), 121.3 (C^{B3}), 121.2 (C^{A3}), 114.1 (C^{C3}), 56.6 (C^{OMe}). IR (solid, v, cm^{-1}) 3079 (w), 3024 (w), 2831 (w), 1696 (w), 1591 (s), 1558 (w), 1541 (w), 1508 (w), 1496 (w), 1397 (w), 1388 (m), 1208 (w), 1181 (w), 1029 (m), 994 (w), 858 (w), 819 (s), 742 (w), 734 (w), 673 (w), 652 (s), 629 (s), 598 (w). ESI-MS m/z 601.6 [M + H]$^+$ (base peak, calc. 601.2). HR ESI-MS m/z 601.2350 [M + H]$^+$ (base peak, calc. 601.2347). UV-Vis λ / nm (ε / dm3 mol–1 cm–1) (CH$_2$Cl$_2$, 2.5 × 10^{-5} mol dm^{-3}) 257 (34300), 316 sh (14550), 340 sh (11200). Satisfactory elemental analysis could not be obtained.

Ligand 8

4-Acetylpyridine (1.27 g, 10.2 mmol) was added to a solution of 2,5-bis(octyloxy)benzene-1,4-dicarbaldehyde (1.00 g, 2.56 mmol) in EtOH (15 cm^3). KOH pellets (0.575 g, 10.2 mmol) were added in one portion, followed by aqueous NH$_3$ (25%, 15 cm^3). The reaction mixture was stirred at room temperature for 20 h, during which time a precipitate formed. This solid was collected by filtration, washed well with H_2O and EtOH, and dried in vacuo over P_2O_5. Compound 2 was recrystallized from EtOH/CHCl$_3$ and was isolated as bright yellow crystals (including single) (0.62 g, 30%). M.pt. = 255 ^{o}C. ^{1}H NMR (500 MHz, CDCl$_3$) δ / ppm 8.81 (m, 8H, H^{A2}), 8.11 (s, 4H, H^{B3}), 8.09 (m, 8H, H^{A3}), 7.16 (m, 2H, H^{C3}), 4.06 (t, J = 6.2 Hz, 4H, H^{OCH_2}), 1.74 (m, 4H, H^{OCH_2CH_2}), 1.37 (m, 4H, H^{OCH_2CH_2CH_2}), 1.28-1.06 (overlapping m, 16H, H^{CH_2}), 0.80 (t, J = 7.0 Hz, 6H, H^{CH_3}). ^{13}C NMR (126 MHz, CDCl$_3$) δ / ppm: 154.8 (C^{B2}), 150.7 (C^{A2}), 148.3 (C^{C2}), 146.3 (C^{B4}), 129.3 (C^{C1}), 121.6 (C^{B3}), 121.3 (C^{A3}), 115.3 (C^{C3}), 69.9 (C^{OCH_2}), 31.9 (C^{CH_2}), 29.6 (C^{OCH_2CH_2}), 29.5 (C^{CH_2}), 29.3 (C^{CH_2}), 26.5 (C^{OCH_2CH_2CH_2}), 22.7 (C^{CH_2}), 14.2 (C^{CH_3}). IR (solid, v, cm^{-1}) 2920 (m), 2853 (m), 1591 (s), 1557 (m), 1538 (w), 1510 (m), 1469 (m), 1425 (m), 1412 (m), 1387 (m), 1209 (m), 1062 (m), 1053 (m), 1022 (m), 992 (m), 967 (m), 861 (m), 838 (m), 825 (s), 737 (m), 705 (m), 652 (s), 648 (m), 627 (s), 610 (m), 508 (s). ESI MS m/z 797.9 [M + H]$^+$ (base peak, calc. 797.5). UV-Vis λ / nm (ε / dm^3 mol^{-1} cm^{-1}) (CH$_2$Cl$_2$, 2.5 ×10^{-5} mol dm^{-3}): 234 (52000), 259 (50500), 349 (11500). Found C 72.37, H 6.66, N 9.58; C$_{52}$H$_{56}$N$_6$O$_2$·$^1/_2$CHCl$_3$·$^1/_2$H$_2$O requires C 72.84, H 6.69, N 9.71%.

Ligand 11

4-Acetylpyridine (1.24 g, 10.2 mmol) was added to a solution of [1,1':4',1''- terphenyl]-4,4''-dicarbaldehyde (0.716 g, 2.50 mmol) in EtOH (250 mL). KOH pellets (0.56 g, 10 mmol) were added in one portion, followed by aqueous NH$_3$ (25%, 13 mL). The reaction mixture was stirred at room temperature for 20 h, during which time a precipitate formed. The product was collected by filtration, washed well with H_2O and EtOH, and dried in vacuo over P_2O_5. 4,4''-Di((4,2':6',4''-terpyridin)-4'-yl)-1,1':4',1''-terphenyl was isolated as a pale yellow solid (0.50 g, 0.72 mmol, 29%). Decomp. > 320 ^{o}C.

^{1}H NMR (500 MHz, CDCl$_3$) δ / ppm 8.82 (m, 8H, H^{A2}), 8.12 (s overlapping m, 12H, H^{A3+B3}), 7.89 (m, 8H, H^{C2+C3}), 7.83 (s, 4H, H^{D2}); ^{13}C NMR (126 MHz, CDCl$_3$) 155.4 (C^{B2}), 150.6 (C^{A2}), 146.1 (C^{A4}), 141.8 (C$^{C1/D1}$), 139.5 (C$^{C1/D1}$), 136.9 (C^{B4+C4}), 127.8 (C^{C2+C3}), 127.7 (C^{D2}), 121.3 (C^{A3}), 118.6 (C^{B3}). IR (solid / v, cm^{-1}) 3974 (w), 3920 (w), 3027 (w), 2919 (w), 2849 (w), 1695 (w), 1592 (m), 1557 (w), 1533 (w), 1490 (w), 1432 (w), 1393 (w), 1386 (w), 1256 (w), 1217 (w), 1125 (w), 1064 (w), 1004 (w), 996 (w), 833 (w), 811 (s), 739 (w), 668 (w), 647 (m), 646 (m), 624 (m), 621 (m), 615 (w), 581 (m), 575 (m), 570 (m), 566 (m), 541 (s), 537 (s), 529 (m), 512 (s), 510 (m). ESI MS *m/z* 693.7 [M + H]$^+$ (base peak, calc. 693.28).

2.2.6 Absorption and emission properties
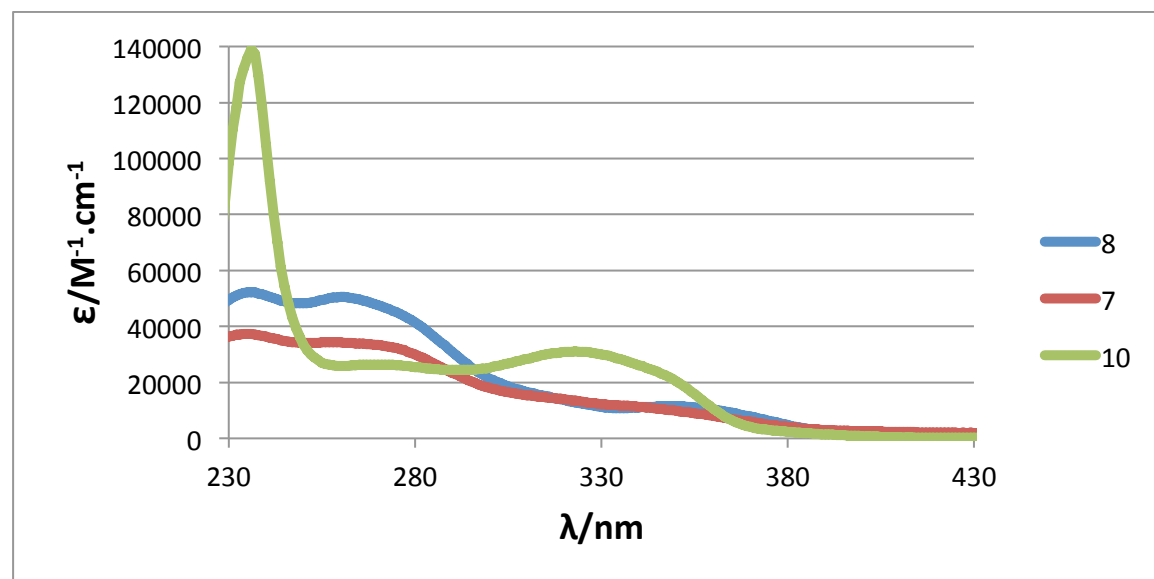
Fig. 18. Absorption spectra of CH$_2$Cl$_2$ solutions of second-generation ligands **7**, **8** and **10**.

All the electronic absorption spectra were recorded in CH$_2$Cl$_2$ and the ligand absorbances were converted into the respective extinction coefficients. The UV-VIS spectrum of both ligands **7** and **8** is governed by a broad absorption arising from π*←π and π*←n transitions (λmax = 257 nm with a higher extinction coefficient for ligand **8**) which tails out into the visible region of the spectrum. For ligand **10** (λmax = 267, 321 nm) it is clear that there is the additional contribution of a futher phenyl ring.

Excitation of the ligands **7**, **8** and **10** (in CH$_2$Cl$_2$ solution) at λ$_{ex}$ = 348, 367 and 350 nm respectively resulted in the emission maxima shown in Table 5.

Ligand	λ$_{em}$ (nm)
7	425
8	429
10	373/385

Table 5. Emission maxima in CH$_2$Cl$_2$ for second-generation ligands **7**, **8** and **10**.

In general alkyl chains do not have an effect on electronic spectra in the energy range recorded. Absorptions are in the vacuum UV. Considering this, the strict similarity between the absorption and emission spectra of ligand **7** and **8** can be fully understood. When it comes to ligand 10 the emission blueshifts due to the spacer with respect to the molecules already taken in consideration. If we consider that the emission for the unsubstituted spacer frame is the range 300-350 nm, it seems that

the emission we see is correlated with that. A similar emission was seen for ligand **1** and **6**. It can be deduced from that if the substituent is polycyclic aromatic (PCA) the emission comer from the PCA. In the presence of a benzene ring the emission seems to come from the phenylene frame and it is very similar to that of the unsubstituted spacer.

2.2.7 Crystal structures

Ligand **8**

When ligand **8** was recrystallized from EtOH/CHCl$_3$ bright yellow crystals were obtained, some of them were even single and suitable for X-ray crystallography. The compound crystallizes in the P2$_1$/c space group and just one half of the molecule is present in the asymmetric unit, the other half being generated by an inversion center. The structure is shown in Fig. 19.
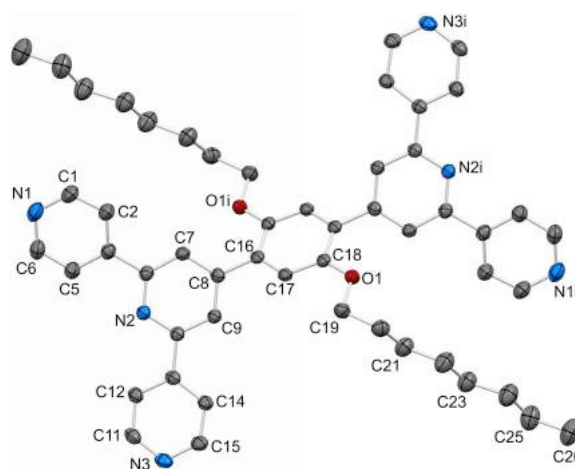
Fig. 19. ORTEP diagram of **8** with ellipsoids plotted at 50% probability level.

In order to minimize steric hindrance between the *ortho* substituents, the phenylene ring containing the C8 side-chains is significantly twisted compared to the plane of the pyridine rings (46.3°). The latter moieties are practically flat and can therefore engage in efficient π-stacking between adjacent molecules (interplane distance 3.44 Å). Each two interacting pyridine rings are sandwiched by two octyloxy chains (Fig. 17), which in turn seem to be implicated in hydrophobic interactions with other neighboring chains that point in the same direction.
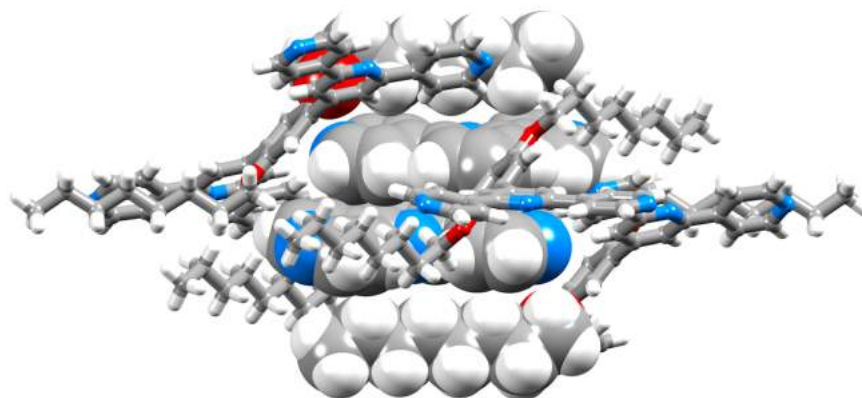
Fig. 20. Alkoxy/tpy/tpy/alkoxy stacking motif in the crystal lattice of **8**.

40

A coordination polymer was attempted to be grown by combining ligand **11** in dichlorobenzene/methanol and a zinc halide in methanol (will be discussed in further detail in one of the next chapters). At least two types of crystals were present and the only ones that diffracted decently turned out to be pure ligand. This is a preliminary structure (R = 20%) as structure refining did not reach the stage when H atoms are added. The compound crystallizes in the space group P2$_1$/c and two half molecules are present in the unit cell (Fig. 21).
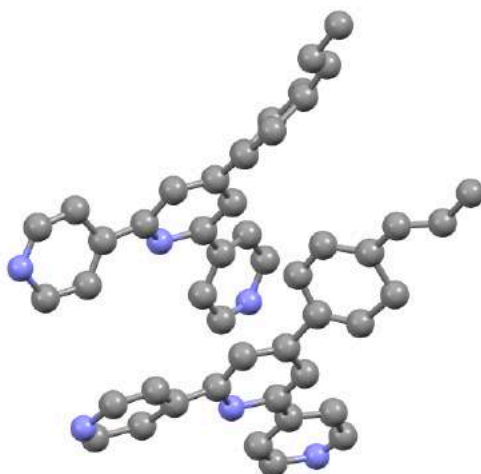
Fig. 21. Contents of the asymmetric unit in the crystal structure of **11.**

The two molecules (now in blue in Fig. 22) interact via each other via π–stacking, that mainly seem to be edge-to-face to be precise (CH…centroid distances could not be calculated because hydrogens were not added in the structure solving process yet). They are surrounded in total by four molecules each, but because of symmetry there are just two different parts of the molecules that engage in the same type of interaction. The two tpy parts of the blue molecules connect with the terphen part of adjacent molecules via CH...N interactions. Much in the same way, the terphen parts of the blue units link with neighboring molecules via CH…N interactions.
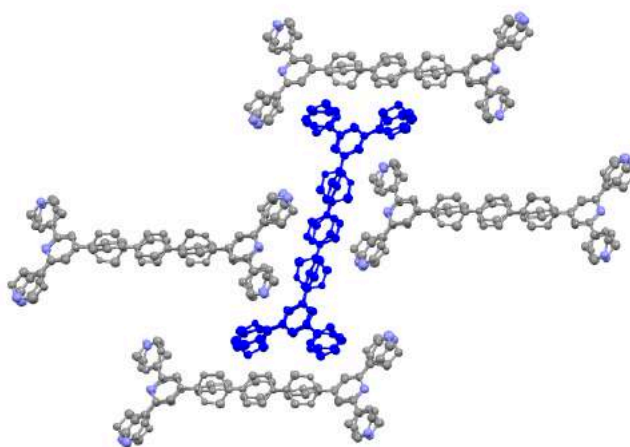
Fig. 22. Face-to-face π–stacking and CH…N interactions as viewed along the a-axis.

2.3 References

1   J. Wang and G. S. Hanan, Synlett., 2005, 8, 1251.

2   N. Miyaura and A. Suzuki, Chem. Rev., 1995, 95, 2457.

3   G. Zhang, Synthesis, 2005, 4, 537.

4   Y. Teki, S. Miyamoto, M. Nakatsuji, Y. Miura, J. Am. Chem. Soc., 2001, 123, 294.

5   M. Kasha, Discuss. Faraday. Soc., 1950, 9, 14.

6   J.W. Steed, CrystEngComm, 2003, 5, 169.

7   A.D. Bond, CrystEngComm, 2008, 10, 411.

8   M. J. Mio, L. C. Kopel, J. B. Braun, T. L. Gadzikawa, K. L. Hull, R. C. Brisbois, C. J. Markworth, P. A. Grieco, Org. Lett., 2002, 4, 3199.

9   P. K. Mandali, D. K. Chand, Catalysis Communications, 2013, 31, 16.

Chapter III: Reactions of 4'-substituted 4,2':6',4''-terpyridines with metal acetate salts

3.1. Structures with ligand 1

3.1.1 Reactions with Zn(OAc)$_2$.2H$_2$O

Zinc(II) acetate tends to form dinuclear {Zn$_2$(μOAc)$_4$} nodes when reacted with 4,2':6',4''-tpy ligands. One-dimensional coordination polymers are obtained in reactions between two equivalents of Zn(OAc)$_2$.2H$_2$O with one equivalent of 4'-X-4,2':6',4''-tpy (X = Ph[1], ^{t}Bu[2], 4-BrC$_6$H$_4$[3], 4-MeSC$_6$H$_4$[3]).

Ligand **1** and Zn(OAc)$_2$.2H$_2$O were reacted using a variety of conditions and ratios. Namely, four vapor diffusion crystal growth experiments were performed with a metal to ligand ratio of 1:1 (using two different anti-solvents), 2:1 and 1:2. All those experiments were performed in the same way: **1** was dissolved in a CH$_2$Cl$_2$/MeOH (3:1) mixture and solid Zn(OAc)$_2$.2H$_2$O was added while stirring the solution. The mixture (it is important that no precipitate was present) was transferred into a small vial, which in turn was inserted into a much bigger vial and the latter was filled with counter-solvent. Vapor diffusion of hexane into the reaction mixture with a 1:1 ratio gave single crystals suitable for X-ray crystallography, which correspond to the coordination polymer [{Zn$_2$(μ-OAc)$_4$(**1**)}$_n$] without any solvent present in the lattice. Keeping the ratio constant, the anti-solvent was changed to Et$_2$O and colorless single crystals of the same compound were obtained after a few days. When the metal to ligand ratio was 2:1 a precipitate was formed as soon as the metal was added to the solution in its solid form. The suspension was evaporated to dryness and the resulting solid was dissolved in a minimal amount of MeOH. A crystal growth experiment using the layering methodology was also performed with this ratio. After slow evaporation of the MeOH solution X-ray quality crystals of again the same compound formed. With the ligand being in excess (metal to ligand ratio of 1:2) Et$_2$O was diffused into the reaction mixture in order to produce single crystals. All experiments yielded crystals of similar morphologies and same unit cell dimensions.
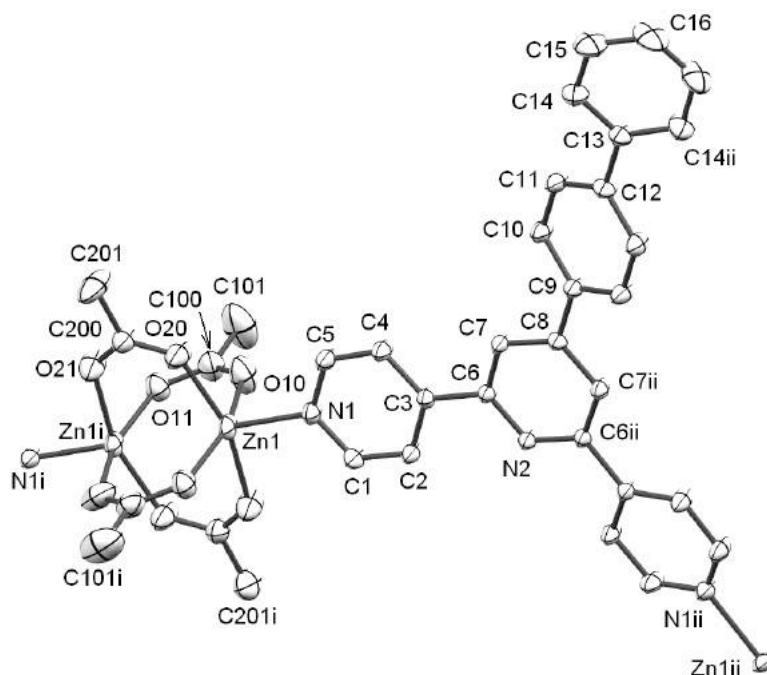
Fig. 1. Part of one chain in [{Zn$_2$(μ-OAc)$_4$(**1**)}$_n$] with ellipsoids plotted at 40% probability level (H atoms omitted for clarity).

44

Indeed, the structural determination proves that the 1D coordination polymer [{Zn$_2$(μ-OAc)$_4$(**1**)}$_n$] has been formed, where ligand **1** bridges the {Zn$_2$(μ-OAc)$_4$} paddle-wheel-like motive (Fig. 1). The polymer crystallizes in the *C*2/*c* space group, which is monoclinic and half of ligand **1** and half of a {Zn$_2$(μ-OAc)$_4$} paddle-wheel are to be found in the asymmetric unit. The central N atom of **1** is not coordinated to a metal, which is common for coordination polymers containing a 4,2':6',4"–tpy ligand. The distance between the two Zn nodes is 2.9000(6) Å, which is within the range (2.87-3.05 Å) for this and similar motifs[4]. Compared to the free ligand **1** (structure described in the previous chapter) the same coordinated ligand is more planar. The chain that makes up the coordination polymer has a zigzag backbone where each biphenyl substituent fits into a V-shaped cavity of an adjacent chain. This leads to efficient packing of chains into sheets. Between adjacent sheets, chains are arranged as shown in Fig. 2, where face-to-face π–stacking between tpy domains can be seen (separation of 3.44 Å).
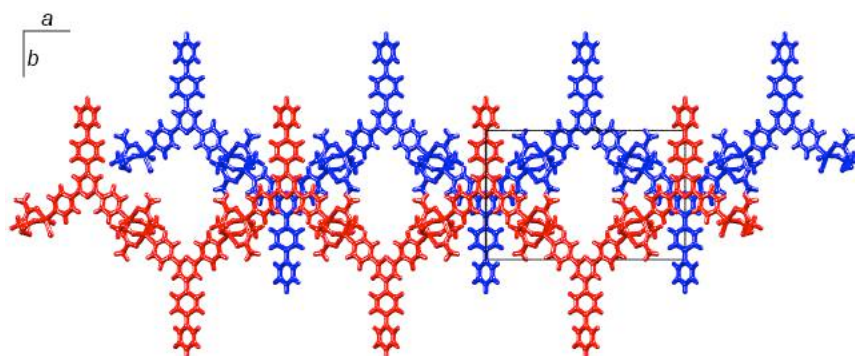
Fig. 2. Crystal packing in [{Zn$_2$(μ-OAc)$_4$(**1**)}$_n$]: relative orientations of zigzag chains in adjacent sheets.

Furthermore, biphenyl moieties of adjacent chains engage in face-to-face stacking in a head-to-tail manner. Even though there is a 31.41(18)° twist between the C and D rings the interaction is still effective (inter-centroid distance of 4.26 Å)[5,6] (Fig. 3.).
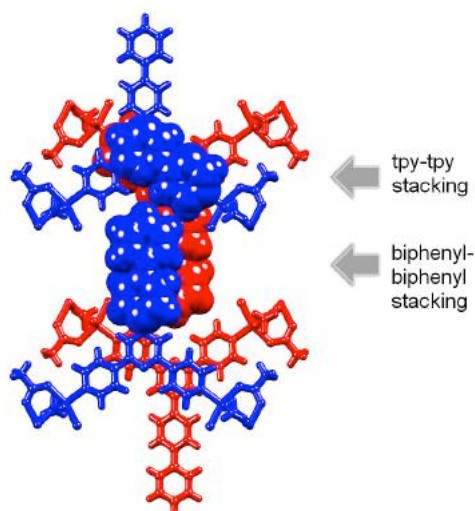
Fig. 3. Crystal packing in [{Zn$_2$(μ-OAc)$_4$(**1**)}$_n$]: Face-to-face π–stacking occurring between tpy domains and between biphenyl units in adjacent chains.

Unit cell dimensions of [{Zn$_2$(μ-OAc)$_4$(**1**)}$_n$] are very similar to those of the previously reported related structures with 4'-X-4,2':6',4''-tpys (X = Ph[1], ^{t}Bu[2], 4-BrC$_6$H$_4$[3]). All compounds are structurally similar, both in the presence of zig-zag chains and in their packing; the dominant packing interactions are face-to-face stacking of tpy domains. The polymer obtained with X = 4-MeSC$_6$H$_4$[3] is structurally analogous to the latter compounds, but crystallizes in the P2$_1$/c space group.

Out of all those compounds, the one where X = Ph is the only one that crystallizes with solvent (CH$_2$Cl$_2$) in the lattice. Significantly, the partial occupancy solvent molecules occupy sites coincident with the positions of the peripheral phenyl rings in [{Zn$_2$(μ-OAc)$_4$(**1**)}$_n$], which shows that the additional Ph ring increases the surface that engages in stacking. When X = Ph, if the crystallization period is months rather than days, the preferred product is a mononuclear species. In the case of [{Zn$_2$(μ-OAc)$_4$(**1**)}$_n$] no interconversion to another species is observed, which might indicate that the obtained compound presents a higher stability.

If X = 4-BrC$_6$H$_4$, the Br atoms reside in the sites occupied by the outer phenyl rings in [{Zn$_2$(μ-OAc)$_4$(**1**)}$_n$]. Each Br atoms lies over a phenyl ring in an adjacent chain (Ph$_{centroid}$…Br separation = 4.01 Å), which prevents stacking of phenyl rings. Compound [{Zn$_2$(μ-OAc)$_4$(**1**)}$_n$] presents an improvement in the packing interaction since its biphenyl moiety is involved in stacking between adjacent chains. Similarly, in the case of X = 4-MeSC$_6$H$_4$ each SMe group occupies the site taken by the outer phenyl ring, which results in Ph$_{centroid}$…SMe contacts (separation = 3.95 Å), which prevent face-to-face stacking that helps stabilize the packing in [{Zn$_2$(μ-OAc)$_4$(**1**)}$_n$].

3.1.2 Reactions with Cu(OAc)$_2$.H$_2$O

Layering a solution containing 2 equivalents of Cu(OAc)$_2$.H$_2$O (in MeOH) over a solution of 1 equivalent of ligand **1** (in CHCl$_3$) resulted in the formation of turquoise colored crystals of [{Cu$_2$(μ-OAc)$_4$(**1**)}$_n$]. This structure (shown in Fig. 4) is isostructural to previously described [{Zn$_2$(μ-OAc)$_4$(**1**)}$_n$] as confirmed by single crystal X-ray diffraction.
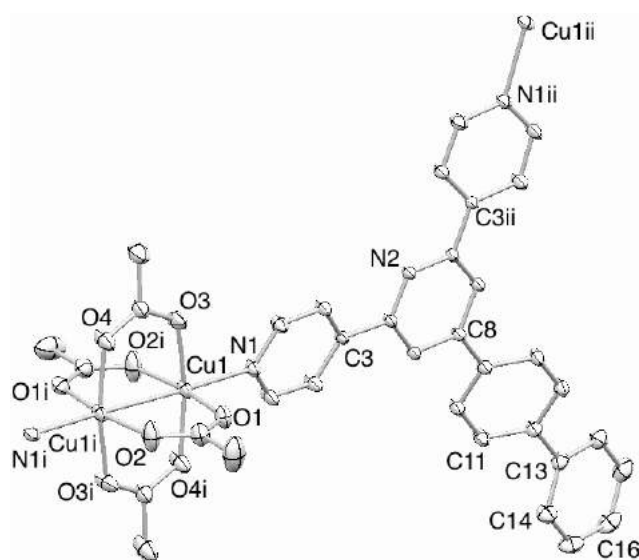

Fig. 4. Part of on chain in [{Cu$_2$(μ–OAc)$_4$(**1**)}$_n$].

This is not surprising considering that $\{Cu_2(\mu\text{-OAc})_4\}$ motifs have a tendency to form[4] (and have a similar size to the $\{Zn_2(\mu\text{-OAc})_4\}$ unit) as well as the fact that the face-to-face π-stacking between biphenyl and tpy moieties of neighboring chains has a prevalent role in the packing interactions.

3.1.3 Reactions with Cd(OAc)$_2$.2H$_2$O

Moving from zinc(II) to cadmium(II), cobalt(II) or nickel(II) increases the coordination number of the metal node and the assembly of 2-D sheets, 1-D, chains or 1-D ladders was reported[2, 7, 8, 9]. The next candidate for reactions with ligand **1** was Cd(II) acetate, which does not have a propensity to form paddle-wheel units (only seven examples are contained in the CSD)[4] but the Cd(II) center can possibly have a higher coordination number (thus more structural flexibility) than Zn(II). A solution of **1** (in CHCl$_3$) was inserted into a test tube and a solution containing 2 equivalents of Cd(OAc)$_2$.2H$_2$O (in MeOH) was carefully layered on top of it, which yielded colorless crystals. X-ray diffraction structural analysis indicated the formation of the coordination polymer with the formula [$\{Cd_2(OAc)_4(\mathbf{1})_2\}_n$] meaning that contrary to the two previously defined structures the metal: ligand ratio is 1:1. Unfortunately, due to the size of the crystals being small and to their rapid decomposition upon being taken out of solution, the quality of the structure is low. Therefore, the program SQUEEZE[10] was used to improve the quality of the main framework as much as possible by removing electron density from the cavities that are present due to the loss of solvent. The polymer crystallizes in the space group P-1, which is triclinic and the contents of the asymmetric unit (shown in Fig. 5.) include two independent Cd(OAc)$_2$ moieties consisting of chelating acetate ligands as well as two independent molecules of ligand **1**. Each of atoms O2 and O6 is not only involved in chelation but also bridges a pair of symmetry related Cd atoms yielding the planar [$\{Cd_2(\mu,\kappa^3\text{-}O,O':O'\text{-}OAc)_2(\kappa^2\text{-}O,O'\text{-}OAc)_2(\mathbf{1})\}_n$] motif. This $\{Cd_2(OAc)_4\}$ unit occurs in 47 structures in the CSD[4].
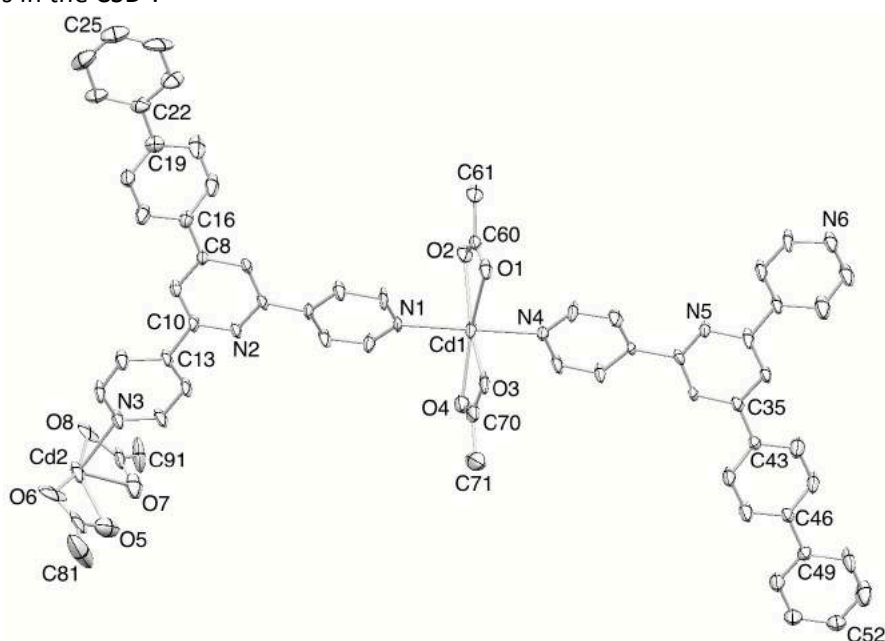
Fig. 5. Contents of the asymmetric unit in [$\{Cd_2(\mu,\kappa^3\text{-}O,O':O'\text{-}OAc)_2(\kappa^2\text{-}O,O'\text{-}OAc)_2(\mathbf{1})\}_n$] (ellipsoids plotted at 30% probability level, H atoms omitted).

The coordination sphere around the Cd atom is pentagonal bipyramidal where five O donors form the equatorial plane and two nitrogen donors from two ligands **1** occupy the two remaining sites (Fig. 6). The global polymer chain can be described as a ladder where the $\{Cd_2(OAc)_4\}$ fragments act as the rungs and the sides of the ladder are made of ligands **1**. As can be seen in Fig. 5 the central N atoms (N2 and N5) of the tpy groups are not coordinated. Face-to-face stacking of ligands, which lie practically over one another but are slightly slipped in order to allow adequate π–interactions, holds this structure together (centroid...centroid distance is 3.88 Å).
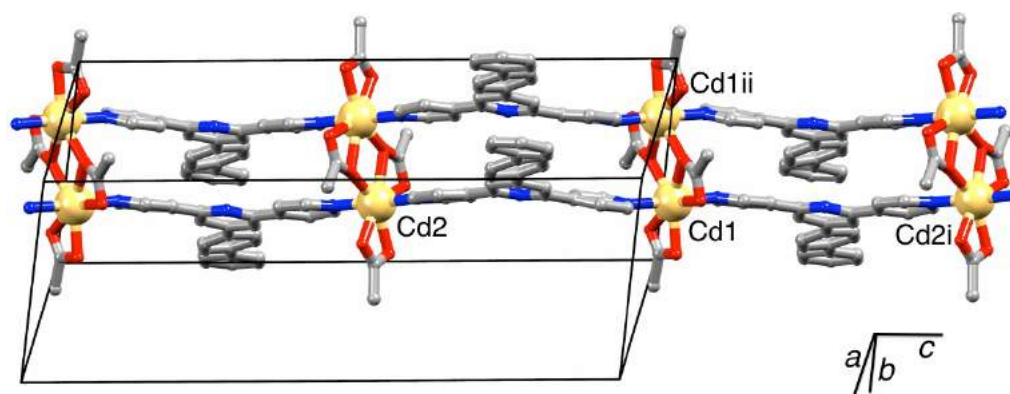
Fig. 6. Part of one ladder (double chain) assembled through bridging acetate ligands.

Alternatively the ladder topology can also be described as being a double zig-zag chain, which assembles into sheets (Fig. 7) and where the packing is similar to the two structures previously described.
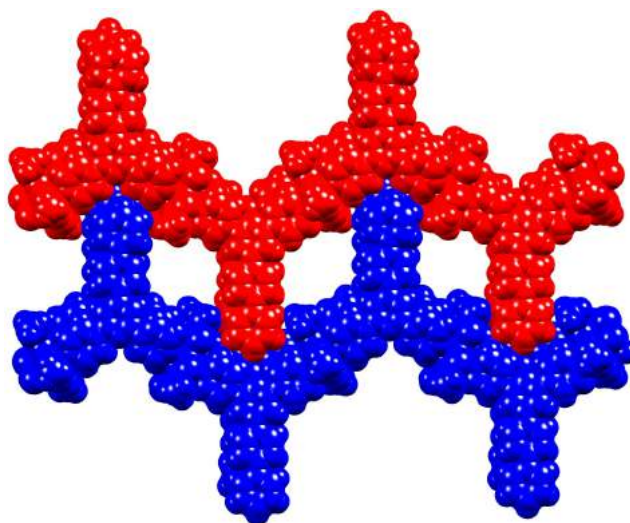
Fig. 7. Packing of zig-zag chains into sheets: parts of two ladders shown.

Each side of the sheet has protruding acetato ligands and different sheets pack in a "peg-and-hole" mode in a way that the holes seen in Fig. 7 are filled by the pegs (acetate ligands) of a neighboring sheet (Fig. 8).

Even though the metal size is increased in going from Zn^{2+} or Cu^{2+} to Cd^{2+} produces a structural change in the $\{M_2(OAc)_4\}$ unit and a change in the metal:ligand stoichiometry in

48

the coordination polymer, the recurrence of biphenyl…biphenyl and tpy…tpy face-to-face interactions in all three complexes in noteworthy.
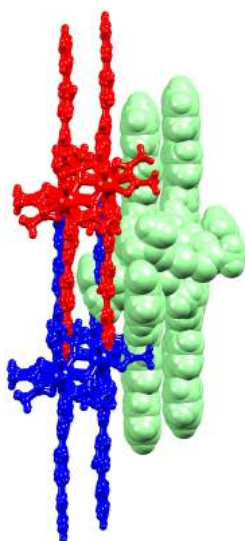
Fig. 8. Penetration of acetate-groups into cavities in adjacent sheets; red and blue ladders are in one sheet, green ladder is in the adjacent sheet.

3.1.4 Absorption and emission spectroscopic properties

In the last decade, a range of photoactive zinc(II)-containing coordination polymers has been reported, some exhibiting promising performance in electroluminescent devices[11, 12, 13, 14, 15].
In the solid-state diffuse reflection spectrum of a crystalline sample of $[\{Zn_2(\mu\text{-OAc})_4(\mathbf{1})\}_n]$ showed minimum reflection (which is maximum absorption) at 286 and 352 nm whereas the absorption spectrum of an EtOH solution of the complex displayed maxima at 233, 278 and 306 nm. Comparing this solution spectrum with the solution spectrum of **1** (discussed in the previous chapter) it can be assumed that the coordination polymer dissociated in solution (Fig. 9). The fact that he emission of an EtOH solution of the complex (λ_{em} = 384 nm) mirrors that of ligand **1** and the two spectra are practically superimposable.
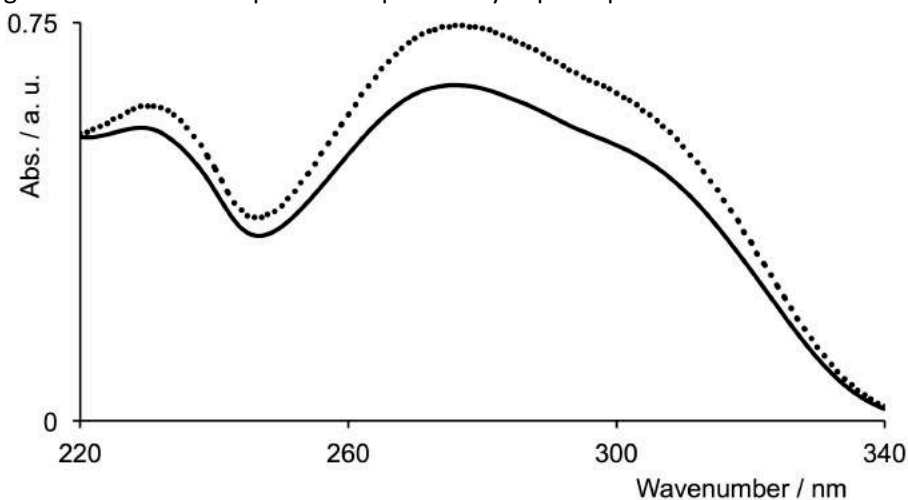
Fig. 9. Absorption spectra of EtOH solutions of 1 (solid line) and $[\{Zn_2(\mu\text{-OAc})_4(\mathbf{1})\}n]$ (dotted line).

A thin film of the complex was prepared (5% in PMMA) and showed an emission maximum at 362 nm with a shoulder at 245 nm (λ_{ex} = 300 nm) but because during the casting, the complex had to be dissolved (in CH_2Cl_2/MeOH) it is uncertain which species is emitting (ie. polymer or dissociated ligand). Comparing the PMMA films of the ligand and the complex it is clear that the spectrum of the latter is dictated by the one of the former. The shoulder at 425 nm is assigned to come from the complex.
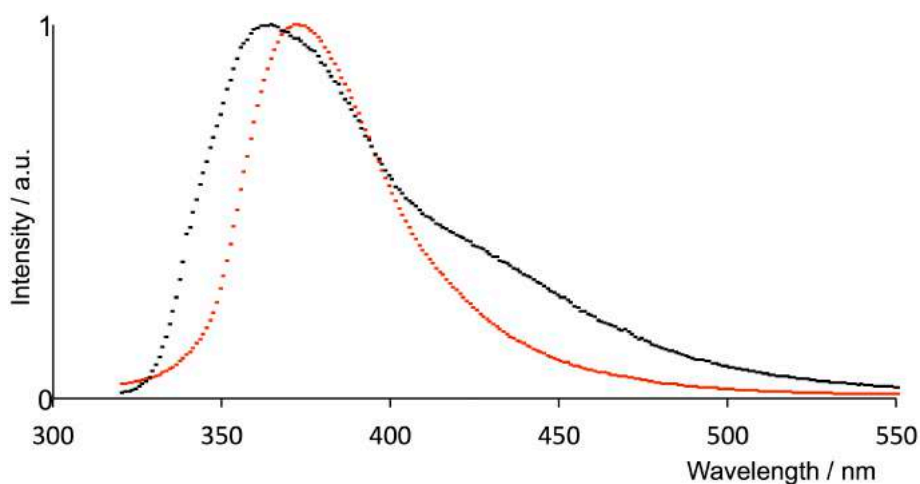
Fig. 10. Normalised emission spectra (λ_{ex} = 300 nm) of 1 (red) and [{$Zn_2(\mu$-OAc$)_4$(**1**)}$_n$] (black) 5% in PMMA film.

The emission maximum for **1** in the solid state is 395 nm, which is close to that in solution (385 nm). Going from **1** to [{$Zn_2(\mu$-OAc$)_4$(**1**)}$_n$] (λ_{em} = 425 nm), a red shift is observed and the complex is a blue emitter (Fig. 11). Using ex = 300 nm the emissions of the solid samples of **1** and the complex have quantum yields of 9.5 and 7.7% respectively.
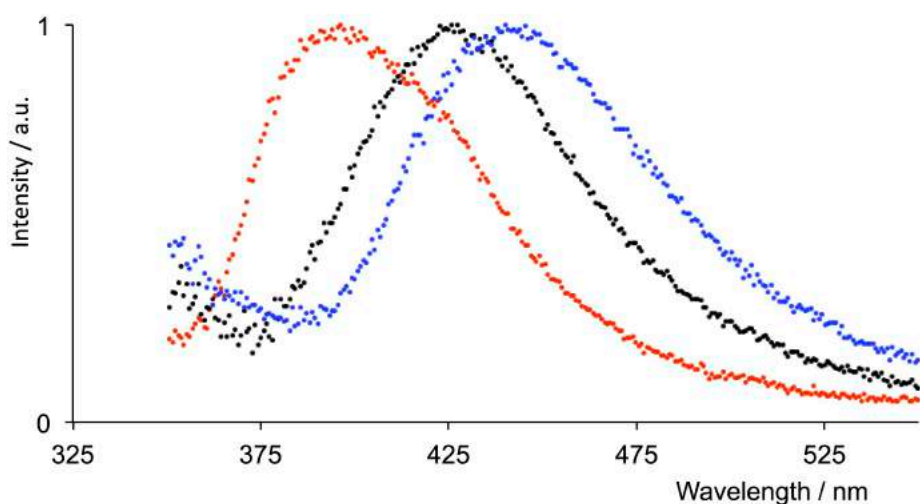
Fig. 11. Normalised emission spectra of **1** (red) [{$Zn_2(\mu$-OAc$)_4$(**1**)}$_n$] (black) and [{$Cd_2(OAc)_4$(**1**)$_2$}$_n$] (blue) in the solid state.

The Cd(II) complex behaves analogously to the Zn(II) one. In the solid state diffuse reflectance spectrum of crystalline [{$Cd_2(OAc)_4$(**1**)$_2$}$_n$] two broad bands with a minimum reflectance at 293 and 382 nm are to be seen and assigned to ligand-based transitions. As

for the previous complexes the absorption spectrum of an EtOH solution of $[\{Cd_2(OAc)_4(\mathbf{1})_2\}_n]$ shows the presence of free ligand **1** as well. This is also backed by the emission spectrum, which again mirrors that of **1**. Like the $[\{Zn_2(\mu\text{-}OAc)_4(\mathbf{1})\}_n]$ complex, the $[\{Cd_2(OAc)_4(\mathbf{1})_2\}_n]$ one is a blue emitter as well and a further red-shift is observed by going from the Zn (λ_{em} = 425 nm) to the Cd (λ_{em} = 439 nm), the latter one having a quantum yield of 9.5% (λ_{ex} = 300 nm).

In the diffuse reflectance spectrum of crystalline $[\{Cu_2(\mu\text{–}OAc)_4(\mathbf{1})\}_n]$ a broad band can be distinguished at 681 nm, corresponding to an MLCT process. Shoulders at 344 and 398 nm arise from ligand-based transitions. When the complex is dissolved in EtOH, these characteristics are lost and the observed bands (231 and 273 nm) match the spectrum of **1**, just as the emission behavior of an EtOH solution of the complex (λ_{em} = 388 nm with λ_{ex} = 280 nm) mirrors that of the free ligand. As for the solid state, the complex is non-emissive which is due to the fact that coordination of ligand **1** to the Cu(II) quenches the ligand-based emission[16, 17, 18, 19].

3.1.5 Experimental part

$[\{Zn_2(\mu\text{-}OAc)_4(\mathbf{1})\}_n]$: (ratio Zn:ligand = 1:1)

$Zn(OAc)_2 \cdot 2H_2O$ (10.9 mg, 0.0497 mmol) was added to a solution of **1** (19.1 mg, 0.0496 mmol) in CH_2Cl_2/MeOH (10 cm³, v/v, 3:1). The mixture was stirred at room temperature for 10 min and then split into several glass vials. Hexane was allowed to diffuse slowly into the vials and after several days, colourless crystals of $[\{Zn_2(\mu\text{-}OAc)_4(\mathbf{1})\}_n]$ had formed. A crystal was selected for structure determination. Method 1 was repeated using Et_2O in place of hexane. Colourless crystals of $[\{Zn_2(\mu\text{-}OAc)_4(\mathbf{1})\}_n]$ formed; the identity of the compound was confirmed by a crystal cell check (see text).

$[\{Zn_2(\mu\text{-}OAc)_4(\mathbf{1})\}_n]$: (ratio Zn:ligand = 2:1)

$Zn(OAc)_2 \cdot 2H_2O$ (21.8 mg, 0.0993 mmol) was added to a solution of **1** (19.1 mg, 0.0496 mmol) in CH_2Cl_2/MeOH (10 cm³, v/v, 3:1). The mixture was stirred at room temperature for 10 min and a precipitate appeared. Solvent was evaporated and the solid redissolved in MeOH. The solution was left to stand at room temperature and after several days, colourless crystals of $[\{Zn_2(\mu\text{-}OAc)_4(\mathbf{1})\}_n]$ had formed. IR (solid) v/cm^{-1} 3630w, 3500w, 3300w, 3150w, 3050w, 2925w, 2850w, 1684w, 1653m, 1595s, 1560s, 1533w, 1490m, 1394m, 1317w, 1271w, 1217w, 1121w, 1065m, 1060sh, 1001vs, 995vs, 950sh, 908s, 823vs, 764vs, 727m, 692m, 663m, 627m, 613sh, 540m.

$[\{Zn_2(\mu\text{-}OAc)_4(\mathbf{1})\}_n]$: (ratio Zn:ligand = 1:2)

Starting with with $Zn(OAc)_2 \cdot 2H_2O$ (5.5 mg, 0.025 mmol) and **1** (19.1 mg, 0.0496 mmol). Crystals $[\{Zn_2(\mu\text{-}OAc)_4(\mathbf{1})\}_n]$ grew after of diffusion of Et_2O into the CH_2Cl_2/MeOH solutions and the product was identified by a unit cell check. IR (solid) v/cm^{-1} 3630w, 3500w, 3053w, 3030w, 2923w, 2851w, 1684w, 1653m, 1593s, 1558m, 1533m, 1489m, 1448w, 1423w, 1393m, 1315w, 1269w, 1215w, 1118w, 1064sh, 1061m, 1038sh, 1004vs, 995vs, 950sh, 912s, 848sh, 820vs, 762s, 727m, 696s, 662s, 626s, 613m, 546m.

[{Zn$_2$(μ-OAc)$_4$(**1**)}$_n$]: (ratio Zn:ligand = 2:1)

A solution of **1** (19.1 mg, 0.0497 mmol) in CHCl$_3$ (6.0 mL) was placed in a long test tube and MeOH (3.0 cm^3) was layered over it. A solution of Zn(OAc)$_2$·2H$_2$O (21.8 mg, 0.0993 mmol) in MeOH (5.0 cm^3) was layered over the MeOH. The tube was sealed with parafilm and left to stand for 10 d at room temperature. Colourless crystals formed at the MeOH/CHCl$_3$ interface and were isolated by decantation. . IR (solid) v/cm^{-1} 3630w, 3500w, 3050w, 2926w, 2852w, 1684w, 1653m, 1637w, 1591m, 1562m, 1530sh, 1420m, 1394m, 1320w, 1270w, 1217m, 1198sh, 1116w, 1065m, 1064sh, 1049m, 1004vs, 991vs, 950sh, 914s, 837vs, 762s, 730m, 685m, 663m, 613m, 543m. ESI MS m/z 386.2 [1+H]$^+$ (base peak, calc. 386.2). *Anal.* calc. for C$_{35}$H$_{31}$N$_3$O$_8$Zn$_2$ + 1/5 MeOH: C, 55.49; H, 4.33; N, 5.47. Found: C, 54.88; H, 4.24; N, 5.53%.

[{Cu$_2$(μ-OAc)$_4$(**1**)}$_n$]

A solution of **1** (19.1 mg, 0.050 mmol) in CHCl$_3$ (6.0 cm^3) was placed in a long test tube and MeOH (3.0 cm^3) was layered on the solution. A solution of Cu(OAc)$_2$·H$_2$O (18.5 mg, 0.10 mmol) in MeOH (5.0 cm^3) was layered over the MeOH, and the tube was sealed with parafilm and left to stand for 3 weeks at room temperature. Turquoise crystals of [{Cu$_2$(μ-OAc)$_4$(**1**)}$_n$] formed at the interface and were isolated by decantation. *Anal.* calc. for C$_{35}$H$_{31}$Cu$_2$N$_3$O$_8$ + H$_2$O: C, 54.83; H, 4.34; N, 5.48. Found: C, 54.99; H, 4.30; N, 5.62%.

[{Cd$_2$(μ,κ^3-O,O':O'-OAc)$_2$(κ^2-O,O'-OAc)$_2$(**1**)}$_n$]

The method was as for [{Cu$_2$(μ-OAc)$_4$(**1**)}$_n$] starting with **1** (19.1 mg, 0.050 mmol) and Cd(OAc)$_2$·2H$_2$O (26.7 mg, 0.10 mmol). Small, colourless crystals of [{Cd$_2$(μ,κ^3-O,O':O'-OAc)$_2$(κ^2-O,O'-OAc)$_2$(**1**)}$_n$] were isolated by decantation.

Crystallography

[{Zn$_2$(μ-OAc)$_4$(**1**)}$_n$]

C$_{35}$H$_{31}$N$_3$O$_8$Zn$_2$, M = 752.41, colourless block, monoclinic, space group $C2/c$, a = 26.210(5), b = 16.151(2), c = 8.3410(15) Å, $β$ = 108.050(14)°, U = 3357.0(9) Å^3, Z = 4, D_{calc} = 1.489 Mg m^{-3}, μ(Mo-Kα) = 1.485 mm^{-1}, T = 173 K. Total 39 302 reflections, 3356 unique, R_{int} = 0.0841. Refinement of 3096 reflections (222 parameters) with $I > 2σ(I)$ converged at final R_1 = 0.0393 (R_1 all data = 0.0434), wR_2 = 0.0920 (wR_2 all data = 0.0937), Goodness-of-fit (GOF) = 1.261.

[{Cu$_2$(μ-OAc)$_4$(**1**)}$_n$]

C$_{35}$H$_{31}$Cu$_2$N$_3$O$_8$, M = 748.73, green block, monoclinic, space group $C2/c$, a = 26.0528(9), b = 16.1512(9), c = 8.2267(3) Å, $β$ = 108.113(2)°, U = 3290.1(2) Å^3, Z = 4, D_{calc} = 1.512 Mg m^{-3}, μ(Mo-Kα) = 1.350 mm^{-1}, T = 123 K. Total 57 542 reflections, 4365 unique, R_{int} = 0.0367. Refinement of 3761 reflections (222 parameters) with $I > 2σ(I)$ converged at final R_1 = 0.0308 (R_1 all data = 0.0384), wR_2 = 0.0877 (wR_2 all data = 0.0924), Goodness-of-fit (GOF) = 1.070.

[{Cd$_2$(μ,κ^3-O,O':O'-OAc)$_2$(κ^2-O,O'-OAc)$_2$(**1**)}$_n$]

After SQUEEZE: C$_{62}$H$_{50}$Cd$_2$N$_6$O$_8$, M = 1231.90, colourless block, triclinic, space group P-1, a = 9.8395(15), b = 11.6635(18), c = 26.523(4) Å, $α$ = 96.577(10), $β$ = 97.513(9), $γ$ = 96.040(1

0)°, U = 2975.5(8) Å^3, Z = 2, D_{calc} = 1.374 Mg m^{-3}, μ(Mo-Kα) = 0.772 mm^{-1}, T = 123 K. Total 35 702 reflections, 11 083 unique, R_{int} = 0.0818. Refinement of 5292 reflections (708 parameters) with $I > 2\sigma(I)$ converged at final R_1 = 0.1135 (R_1 all data = 0.1715), wR_2 = 0.2810 (wR_2 all data = 0.3199), Goodness-of-fit (GOF) = 0.496.

3.2. Structures with ligands 2 and 3

3.2.1 Reactions of 3 with Zn(OAc)$_2$.2H$_2$O

A three-layer crystallization set-up where the ligand **3** was dissolved in in CHCl$_3$ and Zn(OAc)$_2$.H$_2$O in MeOH and the middle layer being just MeOH was performed. Yellow plates suitable for X-ray crystallography were collected and the structural determination showed that a one-dimensional, helical polymer [{Zn(OAc)$_2$(**3**)}n]. Upon taking the crystals out of the solution, rapid solvent loss proved to be a problem and therefore numerous crystals were measured. The bulk sample turned out to me made up from two types of yellow plates, either the racemate crystallizing in the centrosymmetric group Pnna or as the homochiral complex in the space group P2$_1$2$_1$2$_1$. The two different crystals were obtained starting from achiral building blocks, from the same vial and under the same conditions. Simultaneous formation of homo- and heterochiral coordination polymers from achiral modules is not a common observation[20], but may be assisted by judicious ligand design[21]. Pertinent to the system described here is a report from Li and coworkers that both homo- and heterochiral [{ZnCl$_2$(4'-tolyl-4,2':6',4''-tpy)}n] assemble during the reaction of ZnCl$_2$ with 4'-tolyl-4,2':6',4''-tpy in EtOG and water at 140°C[22].
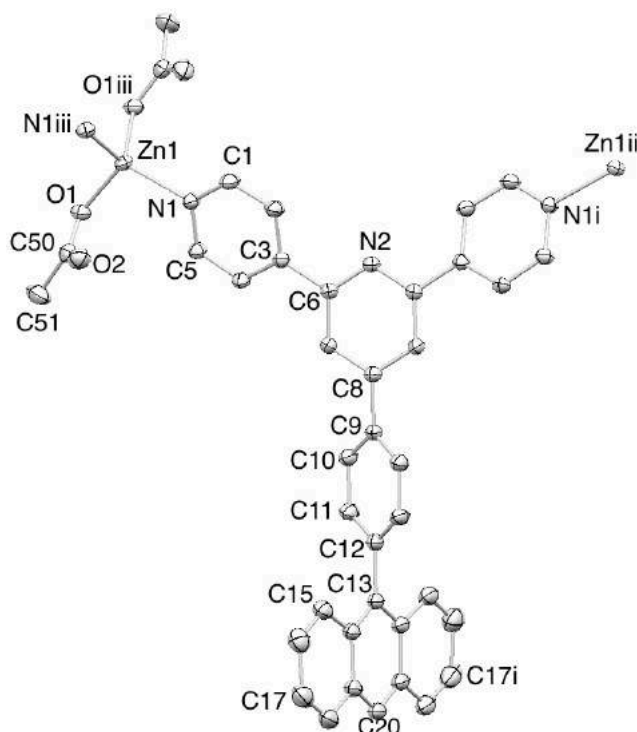

Fig. 12. Repeat unit in the polymer chain in 2[{Zn(OAc)$_2$(**3**)}n].CHCl$_3$.2H$_2$O (ellipsoids plotted at 40% probability level and H atoms omitted).

Fig. 12 shows the repeat unit in one chain of the coordination polymer $2[\{Zn(OAc)_2(\mathbf{3})\}_n]$.$CHCl_3.2H_2O$ where the two halves of ligand **3** are complementary by a 2-fold axis passing from atom N2 through to C20. The coordination sphere around the metal Zn1 has a tetrahedral geometry where the bond angles range from 100.85(8)° to 114.29(8)°. Metal Zn^{2+} ions are connected to the ligand via the outlying pyridine rings (through atoms N1 and N1i) leaving N2 uncoordinated. There is a twisting of the tpy unit (angle between A and B rings 19.2°), which is the origin of the helical twist of the whole polymer chain. As far as the twisting in the remaining part of the molecule is concerned, the values are similar to the free ligand **3** (B/C 38.1° and C/D 64.7°). The different chains that make up the coordination polymer stack with P- and M-helices neighboring to one another and with anthracene moieties lying on top of the pyridine ring, which contains atom N2[iii] of the adjoining chain (Fig. 13).
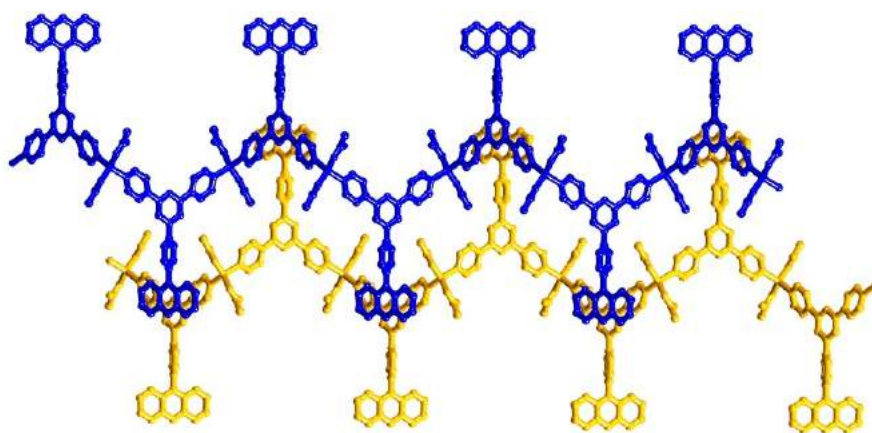
Fig. 13. Face-to-face stacking interactions between anthracene and tpy domains of chains of opposite handedness (H atoms omitted).

The face-to-face stacking is efficient as the angle between the mean planes is just 0.2° (distance between centroids 3.87 Å). Solvent molecules (modeled as disordered $CHCl_3$, MeOH and H_2O) fill the voids in the lattice.

Due to crystals of the homochiral polymer M-$[\{Zn(OAc)_2(\mathbf{3})\}_n]$ being subject to rapid solvent loss the data quality was low and therefore SQUEEZE[10] had to be used in order to refine the structure. It is inconclusive if the two obtained structures are polymorphs (as in Ref. 22) because due to the disorder, the solvent molecules could not be identified. The two exterior pyridine rings are crystallographically independent and the angles between the rings contining N1/N2 and N2/N3 are 16.5° and 5.9°. These values being different than in the racemate, leads to distinct pitches of the helical chains in the two polymers. The ligand-bridged Zn…Zn distances in the polymers are expected to be similar; the separation of pairs of alternate Zn atoms does in fact depend upon the pitch of the helix (Fig. 14).
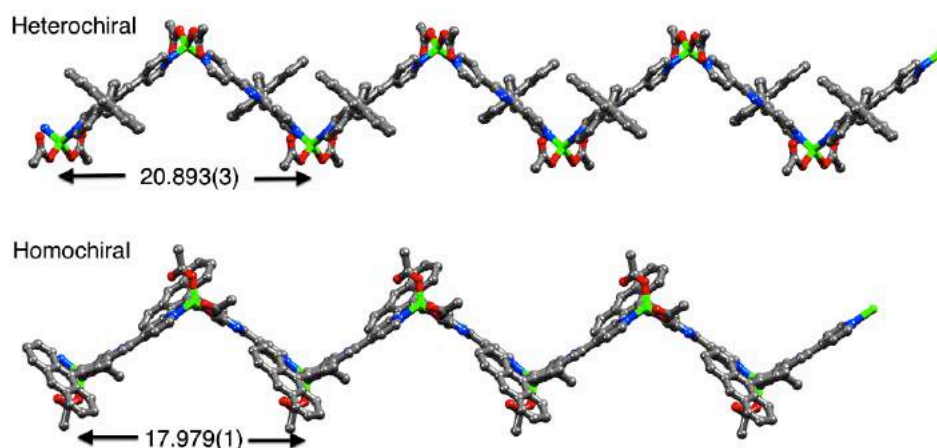
Fig. 14. Comparison of the pitches of the helical chains in heterochiral and homochiral [{Zn(OAc)$_2$(**3**)}$_n$]. Distances are Zn..Zn separations in Å; H atoms omitted.

Face-to–face interactions between anthracene and tpy moieties make up the packing of the polymer chains. Tpy and anthracene parts of a given ligand in the racemate, stack with anthracene and tpy domains respectively of different neighboring chains. In M-[{Zn(OAc)$_2$(**3**)}$_n$] tpy and anthracene units of a given ligand engage in a head-to-tail interaction with anthracene and tpy domains respectively with a single ligand of a neighboring chain (Fig. 15). The more efficient inter-chain stacking interactions in the homochiral versus heterochiral polymer mimic the observations of Li and coworkers[22]; these authors argue that denser packing encourages spontaneous resolution.
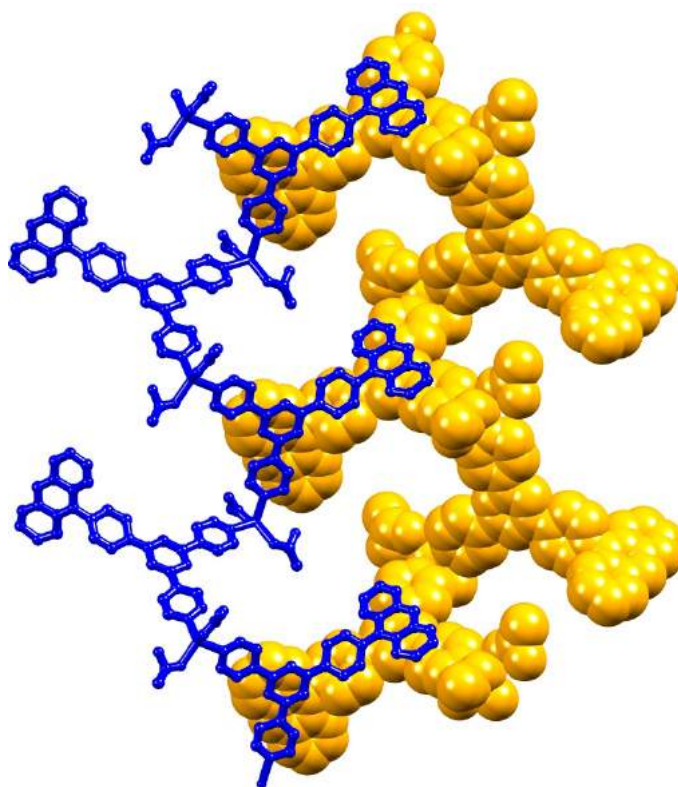
Fig. 15. Stacking interactions between anthracene and tpy domains in adjacent chains of M-[{Zn(OAc)$_2$(**3**)}$_n$].

3.2.2 Reactions of **2** with Zn(OAc)$_2$.2H$_2$O

Using the same conditions as for ligand **3**, ligand **2** and Zn(OAc)$_2$.2H$_2$O were reacted in a long vial. Even though this setup yielded crystals, their quality always proved to be poor. Preliminary crystallographic data confirmed that the coordination polymer [{Zn$_2$(μ-OAc)$_4$(**2**)}$_n$], which is analogous to the structure obtained with ligand **1** was made. Nevertheless it can be assumed that a structure containing the paddle-wheel nodes still forms when a naphthyl group replaces the terminal phenyl substituent but not when an anthracyl moiety is introduced in which case a mononuclear {Zn(OAc)$_2$} is involved. Just as with the ligand **1**, reactions with Zn(OAc)$_2$.2H$_2$O were put by varying the metal to ligand ratio. Again, the ligand was dissolved in CH$_2$Cl$_2$/MeOH (3:1) and the metal salt was added to the reaction mixture in its solid form. A variety of techniques were used afterwards in order to grow crystals from the solution. Using a 1:2 ratio of Zn$^{2+}$:**2** some X-ray quality single crystals (colorless blocks) were obtained and structural determination confirmed a one-dimensional coordination polymer 2[{Zn$_7$(μ-OAc)$_{10}$(μ$_4$-O)$_2$(**2**)}$_n$].CH$_2$Cl$_2$. By using a higher Zn^{2+}:**2** ratio the formation of this product was attempted to be forced and its yield increased but without any success. The space group in which the complex crystallizes in is orthorhombic, P2$_1$2$_1$2$_1$ and has a Flack parameter of 0.489(14), which is consistent with twinning by inversion. The structure of the repeat unit of the complex can be seen in Fig. 16.
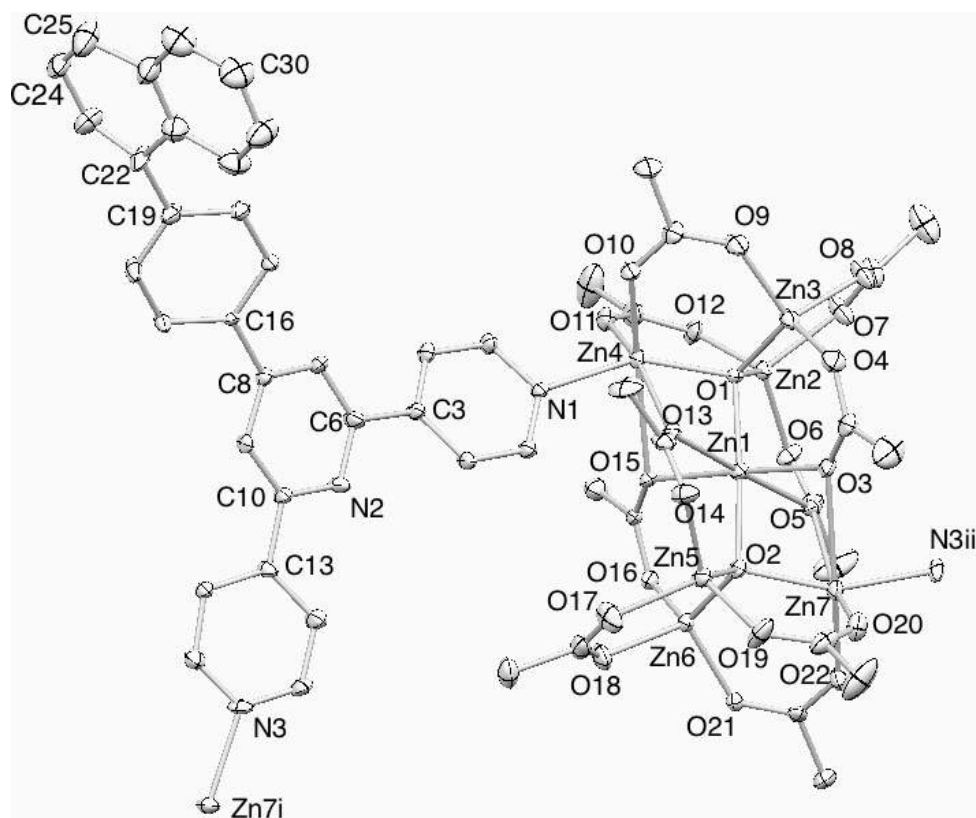
Fig. 16. Repeat unit in the polymer chain in 2[{Zn$_7$(μ-OAc)$_{10}$(μ$_4$-O)$_2$(**2**)}$_n$].CH$_2$Cl$_2$ (ellipsoids plotted at 30% probability level; H atoms omitted).

Even though crystallization in this chiral space group excludes the presence of a crystallographic inversion centre, the cluster {Zn$_7$(μ-OAc)$_{10}$(μ$_4$-O)$_2$} is best described as

centrosymmetric. All examples of this structural motif in the CSD are centrosymmetric[23-31]. The coordination sphere around the central Zn1 atom is octahedral, both O1 and O2 are oxido ligands and connect four Zn atoms in an approximately tetrahedral cluster. Atom pairs are either bridged by acetate ligands in a μ–O,O' mode or by acetato ligands which adopt μ,κ-O, O':O' mode. The coordination sphere of atoms Zn2, Zn3, Zn5 and Zn6 is tetrahedral while the one of Zn4 and Zn7 is octahedral (Fig. 17).
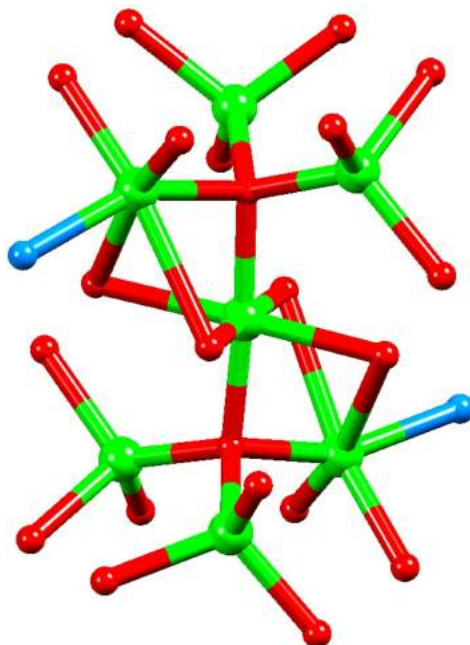
Fig. 17. Connectivities in the Zn$_7$-cluster.

As can be seen on Fig. 16 the cluster is connected to ligand **3** via atoms N1 and N3[ii]. The twist in the tpy part (angle between rings containing N1/N2 is 29.2^o and 21.3^o between rings containing N2/N3) is responsible for the helical twist of the whole polymer. Chains of the same handedness pack in a way that the naphthyl moieties are enclosed within a cavity between two tpy units (Fig. 18).
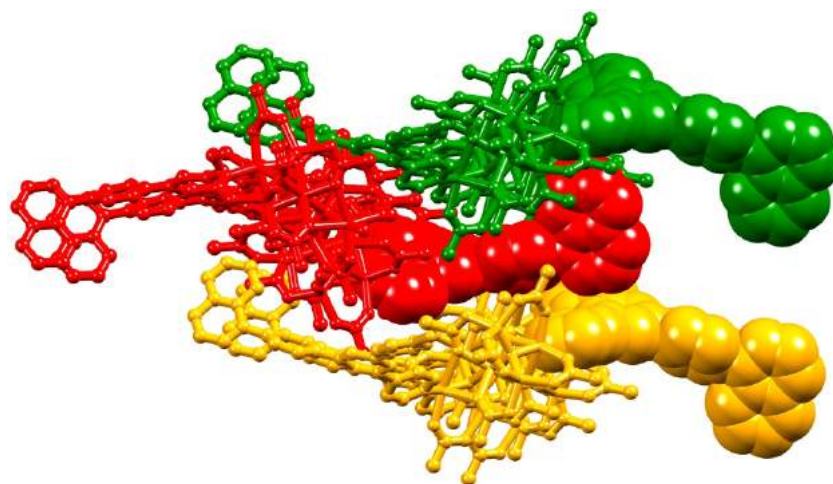
Fig. 18. Packing of chains in (H atoms and CH$_2$Cl$_2$ molecules omitted) viewed down the c-axis.

Edge-to-face interactions take place between the naphthyl substituent (edge) and the tpy part (CH…centroid distances of 2.8 and 2.65 Å).
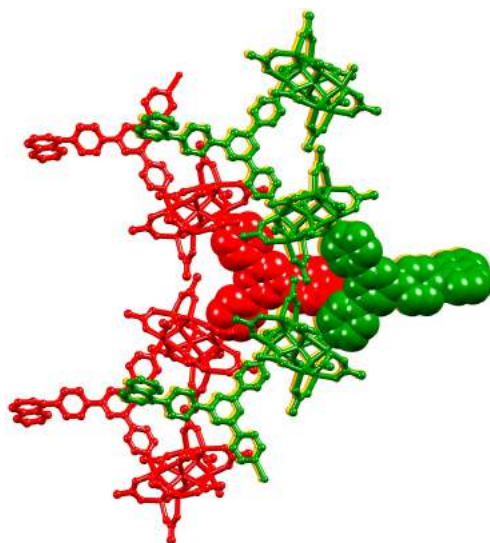
Fig. 19. Packing of chains in (H atoms and CH_2Cl_2 molecules omitted) viewed down the a-axis.

Four examples of coordination polymers containing the same cluster have previously been reported[26, 30, 31]. All were synthesized using a 7:1 ratio of metal: bridging ligand, which contrasts to the assembly described here. Our example is reminiscent of the unexpected assembly of the discrete cluster $[Zn_7(\mu\text{-OAc})_{10}(\mu_4\text{-O})_2(pz)_2]$ (pz = pyrazine) from reaction of equimolar amounts of pz and $Zn(OAc)_2\cdot 2H_2O$[25], or the formation of $[Zn_7(\mu\text{-OAc})_{10}(\mu_4\text{-O})_2(3\text{-}HOCH_2py)_2]$ (3-$HOCH_2py$ = 3-hydroxymethylpyridine) from the 2:1 reaction of $Zn(OAc)_2.2H_2O$ with $Ph_2P(3\text{-}OCH_2py)$[27]. The appearance of this heptazinc motif is very scarce compared to that of $[Zn_4(\mu\text{-OAc})_6(\mu_4\text{-O})]$ (basic zinc acetate)[32], derivatives of which are widespread building blocks in metal–organic frameworks[33]. The driving forces which favour the assembly of {Zn7(μ-OAc)10(μ4-O)2} clusters remain to be explored.

3.2.3 Absorption and emission spectroscopic properties

The electronic absorption spectra of EtOH solutions of ligands **2** and **3** can be seen in Fig. 20.
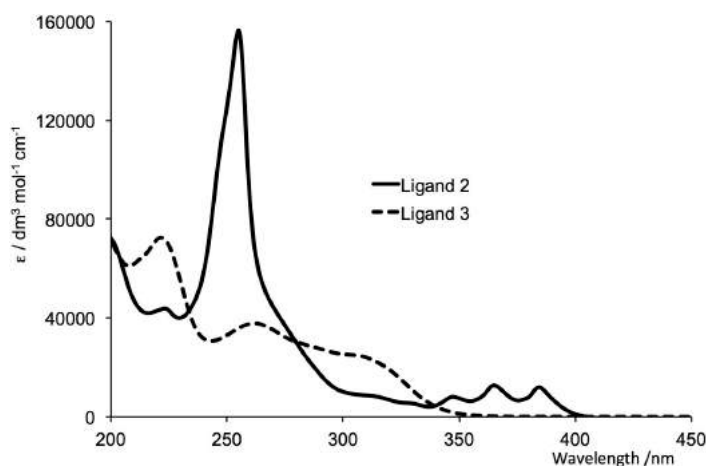
Fig. 20. Absorption spectra of EtOH solutions of **2** and **3** (1.10^{-5} mol.dm^{-3}).

58

Between 350 and 400 nm the fine structure is typical of the anthracene moiety. By going from a naphthyl substituent to an anthracyl, the shift to lower energy in the absorption bands in consistent with the extension of the π-conjugation. Exciting EtOH solutions of ligands **2** and **3** lead to broad emission at 480 and 440 nm repectively (Fig. 21) with quantum yields of 12 and 52%.
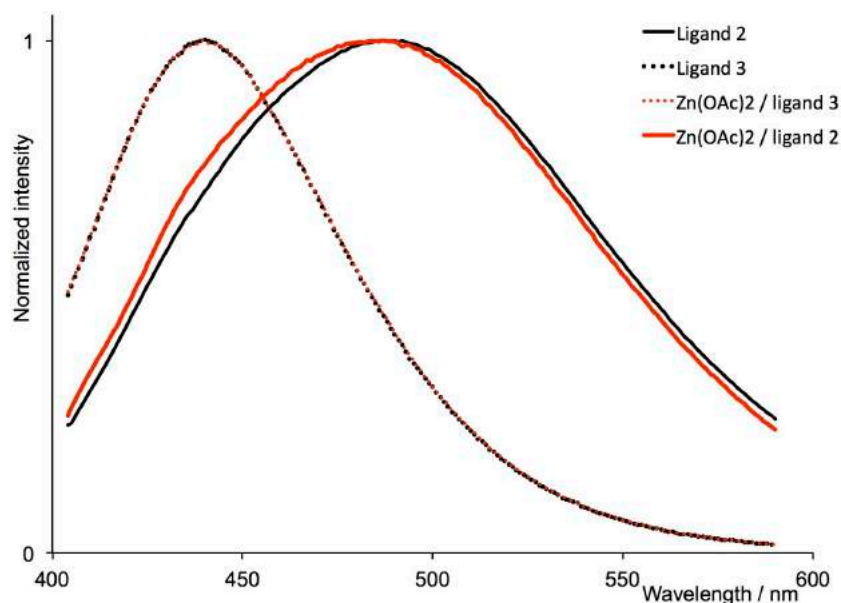
Fig. 21. Emission spectra of EtOH solutions of **3** (λ_{ex} = 365 nm), **2** (λ_{ex} = 305 nm), [{Zn(OAc)$_2$(**3**)}$_n$] (λ_{ex} = 365 nm) and [{Zn$_2$(μ-OAc)$_4$(**2**)}$_n$] (λ_{ex} = 313 nm).

The coordination polymers dissociate in solution as confirmed by the fact that the emission spectra of EtOH of bulk samples of the complexes mirror those of the free ligands **2** and **3**. Powdered-crystalline samples were prepared in order to study the solid state emission behavior of the ligands and their complexes. When ligand **3** was excited at 280 nm an emission at 510 nm was observed, which is red-shifted from the solution value of 480 nm. The emission is almost quenched after complexation with Zn(OAc)$_2$ occurs which might be due to the fact that in the solid-state ligand anthracene units stack with one another whereas in the complex anthracene parts interact with a tpy domain. In the case of ligand **2** (λ_{ex} = 370 nm) the observed emission maximum was 416 nm and in [{Zn$_2$(μ-OAc)$_4$(**2**)}$_n$] a red-shift to 434 nm occurs (λ_{ex} = 330 nm). Such a red-shift upon complexation is consistent with the one observed for ligand **1**. The quantum yield of the solid-state emission of that complex is 1.6% that is the same as the one of the free ligand **2** in the solid state (1.7%).

3.2.4 Experimental part

[{Zn(OAc)$_2$(**3**)}$_n$]

A solution of **3** (24.1 mg, 0.050 mmol) in CHCl$_3$ (6.0 cm^3) was placed in a test tube (1.5 × 15 cm). Then MeOH (3.0 cm^3) was layered on the top of the solution, followed by a solution of Zn(OAc)$_2$·2H$_2$O (21.8 mg, 0.050 mmol) in MeOH (5.0 cm^3). The test tube was sealed with parafilm and allowed to stand for 10 d at room temperature. Crystals formed at

the interface and were isolated by decantation. Satisfactory elemental analysis for the bulk sample could not be obtained.

[{Zn₂(µ-OAc)₄(**2**)}ₙ]

A solution of **2** (21.6 mg, 0.050 mmol) in $CHCl_3$ (6.0 cm^3) was placed in a test tube (1.5 × 15 cm). Methanol (3.0 cm^3) was layered on the top of the first solution, followed by a solution of $Zn(OAc)_2 \cdot 2H_2O$ (21.8 mg, 0.050 mmol) in MeOH (5.0 cm^3). The test tube was sealed with parafilm and allowed to stand for 10 d at room temperature. Colourless crystals formed at the interface and were isolated by decantation. Found: C 57.03, H 4.43, N 5.21; $C_{39}H_{33}N_3O_8Zn_2 \cdot H_2O$ requires C 57.09, H 4.30, N 5.12%.

[{Zn₇(µ-OAc)₁₀(µ₄-O)₂(**2**}ₙ]

Solid $Zn(OAc)_2 \cdot 2H_2O$ (5.5 mg, 0.0250 mmol) was added to a solution of ligand **2** (21.6 mg, 0.0500 mmol) in CH_2Cl_2/MeOH (10 cm^3, v/v, 3:1). The reaction mixture was stirred at room temperature for 10 min, and was then split into several small vials. After standing at room temperature for several days, a few crystals formed. Insufficient material was obtained for analysis of the bulk sample.

Crystallography

2[{Zn(OAc)₂(**3**)}ₙ]·CHCl₃·5MeOH·2H₂O

$C_{84}H_{83}Cl_3N_6O_{15}Zn_2$, M = 1653.70, yellow plate, orthorhombic, space group $Pnna$, a = 20.402(3), b = 20.893(3), c = 9.0595(11) Å, U = 3861.7(8) $Å^3$, Z = 2, D_c = 1.419 Mg m^{-3}, μ(Mo Kα) = 0.796 mm^{-1}, T = 123 K. Total 62344 reflections, 4658 unique, R_{int} = 0.0638. Refinement of 3279 reflections (302 parameters) with $I > 2\sigma(I)$ converged at final R_1 = 0.0430 (R_1 all data = 0.0734), wR_2 = 0.1092 (wR_2 all data = 0.1305), goodness-of-fit = 1.078.

M-[{Zn(OAc)₂(**3**)}ₙ]

After SQUEEZE: $C_{39}H_{29}N_3O_4Zn$, M = 669.04, yellow plate, orthorhombic, space group $P2_12_12_1$, a = 8.5662(4), b = 17.9692(8), c = 30.9785(15) Å, U = 4768.5(4) $Å^3$, Z = 4, D_c = 0.932 Mg m^{-3}, μ(Mo Kα) = 0.547 mm^{-1}, T = 123 K. Total 46559 reflections, 10071 unique, R_{int} = 0.1128. Refinement of 4404 reflections (404 parameters) with $I > 2\sigma(I)$ converged at final R_1 = 0.0946 (R_1 all data = 0.1630), wR_2 = 0.2255 (wR_2 all data = 0.2559), goodness-of-fit = 0.876, Flack parameter = 0.146(18).

2[{Zn₇(µ-OAc)₁₀(µ₄-O)₂(**2**)}ₙ]·CH₂Cl₂

$C_{103}H_{104}Cl_2N_6O_{44}Zn_{14}$, M = 3116.29, colourless block, orthorhombic, space group $P2_12_12_1$, a = 11.861(2), b = 20.370(4), c = 25.040(5) Å, U = 6050(2) $Å^3$, Z = 2, D_c = 1.711 Mg m^{-3}, μ(Mo Kα) = 2.849 mm^{-1}, T = 123 K. Total 99202 reflections, 12154 unique, R_{int} = 0.0633. Refinement of 9577 reflections (786 parameters) with $I > 2\sigma(I)$ converged at final R_1 = 0.0594 (R_1 all data = 0.0930), wR_2 = 0.1567 (wR_2 all data = 0.2024), goodness-of-fit = 1.166, Flack parameter = 0.489(14).

3.3. Structures with ligand 6

The replacement of hydrogen in a compound by fluorine may significantly alter solid-state packing interactions. The classic example concerns the crystal packing in solid benzene or hexafluorobenzene versus a 1:1 co-crystallized mixture. Both C_6H_6[34] and C_6F_6[35] exhibit edge-to-face CX...π interactions (X = H[36-38] or F[39]), while the co-crystallized material has infinite columns of alternating C_6D_6 and C_6F_6 molecules which interact through π-stacking interactions[40, 41]. Molecular assembly directed by such arene...perfluoroarene interactions is now well recognized[42]. A wider perspective has been taken by Hulliger and coworkers who have surveyed the roles played in crystal engineering by phenyl...perfluorophenyl (abbreviated as πH...πF), CF...H, F...F and CF...πF interactions; they concluded (in 2005) that 'the role of fluorine in crystal engineering is not yet clear in detail[43]. An update of this picture appeared in 2011, adding CF...M+, CF...C=O and anion...πF contacts to packing interactions in fluorine-containing compounds[44]. Although πH..πF stacking has gained significant attention in crystal engineering and has been utilized to direct host–guest complex formation[45], the coexistence of arene and perfluoroarene rings does not necessarily result in such interactions. Competitive packing motifs may predominate, and hydrogen bonds in particular are favoured over πH...πF contacts[44]. (The strength of the face-to-face πH...πF interaction is ca. 20 to 25 kJ mol^{-1} [42].)

Surprisingly, the use of phenyl...perfluorophenyl interactions to direct the assembly of coordination polymers has received little attention. Reaction of 1,4-bis(4′-pyridylethynyl)-tetrafluorobenzene with zinc(II) nitrate results in the formation of a one-dimensional polymer in which zig-zag chains interact with each other through π_{alkyne}...πF and π_{alkyne}...π pyridine interactions; there is no πH...πF stacking[46]. The related ligand 1,4-bis(4′-pyridyl-methyl)tetrafluorobenzene reacts with $Cd(NO_3)_2$ and aniline to give a one-dimensional coordination polymer in which {$Cd(NO_3)_2(C_6H_5NH_2)_2$} nodes are connected by bridging ligands. In this case, adjacent chains interact through πH...πF stacking. However, replacing aniline by 4-bromoaniline turns off the inter-chain πH...πF interactions[47].

3.3.1 Reactions of **6** with CuOAc)$_2$.H$_2$O

Ligand **6** was dissolved in $CHCl_3$, put into a big vial and a solution of CuOAc)$_2$.H$_2$O in MeOH was carefully layered on top which yielded X-ray quality single crystals of [$Cu_2(\mu\text{-OAc})_4$(**2**)]$_n$. This formula was confirmed by matching elemental analysis and the powder diffraction pattern corresponded to the theoretical calculated one (using the single crystal data). Just as for the complex with ligand **1**, this polymer crystallizes in the space group C2/c, which is monoclinic and the cell dimensions of those two structures are very similar. The compound is practically isostructural to its analogue that contains ligand **1**, which means that replacing the terminal phenyl ring by a pentafluorophenyl one has little effect on the structure in this example. The central N atom of ligand **6** (which acts like a bridge) is uncoordinated while the other two N atoms connect to {$Cu_2(OAc)_4$} paddle-wheel motifs. The two acetate ligands being disordered have therefore been modeled over two positions with site occupancies of 0.36/0.64 and 0.40/0.60, respectively. As shown in Fig. 22 the asymmetric unit contains half of the ligand **2** and half of one paddle-wheel unit, the second part of the polymer's repeat unit being generated by a 2-fold axis.
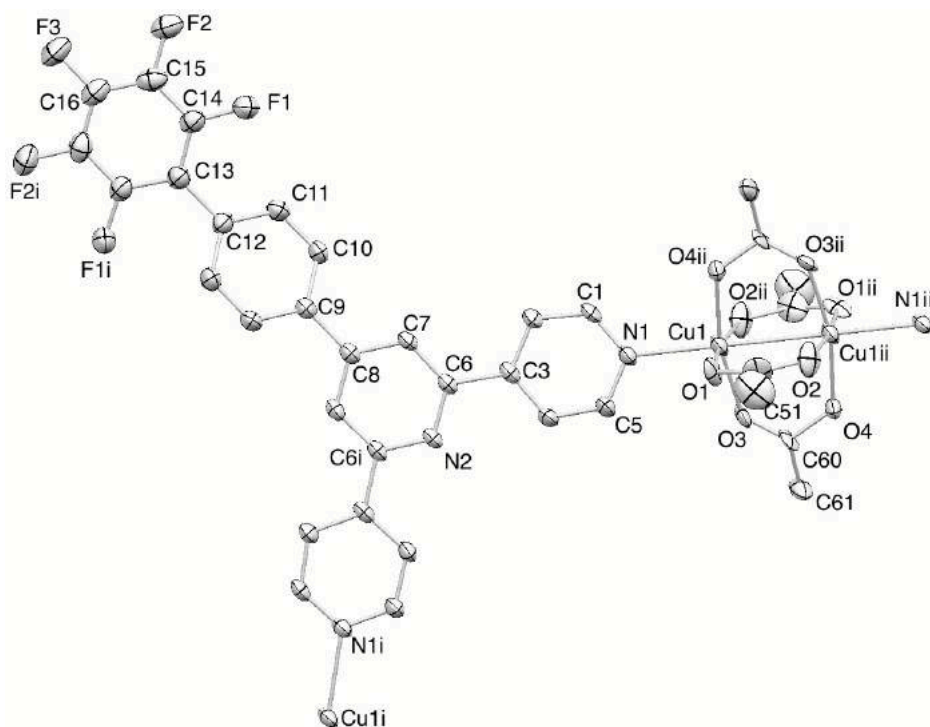
Fig. 22. ORTEP representation of the repeat unit in $[Cu_2(\mu\text{-OAc})_4(\mathbf{6})]_n$ (ellipsoids were plotted at the 30% probability level, and H atoms were omitted for clarity.

The distance between the two metal centers, which is 2.6358(8) Å is typical for such a Cu–Cu paddle-wheel motif[48]. Packing of zig-zag chains implicates the formation of sheets, which in turn stack between each-other via their arene domains. As can be seen on the left-hand side of Fig. 23 the pentafluorophenyl unit slots into the V-shaped cavity of a tpy domain of the adjacent chain with short $CH_{methyl}\cdots F$ (2.51 Å) and $CH_{tpy}\cdots F$ contacts (2.42 and 2.54 Å). These interactions do not seem to be very significant for the assembly of the chains into sheets as for the analogous structure containing ligand **1**, they are simply replaced by CH···H contacts.

Fig. 23. Packing motifs in $[Cu_2(\mu\text{-OAc})_4(\mathbf{6})]_n$: short CH···F contacts shown in red (left) and $\pi_H\cdots\pi_F$ interactions shown in space-filling representation (right).

Tpy-tpy π interactions between chains in adjacent sheets are to be seen in Fig. 24 and are typical for structures containing such tpy's and Zn or Cu paddle-wheel moieties[1-3]. Pyridine rings stack in a face-to-face manner, with the distance between them being 3.48 Å. Finally, pentafluorobiphenyl domains stack in a head-to-tail manner (Fig. 23) yielding $\pi_H...\pi_F$ interactions. Since there is a twist between the pentafluorophenyl part and the phenylene ring it is bonded to (31.5°), the π-interaction is not completely efficient.
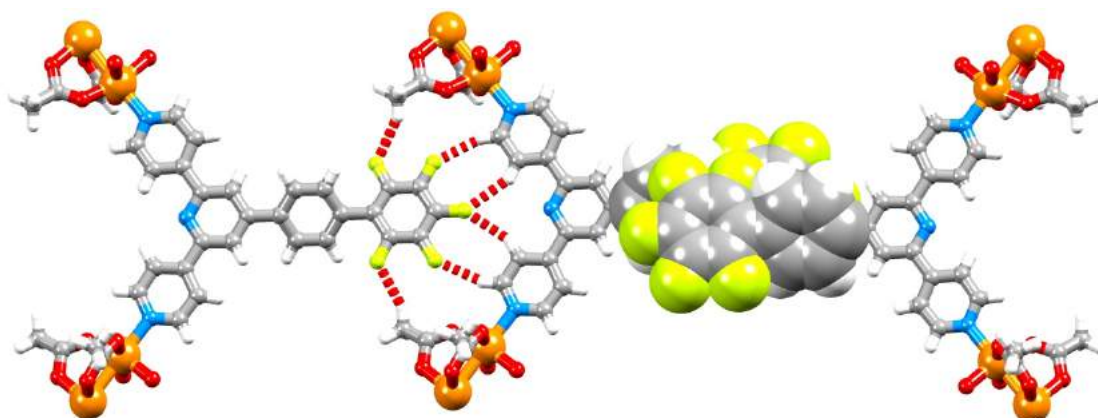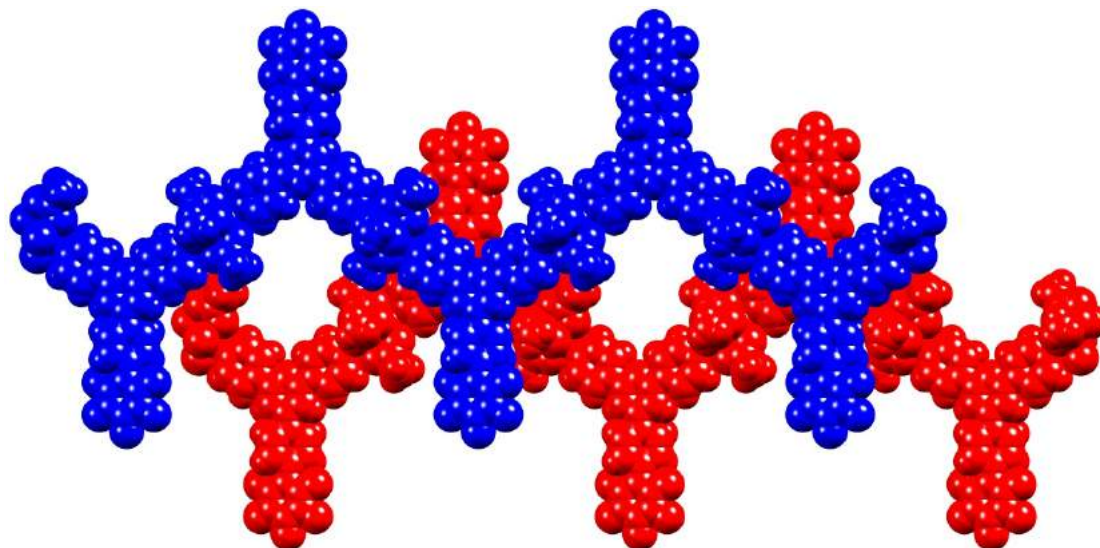

Fig. 24. Packing motifs in [Cu$_2$(μ-OAc)$_4$(**6**)]*n*: tpy...tpy π interactions between zig-zag chains.

3.3.2 Co-crystallization of **1** and **6** with CuOAc)$_2$.H$_2$O

Cu(OAc)$_2$.H$_2$O was reacted with a 1:1 mixture of ligands **1** and **6** in order to find out if the phenyl and pentafluorophenyl substituents recognize one another in the crystal packing. Elemental analysis of the bulk sample confirmed that the overall stoichiometry was [Cu$_2$(μ-OAc)$_4$(**1**)]*n*.[Cu$_2$(μ-OAc)$_4$(**6**)]*n*. The cell dimensions were virtually the same as those for the two isolated coordination polymers containing either ligand **1** or **6** and the product crystallizes in the space group C2/c, which is monoclinic. In fact, it is confirmed by the structural analysis that the asymmetric unit contains both ligands superimposed, which means that the terminal phenyl or pentafluorophenyl ring is disordered and has therefore been modeled with a 0.5/0.5 site occupancy. If the structure would be more ordered, and the position of each ligand better defined (alternating ligands) the unit cell would have to be bigger and more reflections would have to be observed compared to the original intensities, which was not the case. Thus the only sensible way to describe this structure is by considering a disordered model. The powder diffraction pattern for the bulk sample matched with the pattern that was calculated from the single crystal diffraction data.

3.3.3 Reactions of **6** with Zn(OAc)$_2$.2H$_2$O

Knowing that Zn(OAc)$_2$.2H$_2$O reacts with **1** and a number of other 4'-functionalized 4,2':6,4''-tpys[1-3] to give one-dimensional polymers with the same assembly motifs as [Cu$_2$(μ-OAc)$_4$(**1**)]*n* and [Cu$_2$(μ-OAc)$_4$(**6**)]*n*, we expected that reaction of Zn(OAc)$_2$·2H$_2$O with **6** would give [Zn$_2$(μ-OAc)$_4$(**6**)]*n*.

Ligand **6** was reacted with two equivalents of $Zn(OAc)_2.2H_2O$ in a big test tube using the layering technique, which gave colorless blocks and plates. Analysis of the blocks indicated that the one-dimensional coordination polymer $[Zn_2(\mu\text{-}OAc)_4(\textbf{6})]_n$, which is isostructural to its Cu analogue with the same ligand and the Zn and Cu analogues with ligand **1**, was formed and crystallizes in the monoclinic space group C2/c. All attempts to obtain a good quality structure failed. Structure determination by X-ray crystallographic analysis of the plates displayed the formation of $[Zn_5(OAc)_{10}(\textbf{6})_4.11H_2O]_n$, which is an unexpected one-dimensional coordination polymer where four ligands **6** act like bridges and are associated with five Zn atoms. The repeat unit, shown in Fig. 25 consists of five crystallographically independent Zn
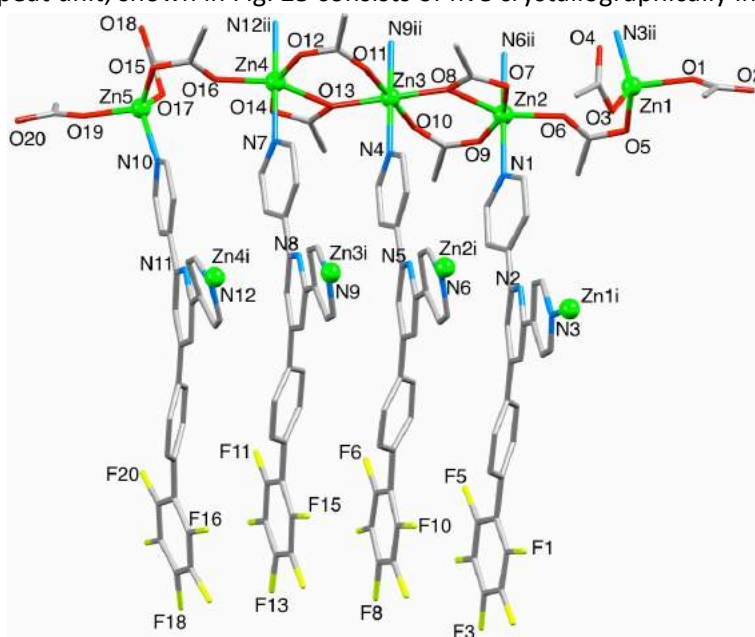
Fig. 25. Repeat unit of the polymer $[Zn_5(OAc)_{10}(\textbf{6})_4.11H_2O]_n$.

atoms , of which Zn1 and Zn5 have a tetrahedral coordination sphere whereas Zn2, Zn3 and Zn4 have a six-membered one. Zn1 and Zn5 thus have a comparable coordination environment being connected to two monodentate (terminal) acetate ligands, one N donor (of a bridging ligand **6**) and one O donor of an acetate ligand that also acts as a bridge. There is a disorder in the monodentate acetato ligands (containing O1/O2 and O17/O18), which have been modeled over two positions 0.51/0.49 and 0.54/0.46. Zn2, 3 and 4 each contain a N_2O_4 coordination shell consisting of trans-N donors and acetato ligands that connect the metal ions can either adopt a μ-O,O' or μ,κ^3–O,O':O' mode. A search of the CSD revealed no analogous pentametal building blocks. However, several examples of coordination polymers and networks containing $\{Zn_3(\mu\text{-}O,O'\text{-}O_2CR)_2(\mu,\kappa^3\text{-}O,O':O'\text{-}O_2CR)_2\}$[49-53], or $\{Zn_3(\mu\text{-}O,O'\text{-}O_2CR)_4(\mu,\kappa_3\text{-}O,O':O'\text{-}O_2CR)_2\}$[54-60], units have been reported. The N of the middle pyridine ring is uncoordinated again while both N of the outer pyridine rings are coordinating to the metal ion. As can be seen in Fig. 25, Zn2, 3 and 4 are bound to two ligands **6**, whereas Zn1 and 5 are connected to only one ligand. Infinite polymer chains that run parallel to the c-axis (Fig. 26 and 27) are made from $\{Zn_5(\textbf{6})_4\}$ units (black arrow in Fig. 26), which are interconnected by $\{Zn_5(OAc)_{10}\}$ ones (red arrow in Fig. 26).
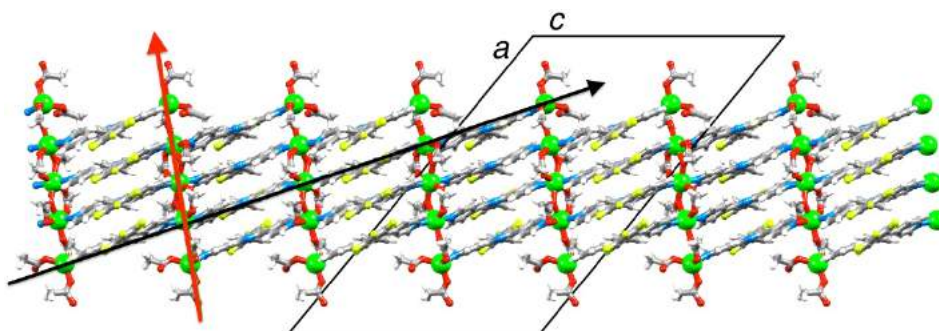
Fig. 26. Assembly of deep chains in $[Zn_5(OAc)_{10}(\mathbf{6})_4.11H_2O]_n$: the red and black arrows define the directionalities of the $\{Zn_5(OAc)_{10}\}$ and $\{Zn_5(\mathbf{6})_4\}$ units, repectively.

The domains of four pentafluorobiphenyl moieties protrude from either side of the chain (in an alternating fashion) as can be seen in Fig. 27. There is face-to-face stacking of tpy domains and of pentafluorobiphenyl domains of the four ligands **6** that make up the repeat unit (Fig. 25).
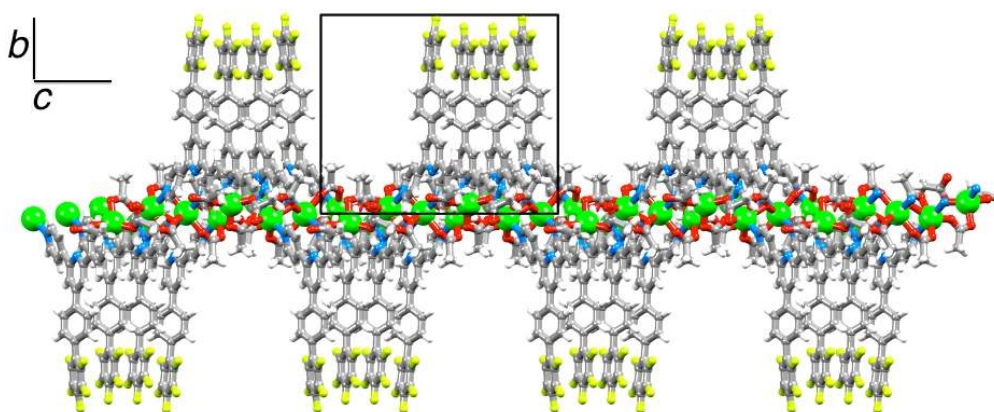
Fig. 27. Assembly of deep chains in $[Zn_5(OAc)_{10}(\mathbf{6})_4.11H_2O]_n$: chains run along the c-axis, and groups of four adjacent pentafluorobiphenyl domains engage in $\pi_F...\pi_F$ and $\pi_H...\pi_H$ stacking interactions.

The chains display a comparable zig-zag look to the single chains previously described when viewed through the π-stacked domains. Just like in the Cu analogue with the same ligand **6**, this means that chains associate into sheets and that this involves π-stacking between arene moieties of neighboring sheets. As can be seen in Fig. 28, two adjacent chains (blue and green) assemble into a sheet and two chains in neighboring sheets (red and blue) π–stack with one another.
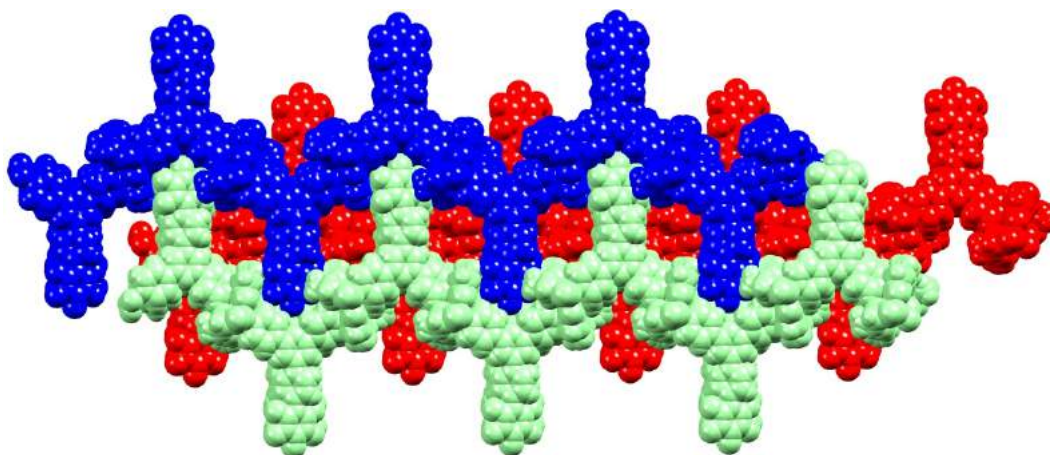
Fig. 28. Packing of adjacent chains in $[Zn_5(OAc)_{10}(\mathbf{6})_4.11H_2O]_n$. The blue and green chains are in the same sheet.

The role of the water molecules in the assembly of the coordination polymer can not be identified clearly because H-atoms could not be located in a reliable manner from the difference map. The powder X-ray diffraction pattern confirmed that the dominant compound was $[Zn_5(OAc)_{10}(\mathbf{6})_4.11H_2O]_n$ but residual $Zn(OAc)_2.H_2O$ was also present as well as an unknown compound.

The outcome of the reaction of zinc(II) acetate and 6 is unexpected and not readily explained. The anticipated single-stranded polymer is indeed formed but the dominant crystalline product is the quadruple-stranded one. It has a 5 : 4 ratio of zinc atoms : bridging ligands, which leads to a thick chain constructed from interconnected, oblique $\{Zn_5(\mathbf{6})_4\}$ subchains (Fig. 26). This assembly is a highly unusual 1D with respect to more commonly cited examples[61-62].

3.3.4 Experimental part

$[Cu_2(\mu\text{-}OAc)_4(\mathbf{6})]_n$

A solution of 6 (23.6 mg, 0.050 mmol) in $CHCl_3$ (6.0 mL) was placed in a long test tube. MeOH (3.0 mL) was layered on the top of the solution, and then a solution of $Cu(OAc)_2 \cdot H_2O$ (18.5 mg, 0.1 mmol) in MeOH (5.0 mL) was added carefully over the pure MeOH layer. The tube was sealed with parafilm and left to stand for 3 weeks at room temperature. The turquoise-green crystals of $[Cu_2(OAc)_4(\mathbf{2})]_n$ that had formed were isolated by decantation. Yield: 25.2 mg, 0.030 mmol, 60%. Found: C 50.21, H 3.54, N 5.05; $C_{35}H_{26}Cu_2F_5N_3O_8$ requires C 50.12, H 3.12, N 5.01%.

$[Cu_2(\mu\text{-}OAc)_4(\mathbf{1})]_n \cdot [Cu_2(\mu\text{-}OAc)_4(\mathbf{6})]_n$

A solution of 1 (9.64 mg, 0.025 mmol) and 6 (11.9 mg, 0.025 mmol) in $CHCl_3$ (6.0 mL) was placed in a long test tube. MeOH (3.0 mL) was layered on the top of the first solution, followed by a solution of $Cu(OAc)_2 \cdot H_2O$ (18.5 mg, 0.1 mmol) in MeOH (5.0 mL). The test tube was sealed with parafilm and allowed to stand for 1 week at room temperature, after which time turquoise-green crystals had formed. Yield: 15.5 mg, 0.0098 mmol, 39.1%. Single

66

crystals of {[Cu$_2$(OAc)$_4$(**1**)]$_n$}·{[Cu$_2$(OAc)$_4$(**2**)]$_n$} were separated by decantation. Found: C 52.46, H 3.75, N 5.62; C$_{70}$H$_{57}$Cu$_4$F$_5$N$_6$O$_{16}$ requires C 52.96, H 3.62, N 5.29%.

Reaction of Zn(OAc)$_2$·2H$_2$O with **6**

A solution of **6** (23.6 mg, 0.050 mmol) in CHCl$_3$ (6.0 mL) was placed in a long test tube, and MeOH (3.0 mL) was then layered on top. A solution of Zn(OAc)$_2$·2H$_2$O (21.8 mg, 0.1 mmol) in MeOH (5.0 mL) was then added carefully, and the tube was sealed with parafilm. After 10 days at room temperature, colourless crystals had formed. These proved to be a mixture of colourless blocks of [Zn$_2$(OAc)$_4$(**6**)]$_n$ and colourless plates of [Zn$_5$(OAc)$_{10}$(**6**)$_4$·11H$_2$O]$_n$. See text for bulk sample analysis.

[Cd$_2$(μ-OAc)$_4$(**6**)$_2$]$_n$

A solution of **6** (23.6 mg, 0.050 mmol) in CHCl$_3$ (6.0 mL) was placed in a long test tube, and MeOH (3.0 mL) was layered on top of the solution. A solution of Cd(OAc)$_2$·2H$_2$O (26.7 mg, 0.100 mmol) in MeOH (5.0 mL) was added carefully, and the tube was sealed with parafilm and left for 3 weeks at room temperature. Over this period, colourless crystals formed and were isolated by decantation. Satisfactory analysis on the bulk sample could not be obtained.

Crystallography

Compound **2**

C$_{27}$H$_{14}$F$_5$N$_3$, M = 475.41, colourless block, monoclinic space group Cc, a = 10.6918(11), b = 17.4451(17), c = 10.9674(11) Å, $β$ = 96.054(4)°, U = 2034.2(4) Å^3, Z = 4, D_c = 1.552 Mg m^{-3}, $μ$(Cu-Kα) = 1.071 mm^{-1}, T= 123 K. Total 15 280 reflections, 3453 unique, R_{int} = 0.0281. Refinement of 3414 reflections (316 parameters) with $I > 2σ(I)$ converged at final R_1 = 0.0293 (R_1 all data = 0.0296), wR_2 = 0.0777 (wR_2 all data = 0.0782), gof = 1.061. CCDC 949634.

[Cu$_2$(OAc)$_4$(**6**)]$_n$

C$_{35}$H$_{26}$Cu$_2$F$_5$N$_3$O$_8$, M = 838.69, green block, monoclinic space group $C2/c$, a = 26.5522(13), b = 16.7313(9), c = 8.0639(4) Å, $β$ = 107.038(3)°, U = 3425.2(3) Å^3, Z = 4, D_c = 1.626 Mg m^{-3}, $μ$(Cu-Kα) = 2.282 mm^{-1}, T = 123 K. Total 18 388 reflections, 3059 unique, R_{int} = 0.0417. Refinement of 2718 reflections (322 parameters) with $I > 2σ(I)$ converged at final R_1 = 0.0610 (R_1 all data = 0.0672), wR_2 = 0.1639 (wR_2 all data = 0.1696), gof = 1.114. CCDC 949632.

[Cu$_2$(OAc)$_4$(**1**)]$_n$·[Cu$_2$(OAc)$_4$(**6**)]$_n$

C$_{70}$H$_{57}$Cu$_4$F$_5$N$_6$O$_{16}$, M = 1587.42, green block, monoclinic space group $C2/c$, a = 26.366(3), b = 16.393(2), c = 8.1433(9) Å, $β$ = 107.648(6)°, U = 3354.2(7) Å^3, Z = 2, D_c = 1.572 Mg m^{-3}, $μ$(Cu-Kα) = 2.182 mm^{-1}, T= 123 K. Total 14 871 reflections, 2950 unique, R_{int} = 0.0306. Refinement of 2663 reflections (245 parameters) with $I > 2σ(I)$ converged at final R_1 = 0.0502 (R_1 all data = 0.0541), wR_2 = 0.1518 (wR_2 all data = 0.1560), gof = 1.125. CCDC 949633.

[Zn$_5$(OAc)$_{10}$(**6**)$_4$·11H$_2$O]$_n$

C$_{128}$H$_{108}$F$_{20}$N$_{12}$O$_{31}$Zn$_5$, M = 3017.26, colourless plate, monoclinic space group Cc, a = 39.181(2), b = 16.5180(9), c = 25.5638(14) Å, β = 129.465(3)°, U = 12772.9(13) Å^3, Z = 4, D_c = 1.557 Mg m^{-3}, μ(Cu-Kα) = 2.019 mm^{-1}, T = 123 K. Total 18 388 reflections, 20 471 unique, R_{int} = 0.0445. Refinement of 15 051 reflections (1879 parameters) with $I > 2\sigma(I)$ converged at final R_1 = 0.0683 (R_1 all data = 0.0962), wR_2 = 0.1802 (wR_2 all data = 0.2057), gof = 1023. CCDC 949635.

3.4 References:

1. E.C. Constable, G. Zhang, C.E. Housecroft, M. Neuburger, J.A. Zampese, CrystEngComm, 12 (2010), p. 2146.
2. E.C. Constable, C.E. Housecroft, P. Kopecky, M. Neuburger, J.A. Zampese, G. Zhang, CrystEngComm, 14 (2012), p. 446.
3. E.C. Constable, G. Zhang, E. Coronado, C.E. Housecroft, M. Neuburger, CrystEngComm, 12 (2010), p. 2139.
4. I.J. Bruno, J.C. Cole, P.R. Edgington, M.K. Kessler, C.F. Macrae, P. McCabe, J. Pearson, R. Taylor, Acta Crystallogr., Sect. B, 58 (2002), p. 389.
5. C.J. Janiak, J. Chem. Soc., Dalton Trans. (2000), p. 2885.
6. D.N. Sredojevic, D.Z. Vojislavljevic, Z.D. Tomic, S.D. Zaric, Acta Crystallogr., Sect. B, 68 (2012), p. 261 and references therein.
7. E.C. Constable, G. Zhang, C.E. Housecroft, M. Neuburger, J.A. Zampese, CrystEngComm, 11 (2009), p. 2279.
8. E.C. Constable, G. Zhang, C.E. Housecroft, M. Neuburger, J.A. Zampese, CrystEngComm, 12 (2010), p. 3733.
9. E.C. Constable, G. Zhang, C.E. Housecroft, J.A. Zampese, CrystEngComm, 14 (2012), p. 1770.
10. A.L. Spek, Acta Crystallogr., Sect. D, 65 (2009), p. 148.
11. Y. Hou, S. Wang, E. Shen, E. Wang, D. Xiao, Y. Li, L. Xu, C. Hu, Inorg. Chim. Acta, 357 (2004), p. 3155.
12. Z. Tian, Chem. Commun., 12 (2009), p. 417.
13. S.-C. Yu, C.-C. Kwok, W.-K. Chan, C.-M. Che, Adv. Mater., 15 (2003), p. 1643.
14. C.-C. Kwok, S.-C. Yu, I.H.T. Sham, C.-M. Che, Chem. Commun. (2004), p. 2758.
15. L. Tian, W. Zhang, B. Yang, P. Lu, M. Zhang, D. Lu, Y. Ma, J. Shen, J. Phys. Chem. B, 109 (2005), p. 6944 and references therein.
16. S. Alves, F. Pina, M.T. Albelda, E. García-España, C. Soriano, S.V. Luis, Eur. J. Inorg. Chem. (2001), p. 405.
17. E. Oliveira, M. Vicente, L. Valencia, A. Macías, E. Bértolo, R. Bastida, C. Lodeiro, Inorg. Chim. Acta, 360 (2007), p. 2734.
18. B. Pedras, V. Rosa, R. Welter, C. Lodeiro, T. Avilés, Inorg. Chim. Acta, 381 (2012), p. 143.
19. J. Jayabharathi, V. Thanikachalam, K. Jayamoorthy, R. SathishkumarSpectrochim. Acta, Part A, 97 (2012), p. 384.

20. X.-D. Chen, M. Du, T.C.W. Mak, Chem. Commun. (2005), p. 4417.
21. S.-Q. Bai, S. Leelasubcharoen, X. Chen, L.L. Koh, J.-L. Zuo, T.S.A. Hor, Cryst. Growth Des., 10 (2010), p. 1715.
22. X.-Z. Li, M. Li, Z. Li, J.-Z. Hou, X.-C. Huang, D. Li, Angew. Chem., Int. Ed., 47 (2008), p. 6371.
23. I.V. Anan'ev, E.V. Perova, S.E. Nefedov, Russ. J. Inorg. Chem., 55 (2010), p. 43.
24. M. Kroger, C. Folli, O. Walter, M. Doring, Adv. Synth. Catal., 348 (2006), p. 1908.
25. A. Waheed, R.A. Jones, J. McCarty, X. Yang, Dalton Trans. (2004), p. 3840.
26. M.-C. Suen, Z.-K. Chan, J.-D. Chen, J.-C. Wang, C.-H. Hung, Polyhedron, 25 (2006), p. 2325.
27. R.P. Feazell, C.E. Carson, K.K. Klausmeyer, Chem. Commun., 10 (2007), p. 873.
28. N. Lalioti, C.P. Raptopoulou, A. Terzis, A.E. Aliev, S.P. Perlepes, I.P. Gerothanassis, E. Manessi-Zoupa, Chem. Commun. (1998), p. 1513.
29. D.J. Darensbourg, J.R. Wildeson, J.C. Yarbrough, Inorg. Chem., 41 (2002), p. 973.
30. M.T. Ng, T.C. Deivaraj, J.J. Vittal, Inorg. Chim. Acta, 348 (2003), p. 173.
31. J. Granifo, M.T. Garland, R.F. Baggio, Polyhedron, 25 (2006), p. 2277.
32. V. Auger, I. Robin, Compt. Rend., 178 (1924), p. 1546.
33. O.M. Yaghi, M. O'Keeffe, N.W. Ockwig, H.K. Chae, M. Eddaoudi, J. Kim, Nature, 423 (2003), p. 705.
34. S. K. Nayak, R. Sathishkumar and T. N. G. Row, CrystEngComm, 12 (2010), p. 3112 and references therein.
35. N. Boden, P. P. Davis, C. H. Stam and G. A. Wesselink, Mol. Phys., 25 (1973), p. 81.
36. M. Nishio, CrystEngComm, 6 (2004), p. 130.
37. M. Nishio, Y. Umezawa, K. Honda, S. Tsuboyama and H. Suezawa, Hiroko, CrystEngComm, 11 (2009), p. 1757.
38. S. Tsuzuki and A. Fujii, Phys. Chem. Chem. Phys., 10 (2008), p. 2584.
39. M. D. Prasanna and T. N. G. Row, Cryst. Eng.,3 (2000), p. 135.
40. J. S. W. Overell and G. S. Pawley, Acta Crystallogr., Sect. B: Struct. Crystallogr. Cryst. Chem., 38 (1982), p. 1966.
41. J. H. Williams, J. K. Cockcroft and A. N. Fitch, Angew. Chem., Int. Ed. Engl., 31 (1992), p. 1655.
42. S. Bacchi, M. Benaglia, F. Cozzi, F. Demartin, G. Filippini and A. Gavezzotti, Chem.– Eur. J., 12 (2006), 3538.
43. R. Berger, G. Resnati, P. Metrangolo, E. Weber and J. Hulliger, Chem. Soc. Rev., 40 (2011), p. 3496.
44. M. Stein, R. Berger, W. Seichter, J. Hulliger and E. Weber, J. Fluorine Chem., 135 (2012), p. 231.
45. See for example: M. Fujita, S. Nagao, M. Iida, K. Ogata and K. Ogura, J. Am. Chem. Soc., 115 (1993), p. 1574; K. Kasai, M. Aoyagi and M. Fujita, J. Am. Chem. Soc., 122 (2000), p. 2140.
46. T. M. Fasina, J. C. Collings, D. P. Lydon, D. Albesa-Jove, A. S. Batsanov, J. A. K. Howard, P. Nguyen, M. Bruce, A. J. Scott, W. Clegg, S. W. Watt, C. Viney and T. B. Marder, J. Mater. Chem., 14 (2004), p. 2395.
47. K. Kasai, Chem. Lett., 35 (2006), p. 54.
48. F. H. Allen, Acta Crystallogr., Sect. B: Struct. Sci., 58 (2002), p. 380.

49. J. D. Woodward, R. V. Backov, K. A. Abboud and D. R. Talham, Polyhedron, 25 (2006), p. 2605.

50. B. Sun, Z. Wang and S. Gao, Acta Sci. Nat. Univ. Pekin., 37 (2001), p. 271.

51. P. Phuengphai, S. Youngme, P. Kongsaeree, C. Pakawatchai, N. Chaichit, S. J. Teat, P. Gamez and J. Reedijk, CrystEngComm, 11 (2009), p. 1723.

52. D. L. Reger, A. Debreczeni and M. D. Smith, Inorg. Chim. Acta, 364 (2010), p. 10.

53. U. Kumar, J. Thomas and N. Thirupathi, Inorg. Chem., 49 (2010), p. 62.

54. P. Ren, M.-L. Liu, J. Zhang, W. Shi, P. Cheng, D.-Z. Liao and S.-P. Yan, Dalton Trans., (2008), p. 4711.

55. H. Kwak, S. H. Lee, S. H. Kim, Y. M. Lee, B. K. Park, E. Y. Lee, Y. J. Lee, C. Kim, S.-J. Kim and Y. Kim, Polyhedron, 27 (2008), p. 3484.

56. J.-H. Cai, Y.-H. Xu and S. W. Ng, Acta Crystallogr., Sect. E: Struct. Rep. Online, 63 (2007), m2940.

57. H. Kwak, S. H. Lee, S. H. Kim, Y. M. Lee, B. K. Park, Y. J. Lee, J. Y. Jun, C. Kim, S.-J. Kim and Y. Kim, Polyhedron, 28 (2009), p. 553.

58. Y.-Z. Zheng, M.-L. Tong and X.-M. Chen, J. Mol. Struct., 796 (2006), p. 9.

59. A. Karmakar, R. J. Sarma and J. B. Baruah, Inorg. Chem. Commun., 9 (2006), p. 1169.

60. C.-Y. Niu, X.-F. Zheng, Y. He, Z.-Q. Feng and C.-H. Kou, CrystEngComm,12 (2010), p. 2847.

61. S. R. Batten, S. M. Neville and D. R. Turner, Coordination Polymers, RSC Publishing, (2008), Chapter 2.

62. E. C. Constable, in Supramolecular Chemistry: From Molecules to Nanomaterials, ed. P. A. Gale and J. W. Steed, Wiley, vol. 6 (2012), p. 3073.

Chapter IV: Reactions of 4'-substituted 4,2':6',4''-terpyridines with Zn(II) halides

Reactions of zinc(II) halides with 4,2':6',4''-tpys (in 1:1 ratios) tend to lead to coordination polymers[1-6] independently of the mode of synthesis. However, reacting $ZnCl_2$ with 4'-(4-ethynylphenyl)-4,2':6',4''-tpy leads to the unexpected formation of a molecular metallohexacycle[7], which is not readily explained. Before the start of this project, this was a unique example of a metallomacrocyclic complex containing a 4,2':6',4''-tpy ligand.

4.1. Structures with ligand 1

4.1.1 [{$ZnCl_2$(1)}$_6$] and [{$ZnBr_2$(1)}$_6$]

At first crystals of ligand **1** with ZnX_2 (X = Cl, Br) were attempted to be grown like the ones with $Zn(OAc)_2.2H_2O$ namely by dissolving the ligand in a 3:1 mixture of chloroform and methanol then adding the metal to the solution in its solid form. In this case immediately upon adding the metal to the ligand solution a precipitate appeared that could either not be redissolved or just in a very dilute form which is unfavorable for growing crystals. Thus, ligand **1** was dissolved in chloroform and reacted with $ZnCl_2$ and $ZnBr_2$, which were dissolved in methanol and carefully layered on top. After about three days colorless blocks grew and only one type of crystal was observed in both vials. Analysis by single crystal X-ray diffraction confirmed the formation of two molecular metallohexacycles [{$ZnCl_2$(1)}$_6$] and [{$ZnBr_2$(1)}$_6$] in the form of solvated [{$ZnCl_2$(1)}$_6$].6$CHCl_3$.6MeOH.5H_2O and [{$ZnBr_2$(1)}$_6$]. 4$CHCl_3$.5MeOH.8H_2O. The space group that both compounds crystallize in is R-3, which is trigonal and the cell parameters are comparable. One molecule of ligand **1** and one ZnX_2 unit (X = Cl, Br) is present in the asymmetric unit of each structure with the hexacycle being generated by a 3-fold rotoinversion. The two metallocycles [{$ZnCl_2$(1)}$_6$] and [{$ZnBr_2$(1)}$_6$] can be seen in Fig. 1 and 2 respectively. The two views highlight the alternating up/down conformation (conformer **I**), which contrasts with the three-up/three down (chair-like conformation) observed with 4'-(4-ethynylphenyl)-4,2':6',4''-tpy[7]. In both complexes the coordination sphere around the Zn atom is tetrahedral and only the outer pyridine rings are coordinating. Fig. 1 shows that the backbone of the ligand is bowed, which is due to the fact that the tpy moiety is not completely planar (angles between the A rings and the B ring = 5.5 and 14.2° for the Cl compound and 4.4 and 12.6° for the Br one). In order to minimize H...H repulsions between adjacent rings within the biphenyl unit there is a twisting between rings B and C and C and D (33.4 and 35.8 for the Cl structure and 34.2 and 36.9 for the Br one).
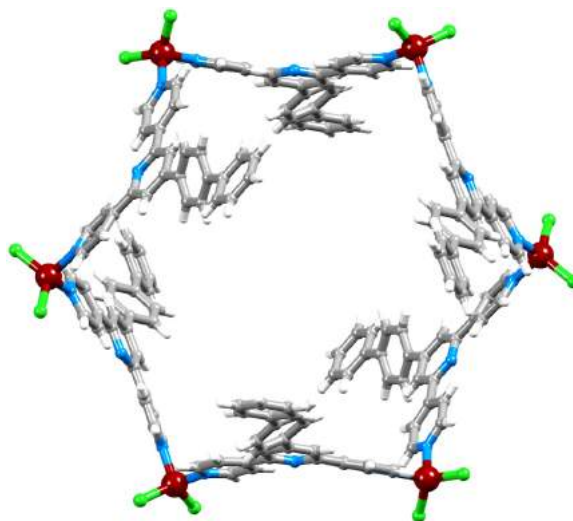
Fig. 1. Structure of [{$ZnCl_2$(1)}$_6$].
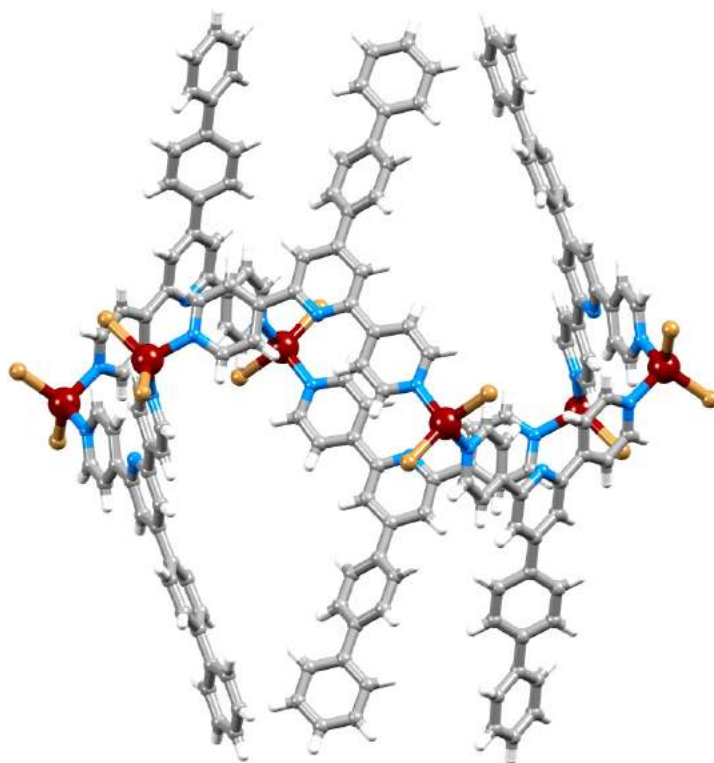
Fig. 2. Structure of [{ZnBr$_2$(**1**)}$_6$].

As can be observed in Fig. 3, the stacking of the hexacycles gives rise to a nanotube architecture with the tubes aligned parallel to the crystallographic c-axis. Due to the fact that the voids are filled with disordered solvent molecules the crystals are very sensitive to the loss of solvent, which made them difficult to handle, and the structure determination was challenging.
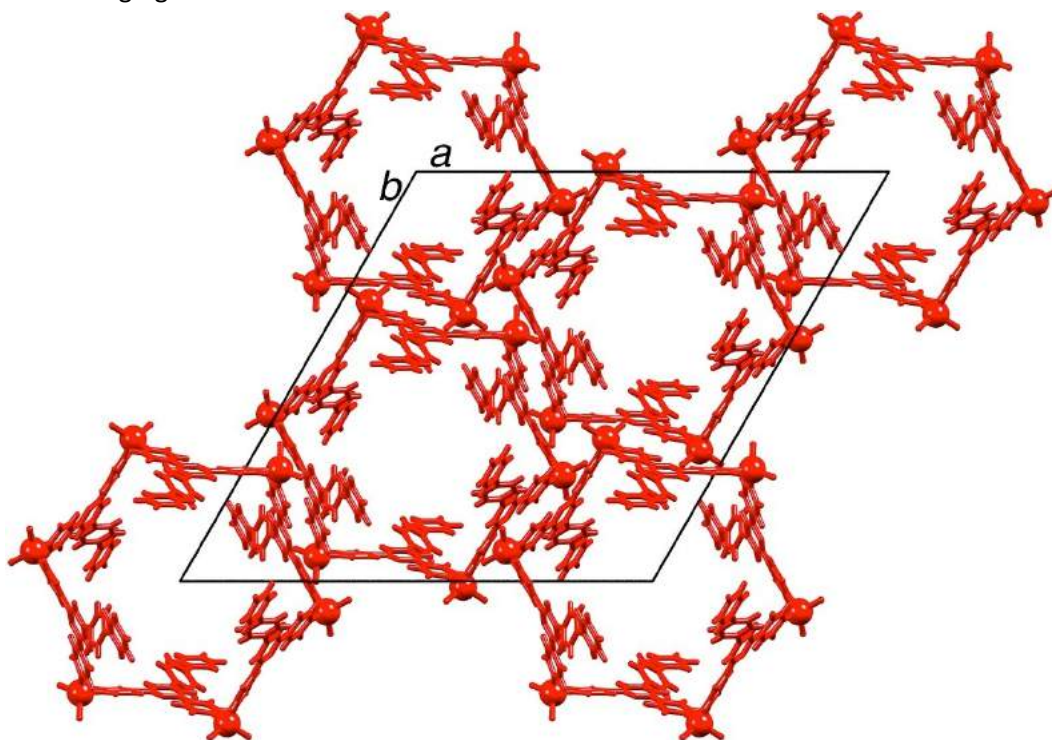
Fig. 3. Hexacycles of [{ZnBr$_2$(**1**)}$_6$] pack into tubes which follow the c-axis.

Association of the units that make up the tubes can best be illustrated by first looking at pendant phenyl rings of the biphenyl groups of every second hexamer that interdigitate (Fig. 4a). Then, when two such motifs interlock, the final nanotubular structure shown in Fig. 4b is obtained.
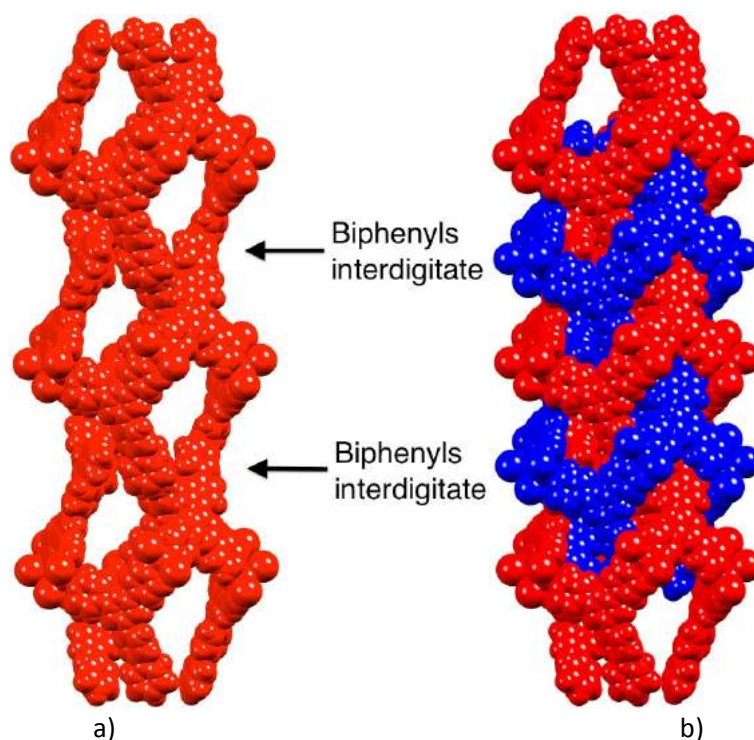
Fig. 4. a) Within each tube, biphenyl domains of every second hexamer are interdigitated. b) Interlocking of two of the motifd shown in a). Solvent molecules are omitted.

The red and blue hexacycles engage in face-to-face π–stacking between one of the A pyridine rings and the terminal phenyl ring D (inter-centroid distance = 3.77 Å for both derivatives). Every hexacycle is involved in six of those interactions, which play an important part in making the general architecture rigid.

Fig. 5. Face-to-face stacking of pyridine and phenyl rings between adjacent [{ZnBr$_2$(**1**)}$_6$] molecules.

Neighboring tubes interact efficiently through π–stacking of tpy domains (inter-centroid distance = 3.68 Å), which is illustrated in Fig. 6. by symmetry each hexamer is entangled in six such interactions. Heavily disordered molecules of solvent have been modeled as partial occupancy water, chloroform and methanol.

Fig. 6. Face-to-face interactions between pairs of tpy units in adjacent tubes.

4.2. Structures with ligand 6

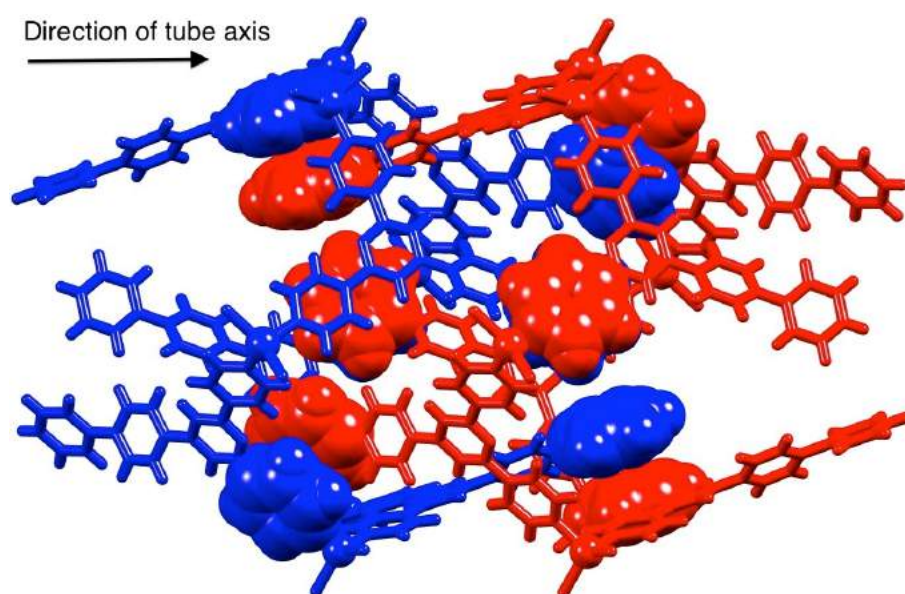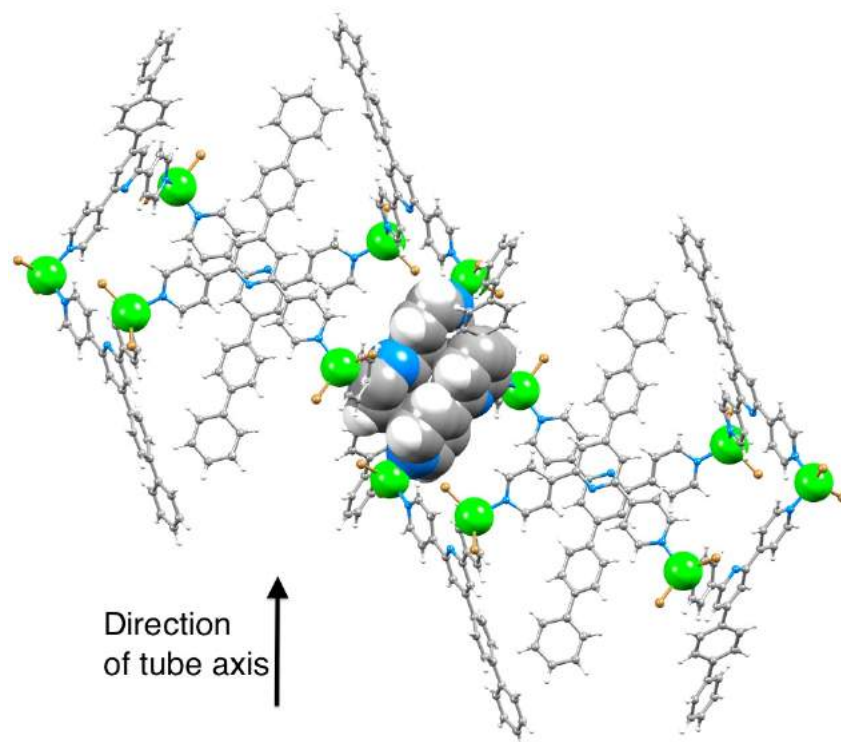As described in the previous chapter, the replacement of hydrogen by fluorine in an organic compound can potentially significantly affect solid-state structures. So far, coordination polymers formed between zinc(II) acetate and ligands **1** and **6** were isostructural and we were interested to find out whether the same would be true when the same ligands are reacted with $ZnCl_2$ and $ZnBr_2$.

4.2.1 [{$ZnCl_2$(**6**)}$_6$] and [{$ZnBr_2$(**6**)}$_6$]

Even though the coordination polymers formed upon reacting ligands **1** and **6** with zinc(II) acetate are isostructural, it was interesting to investigate if the same would be true when both ligand are reacted with ZnX_2 (X = Cl, Br). Therefore ligand **6** was reacted with ZnX_2 (X = Cl, Br) under the same layering conditions as for ligand **1**. Whereas only one type of crystal was obtained in the reactions with **1**, in this case colorless blocks and spear-like blocks (dominant form) were formed. The colorless blocks obtained from the reaction of **6** with $ZnCl_2$ analyzed as discrete macrocycles with the formula [{$ZnCl_2$(**6**)}$_6$].3$CHCl_3$.3MeOH.6H_2O. As for its analogue with **1** (cell dimensions very close) the compound crystallizes in the space group R-3, which is trigonal. Zinc atoms in the [{$ZnCl_2$(**6**)}$_6$] hexamer (Fig. 7) have a tetradehral coordination sphere and the compound also crystallizes in the conformer **I** (alternating up/down arrangement of pentafluorobiphenyl units). Stacking of the hexamers into nanotube-like architectures that run along the crystallographic c-axis imitted that in the

analogue with ligand **1** and contains disordered solvent molecules (modeled with partial occupancies) in the voids. Pentafluorophenyl-pyridine ($\pi_F \ldots \pi_H$) face-to-face stacking (Fig. 8) replaces phenyl-pyridine contacts but otherwise the stacking of the [{ZnCl$_2$(**6**)}$_6$] hexacycles can be characterized in the same way as the one in [{ZnCl$_2$(**1**)}$_6$]. In this case for the $\pi_F \ldots \pi_H$ stacking, the distance between ring centroids is 3.71 Å. Stacking between neighboring tubes (inter centroid separation of 3.58 Å) involves tpy-tpy face-to-face interactions analogous to the ones described for [{ZnBr$_2$(**1**)}$_6$].

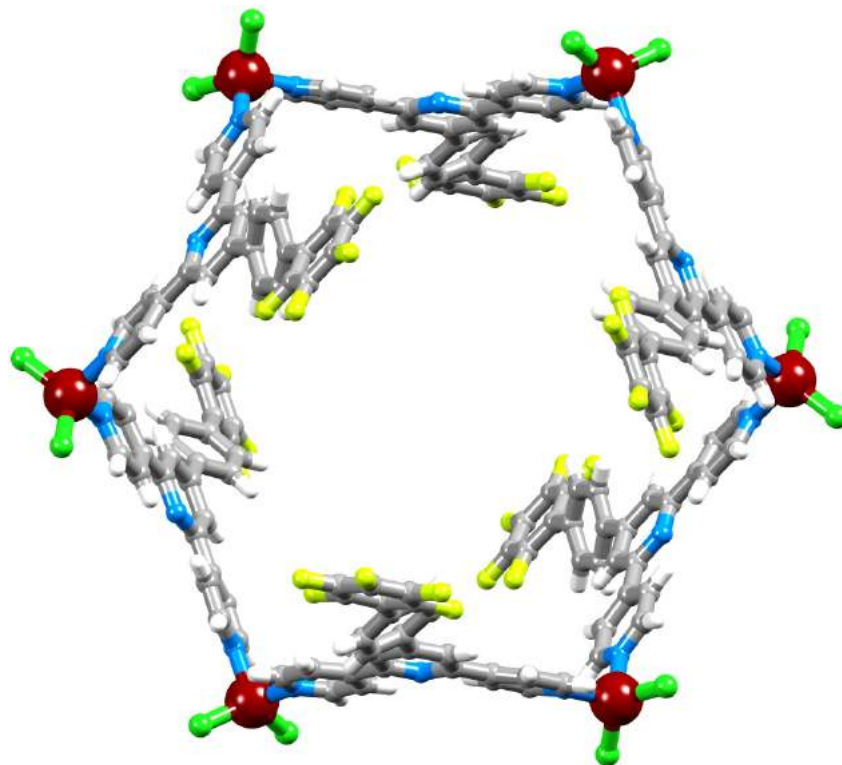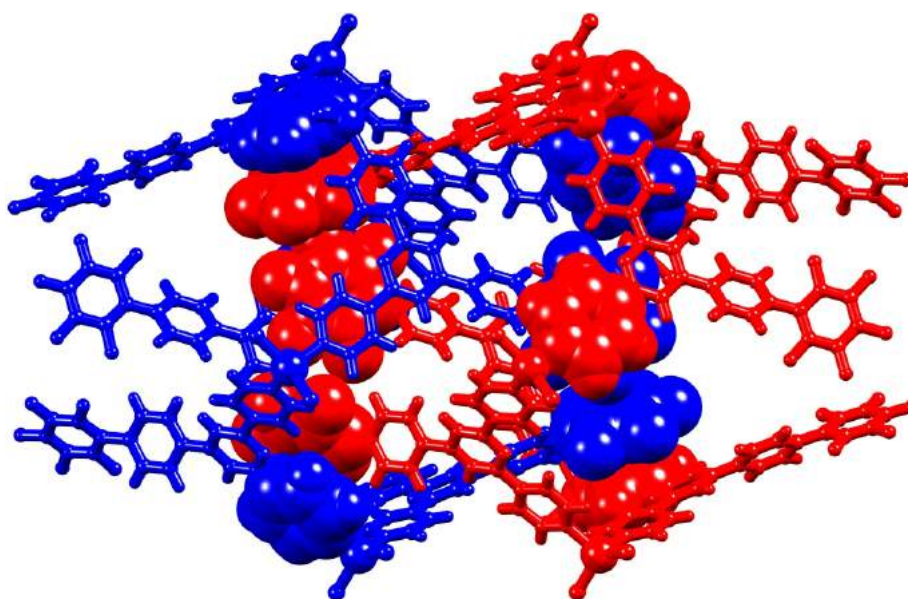Fig. 7 Structure of the [{ZnCl$_2$(**6**)}$_6$] hexamer in [{ZnCl$_2$(**6**)}$_6$].3CHCl$_3$.3MeOH.6H$_2$O.

Fig. 8. Face-to-face stacking of pyridine and pentafluorophenyl rinds between adjacent [{ZnCl$_2$(**6**)}$_6$] hexamers.

Rapid solvent loss from the block-like crystals obtained from the setups of ZnBr$_2$ and **6** as well as heavily disordered solvent molecules meant that the program SQUEEZE[8] had to be used in order to handle the data. Nevertheless, the structural determination established that [{ZnBr$_2$(**6**)}$_6$] hexacycles were formed. The cell dimensions, trigonal space group and the fact that the compound crystallized out in the form of conformer **I** are all consistent with the structures described in this chapter beforehand.
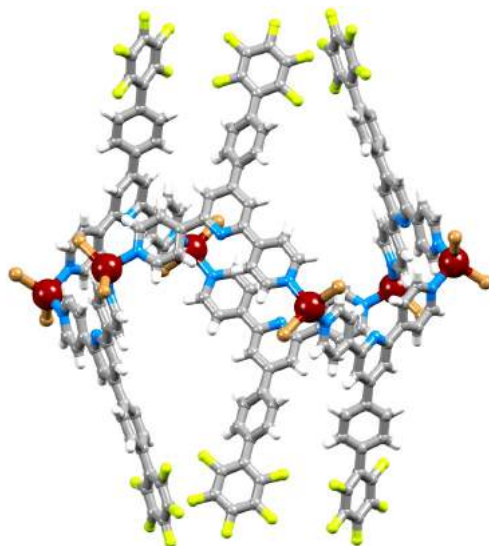
Fig. 9. Structure of hexamer [{ZnBr$_2$(**6**)}$_6$] showing the alternating up/down arrangement of the pentafluorophenyl units (conformer **I**).

Analysis of the spear-like crystals from the reactions with both halides showed that a second conformer (conformer **II**), which replicated the one observed with 4'-(4-ethynylphenyl)-4,2':6',4''-tpy[7], of the metallohexacycle was formed. Structural analysis by X-ray crystallography of the Cl compound [{ZnCl$_2$(**6**)}$_6$] established the presence of a chair conformer. SQUEEZE[8] had to be used in order to deal with the extremely disordered solvent located in the big voids of the structure. The compound crystallizes in the space group P2$_1$/n, which is monoclinic with half a hexamer located in the asymmetric unit and the remaining half being generated via an inversion centre.
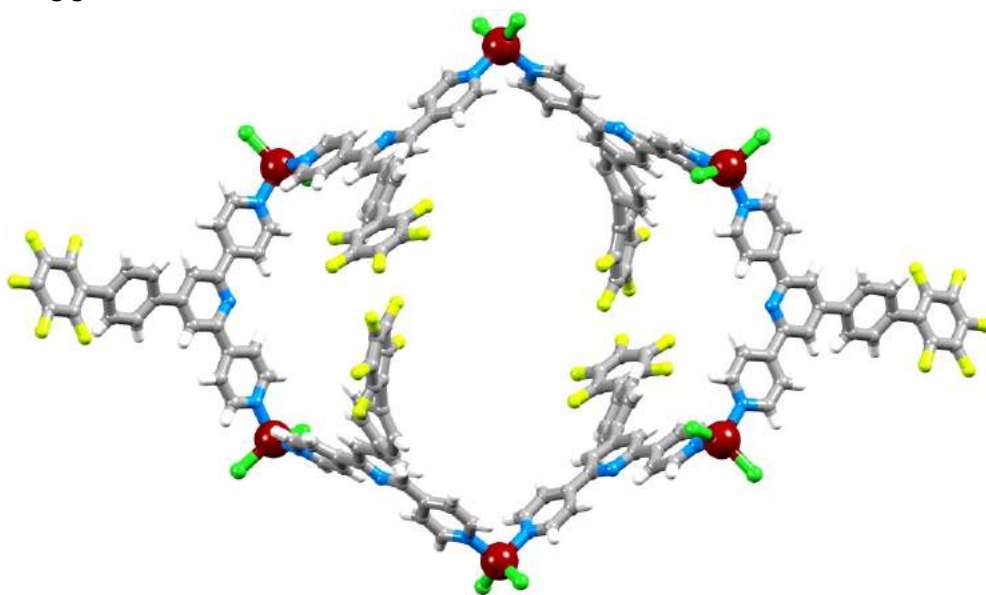
Fig. 10. Structure of conformer **II** of [{ZnCl$_2$(**6**)}$_6$] viewed through the macrocycle.

Two different views of the structure can be seen in Fig. 10 and 11. One of the pentafluorobiphenyl moieties is disordered and had to be modeled over two positions with fractional occupancies of 0.79 and 0.21.
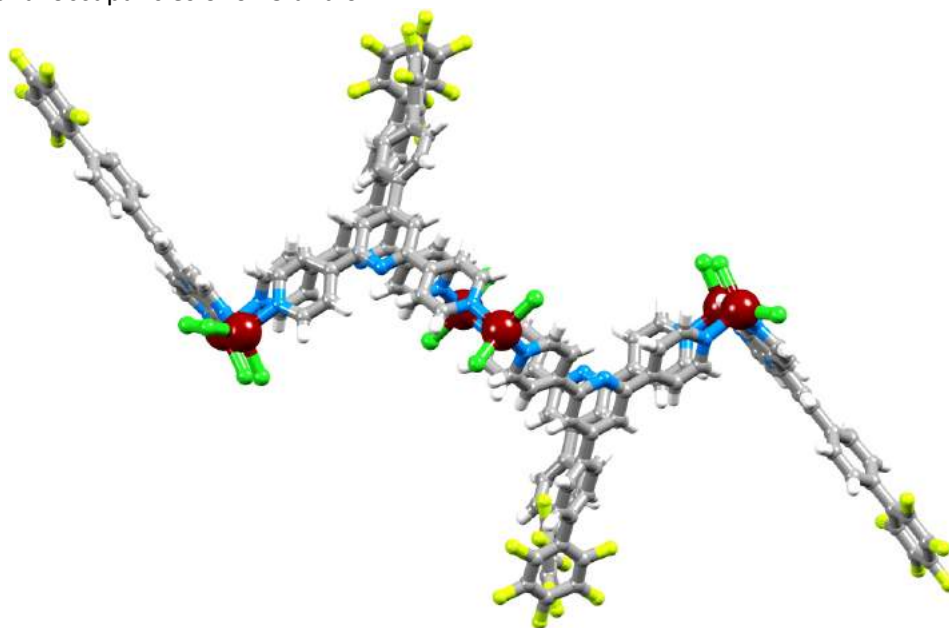
Fig. 11. Structure of conformer **II** of [{ZnCl$_2$(**6**)}$_6$] showing the chair conformation.

Stacking of the chair conformers leads to the formation of columns, which are parallel to the a-axis (Fig. 12) and protruding pentafluorophenyl units of one column interdigitate with those on a neighboring column (green in Fig. 13). Nonetheless, this interaction does not include the pentafluorophenyl domain but implicates $\pi_H\ldots\pi_H$ contacts.
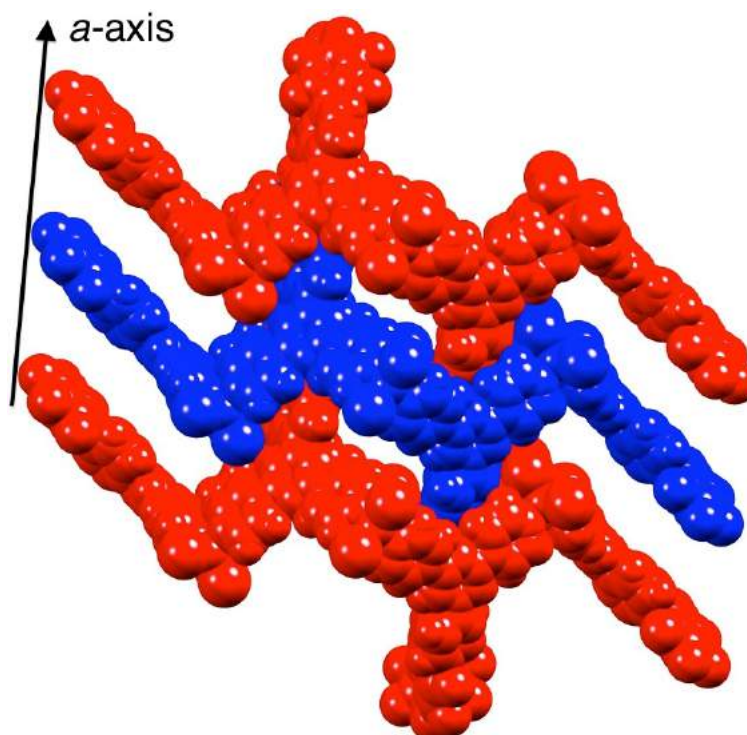
Fig. 12. Packing of molecules of [{ZnCl$_2$(**6**)}$_6$] with conformer **II**: part of one column showing $\pi_F\ldots\pi_H$ (pyridine) contacts.

75

Intermolecular $\pi_F\cdots\pi_H$ (pyridine) contacts occur between neighboring molecules within one column as seen in Fig. 12 (distance between ring centroids = 3.96 Å). Every hexamer is involved if four interactions of this type.
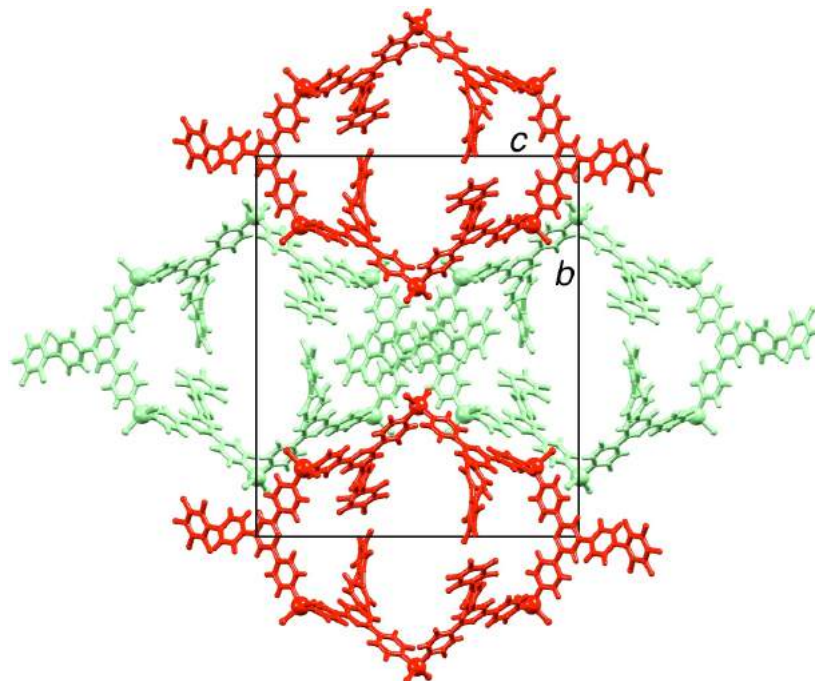
Fig. 13. Packing of molecules of [{ZnCl$_2$(**6**)}$_6$] with conformer **II**: view down the a-axis showing four adjacent columns.

For the spear-like blocks (major product) of ZnBr$_2$ and **6** only a preliminary dataset was obtained due to the crystals being of poor quality and being susceptible to loss of solvent. Still, the structure analysis confirmed the formation of the chair conformer of [{ZnBr$_2$(**6**)}$_6$] which means that ligand **6** crystallizes in conformers **I** and **II** with both zinc(II) halides. Even though through stacking of the hexacycles both conformers pack into tubes, the intermolecular interactions between molecules of conformer **I** (both within a tube and between neighboring tubes) lead to a more rigid architecture compared to the one of conformer **II**. Using PLATON[8] the void spaces in the lattices of the two conformers of [{ZnCl$_2$(**6**)}$_6$] are 26.8% (**I**) and 27.6% (**II**) and for [{ZnBr$_2$(**6**)}$_6$] the values are 28.3 (**I**) and 33.1% (**II**). Intriguingly, when layering a solution of ZnCl$_2$ in methanol over a 1:1 mixture of ligands **1** and **6** in chloroform a compound, which crystallizes in the trigonal space group R-3 was obtained and had cell dimensions which were comparable to the up/down hexamers previously obtained. Structural analysis showed that the obtained product crystallized out in conformation **I**, with both ligands statistically disordered over one ligand site, which is a similar disorder phenomenon as the one in the coordination polymer obtained by reacting ligands **1** and **6** with copper(II) acetate as discussed in the previous chapter.

4.3.1 [{ZnBr$_2$(**2**)}$_6$]

First setups with ZnCl$_2$ were tried and yielded crystals but only preliminary data could be obtained and confirmed the formation of the expected hexamer [{ZnCl$_2$(**2**)}$_6$] in conformation **I**. Unfortunately, due to the fact that the naphthyl units were heavily disordered a good quality dataset could not be obtained despite numerous attempts. Ligand **2** and ZnBr$_2$ were reacted via the same layering procedure and structural analysis of the obtained colorless blocks confirmed the formation of the hexamer [{ZnBr$_2$(**2**)}$_6$] that crystallize out as [{ZnBr$_2$(**2**)}$_6$].3CHCl$_3$.15H$_2$O. The fact that the compound crystallizes in the space group R-3, which is trigonal is consistent with the creation of conformer **I** and the structure of the metallohexacycle can be seen in Fig. 14.
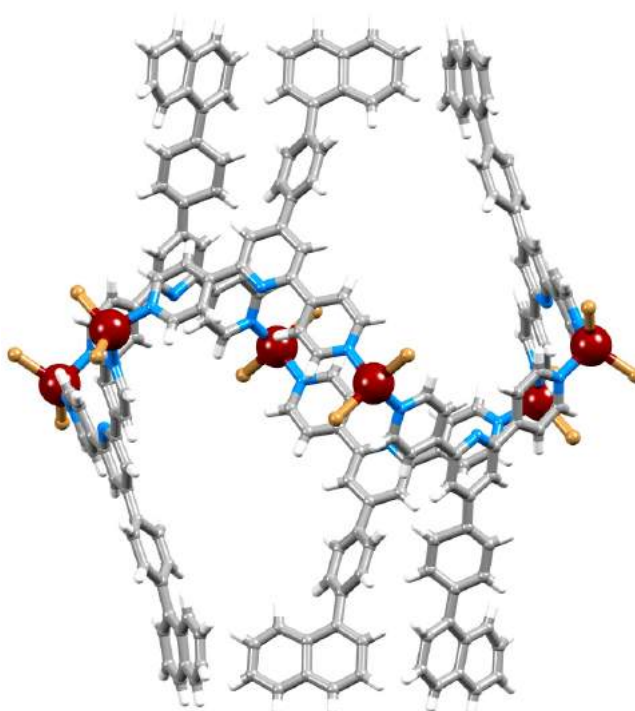
Fig. 14. Structure of the centrosymmetric [{ZnBr$_2$(**2**)}$_6$] molecule in [{ZnBr$_2$(**2**)}$_6$].3CHCl$_3$ .15H$_2$O; the metallohexacycle adopts conformer **I**.

Due to the fact that the naphth-1-ylphenyl unit is disordered it had to be modeled over two positions (related by a wagging motion) of occupancies 0.41 and 0.59. The fact that there is a slight bowing within the tpy backbone (angles between planes of adjacent pyridine rings = 9.7 and 3.3°) and a twisting of the phenyl ring with respect to the pyridine and naphthyl moieties (interplane angles = 40.8 and 44.3°) are consistent with the structures described beforehand. Hexamers pack into tubes, which run along the c-axis and interdigitation of naphth-1-ylphenyl moiety occurs between every second [{ZnBr$_2$(**2**)}$_6$] unit. Neighboring metallohexacycles engage in face-to-face stacking (centroid distances between the pyridine ring and naphthalene unit rings = 3.67 and 4 Å) of naphthyl and pyridine rings, which is illustrated in Fig. 15. In conformer **I** the arrangement of the aromatic backbones seems to be optimal for hosting arene guests of fitting dimensions and such a guest might even favor the formation of conformer **I**. In this case the closest separation of any pair of naphthyl moieties

on one rim of the $[\{ZnBr_2(\mathbf{2})\}_6]$ hexacycle is roughly 11 Å, which compares to the diameter of a C_{60} fullerene (7 Å, van der Waals radius 10 Å) and makes the cavity suitable to acting as a potential host for such systems.

Fig. 15. View down the c-axis in $[\{ZnBr_2(\mathbf{2})\}_6].3CHCl_3.15H_2O$ (solvents omitted) showing face-to-face stacking of naphthyl and pyridine domains between adjacent hexamers.
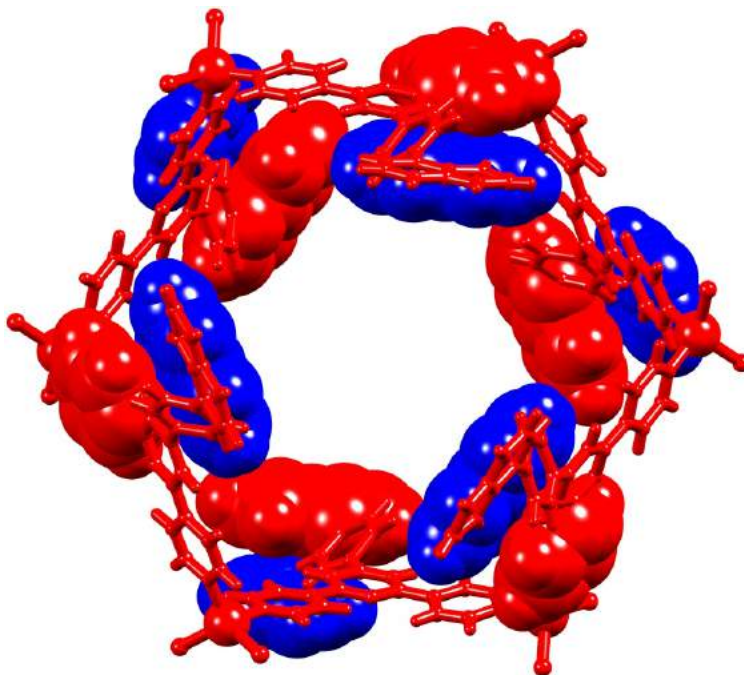
4.3.2 $[2\{ZnCl_2(\mathbf{2})\}_6.C_{60}].6MeOH.16H_2O$

Porphyrin and calixarene[9, 10] especially calix[5]arene[11-14] derivatives are popular choices as hosts for C_{60}, with the fullerene typically occupying the bowl-shaped cavity of the host. An example of a dumb-bell shaped metallo-bi(calixarene) breaks this pattern since the C_{60} guests interact with the concave outer surface of the dumb-bell instead of the calixarene cavities[15]. A porphyrin barrel (tetrameric porphyrin complex) in constrast interacts with C_{60} via both the inner and outer faces, which gives rise to a 1:3 host:guest compound[16]. However, examples of metallomacrocycles hosting such a fullerene appear to be limited. Maverick and coworkers have reported C_{60} encapsulation by a molecular square containing ditopic β–ketonate ligands bound to square planar copper(II) ions[17]. Quite a few examples of cyclic metallo-bisporphyrins binding fullerene guest have been published[18-22]. Particularly relevant to this work is the use of pyridyl-decorated bis(nickellaporphyrin) domains, which assemble into one-dimensional tubes in the solid state via pyridine…pyridine face-to-face interactions augmented by $CH…N_{pyrrole}$ contacts[21, 22].

First, the idea was to trap guest molecules within pre-formed metallomacrocycles under the assumption that they do not dissociate in solutions. Unfortunately, all evidence seems to suggest that that is not the case. An ESI mass spectra could not be obtained and the electronic absorption spectrum of a solution made by dissolving crystalline $[\{ZnCl_2(\mathbf{2})\}_6]$ in methanol (1.10^{-5} mol.dm^{-3}) was identical to the one of the free ligand $\mathbf{2}$. Furthermore, the aromatic region of the ^1H NMR spectrum of a CD_3OD solution of the hexamer was equal to the one of the ligand (similar result obtained in $CDCl_3$). Then, the second thought for the assembly of the host-guest complex was to have all species (ligand = host, metal salt and guest) in solution in their free form and have the complex assemble by co-crystallization of the fragments. Thus, ligand $\mathbf{2}$ was dissolved in a $1,2-Cl_2C_6H_4$-MeOH (8/2) solution and

inserted into a long testing tube and a solution of C_{60} in 1,2-$Cl_2C_6H_4$ was added to it. Then, a 1,2-$Cl_2C_6H_4$-MeOH (1:1) solution was layered on top of it and finally a $ZnCl_2$ solution in MeOH was also carefully layered on top of everything. In anticipation of encapsulation of one C_{60} molecule per hexamer a ratio of $ZnCl_2$: 2 : C_{60} = 6:6:1 was used. After about two weeks, single crystals suitable for X-ray diffraction were recovered. Ensuing setups with different amounts of C_{60} yielded crystals with the same structure as the one described below and separate crystals of pure fullerene. The host-guest complex, which turned out to be [2{$ZnCl_2$(**2**)}$_6$.C_{60}].6MeOH .16H_2O crystallized in the trigonal space group R-3 (same as the hexamers) with a unit cell having a c-axis about twice the length of those obtained in the case of the haxamers (with conformer **I**). The asymmetric unit contains two independent {$ZnCl_2$(**2**)} units and one-sixth of a C_{60} molecule; two mutually stacked hexamers and one entire fullerene molecule (shown in Fig. 16) are generated by 3-fold rotoinversion.
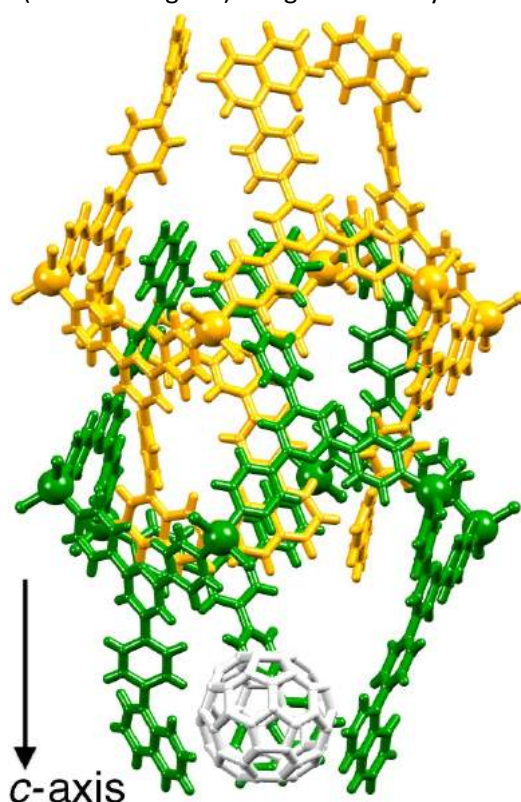
Fig. 16. The two independent {$ZnCl_2$(**2**)} hexamers and one C_{60} molecule present in [2{$ZnCl_2$(**2**)}$_6$.C_{60}].6MeOH .16H_2O. Only the major occupancy sited of the disordered naphthyl groups (yellow) are shown.

Generally speaking the architechtures of the two independent [{$ZnCl_2$(**2**)}$_6$] molecules in the structure are comparable and they do not diverge considerably from the previously described hexamers. It is important to point out that the hexamer that interacts most with the fullerene contains a naphthyl group that is ordered while in the other unit it is disordered and had to be modeled over two positions with site occupancies of 0.67 and 0.33. Between the phenyl and pyridine rings the twist angles are 37.8 and 33.2^o and the angles between the planes of the phenyl and naphthyl moieties are 43.8 and 46.3 (in the molecules colored green and yellow in Fig. 16). The structure can be described best in terms of the interdigitation of naphth-1-ylphenyl units of every second molecule together with an

interlocking of two sets of such assemblies as was the case for [{ZnBr$_2$(**2**)}$_6$]. Two non-adjacent hexamers can be seen in Fig. 17 a) and the interdigitation of naphth-1-ylphenyl units is highlighted. Neighboring hexacycles (yellow and green in Fig. 17 b)) engage in face-to-face stacking of naphthyl and pyridine rings. Every C$_{60}$ molecule is caught between six naphthyl moieties, three from one hexamer and three from its interdigitated partner (as can be seem in the center of Fig. 17 a)). Furthermore, the fullerene-six-naphthyl (green in Fig. 17) association is located at the heart of a second hexamer (yellow in Fig. 17). The fullerene guest is crystallographically ordered, which is probably due to the fact that it is engaging in π-stacking interactions with the naphthyl groups of the hexameric host (closest separations of the centroids between the fullerene and the two rings of the naphthyl moiety are 3.78 and 4.08 Å).
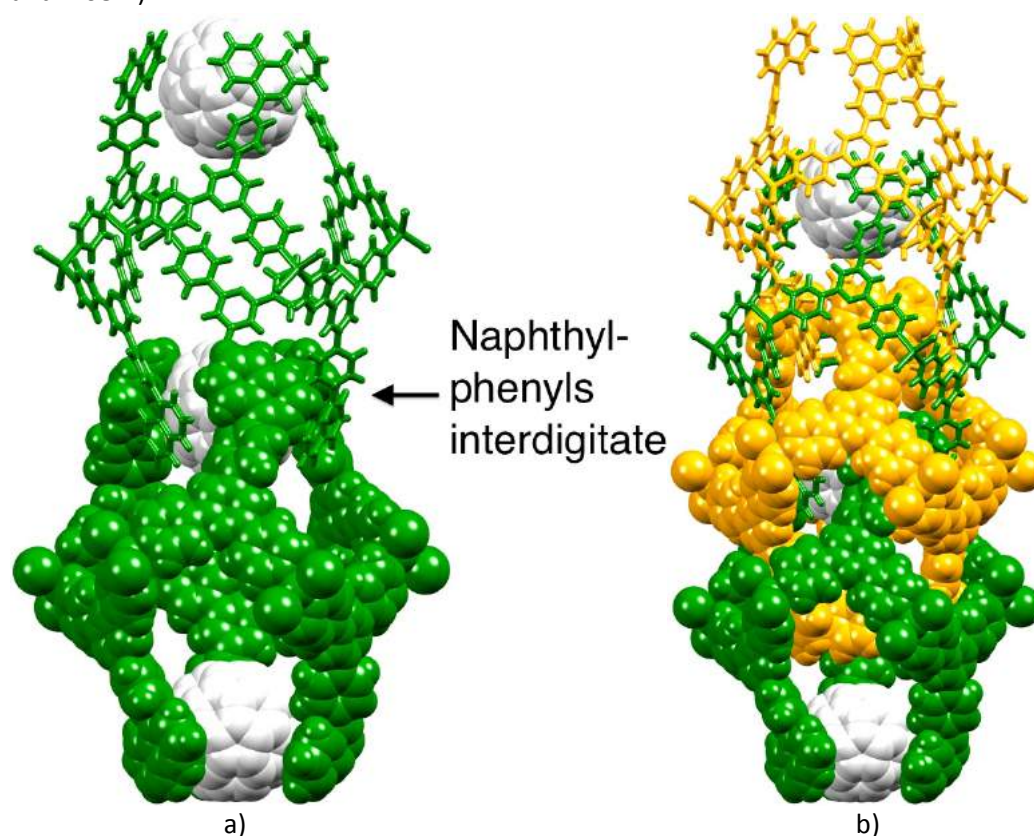
Fig. 17. a) Interdigitated naphthalene-1-ylphenyl units of every second hexamer (colored green) host a C$_{60}$ molecule. Interlocking of the crystallographically independent [{ZnCl$_2$(**2**)}$_6$] hexamers (colored green and yellow) completes the structure. Solvent molecules are omitted.

It is worth mentioning that just every other set of interdigitated naphthyl units (green in Fig. 17) captures a fullerene. Even if the cavity between the naphthalene units of the hexamers (colored yellow in Fig. 17) is similar in size it is just filled with disordered solvent molecules, which have been modeled as partial occupancy water and methanol molecules. As mentioned beforehand, only every second cavity hosts a fullerene and all attempts to introduce further C$_{60}$ guest molecules into the structure failed. The two crystallographically independent cavities are practically identical from a spatial point of view and the distance between an occupied (green) cavity and an unoccupied (yellow) one is 11.27 Å. The corresponding separation in crystalline C$_{60}$ or co-crystallizes C$_{60}$.Z (Z being a small organic

molecule) is close to 10 Å[23-26] which suggests that steric crowding is unlikely the reason for the half-filling. A plausible explanation could be that during the assembly of the structure the molecules of ligand **2** preorganise around the fullerene guest in an early recognition event. Furthermore, the intimate interlocking of hexamers along a tube appears to be a critical feature that precents the C_{60} molecules from occupying every six-naphthyl host. In the example where pyridyl-decorated bis(nickellaporphyrin) domains assemble into one-dimensional tubes[21,22], which are more open than in our case every macrocyclic cavity hosts a C_{60} molecule.

4.4 Experimental part

[{ZnCl$_2$(**1**)}$_6$]

A solution of **1** (19.1 mg, 0.050 mmol) in CHCl$_3$ (6.0 mL) was placed in a long test tube. MeOH (3.0 mL) was layered on the top of the solution, followed by a solution of ZnCl$_2$ (6.76 mg, 0.050 mmol) in MeOH (5.0 mL). The test tube was sealed with parafilm and allowed to stand for 3 days at room temperature after which time, colourless crystals had formed. These were isolated by decantation (19 mg, 0.037 mmol, 73%). Found C 61.69, H 4.26, N 7.63%; $C_{162}H_{114}Cl_{12}N_{18}Zn_6$·3MeOH requires C 61.42, H 3.94, N 7.81%.

[{ZnBr$_2$(**1**)}$_6$]

A solution of **1** (19.1 mg, 0.050 mmol) in CHCl$_3$ (6.0 mL) was placed in a long test tube and MeOH (3.0 mL) was then layered over the first solution, followed by a solution of ZnBr$_2$ (11.2 mg, 0.050 mmol) in MeOH (5.0 mL). The tube was sealed with parafilm and left to stand at room temperature. Within 3 days, colourless crystals had formed and were isolated by decantation (10.3 mg, 0.0169 mmol, 33.7%). Found C 53.01, H 3.64, N 6.73%; $C_{162}H_{114}Br_{12}N_{18}Zn_6$·2MeOH requires C 52.84, H 3.30, N 6.76%.

[{ZnCl$_2$(**2**)}$_6$]

A solution of **2** (23.6 mg, 0.050 mmol) in CHCl$_3$ (6.0 mL) was placed in a long test tube and MeOH (3.0 mL) was layered over the solution. A solution of ZnCl$_2$ (6.76 mg, 0.050 mmol) in MeOH (5.0 mL) was added carefully and the tube was sealed with parafilm and left for 3 days at room temperature. Colourless crystals (blocks and spear-like blocks) formed and were isolated by decantation (15.6 mg, 0.0255 mmol, 51.0%). Found: C 53.62, H 2.31, N 6.87%; $C_{162}H_{84}Cl_{12}F_{30}N_{18}Zn_6$ requires C 53.02, H 2.81, N 6.87%.

[{ZnBr$_2$(**2**)}$_6$]

A solution of **2** (23.6 mg, 0.050 mmol) in CHCl$_3$ (6.0 mL) was placed in a long tube. MeOH (3.0 mL) was layered on top of the solution, followed by a solution of ZnBr$_2$ (11.2 mg, 0.050 mmol) in MeOH (5.0 mL). The test tube was sealed with parafilm and allowed to stand for 3 days at room temperature. The colourless crystals that formed were isolated by decantation

(12.7 mg, 0.0181 mmol, 36.3%). Found C 46.84, H 2.28, N 6.30%; $C_{162}H_{114}Br_{12}F_{30}N_{18}Zn_6$ requires C 46.29, H 2.01, N 6.00%.

[{ZnBr$_2$(**3**)}$_6$]

A solution of **3** (21.8 mg, 0.050 mmol) in CHCl$_3$ (6.0 mL) was placed in a long tube and MeOH (3.0 mL) was layered on top, followed by a solution of ZnBr$_2$ (11.2 mg, 0.050 mmol) in MeOH (5.0 mL). The test tube was sealed with parafilm and left at room temperature for 3 days. The colourless crystals that formed were isolated by decantation (13.6 mg, 0.0206 mmol, 41.2%). Found C 57.38, H 3.81, N 6.21%; $C_{186}H_{126}Br_{12}N_{18}Zn_6$ requires C 56.35, H 3.20, N 6.36%.

[2{ZnCl$_2$(**3**)}$_6$·C$_{60}$]

A solution of **3** (21.8 mg, 0.050 mmol) in a mixture of 1,2-Cl$_2$C$_6$H$_4$ (8.0 mL) and MeOH (2.0 mL) and a solution of C$_{60}$ (6 mg, 0.008 mmol) in 1,2-Cl$_2$C$_6$H$_4$ (2.0 mL) were placed in a long test tube. A mixture of MeOH (2.5 mL) and 1,2-Cl$_2$C$_6$H$_4$ (2.5 mL) was added as a new layer, followed by a solution of ZnCl$_2$ (6.76 mg, 0.050 mmol) in MeOH (8 mL). After sealing the tube with parafilm, it was left for 2 weeks at room temperature. During this time, purple-red blocks formed in addition to small crystals of C$_{60}$. Satisfactory elemental analysis could not be obtained.

Crystallography

[{ZnCl$_2$(**1**)}$_6$]·6CHCl$_3$·6MeOH·5H$_2$O

$C_{174}H_{154}Cl_{30}N_{18}O_{11}Zn_6$, M = 4129.02, colourless block, trigonal, space group $R\bar{3}$, $a = b$ = 37.5778(11), c = 11.4003(4) Å, U = 13 941.5(8) Å^3, Z = 3, D_c = 1.472 Mg m^{-3}, μ(Mo-Kα) = 1.255 mm^{-1}, T = 123 K. Total 73 965 reflections, 9030 unique, R_{int} = 0.0423. Refinement of 6903 reflections (429 parameters) with $I > 2\sigma(I)$ converged at final R_1 = 0.0589 (R_1 all data = 0.0834), wR_2 = 0.1704 (wR_2 all data = 0.2067), gof = 1.091. CCDC 956343.

[{ZnBr$_2$(**1**)}$_6$]·4CHCl$_3$·5MeOH·8H$_2$O

$C_{174}H_{154}Br_{12}Cl_{12}N_{18}O_{13}Zn_6$, M = 4447.12, colourless block, trigonal, space group $R\bar{3}$, $a = b$ = 38.1168(9), c = 11.6852(3) Å, U = 14 702.8(6) Å^3, Z = 3, D_c = 1.501 Mg m^{-3}, μ(Mo-Kα) = 3.390 mm^{-1}, T = 123 K. Total 122 861 reflections, 7121 unique, R_{int} = 0.0446. Refinement of 5926 reflections (420 parameters) with $I > 2\sigma(I)$ converged at final R_1 = 0.0333 (R_1 all data = 0.0454), wR_2 = 0.0902 (wR_2 all data = 0.1020), gof = 1.115. CCDC 956344.

[{ZnCl$_2$(**2**)}$_6$]·3CHCl$_3$·3MeOH·6H$_2$O (conformer I)

$C_{168}H_{111}Cl_{21}F_{30}N_{18}O_9Zn_6$, M = 4232.57, colourless block, trigonal, space group $R\bar{3}$, $a = b$ = 37.998(4), c = 11.3178(11) Å, U = 14 152(2) Å^3, Z = 3, D_c = 1.486 Mg m^{-3}, μ(Cu-Kα) = 4.430

mm^{-1}, T = 123 K. Total 32 865 reflections, 5662 unique, R_{int} = 0.0483. Refinement of 5423 reflections (426 parameters) with $I > 2\sigma(I)$ converged at final R_1 = 0.0613 (R_1 all data = 0.0626), wR_2 = 0.1810 (wR_2 all data = 0.1826), gof = 1.051. CCDC 956347.

[{ZnCl$_2$(**2**)}$_6$] (conformer II)

After SQUEEZE: $C_{162}H_{84}Cl_{12}F_{30}N_{18}Zn_6$, M = 3670.71, colourless block, monoclinic, space group $P2_1/n$, a = 9.2722(4), b = 35.4234(15), c = 30.2123(12) Å, β = 95.305(2), U = 9880.8(7) Å^3, Z = 2, D_c = 1.234 Mg m^{-3}, μ(Cu-Kα) = 2.941 mm^{-1}, T = 123 K. Total 72 063 reflections, 17 471 unique, R_{int} = 0.0753. Refinement of 12 646 reflections (1182 parameters) with $I > 2\sigma(I)$ converged at final R_1 = 0.1069 (R_1 all data = 0.1240), wR_2 = 0.3013 (wR_2 all data = 0.3169), gof = 1.089. CCDC 956348.

[{ZnBr$_2$(**2**)}$_6$]

After SQUEEZE: $C_{162}H_{84}Br_{12}F_{30}N_{18}Zn_6$, M = 4203.61, colourless block, trigonal, space group $R\bar{3}$, a = b = 38.394(4), c = 11.5576(15) Å, U = 14 755(3) Å^3, Z = 3, D_c = 1.419 Mg m^{-3}, μ(Cu-Kα) = 4.311 mm^{-1}, T = 123 K. Total 29 568 reflections, 5754 unique, R_{int} = 0.1096. Refinement of 4031 reflections (343 parameters) with $I > 2\sigma(I)$ converged at final R_1 = 0.0769 (R_1 all data = 0.1008), wR_2 = 0.1903 (wR_2 all data = 0.2024), gof = 1.116. CCDC 956349.

[{ZnBr$_2$(**3**)}$_6$]·3CHCl$_3$·15H$_2$O

$C_{189}H_{159}Br_{12}Cl_9N_{18}O_{15}Zn_6$, M = 4592.60, colourless block, trigonal, space group $R\bar{3}$, a = b = 38.975(2), c = 11.4827(8) Å, U = 15 105.8(17) Å^3, Z = 3, D_c = 1.505 Mg m^{-3}, μ(Mo-Kα) = 3.264 mm^{-1}, T = 123 K. Total 125 042 reflections, 8934 unique, R_{int} = 0.0580. Refinement of 6705 reflections (585 parameters) with $I > 2\sigma(I)$ converged at final R_1 = 0.0425 (R_1 all data = 0.0703), wR_2 = 0.1267 (wR_2 all data = 0.1717), gof = 1.111. CCDC 956345.

[2{ZnCl$_2$(**3**)}$_6$·C$_{60}$]·6MeOH·16H$_2$O

$C_{438}H_{308}Cl_{24}N_{36}O_{22}Zn_{12}$, M = 8062.51, red block, trigonal, space group $R\bar{3}$, a = b = 38.4322(16), c = 22.5450(10) Å, U = 28 838(2) Å^3, Z = 3, D_c = 1.387 Mg m^{-3}, μ(Mo-Kα) = 0.970 mm^{-1}, T = 123 K. Total 279 568 reflections, 17 029 unique, R_{int} = 0.0350. Refinement of 13 522 reflections (1015 parameters) with $I > 2\sigma(I)$ converged at final R_1 = 0.0638 (R_1 all data = 0.0860), wR_2 = 0.1735 (wR_2 all data = 0.2072), gof = 1.115. CCDC 956346.

4.5. Further inclusion attempts and non-hexameric structures

4.5.1 Reactions of **2** with ZnCl$_2$ in the presence of anthracene or perylene

The same conditions that led to the formation of [2{ZnCl$_2$(**2**)}$_6$.C$_{60}$].6MeOH .16H$_2$O were used but C$_{60}$ was replaced by an anthracene (A) or perylene (P) solution in 1,2-dichlorobenzene. After about a month, single crystals were obtained but unfortunately they were sensitive to solvent loss and as a consequence difficult to handle (like the structure of ligand **2** with ZnCl$_2$). Therefore the data were treated with the program SQUEEZE. As such the electron density was modeled as a combination of 1,2-dichlorobenzene and methanol. The presence of 1,2-dichlorobenzene was confirmed by dissolving single crystals of [{ZnCl$_2$(**2**)}$_6$]-A in DMF-d7 and recording a ^{1}H NMR spectrum, which confirmed the presence of the solvent but the absence of anthracene guests. Much the same way, the spectrum of [{ZnCl$_2$(**2**)}$_6$]-P showed that the solvent but no perylene guest was present. These results seem to support the modeling of the electron density that was performed with SQUEEZE. Due to the fact that the ^{1}H NMR spectra of free ligand **2** and the dissolved complex are very similar it can be assumed that the complex breaks down in solution. Nevertheless, this conclusion is not unambiguous because the small shift of the signal around δ 8.5 pm (corresponding to H^{A3}) may indicate that the outer pyridine ring coordinated to Zn(II). Both compounds from the setups containing anthracene and perylene crystallized in the space group R-3 and after applying SQUEEZE had the formulation [{ZnCl$_2$(**2**)}$_6$] with both lattices containing discrete metallohexamers comparable to those described beforehand. The cell parameters of the two compounds are different in the sense that the a- and b-axes are double the length for [{ZnCl$_2$(**2**)}$_6$]-P compared to [{ZnCl$_2$(**2**)}$_6$]-A (the c-axis approximately constant). In the case of [{ZnCl$_2$(**2**)}$_6$]-A there is one {ZnCl$_2$(**2**)} moiety in the asymmetric unit and the molecule that can be seen in Fig. 18 is generated by a 3-fold rotoinversion giving [{ZnCl$_2$(**2**)}$_6$], which adopts a barrel-like conformation.
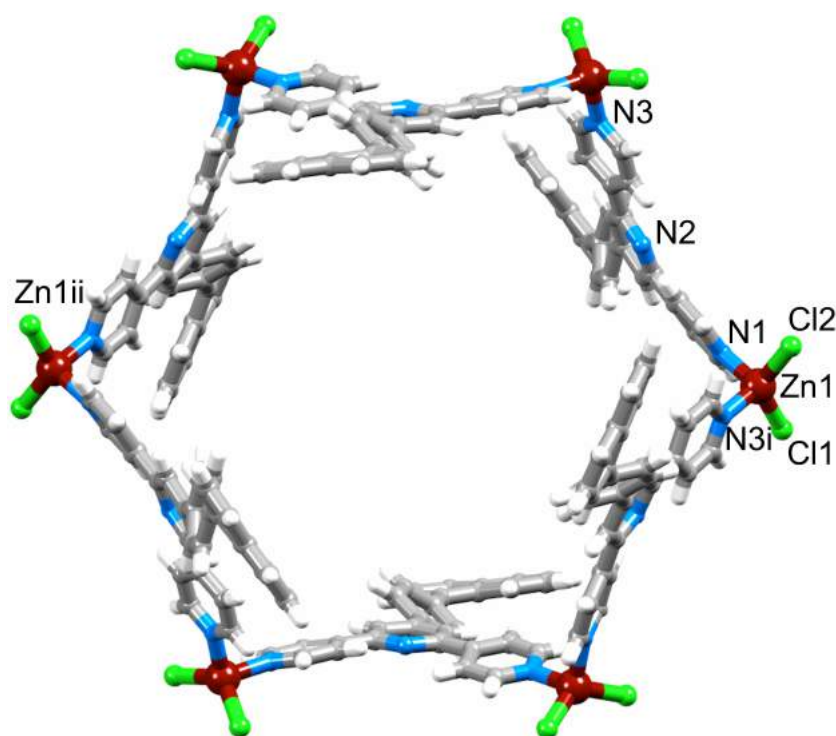

Fig. 18. Structure (looking down the c-axis) of [{ZnCl$_2$(**2**)}$_6$]-A.

The asymmetric unit in [{ZnCl$_2$(**2**)}$_6$]-P contains one {ZnCl$_2$(**2**)} unit and one {Zn$_3$Cl$_6$(**2**)$_3$} one, thus defining two independent [{ZnCl$_2$(**2**)}$_6$] hexamers, which are generated by 3-fold rotoinversion (Fig. 19 a)) or inversion (Fig. 19 b)) respectively.

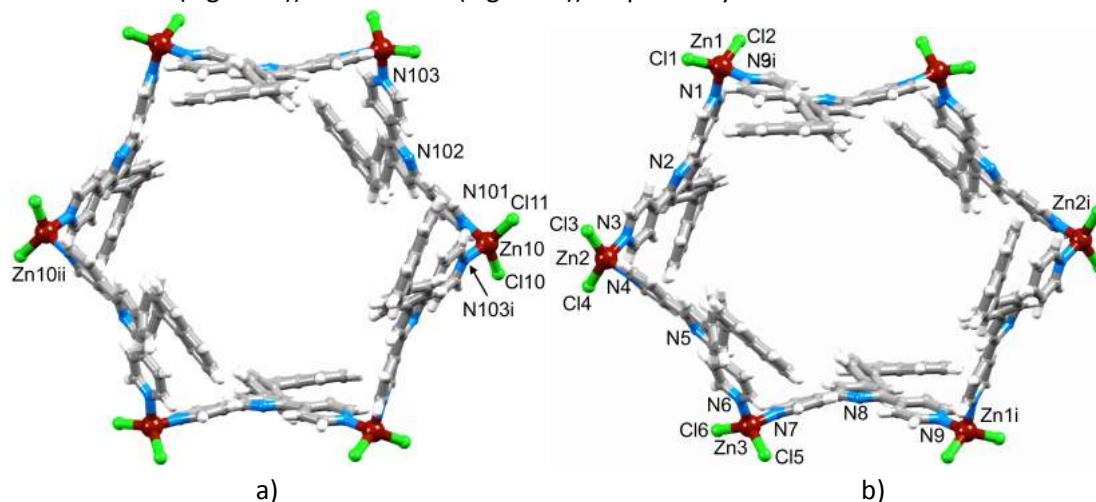a)   b)

Fig. 19. Structured (looking down the c-axis) of: a) one of two independent molecules of [{ZnCl$_2$(**2**)}$_6$]-P and b) the second independent molecule of [{ZnCl$_2$(**2**)}$_6$]-P.

The two structures have the same conformation as [{ZnCl$_2$(**2**)}$_6$]-A and are very similar between each other (the second independent molecule of [{ZnCl$_2$(**2**)}$_6$]-P being a bit flatter). As is the case in the previously discussed related structures, the barrel-like molecules pack to form tubes that go along the c-axis. The cell dimensions of [{ZnCl$_2$(**2**)}$_6$]-A and the fullerene-inclusion complex [2{ZnCl$_2$(**2**)}$_6$.C$_{60}$].6MeOH .16H$_2$O are comparable. As previously mentioned the fact that the length of the c-axis doubles by going from the simple hexamer to [2{ZnCl$_2$(**2**)}$_6$.C$_{60}$].6MeOH .16H$_2$O is a sign that the host-guest complex has been formed. Initially, the elongated unit cell [{ZnCl$_2$(**2**)}$_6$]-A was taken as a positive sign as far as the inclusion of anthracene is concerned but as discussed beforehand this was not the case. Comparing the packing of [{ZnCl$_2$(**2**)}$_6$]-A hexamers and those in [{ZnBr$_2$(**2**)}$_6$].3CHCl$_3$ .15H$_2$O some differences, which might explain the fact that the c-axis is doubled in length, are evident. Packing of the [{ZnBr$_2$(**2**)}$_6$] hexamers has been previously described in detail and is shown for comparison's sake in Fig. 20 a), which shows that the naphthyl moieties point into the tube and therefore do not engage in interactions with adjacent tubes. Crystals of [{ZnCl$_2$(**2**)}$_6$]-A consist of tubular assemblies of metallohexacycles [{ZnCl$_2$(**2**)}$_6$], which only correspond to half of the molecules in [{ZnBr$_2$(**2**)}$_6$].3CHCl$_3$ .15H$_2$O (red molecules in Fig. 20 a) and b)). The two structures are different in terms of inter-tube interactions as the comparison shows that the grey hexacycle is translated along the c-axis by going from [{ZnBr$_2$(**2**)}$_6$].3CHCl$_3$ .15H$_2$O to [{ZnCl$_2$(**2**)}$_6$]-A. As can be seen in Fig. 20 b) face-to-face interactions between a centrosymmetric pair of tpy-C$_6$H$_4$-naphthyl domains in neighboring tubes occur and they replace the naphthyl intra-tube contacts found in previously described hexamers. As illustrated in Fig. 21, the tubular assemblies in [{ZnCl$_2$(**2**)}$_6$]-A interlock with one another.

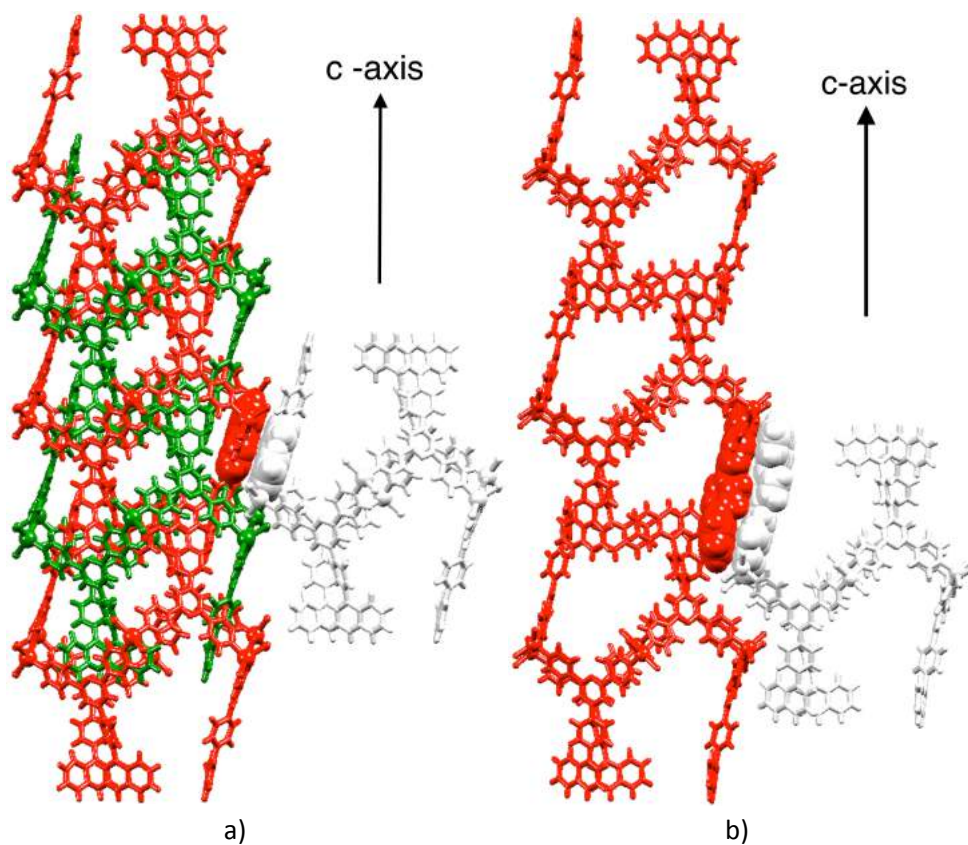Fig. 20. a) In [{ZnBr$_2$(**2**)}$_6$].3CHCl$_3$.15H$_2$O, red and green (crystallographically identical) hexacycles engage in efficient face-to-face stacking of naphthyl and pyridine domains within a tube; between tubes (green and grey) there are face-to-face pyridine/phenyl interactions. b) Tube-assembly in [{ZnCl$_2$(**2**)}$_6$]-A, hexacycles and face-to-face interactions between columns which involves tpy-C$_6$H$_4$-naphthyl stacking.
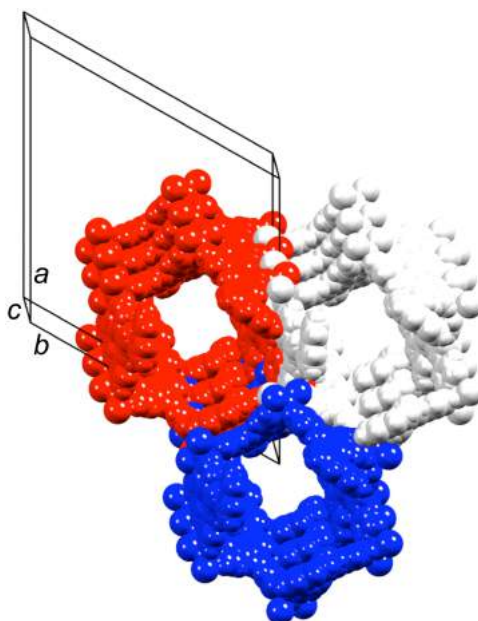

Fig. 21. View down the c-axis in [{ZnCl$_2$(**2**)}$_6$]-A to emphasize intermeshing of macrocycles.

In both structures the naphthyl substituents have a similar orientation with respect to the c-axis but as shown in Fig. 22 the tight nesting of the hexamers in [{ZnBr$_2$(**2**)}$_6$].3CHCl$_3$.15H$_2$O leads to a narrower axial cavity than the one in [{ZnCl$_2$(**2**)}$_6$]-A.
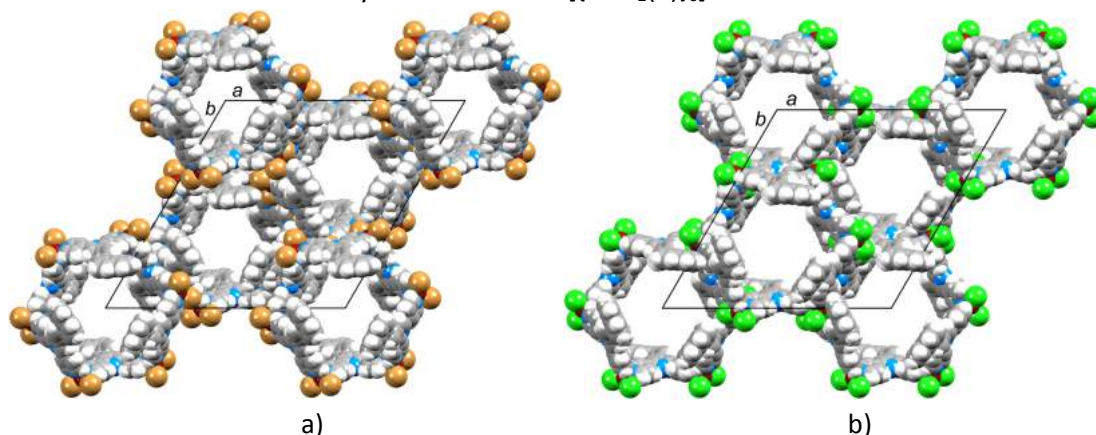

a)	b)

Fig. 22. Views down the c-axis highlighting the difference in void space between the tubular array in a) [{ZnBr$_2$(**2**)}$_6$].3CHCl$_3$.15H$_2$O and b) [{ZnCl$_2$(**2**)}$_6$]-A.

In this case the voids are occupied by solvent molecules (shown in the formula) and generally speaking this structure is far more porous than that of previous metallohexacycles. The cannels that run parallel to the a-axis are shown in Fig. 23; symmetry dictated that a comparable set of channels follow the b-axis.
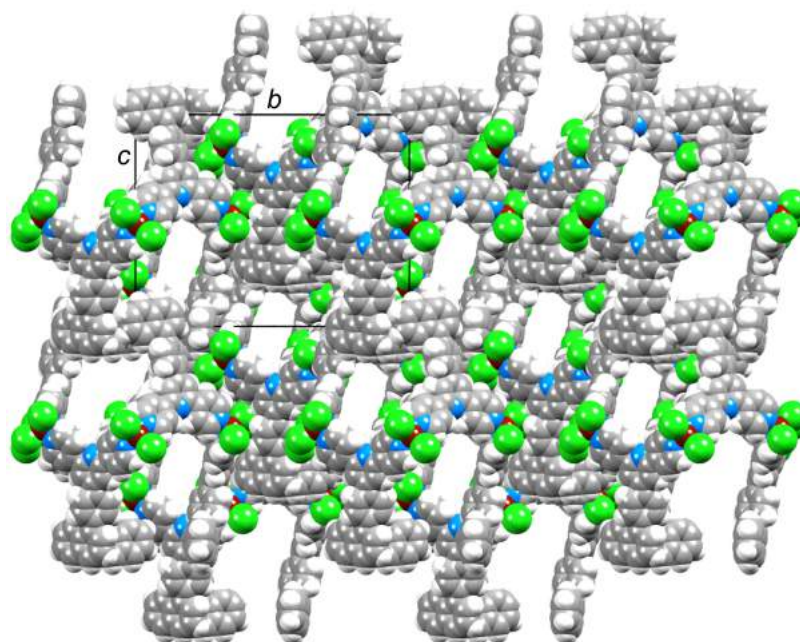
Fig. 23. Channels run parallel to the a-axis in [{ZnCl$_2$(**2**)}$_6$]-A.

[{ZnCl$_2$(**2**)}$_6$]-B is similar to [{ZnCl$_2$(**2**)}$_6$]-A but is different in the sense that it contains two crystallographically independent [{ZnCl$_2$(**2**)}$_6$] units. Tubular arrays, which are parallel to the c-axis, are found in the lattice and are made of one or the other of the two possible independent molecule in a ratio of 3 : 1 (Fig. 24).

87

Fig. 24. Packing of columns of metallohexacycles in $[\{ZnCl_2(\mathbf{2})\}_6]$-P with a 3 : 1 ratio of independent molecules.

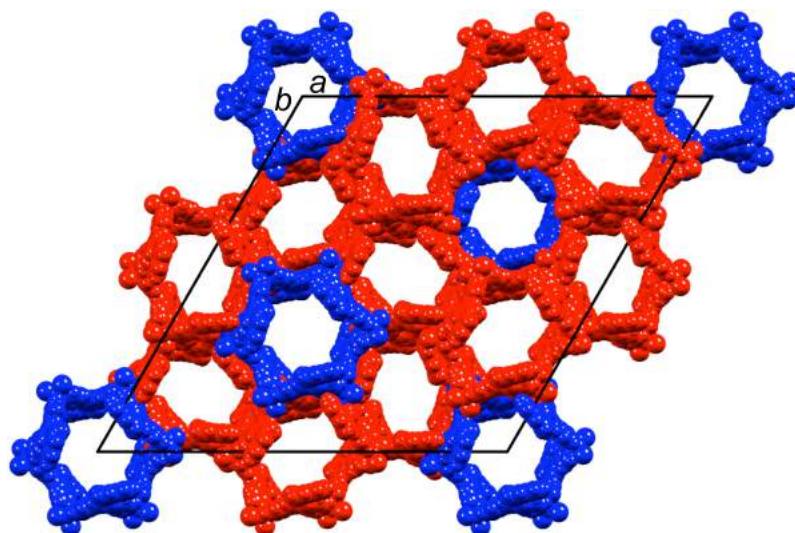Centrosymmetric pairings of tpy-C_6H_4-naphthyl domains interact with one-another (Fig. 25) in a similar way to those in $[\{ZnCl_2(\mathbf{2})\}_6]$-A. Infinite channels are revealed when looking down the a- or b-axes of the lattice of $[\{ZnCl_2(\mathbf{2})\}_6]$-P, which are again analogous to those in $[\{ZnCl_2(\mathbf{2})\}_6]$-A. The solvent loss that was encountered when dealing with $[\{ZnCl_2(\mathbf{2})\}_6]$-A and $[\{ZnCl_2(\mathbf{2})\}_6]$-P is easily explained by considering the porous nature of the two structures.
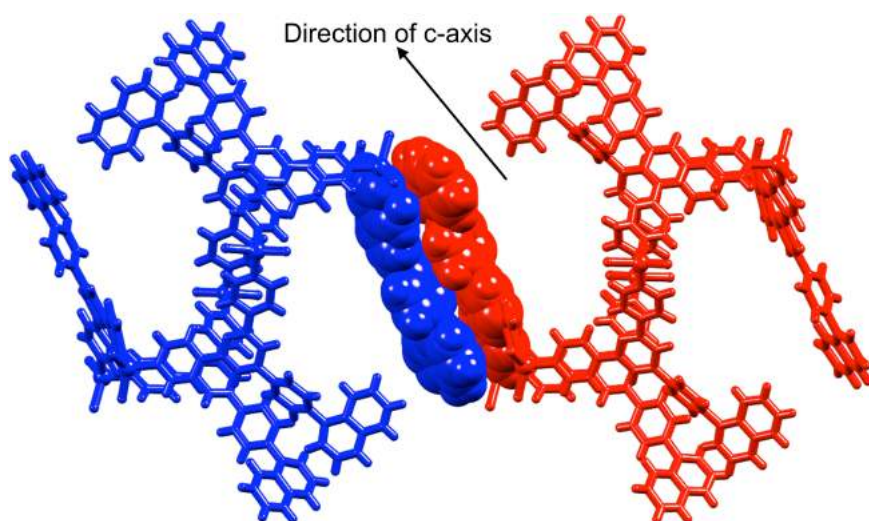
Fig. 25. Head-to-tail face-to-face stacking of tpy-C_6H_4-naphthyl domains.

4.5.2 Reactions with ligand **2** and pyrene as potential guest

Continuing the investigation concerning the attempt of inserting a host into the cavity of a hexamer, further setups with pyrene (as the potential host) and ligand **2** (as the hexamer building block) were performed. The obtained compound crystallizes in the space group P-1 and turned out to be a one-dimensional coordination polymer $[ZnCl_2(\mathbf{2})]_n$ with a crenellated topology as can be seen in Fig. 26.

Fig. 26. Part of one polymer chain in [ZnCl$_2$(**2**)]$_n$.

The reflection data had to be treated with SQUEEZE due to the presence of disordered solvent molecules. In the asymmetric unit four {ZnCl$_2$(**2**)} units are to be found and define an up/up/up/down conformation of the 4'-(4-(naphth-1-yl)phenyl) units that propagates al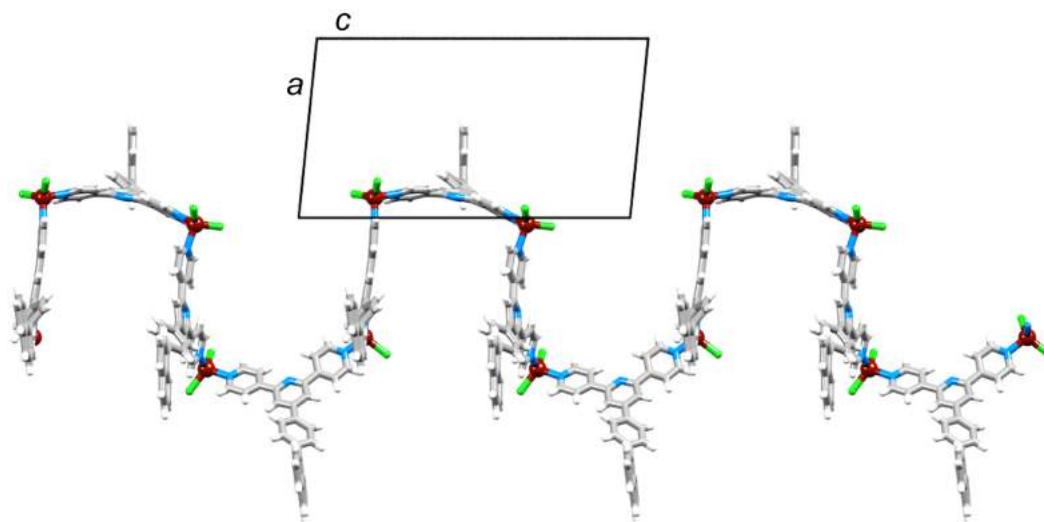ong the chain. The coordination sphere of the Zn(II) centers is tetrahedral but with a distorted geometry. Angles between the planes of pyridine rings range from 5.4 to 27.5°. As can be seen in Fig. 27 pyridine rings located on centrosymmetric pairs of chains interact through π–stacking (distance between the least square planes = 3.41 Å).
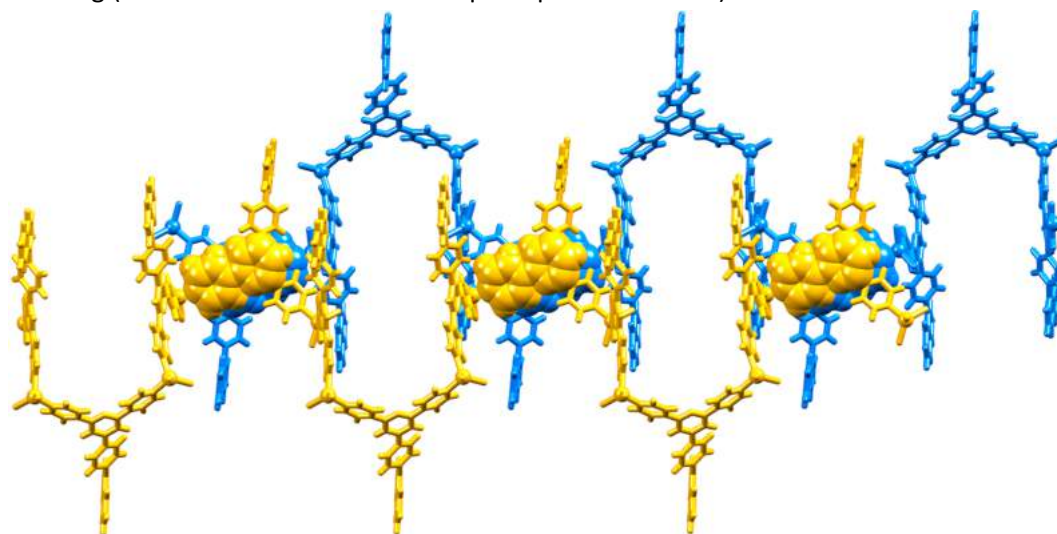
Fig. 27. π-Interactions between tpy domains of centrosymmetric pairs of chains in [ZnCl$_2$(**2**)]$_n$.

4.5.3 Reactions with ligand **6** and pyrene as potential guest

The same chain structure is observed in [ZnCl$_2$(**6**)]$_n$ of which crystals were grown in the presence of pyrene in the same manner as those of [ZnCl$_2$(**2**)]$_n$. Crystallizing in the space group P-1, the asymmetric unit of this compound contains four independent zinc atoms with a tetrahedral coordination sphere. Two ZnCl$_2$ units are bridged by a ligand **6**, which generated a one-dimensional chain that propagates along the c-axis. Even though the

general features of this chain are comparable to the ones of [ZnCl$_2$(**2**)]$_n$, the interaction between neighboring chains are different. π-Interactions between phenyl-tpy domains (separation between the planes = 3.65 Å) are illustrated in Fig. 28.
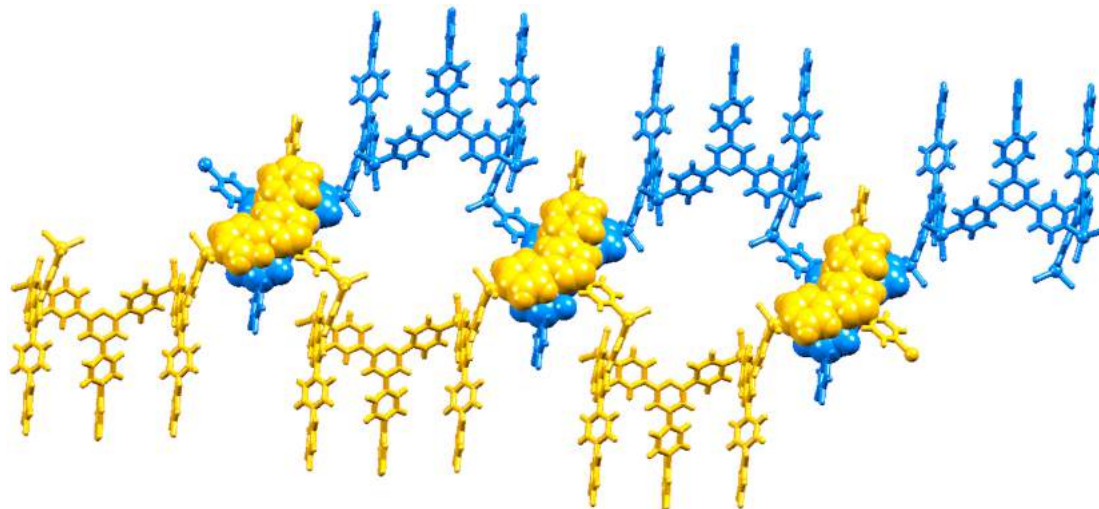

Fig. 28. π-Interactions between phenyl-tpy domains of centrosymmetric pairs of chains in [ZnCl$_2$(**6**)]$_n$.

Views down the c-axis presented in Fig. 29 highlight the difference between the stacking in the two structures.

a)   b)
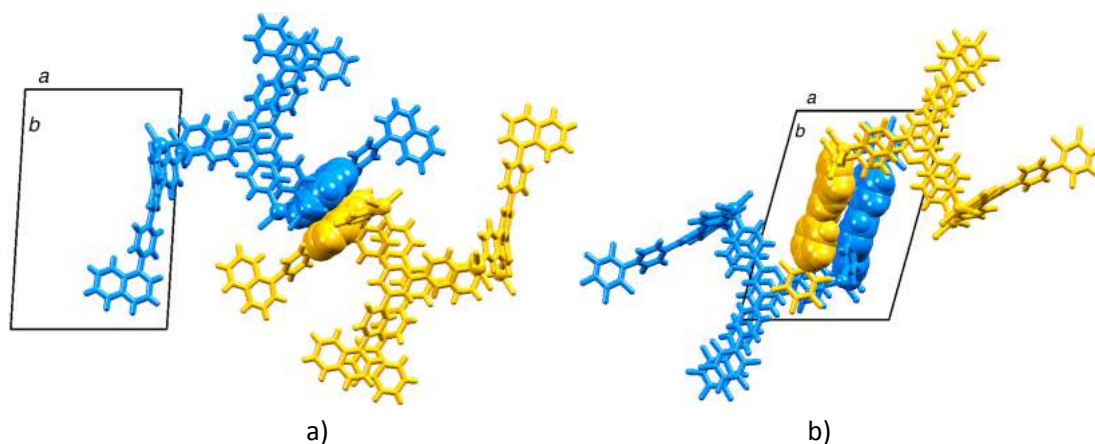
Fig. 29. π-Interactions between centrosymmetric pairs of chains in a) [ZnCl$_2$(**2**)]$_n$ and b) [ZnCl$_2$(**6**)]n, viewed along the c-axis.

Both one-dimensional structures contain repeat units that mirror three sides of a square box (for example Fig. 26). The two structures were partly refined without the use of SQUEEZE, which confirmed the presence of 1,2-dichlorobenzene and pyrene molecules in the lattice but unfortunately the datasets were not of publishable quality in that case.

In the crystallization tube of [ZnCl$_2$(**6**)]$_n$ colorless plates turned out to be crystallographically different and crystallize in the space group P-42$_1$c, which is tetragonal. Structural determination confirmed in fact that not a coordination polymer but a discrete metallosquare [{ZnCl$_2$(**6**)}$_4$] (Fig. 30) was obtained.
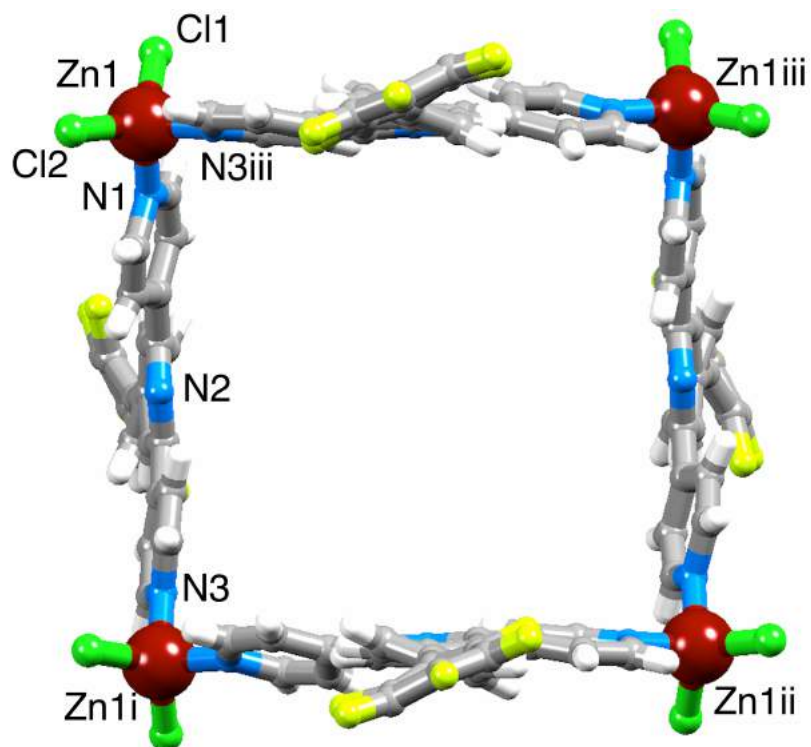
Fig. 30. Structure of [{ZnCl$_2$(**6**)}$_4$].

Even though the quality of the structure is low the main features are clearly determined. One {ZnCl$_2$(**6**)} unit is located in the asymmetric unit and since the molecule displays 4-symmetry the pentafluorophenyl moieties have an up/down/up/down alternation around the square. The four metal centers are almost located in one plane. Because of this, the conformation of [{ZnCl$_2$(**6**)}$_4$] is evocative of the 1,3-alternate form of a calix[4]arene or cyclophane such as the tetrapyridino-cyclophane[27]. Interdigitation of adjacent molecules (Fig. 31) via H…F contacts (2.27, 2.40 and 2.55 Å) lead to the assembly of tubes along the c-axis.

Fig. 31. Interdigitation of adjacent [{ZnCl$_2$(**6**)}$_4$] with H...F interactions shown in red hashed lines.

The space-filling representation of the structure and depicts the tight interlocking of adjacent molecules in the tube-like cluster can be seen in Fig. 32.

Fig. 32. Packing of metallosquares in [{ZnCl$_2$(**6**)}$_4$]. Interlocking of molecules (all crystallographically equivalent) in part of one tube.

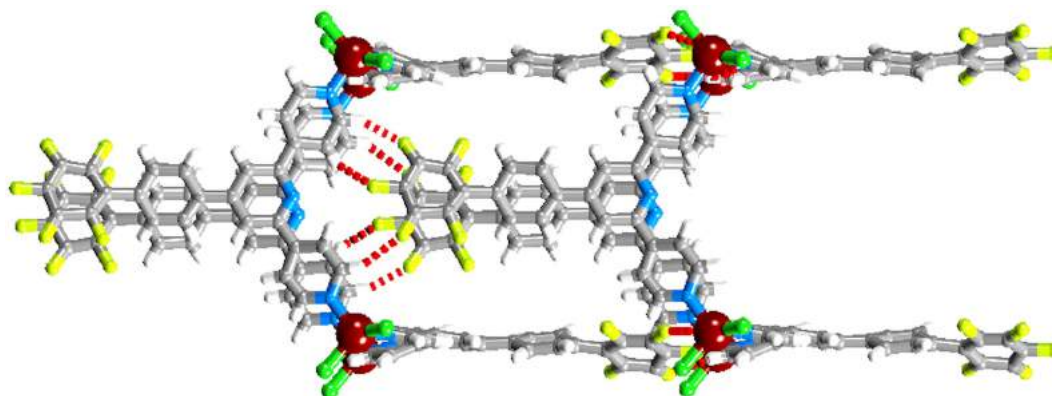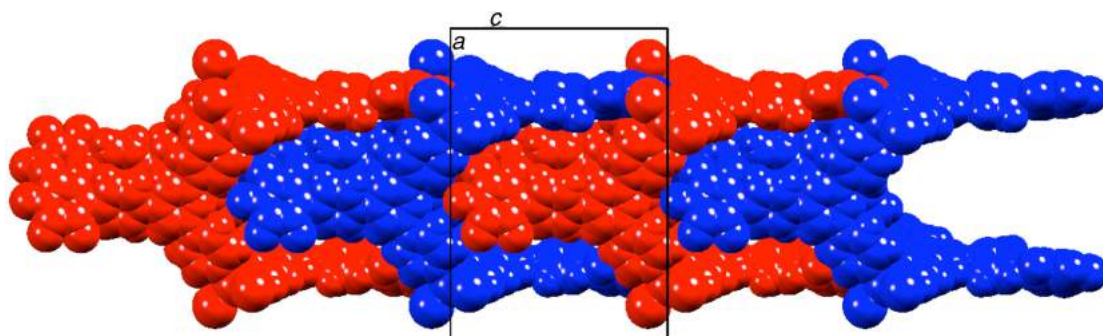The packing of tubes in the crystal lattice is displayed in Fig. 33. In this structure there is absolutely no π–stacking neither within a tube nor between neighboring tubes. Intra- and inter-tube voids that propagate along the c-axis are full of solvent molecules but since they are disordered no detailed understanding into their role in this structure could be gained.
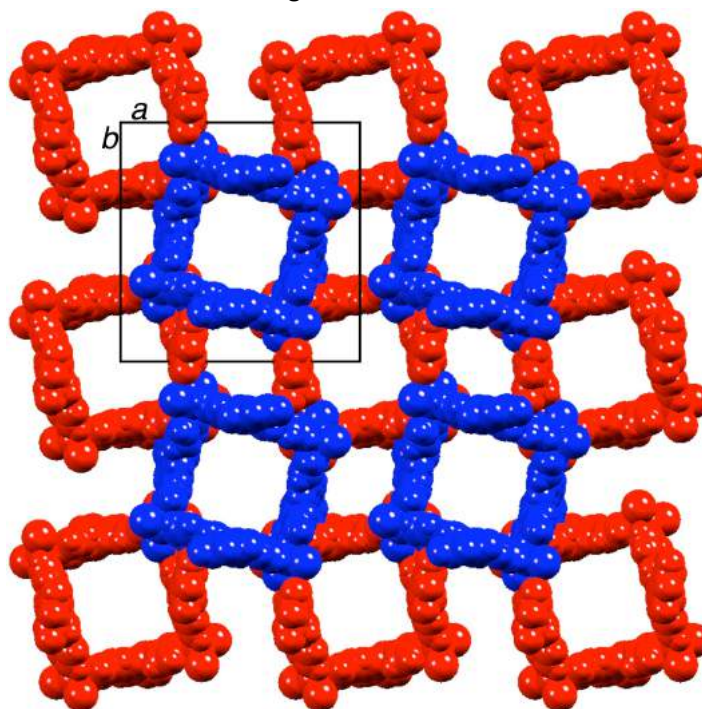
Fig. 33. Packing of metallosquares in [{ZnCl$_2$(**6**)}$_4$]. View down the tube axes.

4.5.4 Reactions with ligand **2** and ZnI$_2$

A solution of ZnI$_2$ in MeOH was layered over a solution of ligand 2 in CHCl$_3$ and after a while crystals of the one-dimensional coordination polymer [2{ZnI$_2$(**2**).CHCl$_3$}]$_n$ were formed. The compound crystallizes in the space group P2$_1$/c, which is monoclinic and two independent {ZnI$_2$(**2**)} entities are to be found in the asymmetric unit. The coordination sphere around the Zn centers is tetrahedral with a distorted geometry. Ligand **2** acts as a bridge between two Zn atoms with the central N of the tpy being uncoordinated. Both independent polymer chains are assembled through a glide plane similar to those observed for [ZnY$_2$(4'-(4-(3-chloropyridyl))-4,2':6',4''-tpy)]$_n$ (Y = Cl or I)[7] and [ZnI$_2$(4'-(4-pyridyl)-4,2':6',4''-tpy)]$_n$[28]. and

92

therefore because of this symmetry operation, the 4'-(4-(naphthyl-1-yl)phenyl) moieties are all located on the same side of the chain as can be seen in Fig. 34.
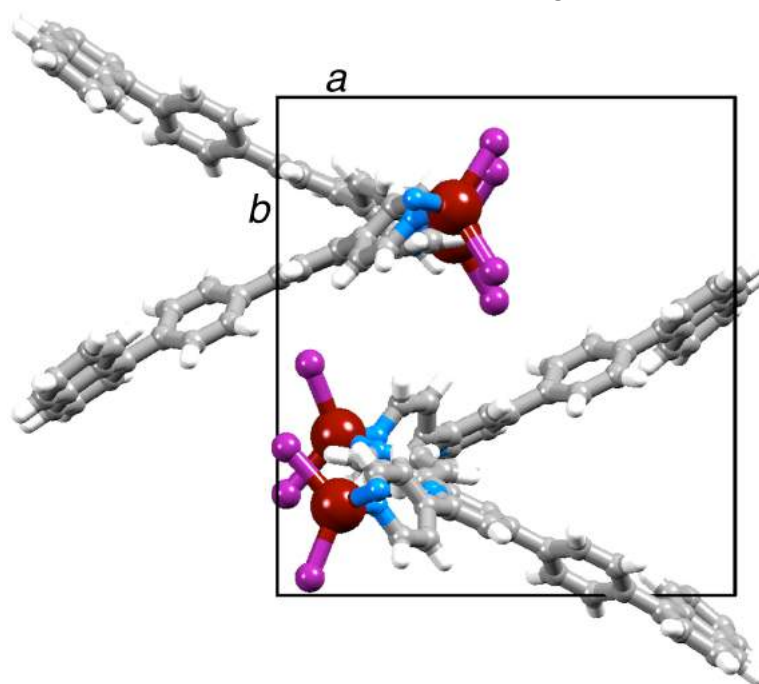
Fig. 34. View down the c-axis in $[2\{ZnI_2(\mathbf{2}).CHCl_3\}]_n$ showing the two independent coordination polymer chains (chain A, top; chain B, bottom); solvent molecules are omitted.

Chains A combine with each other via head-to-tail parings of ligand **2** as illustrated in Fig. 35.
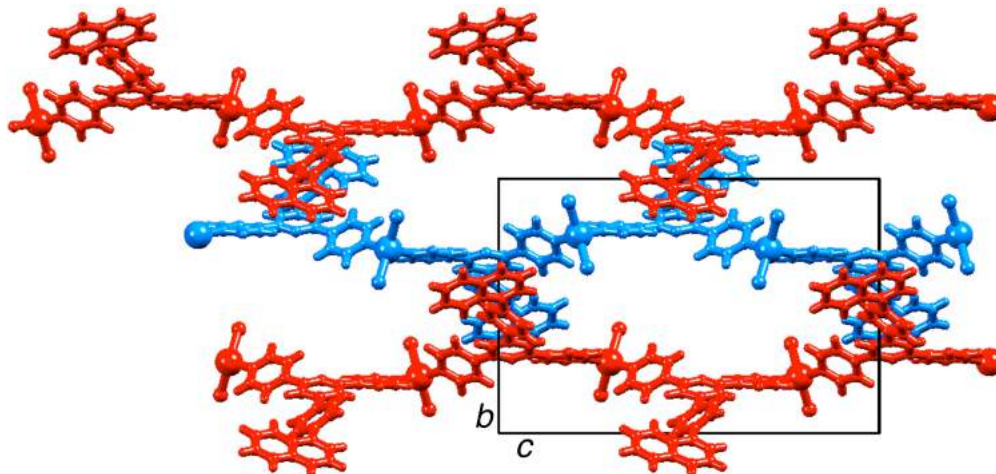
Fig. 35. Alternate ligands in independent chains A in $[2\{ZnI_2(\mathbf{2}).CHCl_3\}]_n$ stack with those of the next chain to form a corrugated sheet.

Yet, the face-to-face stacking is less than ideal due to the fact that the rings are mutually twisted within the ligand (angles between the planes of rings D/C, C/B, B/A =48.5, 57.6, 65.2 and 23.3°, respectively). The resulting assembly is a corrugated sheet, which propagates in the bc-plane as shown in the space-filling diagram in Fig. 36.

93
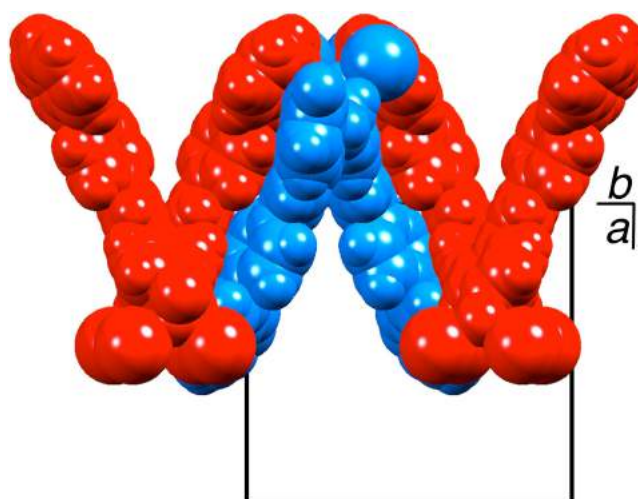
Fig. 36. Part of a corrugated sheet; each coordination polymer chain follows the c-axis.

Comparable packing is seen for the chains B, which leads to two crystallographically independent, combined corrugated sheets (brown and orange in Fig. 37).
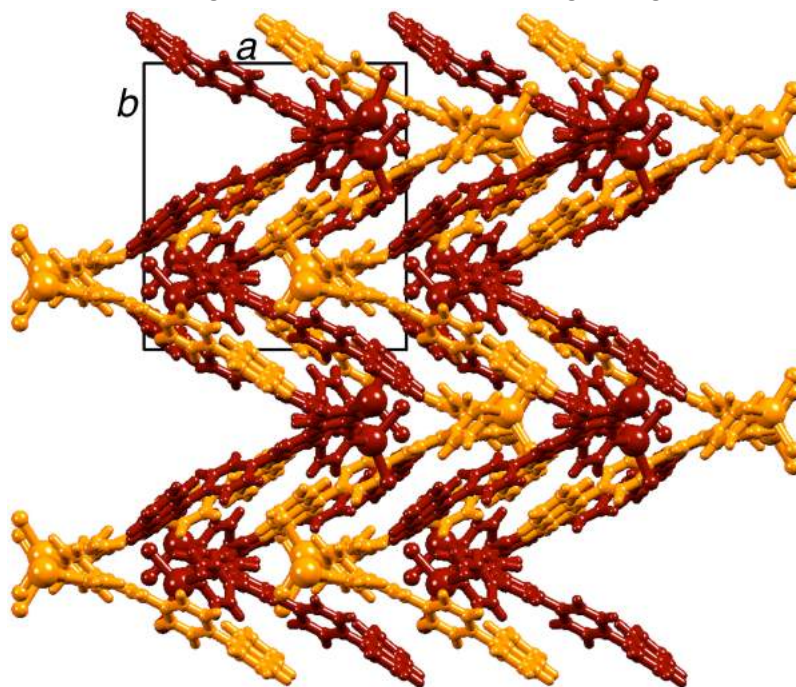
Fig. 37. Packing of crystallographically independent (brown and orange) corrugated sheets in [2{ZnI$_2$(**2**).CHCl$_3$}]$_n$; solvent molecules are omitted.

4.6 Experimental part

[{ZnCl$_2$(**1**)}$_6$]-A.

Compound **1** (21.8 mg, 0.0500 mmol) was dissolved in a mixture of 1,2-dichlorobenzene (6 mL) and MeOH (2 mL) in a long test tube. A solution of anthracene (36 mg, 0.20 mmol) in 1,2-dichlorobenzene (2 mL) was added and then a 1,2-dichlorobenzene and MeOH mixture (3.0 mL of each) was layered on top. Finally, a solution of ZnCl$_2$ (6.7 mg, 0.049 mmol) in MeOH (8.0 mL) was added carefully, and the tube was sealed with Parafilm 'M'. After a month at room temperature, colourless crystals had formed. Yield: 6.8 mg, 24%. Found C 62.75, H 3.74, N 6.59; C$_{31}$H$_{21}$Cl$_2$N$_3$Zn·H$_2$O requires C 63.13, H 3.93, N 7.23%.

[{ZnCl$_2$(**1**)}$_6$]-P.

The reaction scale and conditions were as for [{ZnCl$_2$(**1**)}$_6$]-A, replacing anthracene by perylene (50.5 mg, 0.2 mmol). After a month at room temperature, yellow crystals had formed. Yield: 11.7 mg, 40.9%. Found 63.81, H 3.95, N 7.09; [{ZnCl$_2$(**1**)}$_6$]·H$_2$O requires C 63.13, H 3.93, N 7.12%.

[ZnCl$_2$(**1**)]$_n$.

Compound **1** (21.8 mg, 0.050 mmol) was dissolved in a mixture of 1,2-dichlorobenzene (6 mL) and MeOH (2 mL) in a long test tube. A solution of pyrene (41.3 mg, 0.204 mmol) in 1,2-dichlorobenzene (2 mL) was added, followed by a mixture of 1,2-dichlorobenzene (2.5 mL) and MeOH (2.5 mL). A solution of ZnCl$_2$ (6.7 mg, 0.049 mmol) in MeOH (8.0 mL) was then added carefully. The tube was sealed with Parafilm 'M' and left to stand at room temperature. Colourless crystals grew over a period of about a month. Yield: 8.1 mg, 28%. Found C 64.75, H 3.93, N 6.76; C$_{31}$H$_{21}$Cl$_2$N$_3$Zn requires C 65.12, H 3.70, N 7.35%.

[ZnCl$_2$(**2**)]$_n$ and [{ZnCl$_2$(**2**)}$_4$].

Compound **2** (23.6 mg, 0.050 mmol) was dissolved in a mixture of 1,2-dichlorobenzene (6 mL) and MeOH (2 mL) in a long test tube. A solution of pyrene (41.3 mg, 0.204 mmol) in 1,2-dichlorobenzene (2 mL) was layered on top, followed by a mixture of 1,2-dichlorobenzene (2.5 mL) and MeOH (2.5 mL), and then a solution of ZnCl$_2$ (6.7 mg, 0.049 mmol) in MeOH (8.0 mL). The tube was sealed with Parafilm 'M' and over a period of a month at room temperature, colourless crystals grew. Satisfactory elemental analysis for the bulk sample was not obtained.

[ZnI$_2$(**1**)]$_n$.

A solution of **1** (21.8 mg, 0.050 mmol) in CHCl$_3$ (6.0 mL) was placed in a long test tube, and MeOH (3.0 mL) was layered on top, followed by a solution of ZnI$_2$ (15.8 mg, 0.0495 mmol) in MeOH (5.0 mL). The tube was sealed with Parafilm 'M' and was left at room temperature.

95

Over a period of a week, yellowish crystals grew. Yield: (18.1 mg, 47.7%). Found C 43.20, H 3.09, N 4.70; $C_{31}H_{21}I_2N_3Zn \cdot CHCl_3$ requires C 43.97, H 2.54, N 4.81%.

Crystallography

[{ZnCl$_2$(**1**)}$_6$]·3C$_6$H$_4$Cl$_2$·6MeOH = [{ZnCl$_2$(**1**)}$_6$]-A.

After SQUEEZE and with modelled solvent: $C_{210}H_{146}Cl_{18}N_{18}O_6Zn_6$, M = 4064.14, colourless block, trigonal, space group $R\bar{3}$, $a = b$ = 35.744(2), c = 23.9081(16) Å, U = 26 453(4) Å^3, Z = 3, D_c = 0.765 Mg m^{-3}, μ(Cu-Kα) = 1.503 mm^{-1}, T = 123 K. Total 49 363 reflections, 10 603 unique, R_{int} = 0.0765. Refinement of 6980 reflections (334 parameters) with $I > 2\sigma(I)$ converged at final R_1 = 0.0311 (R_1 all data = 0.0526), wR_2 = 0.0626 (wR_2 all data = 0.0661), gof = 0.799. CCDC 992575.

[{ZnCl$_2$(**1**)}$_6$]·3C$_6$H$_4$Cl$_2$·2MeOH = [{ZnCl$_2$(**1**)}$_6$]-P.

After SQUEEZE and with modelled solvent: $C_{206}H_{146}Cl_{18}N_{18}O_2Zn_6$, M = 3959.99, yellow block, trigonal, space group $R\bar{3}$, $a = b$ = 70.6015(18), c = 23.9920(6) Å, U = 103 568(6) Å^3, Z = 12, D_c = 0.762 Mg m^{-3}, μ(Cu-Kα) = 1.536 mm^{-1}, T = 123 K. Total 207 036 reflections, 42 281 unique, R_{int} = 0.1874. Refinement of 20 632 reflections (1339 parameters) with $I > 2\sigma(I)$ converged at final R_1 = 0.1199 (R_1 all data = 0.1790), wR_2 = 0.2869 (wR_2 all data = 0.3228), gof = 0.971. CCDC 992580.

[ZnCl$_2$(**1**)]$_n$.
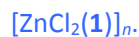
After SQUEEZE: $C_{124}H_{84}Cl_8N_{12}Zn_4$, M = 2287.20, colourless block, triclinic, space group $P\bar{1}$, a = 14.3701(12), b = 22.089(2), c = 26.512(3) Å, α = 95.414(6), β = 95.480(6), γ = 92.935(5), U = 8324.2(13) Å^3, Z = 2, D_c = 0.912 Mg m^{-3}, μ(Cu-Kα) = 2.123 mm^{-1}, T = 123 K. Total 76 749 reflections, 29 093 unique, R_{int} = 0.0600. Refinement of 19 792 reflections (1333 parameters) with $I > 2\sigma(I)$ converged at final R_1 = 0.0714 (R_1 all data = 0.0941), wR_2 = 0.1933 (wR_2 all data = 0.2079), gof = 1.034. CCDC 1006953.

[ZnCl$_2$(**2**)]$_n$.
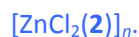
After SQUEEZE: $C_{108}H_{56}Cl_8F_{20}N_{12}Zn_4$, M = 2446.81, colourless plate, triclinic, space group $P\bar{1}$, a = 14.3665(6), b = 20.7814(8), c = 26.2162(13) Å, α = 99.654(3), β = 97.510(3), γ = 103.905(3), U = 7369.5(6) Å^3, Z = 2, D_c = 1.103 Mg m^{-3}, μ(Cu-Kα) = 2.629 mm^{-1}, T = 123 K. Total 57 651 reflections, 25 727 unique, R_{int} = 0.0583. Refinement of 16 085 reflections (1369 parameters) with $I > 2\sigma(I)$ converged at final R_1 = 0.0695 (R_1 all data = 0.1002), wR_2 = 0.1763 (wR_2 all data = 0.1906), gof = 0.932. CCDC 1006954.

[{ZnCl$_2$(**2**)}$_4$]·2C$_6$H$_4$Cl$_2$·5MeOH.

After SQUEEZE and with modelled solvent: C$_{125}$H$_{85}$Cl$_{12}$F$_{20}$N$_{12}$O$_5$Zn$_4$, M = 2901.04, colourless plate, tetragonal, space group $P\bar{4}2_1c$, $a = b$ = 23.6145(15), c = 16.4568(10) Å, U= 177.0(13) Å^3, Z = 2, D_c = 1.050 Mg m^{-3}, μ(Cu-Kα) = 2.111 mm^{-1}, T = 123 K. Total 75 018 reflections, 8428 unique, R_{int} = 0.2237. Refinement of 3283 reflections (344 parameters) with $I > 2\sigma(I)$ converged at final R_1 = 0.0769 (R_1 all data = 0.1907), wR_2 = 0.1590 (wR_2 all data = 0.1884), gof = 0.853. CCDC 992577.

[2{ZnI$_2$(**1**)}·CHCl$_3$]$_n$.
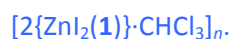
C$_{63}$H$_{43}$Cl$_3$I$_4$N$_6$Zn$_2$, M = 1628.76, colourless plate, monoclinic, space group $P2_1/c$, a = 14.9652(10), b = 16.3097(12), c = 24.4444(18) Å, $β$ = 91.698(2)°, U = 5963.7(7) Å^3, Z = 4, D_c = 1.814 Mg m^{-3}, μ(Cu-Kα) = 3.055 mm^{-1}, T = 123 K. Total 86 490 reflections, 11 089 unique, R_{int} = 0.0766. Refinement of 8572 reflections (741 parameters) with $I > 2\sigma(I)$ converged at final R_1 = 0.0493 (R_1 all data = 0.0728), wR_2 = 0.1034 (wR_2 all data = 0.1195), gof = 1.138. CCDC 992579.

4.7 References:

1. M. Barquin, J. Cancela, M. J. González Garmendia, J. Quintanilla and U. Amador, Polyhedron, 17, (1998), p. 2373.
2. B.-C. Wang, Q.-R. Wu, H.-M. Hu, X.-L. Chen, Z.-H. Yang, Y.-Q. Shangguan, M.-L. Yang and G.-L. Xue, CrystEngComm, 12, (2010), p. 485.
3. X.-Z. Li, M. Li, Z. Li, J.-Z. Hou, X.-C. Huang and D. Li, Angew. Chem., Int. Ed., 47, (2008), p. 6371.
4. L. Hou and D. Li, Inorg. Chem. Commun., 8, (2005), p. 190.
5. G. W. V. Cave and C. L. Raston, J. Supramol. Chem., 2, (2002), p. 317.
6. E. C. Constable, C. E. Housecroft, P. Kopecky, M. Neuburger, J. A. Zampese and G. Zhang, CrystEngComm, 14, (2012), 446.
7. E. C. Constable, G. Zhang, C. E. Housecroft and J. A. Zampese, CrystEngComm, 13, (2011), 6864.
8. A. L. Spek, Acta Crystallogr., Sect. D: Biol. Crystallogr., 65, (2009), p. 148.
9. K. Tashiro and T. Aida, Chem. Soc. Rev., 36, (2007), p. 189.
10. D. Canevet, E. M. Pérez and N. Martín, Angew. Chem., Int. Ed., 50, (2011), p. 9248.
11. T. Haino, M. Yanase and Y. Fukazawa, Tetrahedron Lett., 38, (1997), p. 3739.
12. J. L. Atwood, L. J. Barbour, P. J. Nichols, C. L. Raston and C. A. Sandoval, Chem.–Eur. J., 5, (1999), p. 990.
13. J. L. Atwoood, L. J. Barbour, M. W. Heaven and C. L. Raston, Angew. Chem., Int. Ed., 42, (2003), p. 3254.
14. M. Makha, M. J. Hardie and C. L. Raston, Chem. Commun., 2002, p. 1446.
15. Y. Bi, W. Liao, X. Wang, X. Wang and H. Zhang, Dalton Trans., 40, (2011), p. 1849.
16. J. Song, N. Aratani, H. Shinokubo and A. Osuka, J. Am. Chem. Soc., 132, (2010), p. 16356.

17. C. Pariya, C. R. Sparrow, C.-K. Back, G. Sandí, F. R. Fronczek and A. W. Maverick, Angew. Chem., Int. Ed., 46, (2007), p. 6305.

18. J.-Y. Zheng, K. Tashiro, Y. Hirabayashi, K. Kinbara, K. Saigo, T. Aida, S. Sakamoto and K. Yamaguchi, Angew. Chem., Int. Ed., 40, (2001), p. 1858.

19. M. Yanagisawa, K. Tashiro, M. Yamasaki and T. Aida, J. Am. Chem. Soc., 129, (2007), p. 11912.

20. L. P. Hernández-Eguía, E. C. Escudero-Adán, I. C. Pintre, B. Ventura, L. Flamigni and P. Ballester, Chem.–Eur. J., 17, (2011), p. 14564.

21. H. Nobukuni, Y. Shimazaki, F. Tani and Y. Naruta, Angew. Chem., Int. Ed., 46, (2007), p. 8975.

22. H. Nobukuni, Y. Shimazaki, H. Uno, Y. Naruta, K. Ohkubo, T. Kojima, S. Fukuzumi, S. Seki, H. Sakai, T. Hasobe and F. Tani, Chem.–Eur. J., 16, (2010), 16, 11611.

23. H.-B. Burgi, E. Blanc, D. Schwarzenbach, S. Liu, Y.-J. Lu, M. M. Kappes and J. A. Ibers, Angew. Chem., Int. Ed. Engl., 31, (1992), p. 640.

24. M. Fujiwara, T. Kambe and K. Oshima, Phys. Rev. B: Condens. Matter Mater. Phys., 71, (2005), p. 174424.

25. A. O'Neil, C. Wilson, J. M. Webster, F. J. Allison, J. A. K. Howard and M. Poliakoff, Angew. Chem., Int. Ed., 41, (2002), p. 3796.

26. D. V. Konarev, A. Yu. Kovalevsky, A. L. Litvinov, N. V. Drichko, B. P. Tarasov, P. Coppens and R. N. Lyubovskaya, J. Solid State Chem., 168, (2002), p. 474.

27. C. Klein, E. Graf, M. W. Hosseini and A. De Cian, New J. Chem., 25, (2001), p. 207.

28. J. Heine, J. Schmedt auf der Günne and S. Dehnen, J. Am. Chem. Soc., 133, (2011), p. 10018.

Chapter V: Reactions of back-to-back 4,2':6',4''-terpyridines with Zn(II) halides

Multitopic ligands incorporating multiple 2,2':6',2''-terpyridine domains[1-6] have significantly expanded the diversity of structures accessible with the chelating 2,2':6',2''-tpy unit and have led to a wide range of architectures. Outside the patent literature, reports of multidomain 4,2':6',4''-tpy ligands are remarkably sparse,[7-9] although Yoshida et al. have investigated the coordination behaviour of 1,3-di((4,2':6',4''-terpyridin)-4'-yl)benzene, which forms a triply interpenetrating network with cobalt(II)[8].

5.1. Structures with ligand 8

5.1.1 Reactions with ZnCl$_2$

A chloroform solution of ligand **8** was inserted into a long test tube and a methanol solution of two equivalents of ZnCl$_2$ with respect to the ligand was carefully layered on top. After a month yellow crystals were obtained, which analyzed as {[Zn$_2$Cl$_4$(**8**)].4H$_2$O}n where every ligand binds to the metal ion only through its outer pyridine rings. The compound crystallizes in the space group C2/c where half a ligand and one ZnCl$_2$ unit are to be found in the asymmetric unit. The fatty C8 chain is disordered and was modeled in a way that each of the last five C atoms has two sites with the fractional occupancies being 0.46 and 0.54 while the residual electron density in the lattice has been modeled as partial occupancy H$_2$O molecules. There is not a big difference between the conformation of the free ligand and its conformation within the coordination polymer. Every ligand **8** acts as a 4-connecting node (coordination through the four outer pyridine rings) the tetrahedral Zn(II) centers being the linkers. As can be seen on Fig. 1 four Zn(II) ions and four ligands assemble to form the primary unit of the structure, which is a macrocycle.
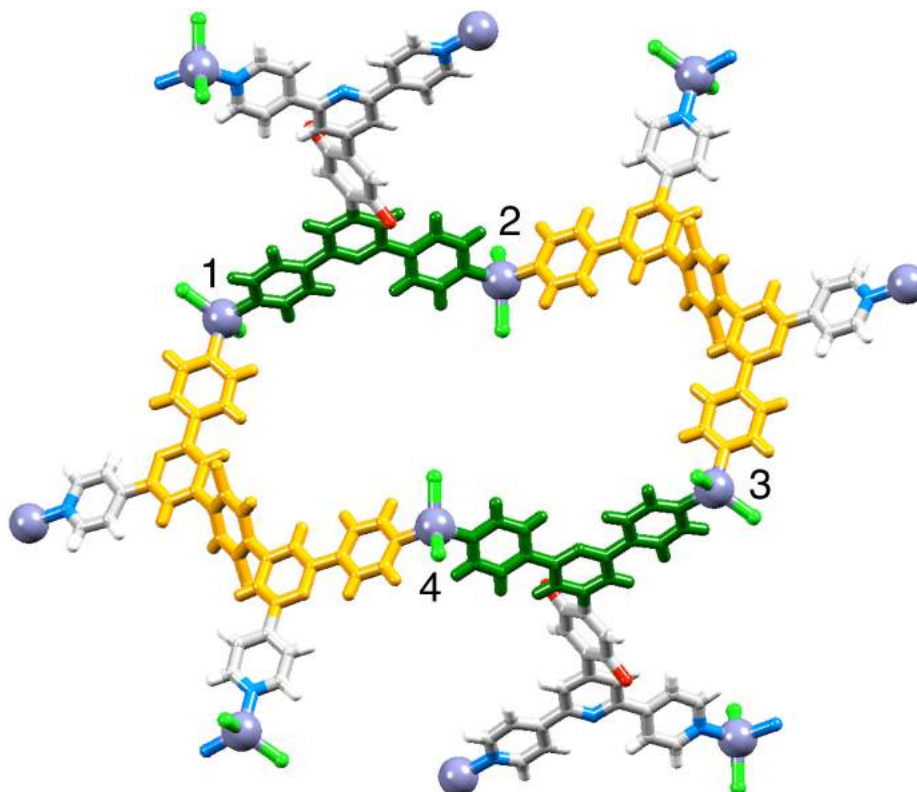

Fig. 1. One macrocyclic unit in {[Zn$_2$Cl$_4$(**8**)].4H$_2$O}n, emphasizing the two different bridging modes of **8**. Alkyl chains omitted for clarity.

99

Ligand **8** has two distinct bridging modes: metal centers 1 and 2 and centers 3 and 4 are connected by a single tpy domain (green in Fig. 1) while centers 2 and 3 and 4 and 1 are bridged by two nitrogen donors from two different tpy domains (yellow in Fig. 1) of one single ligand. Consequently, the macrocycle is not planar and the interconnection of those generates a (4,4) sheet that lies in the bc-plane and a part of that sheet is shown in Fig. 2.
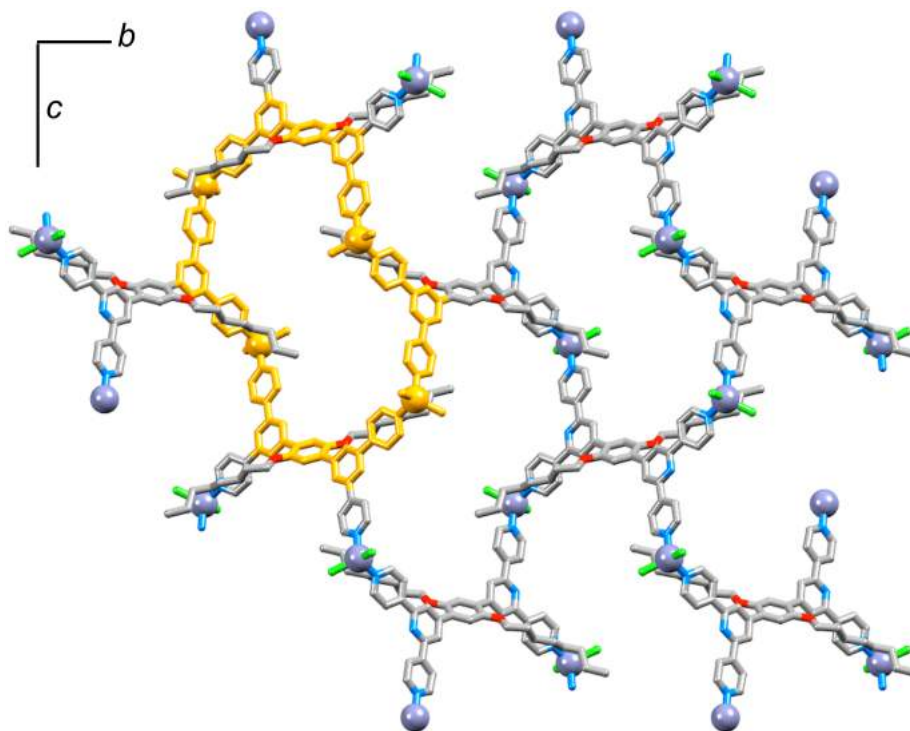

Fig. 2. Part of one (4,4) sheet in $\{[Zn_2Cl_4(\mathbf{8})].4H_2O\}n$ with one macrocyclic unit highlighted in orange; view down the a-axis.

When the same sheet is viewed down the c-axis (Fig. 3) its corrugated topology can be seen and the alkoxy chains sort of face towards each other and are threaded through the middle of the sheet.
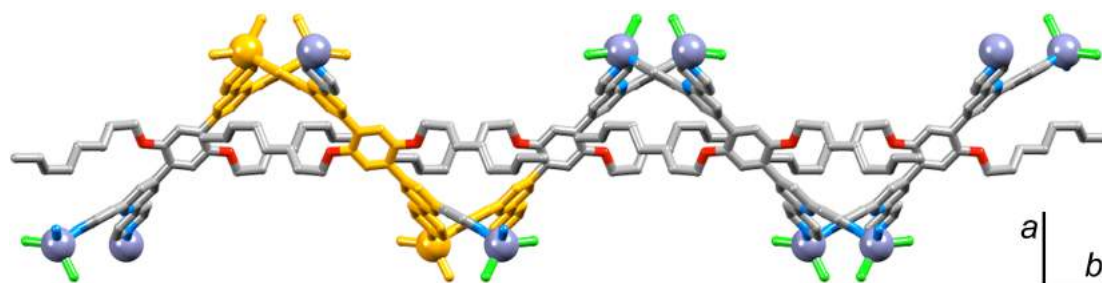

Fig. 3 Part of one (4,4) sheet in $\{[Zn_2Cl_4(\mathbf{8})].4H_2O\}n$ with one macrocyclic unit highlighted in orange; view down the c-axis. Hydrogen atoms are omitted.

The corrugated, wave-like form of each sheet allows two of those sheets to interpenetrate[10] in a 2D➔2D parallel manner[11,12] in order to optimize packing (Fig. 4 and 5). ZnCl₂ units stick

out from the top and bottom of a layer and are to be found in V-shaped cavities (Fig. 4) of an adjacent layer.
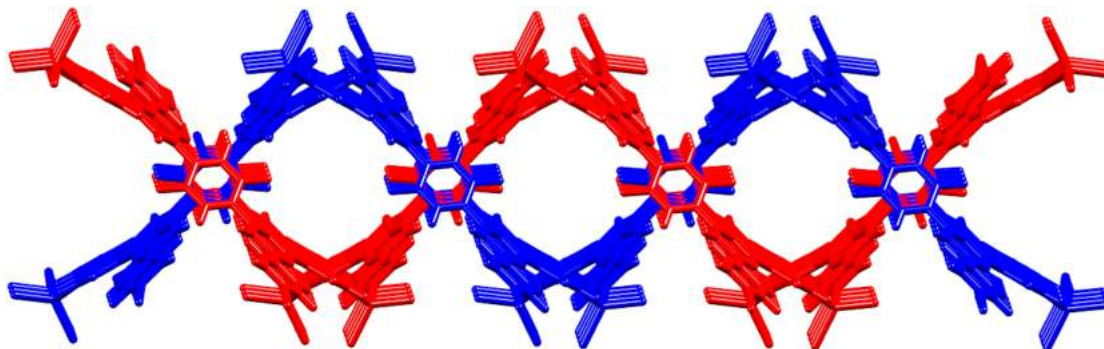

Fig. 4. View down the c-axis showing 2D➔2D parallel interpenetration of sheets in one layer of the lattice in $\{[Zn_2Cl_4(\mathbf{8})].4H_2O\}n$. Alkyl chains have been deleted for clarity.

Packing between the various layers comprises face-to-face stacking of tpy units that are at a distance of 3.59 Å. In one particular layer there are no such stacking interactions between aromatics but the C8 chains are sandwiched between two tpy moieties.
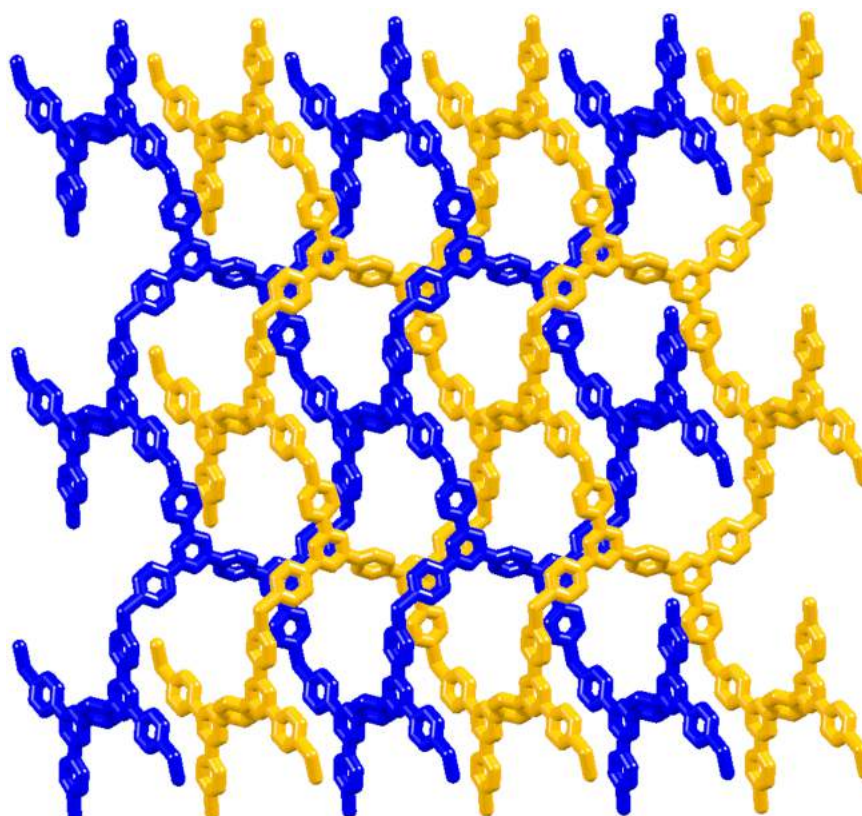
Fig. 5. View down the a-axis showing interpenetration of two sheets in one layer of the lattice in $\{[Zn_2Cl_4(\mathbf{8})].4H_2O\}_n$. Alkyl chains have been deleted for clarity.

5.1.2 Reactions with ZnBr$_2$

Using the same crystal growing conditions as for the setup with ZnCl$_2$, ligand **8** was reacted with ZnBr$_2$ and the coordination polymer $[\{Zn_2Br_4(\mathbf{8})]_n$ was obtained. It crystallizes in the C2/c space group, which is monoclinic and the unit cell parameters are similar to the previously

described $\{[Zn_2Cl_4(\mathbf{8})]\cdot 4H_2O\}_n$. Half a ligand **8** and one $ZnBr_2$ unit are to be found in the asymmetric unit and the repeat unit can be seen in Fig. 6.
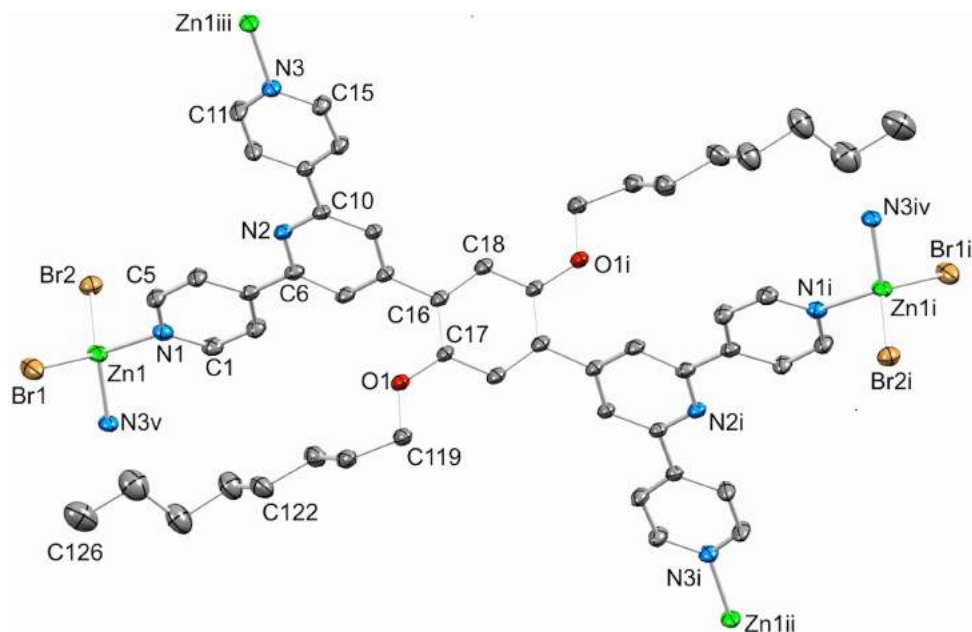
Fig. 6. The repeat unit (with symmetry generated connected atoms) in $[\{Zn_2Br_4(\mathbf{8})\}]_n$ (H atoms omitted; ellipsoids plotted at 30% probability level; for the disordered alkyl chain, only one site is shown)

There is again some disorder in the alkyl chain and it had been modeled over two positions, which have fractional occupancies of 0.49 and 0.51. Zn1 has a tetrahedral coordination sphere and ligand **8** coordinates only through its outer pyridine rings. Metallomacrocycles, made up from four Zn(II) nodes, two entire tpy domains from two different ligands 8 (purple in Fig. 7) and two halves of ligands **8** (dark green in Fig. 7) propagate along the coordination polymer generating a (4,4) net. It is assembled in the same way as the analogue with $ZnCl_2$ instead of $ZnBr_2$.
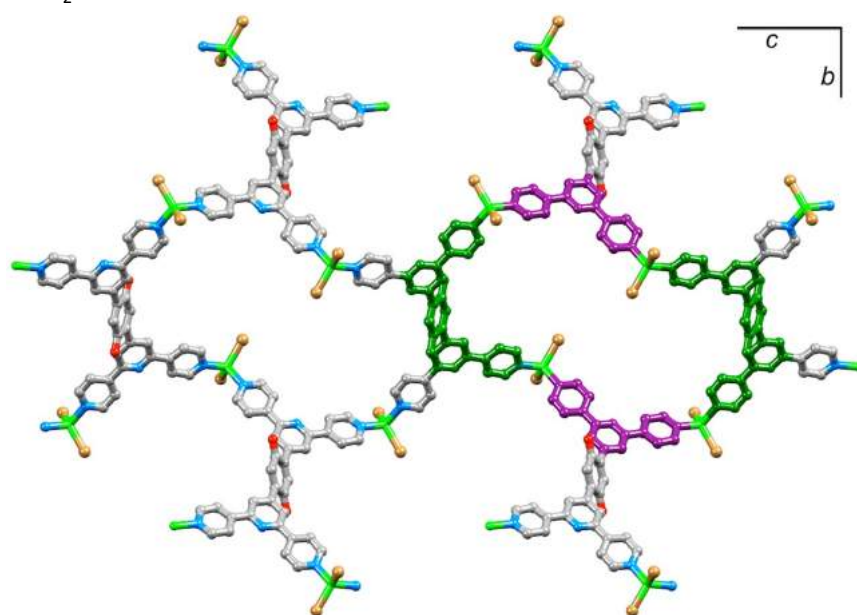
Fig. 7. Formation of metallomacrocyclic units in each (4,4) net in $[\{Zn_2Br_4(\mathbf{8})\}]_n$. Octyl chains and H atoms are omitted for clarity.

Every sheet has a corrugated topology as can be seen in Fig. 8 and the C8 chains are located along the middle of the sheet (Fig. 8 and 9).
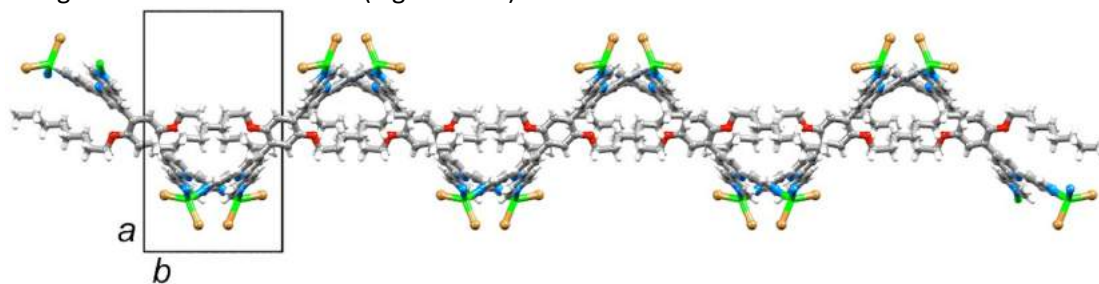
Fig. 8. Part of one (4,4) sheet in $[\{Zn_2Br_4(\mathbf{8})\}]_n$ viewed down the a-axis.
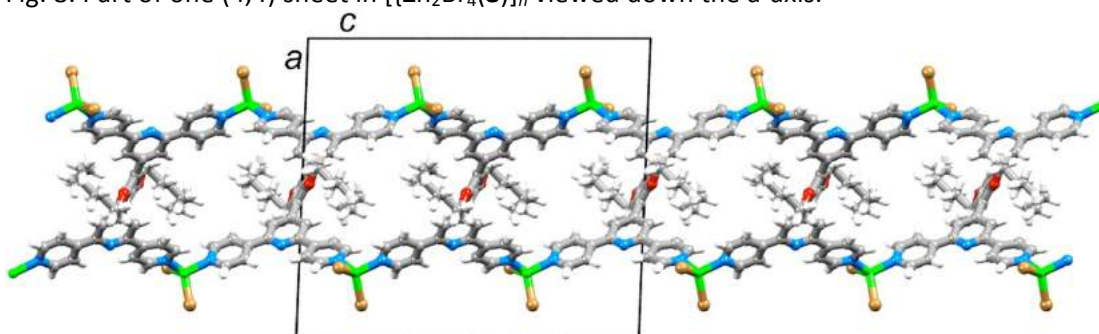
Fig. 9. Part of one (4,4) sheet in $[\{Zn_2Br_4(\mathbf{8})\}]_n$ viewed down the b-axis showing alignment of the octoxy chains within the sheet.

The sheets interpenetrate[10] in a 2D➔2D parallel fashion[11,12] due to the fact that they are relatively open. A TOPOS[13] representation of the structure is shown in Fig. 10 and 11, the 2D➔2D parallel interpenetration and the nesting of neighboring sheets with the $ZnBr_2$ units located in the V-shaped cavities in the subsequent layer can be seen.
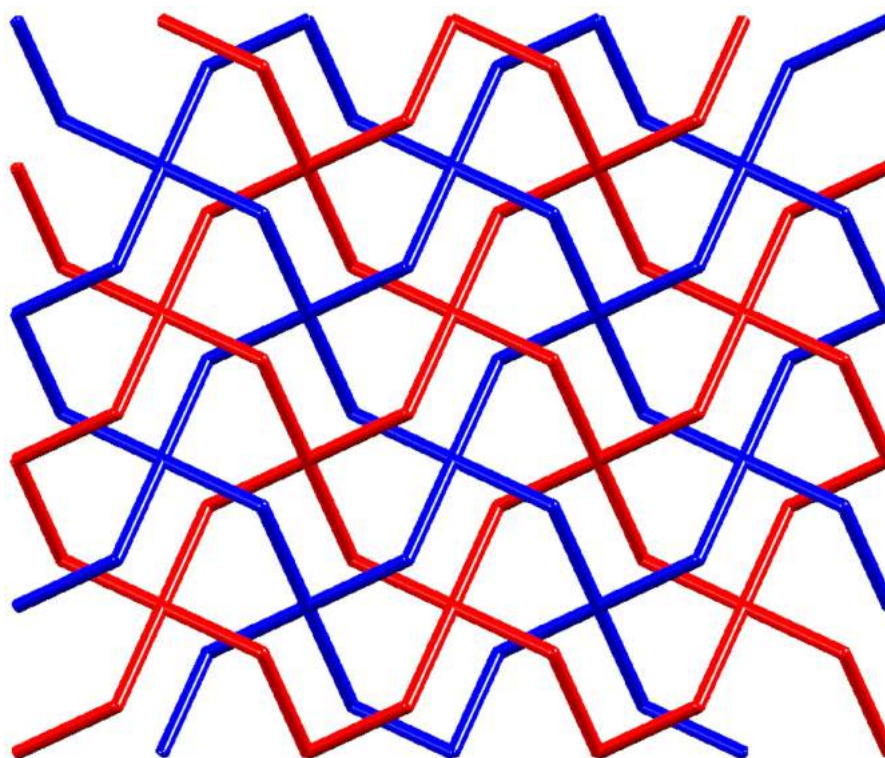
Fig. 10. TOPOS representation of parallel 2D➔2D interpenetrating sheets $[\{Zn_2Br_4(\mathbf{8})\}]_n$. (TOPOS figure generated by Max Klein)

103

Each of the nets can be considered as a 2-nodal one but can be simplified to a (4,4)-descriptor because of the fact that the 4-connecting nodes can be connected through a loop or a straight line but topologically speaking the nets are identical. But since the interpenetration occurs through the loops it is sensible for the Zn atoms to be retained as nodes[11].

Fig. 11. TOPOS representation of the nesting of two adjacent layers (labeled 1 and 2 for clarity) in [{Zn$_2$Br$_4$(**8**)}]$_n$. (TOPOS figure generated by Max Klein)

5.2. Structures with ligand 7

5.2.1 Reactions with ZnBr$_2$ and ZnI$_2$

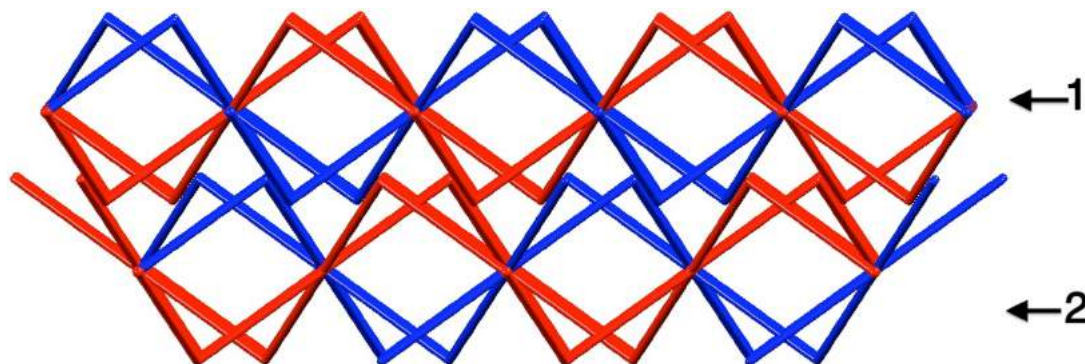As discussed in the previous section, when ligand **8** is reacted with ZnCl$_2$ or ZnBr$_2$ interpenetrating sheets are obtained and the long C8 chains seem to play an important role in stabilizing the structure. It is in fact interesting to examine the effects of shortening or removing the chains. Setups with ligand **9** were attempted but since its solubility was so low, ligand **7** was used instead, having a better solubility and the shortest chains possible. First the same conditions were used as for ligand **8**, namely dissolving ligand **7** in chloroform and layering a solution of metal in methanol on top of it. Even though those setups yielded some crystals they were of poor quality and losing solvent rapidly, which made them tough to handle. The preliminary structure that was obtained indicated that the compound crystallizes in the space group P2$_1$/c, which is monoclinic and that ligand **7** behaves as a 4-connecting node and creates a repeat unit close to the one that were previously described. Since the C8 chains are threaded through the cavities (thus stabilizing the structure) and ligand **7** seems to form a very similar macrocycle, a solution had to be found to have something in the cavity, which would not go out that easily. Therefore, in order to preserve the crystals and make them less sensitive to solvent loss, the ligand was dissolved in a 1:1 mixture of C$_6$H$_4$Cl$_2$ and MeOH instead of chloroform the idea being that C$_6$H$_4$Cl$_2$ could interact with the aromatic rings that make up the macrocycle. Those setups gave some X-ray quality crystals of [{Zn$_2$Br$_4$(**7**).2 C$_6$H$_4$Cl$_2$}]$_n$ and [{Zn$_2$I$_4$(**7**).2.3C$_6$H$_4$Cl$_2$}]$_n$. SQUEEZE was used in order to treat problems relative to solvent disorder in both structures. Both compounds crystallize in the space group P2$_1$/n, which is monoclinic and the cell parameters are similar to the one of the preliminary structure of the product of ligand **7** with ZnCl$_2$. The repeat unit of the coordination polymer [{Zn$_2$Br$_4$(**7**).2 C$_6$H$_4$Cl$_2$}]$_n$ can be seen in Fig. 12.
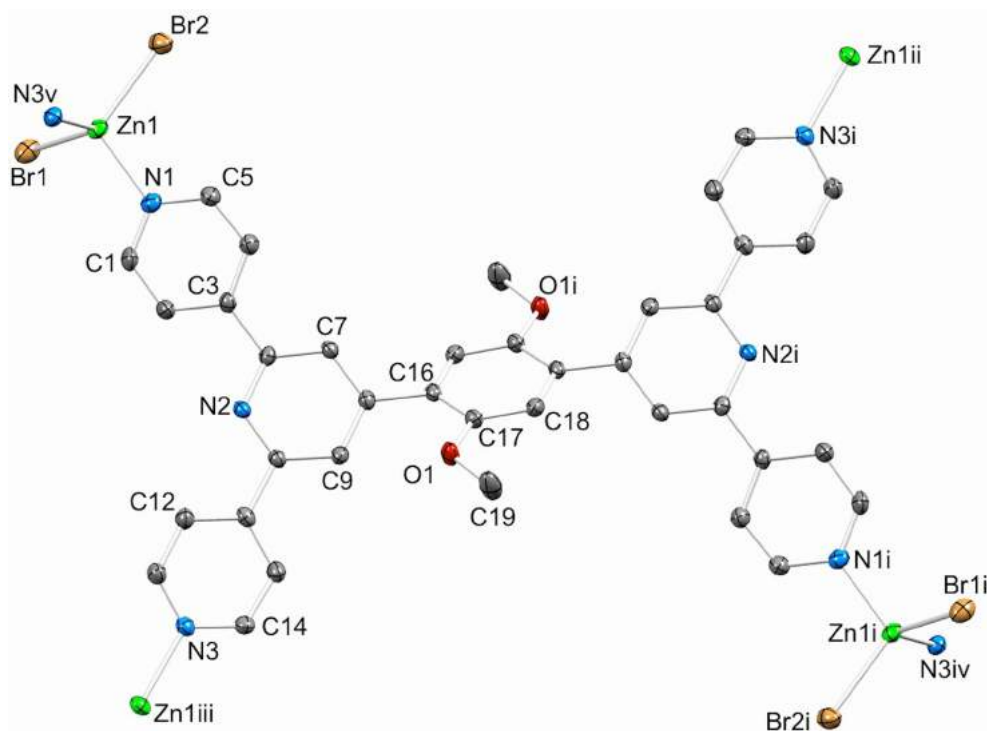
Fig. 12. The repeat unit (with symmetry generated connected atoms) in [{Zn_2Br_4(**7**).2 $C_6H_4Cl_2$}]$_n$ (H atoms omitted; ellipsoids plotted at 40% probability level).

Half of a molecule of ligand **7** and one $ZnBr_2$ unit are to be found in the asymmetric unit, with the second half of the ligand being generated by inversion. The coordination sphere of the Zn atom is tetrahedral and the ligand behaves as a planar 4-connecting node. Propagation into a single sheet follows the same connection patters as for the $ZnBr_2$ analogue with ligand **8**. Looking at the metallomacrocycles of the 2D sheet shown in Fig. 13 it
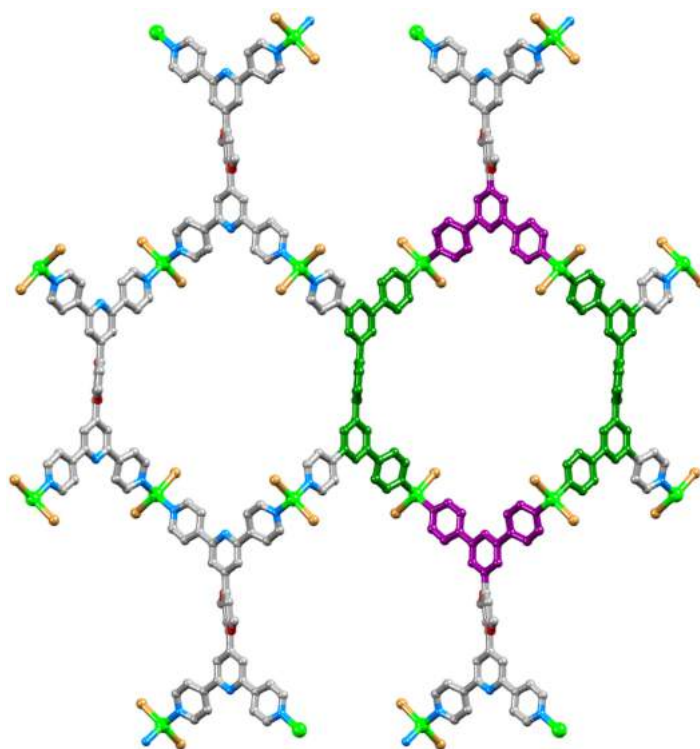
Fig. 13. Formation of metallomacrocyclic units in each (4,4) net in [{Zn_2Br_4(**7**).2 $C_6H_4Cl_2$}]$_n$.

is clear that they are assembled in the same way in term of connectivities as the macrocycles containing ligand **8**. Nonetheless, as can be seen in Fig. 14 the profile of this corrugated sheet is different to the one described in the first part of this chapter.
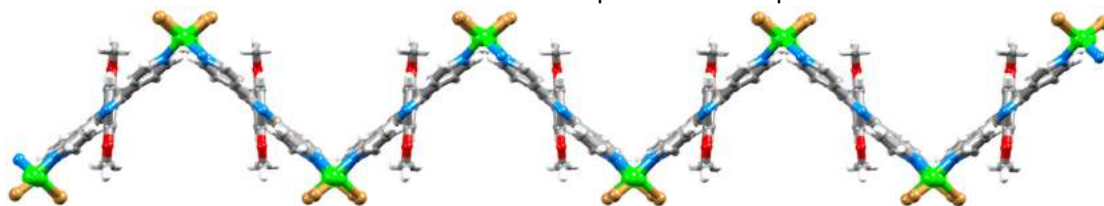
Fig. 14. Part of one corrugated (4,4) sheet in [{Zn_2Br_4(**7**).2 $C_6H_4Cl_2$}]$_n$.

This is due to the fact that the short chains (OMe substituents) point towards the top and the bottom of the sheet whereas the C8 chains were oriented along the sheet. Furthermore, in this case the 4-connecting nodes along each row in a sheet are coplanar while they are tilted in the case of [{Zn_2Br_4(**8**)}]$_n$ which is clearly seen in the two profiles in Fig. 15 and 16.
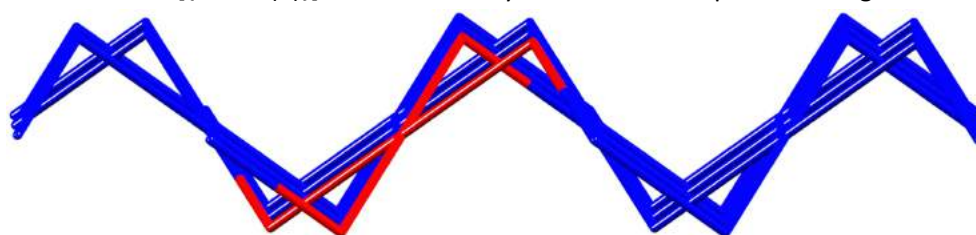
Fig. 15. One (4,4)-net in [{Zn_2Br_4(**7**).2 $C_6H_4Cl_2$}]$_n$ with one 4-connecting node shown in red. (TOPOS figure generated by Max Klein)
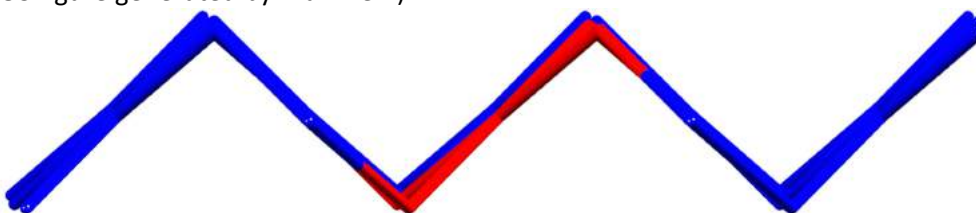
Fig. 16. One (4,4)-net in [{Zn_2Br_4(**8**)}]$_n$ with one 4-connecting node shown in red. (TOPOS figure generated by Max Klein)

In Fig. 17 a TOPOS representation of part of one sheet in [{Zn_2Br_4(**7**).2 $C_6H_4Cl_2$}]$_n$ is displayed and comparing it with Fig. 10 it is evident that there is no interpenetration in the structure.
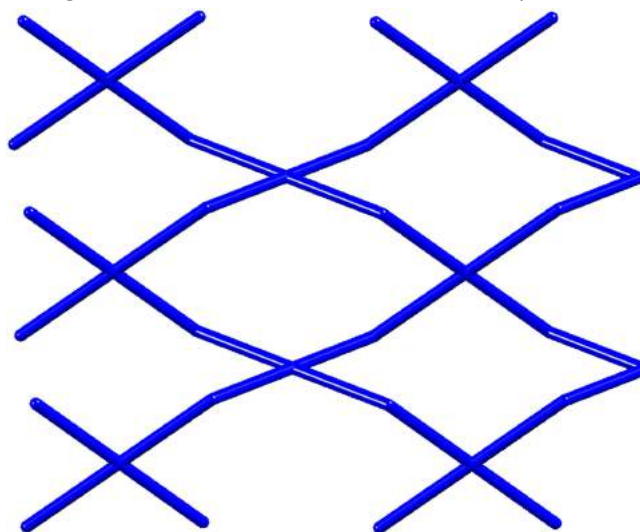
Fig. 17. TOPOS representation of part of one sheet in [{Zn_2Br_4(**7**).2 $C_6H_4Cl_2$}]$_n$. (TOPOS figure generated by Max Klein)

The two coordination polymers described in this section are generally isostructural and their corrugated sheets link closely through face-to-face interactions of their tpy domains as shown for example for the Br analogue in Fig. 18 and 19. The stacking takes place between the least-twisted bipyridine domains of neighboring ligands.
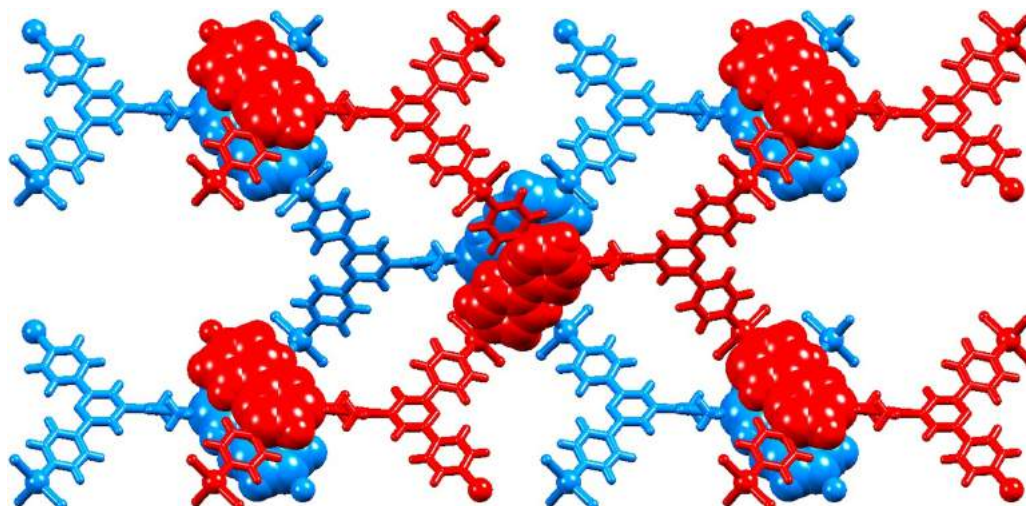
Fig. 18. Inter-sheet face-to-face interactions in $[\{Zn_2Br_4(\mathbf{7}).2\ C_6H_4Cl_2\}]_n$.
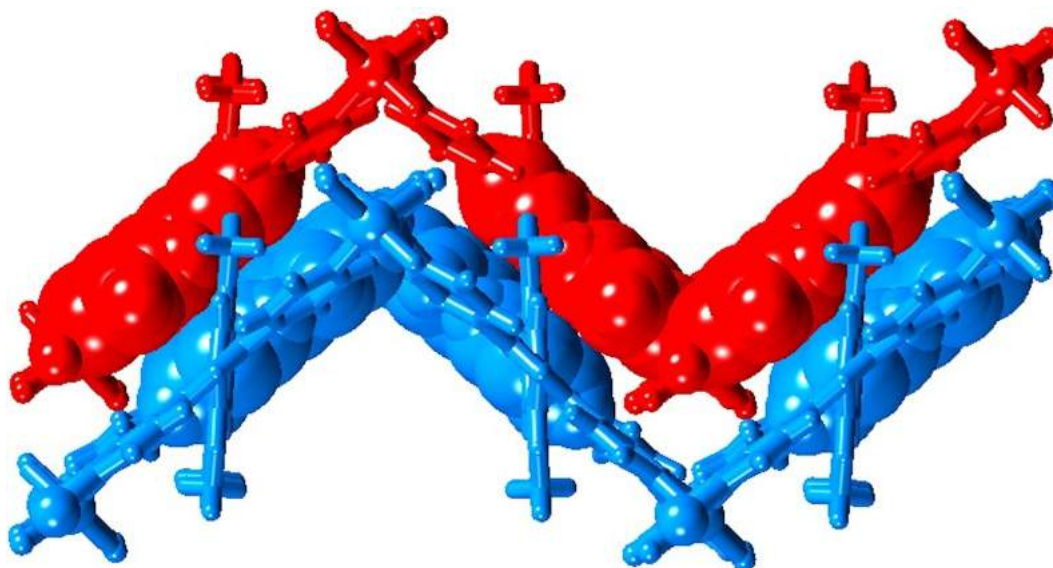
Fig. 19. Same inter-sheet face-to-face interactions in $[\{Zn_2Br_4(\mathbf{7}).2\ C_6H_4Cl_2\}]_n$ seen from a different angle.

The inter plane (least squares planes through the bpy units) separation is 3.38 Å for the Br analogue and 3.48 Å for the I one (the respective inter-centroid distances are 3.59 and 3.68 Å). Dichlorobenzene solvent molecules fit nicely into the remaining cavities as shown in Fig. 20 where face-to-face and edge-to-face interactions dominate. The fact that aromatic solvent molecules are encapsulated in the voids seems to be a major factor during the formation of the crystals as setups grown from chloroform yielded crystals that were very sensitive to solvent loss. Therefore, the assumption that the empty space has to be filled with something that is likely to be bound to the ligand in order to obtain better quality crystals that are easier to work with appears to be correct.
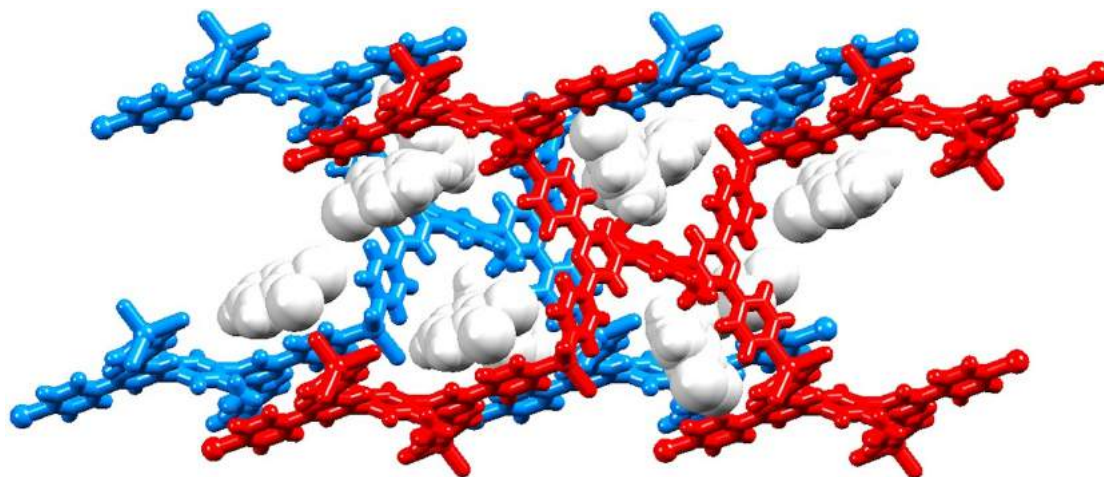
Fig. 20. Accommodation of $C_6H_4Cl_2$ molecules in cavities in the lattice of $[\{Zn_2Br_4(\textbf{7}).2\ C_6H_4Cl_2\}]_n$.

5.3 Experimetal part

[$Zn_2Cl_4(\textbf{8})$]

A solution of **8** (19.9 mg, 0.025 mmol) in $CHCl_3$ (6.0 mL) was placed in a long test tube, and MeOH (3.0 mL) was layered on top, followed by a solution of $ZnCl_2$ (6.8 mg, 0.05 mmol) in MeOH (5.0 mL). The tube was sealed with parafilm and after a month at room temperature, yellow crystals had formed. Yield (11.3 mg, 0.011 mmol, 42.3%). Found C 57.77, H 5.64, N 7.21; $C_{52}H_{56}Cl_4N_6O_2Zn_2$ requires C 58.39, H 5.28, N 7.86.

[$\{Zn_2Br_4(\textbf{1})\}$]

A solution of **1** (19.9 mg, 0.025 mmol) in $CHCl_3$ (6.0 mL) was prepared in a test tube, and MeOH (3.0 mL) was layered on top, followed by a solution of $ZnBr_2$ (11.3 mg, 0.05 mmol) in MeOH (5.0 mL). The tube was sealed with parafilm and after a month at room temperature, pale yellow crystals had formed. Found C 50.35, H 4.83, N 6.87; $C_{52}H_{56}Br_4N_6O_2Zn_2$ requires C 50.07, H 4.53, N 6.74%.

[$\{Zn_2Br_4(\textbf{2})\}\cdot 2C_6H_4Cl_2$]$_n$

A solution of **2** (15 mg, 0.025 mmol) in $C_6H_4Cl_2$/MeOH (6.0/2.0 mL) was placed in a test tube, and a mixture of $C_6H_4Cl_2$ (1.5 mL) and MeOH (1.5 mL) was layered on top, followed by a solution of $ZnBr_2$ (11.3 mg, 0.05 mmol) in MeOH (5.0 mL). The tube was sealed with parafilm and after a month at room temperature, pale yellow crystals had formed. Found C 44.17, H 3.05, N 8.40; $C_{38}H_{28}Br_4N_6O_2Zn_2$ requires C 43.42, H 2.69, N 8.00%.

[$\{Zn_2I_4(\textbf{2})\}\cdot 2.3C_6H_4Cl_2$]$_n$

A solution of **2** (15 mg, 0.025 mmol) in $CHCl_3$ /MeOH (6.0/2.0 mL) was prepared in a test

tube, and a mixture of $C_6H_4Cl_2$ (1.5 mL) and MeOH (1.5 mL) was layered on top, followed by a solution of ZnI_2 (16.3 mg, 0.05 mmol) in MeOH (5.0 mL). The tube was sealed with parafilm and after a month at room temperature, yellow crystals had formed. Found C 37.69, H 2.51, N 6.71; $C_{38}H_{28}I_4N_6O_2Zn_2 \cdot C_6H_4Cl_2$ requires C 38.13, H 2.33, N 6.06%.

[{Zn_2Br_4(**1**)}]

After SQUEEZE: $C_{52}H_{56}Br_4N_6O_2Zn_2$, M = 1247.43, colourless block, monoclinic, space group $C2/c$, a = 20.6639(16), b = 11.9145(10), c = 23.6388(17) Å, β = 92.289(5)^O, U = 5815.2(8) Å^3, Z = 4, D_C = 1.425 Mg.m^{-3}, μ(Cu-Kα) = 4.549 mm^{-1}, T = 123 K. Total 19113 reflections, 5293 unique, R_{int} = 0.044. Refinement of 3765 reflections (198 parameters) with I >2σ (I) converged at final $R1$ = 0.0607 ($R1$ all data = 0.0808), $wR2$ = 0.0646 ($wR2$ all data = 0.0845), gof = 0.9359. CCDC 1038251.

[{Zn_2Br_4(**2**)}·$2C_6H_4Cl_2$]$_n$

After SQUEEZE: $C_{50}H_{36}Br_4Cl_4N_6O_2Zn_2$, M = 1492.06, colourless block, monoclinic, space group $P21/n$, a = 12.0911(16), b = 18.972(3), c = 13.5812(18) Å, β = 111.805(5)^O, U = 2892.5(4) Å^3, Z = 2, D_C = 1.71 Mg.m^{-3}, μ(Cu-Kα) = 7.186 mm^{-1}, T = 123 K. Total 21568 reflections, 5069 unique, R_{int} = 0.030. Refinement of 4994 reflections (307 parameters) with I >2σ (I) converged at final $R1$ = 0.0530 ($R1$ all data = 0.0560), $wR2$ = 0.1358 ($wR2$ all data = 0.1390), gof = 0.9466. CCDC 1038252.

[{Zn_2I_4(**2**)}·$2.3C_6H_4Cl_2$]$_n$

After SQUEEZE: $C_{52}H_{37.50}Cl_{4.50}I_4N_6O_2Zn_2$, M = 1576.32, yellow block, monoclinic, space group $P21/n$, a = 11.997(2), b = 19.440(3), c = 13.828(2) Å, β = 112.664(7)^O, U = 2976.0(5) Å^3, Z=2, D_C =1.76 Mg.m^{-3}, μ(Cu-Kα)=19.476mm^{-1}, T= 123 K. Total 20800 reflections, 5181 unique, R_{int} = 0.045. Refinement of 5173 reflections (267 parameters) with I >2σ (I) converged at final $R1$ = 0.0683 ($R1$ all data = 0.0733), $wR2$ = 0.1811 ($wR2$ all data = 0.1843), gof = 0.9589. CCDC 1038253.

5.4 References

1. E. C. Constable, A. M. W. Cargill Thompson, P. Harveson, L. Macko and M. Zehnder, Chem.–Eur. J., 1, (1995), p. 360.
2. A. Wild, A. Winter, F. Schluetter and U. S. Schubert, Chem. Soc. Rev., 40, (2011), p. 1459.
3. Y. Yan and J. Huang, Coord. Chem. Rev., 254, (2010), p. 1072.
4. E. C. Constable, Chimia, 67, (2013), p. 388.
5. E. C. Constable, Coord. Chem. Rev.,252, (2008), p. 842.
6. E. C. Constable, Chem. Soc. Rev., 36, (2007), p. 246.
7. G. W. V. Cave and C. L. Raston, J. Chem. Soc., Perkin Trans. 1, (2001), p. 3258.

8. J. Yoshida, S.-I. Nishikiori and H. Yuge, J. Coord. Chem., 66, (2013), p. 2191.
9. S. A. S. Ghozlan and A. Z. A. Hassanien, Tetrahedron, 58, (2002), p. 9423.
10. H. Guo, D. Qiu, X. Guo, S. R. Batten and H. Zhang, CrystEngComm, 11, (2009), p. 2611.
11. S. R. Batten in *Supramolecular Chemistry: From Molecules to Nanomaterials*, eds. P. A. Gale and J. W. Steed, Wiley, Chichester, 2012, vol. 6, p. 3107.
12. S. R. Batten, CrystEngComm, 18, (2001), p. 1.
13. V.A. Blatov, A.P. Shevchenko, TOPOS Professional v. 4.0, Samara State University, Russia.

6. Conclusion and outlook

The synthesis and characterization of a number of novel 4'-substituted divergent 4,2':6',4''-terpyridine ligands was presented. It has been shown that the synthetic route where the tpy fragment is formed in the last step works best. Due to the fact that the 4'-position can be readily functionalized, a large number of ligands can be prepared via this route. The 4'-substituent can be selected depending on the interactions that are wished to be used in the formation of the structure.

Reacting the obtained ligands with zinc(II) acetate results in $[Zn_2(-OAc)_4(4'-X-4,2':6',4''-tpy)]_n$ (where X is an extended aryl system) one-dimensional coordination polymers being dominant. The chains propagate in a zig-zag manner and combine into flat sheets, which interact via π–stacking to yield efficiently packed structures. Propensity for metal acetate cluster formation did lead to the formation of a number of unexpected structures, some which are multiply-stranded chains. However, even in that case the key aspects of the packing characteristics found in the single-stranded polymers are observed. Ligand **6** was prepared in order to be complementary and interact specifically with ligand **1**, which was not the case. One could imagine that an analogue of ligand **6**, where the phenylene spacer is replaced by a tetrafluorophenylene would possibly be able to "recognize" the biphenyl moiety of ligand **1**.

Before this project, 4'-X-4,2':6',4''-tpy ligands (where X is not an extended aryl system for example ^tBu or Ph) showed a tendency to form one-dimensional coordination polymers, which are mostly helical, upon reaction with zinc(II) halides. When the ligands presented in this work are reacted with $ZnCl_2$ or $ZnBr_2$ the formation of metallohexacycles is promoted due to the extended aryl domains present in the 4'-position. The preference over the polymer formation can be explained by the interlocking of the metallocycles via π–stacking, which necessitates large aromatic substituents in order to form robust tube-like structures. It has been proven by fullerene encapsulation that those materials can act as hosts due to the presence of large voids. However, since all other inclusion attempts have been unsuccessful or could not be confirmed by single-crystal X-ray diffraction, other reactions with more suitable guest molecules could be tried in the future. Alternatively, new divergent 4,2':6',4''-tpy ligands with different 4'-substituents could be prepared and would maybe better interact and capture these guest molecules.

Also, the preparation of a novel family of back-to-back 4,2':6',4''-terpyridine ligands was shown. Just as in the case with the mono-tpys the tpy forming reaction should be performed in the end and works just as well in its double version. Via that route a considerable number of back-to-back tpys bearing different spacers could be synthesized. The type of spacer will have a direct influence on the separation of the two tpy moieties, as well as on the rigidity and on the solubility of the ligand.

When ligands **7** and **8** were reacted with zinc(II) halides 2D-(4,4) nets presenting a corrugated topology were formed. Nonetheless, the structural features are quite different. The single sheets containing ligand **7** have methoxy substituents that point above and below the sheet and neighboring sheets can thus engage in face-to-face π–interactions. On the contrary, structures with ligand **8** interpenetrate in a 2D➔2D parallel manner with extended octoxy chains propagating through the middle of the sheet. The successfully measured

crystals with ligand **7** had to be grown from an aromatic solvent, which seems to have an important stabilizing influence as crystals obtained with a non-aromatic solvent never gave a good quality structure. It would be interesting to synthesize analogs of ligands **7** and **8** with chain lengths between 2 and 7 carbon atoms in order to find out where the tipping point is, i.e. what the minimal chain length needs to be in order to observe 2D➔2D parallel interpenetration. Also, it would be interesting to investigate if the interpenetrated structure with the shortest chain is also the first one that can be grown successfully from chloroform without needing an aromatic solvent.

Furthermore, the described back-to-back ligands can be reacted with a number of suitable metal salts, such as Zn(II), Cu(II) Cd(II), which would produce new structures. Also, a "third generation" of back-to-back-to-back ligands could be designed and prepared, where the 4,2':6',4''-terpyridines are at an angle of 120 ^{o}C.

Curriculum Vitae

Personal information

Family name: Vujovic
First name: Srboljub
Address: Croisee des Lys 7, 68300 St. Louis, France

Cell phone: (+33) 6.28.34.10.51
E-mail: srijeca@hotmail.com

Date of birth: 8 March 1987
Place of birth: Belgrade, Serbia
Nationality: Austrian
Languages: English, German, French (trilingual), Serbian (mother tongue), Spanish (fluent)
Family situation: Single

Education

2011-2015   ***PhD student in Chemistry***, University of Basel (Switzerland)
Main areas : Design and synthesis of Organic ligands, formation of coordination polymers and networks by crystal growth, XRD.
supervised by Prof. Catherine E. Housecroft and Prof. Edwin C. Constable

2008-2010   ***Masters of Molecular and Supramolecular Chemistry, cum laude distinction***, Université Louis Pasteur (Strasbourg I)
Main subjects : Organic Chemistry, Inorganic Chemistry and Supramolecular Chemistry.
Master thesis: "Total synthesis of Tephrosin and analogs" supervised by Prof. Nicolas Winssinger

2005-2008   ***Bachelors of Chemistry, cum laude distinction,***Université Louis Pasteur (Strasbourg I)
Main subjects : Organic Chemistry, Inorganic Chemistry, Physical Chemistry and Analytical Chemistry

2002-2005   ***Baccalauréat and Matura, magna cum laude distinction,*** with major in Science, Lycee Francais, Vienna, Austria
Main subjects : Biology, Chemistry, Physics and Mathematics

Professional experiences

April-July 2009   Internship in *Laboratoire de Chimie Organo-Minérale,* Prof. J.P. Sauvage, Strasbourg
Synthesis of a ligand for the elaboration of multi-rotaxanes.

July-August 2008   Internship at University of Belgrade in Prof. Bogdan Solaja's lab (5 weeks)
Synthesis of antimalarial compounds.

Technical skills: Experience in organic and organometallic synthesis, crystal growth and XRD.
Skills in following analytical techniques: NMR, UV-VIS, IR, LCMS.

Special skills: Windows XP, Vista, Mac
Excel, Word, Powerpoint, Origin
NMR notebook, Mestrenova, Mercury, Chemdraw

Extra-curricular activities Sport: Member of Tennis club T.C. SAINT LOUIS and playing competitively. Part time tennis coach for kids in Belgrade. Training Karate in the Karate club of Saint Louis. Former member of the basketball team « basket 2000 » competing in the league in Vienna. Also fitness and other sports as hobby.

Tutoring: Part time tutoring in science during high-school and also part time tutor in organic chemistry during the masters and PhD (for bachelors students).

Publications:

1. Cobalt(II) coordination polymers with 4'-substituted 4,2':6',4"- and 3,2':6',3"-terpyridines: engineering a switch from planar to undulating chains and sheets E.C. Constable, C.E. Housecroft, M. Neuburger, S. Vujovic, J.A. Zampese and G. Zhang *CrystEngComm.,* 2012, **14**, 3554-3563

2. Molecular recognition between 4'-(4-biphenylyl)-4,2':6',4"-terpyridine domains in the assembly of d9 and d10 metal ion-containing one-dimensional coordination polymers E.C. Constable, C. E.Housecroft, M.Neuburger, J.Schönle, S.Vujovic and J.A.Zampese *Polyhedron ,* 2013, **60**, 120-129

3. Coordination polymers with 4'-(4-(anthracen-9-yl)phenyl)- and 4'-(4-(naphthalen-1-yl)phenyl)-4,2':6',4"-terpyridines: Mono-, di and heptazinc(II) nodes E.C. Constable, C. E.Housecroft, M.Neuburger, J.Schönle, S.Vujovic and J.A.Zampese *Polyhedron ,* 2013, **62**, 260-267

4. Do perfluoroarene..arene and C-H...F interactions make a difference to 4,2':6',4"-terpyridine-based coordination polymers? E.C. Constable, C. E.Housecroft, S.Vujovic, J.A.Zampese, A.Crochet and S.R.Batten, *CrystEngComm ,* 2013, **15**, 10068-10078.

5. Metallohexacycles containing 4'-aryl-4,2':6',4"-terpyridines: conformational preferences and fullerene capture E.C. Constable, C. E.Housecroft, S.Vujovic and J.A.Zampese *CrystEngComm ,* 2014, **16**, 328-338.

6. 2D → 2D Parallel interpenetration of (4,4) sheets constructed from a ditopic bis(4,2':6',4"-terpyridine) E.C. Constable, C. E.Housecroft, S.Vujovic and J.A.Zampese *CrystEngComm ,* 2014, **16**, 3494-3497.

7. Environmental control in the assembly of metallomacrocycles and one-dimensional polymers with 4,2':6':4"-terpyridine linkers and zinc(II) nodes E.C. Constable, C. E.Housecroft, S.Vujovic and J.A.Zampese *CrystEngComm ,* 2014, **16**, 8691-8699.